From photosensitive glycopolymers to smart drug delivery systems

Soliman Mehawed Abdellatif Soliman

UNIVERSITÉ DE LORRAINE

Laboratoire de Chimie Physique Macromoléculaire

RP2E

Doctoral Thesis

From photosensitive glycopolymers to smart drug delivery systems

Laboratory Physical Chemistry of Macromolecules (LCPM)- Nancy

Doctoral School Resources, Processes, Products and Environment (RP2E)

Publicly presented for the degree of Doctor of Philosophy of

University of Lorraine

By

Soliman Mehawed Abdellatif SOLIMAN

Defense: October 31th, 2014

The Jury:

Prof. Etienne FLEURY	Reviewer
Prof. Jean-Francois GOHY	Reviewer
Prof. Dominique HOURDET	Examiner
Dr. Cécile NOUVEL	Examiner
Dr. Jérome BABIN	Co-Director of thesis
Prof. Jean-Luc SIX	Director of thesis

The work presented in this manuscript was carried out within the `Biomolecules and targeting_ theme of Laboratory Physical Chemistry of Macromolecules (LCPM, FRE 3564, Nancy F-54000). Thanks to Prof. Dr. Alain Durand, Laboratory Director of LCPM for hosting me.

I wish to express my deepest appreciation and gratitude to Prof. Dr. Jean-Luc Six, Professor at the European School of Materials Engineering (EEIGM), and to Dr. Jérome Babin, Lecturer at the National School of Chemical Industries (ENSIC), for suggesting the topic of this work for their supervision, constructive comments, valuable criticism and continuous encouragement. However, these words are not enough to express my gratitude.

I also wish to express my appreciation to Prof. Dr. Muriel Barberi-Heyob, Professor at Research Center for Automatic Nancy (CRAN), University of Lorraine, for her assistance through cyctotoxicity test.

I'm much thankful to Dr. Cécile Nouvel, Lecturer at the National School of Chemical Industries (ENSIC), Prof. Brigitte Jamart Gregory, Professor and Director of European School of Materials Engineering (EEIGM), Prof. Anne Jonquières, Professor at ENSIC, Dr. Michelle Léonard, Head of Research CNRS, Dr. Carole Arnal-Herault, Lecturer at ENSIC, Dr. Marie-Christine Averlant-Petit, Head of Research at the CNRS, for their scientific support and kindness.

My thanks to Mr. Olivier Fabre, Engineer at LCPM for NMR analyzes and Mrs Chrystel Beaufils, Engineer at LCPM, for their appreciation assistance.

I would like also to thank Mrs. Marie-Christine Grassiot for SEC analysis, Mrs. Mathilde Achard, Mr. Jean-Claude Silvaut and Mr. Henri Lenda for their help and technical support throughout these years. Also thank to Jeanine Fourier, Amélie Trottman and Nathalie Brenon for their administrative assistance and usual kindness.

I'm much thankful to all my current and former colleagues with whom I had a great time and were able to put a good friendly atmosphere in the laboratory: Dr. Khalid Ferji, Dr. Charlotte Duval, Dr. Ancuta Rusu, Dr. Maxime Laville, Dr. Ludovic Colombeau, Dr. Hicham Qayouh, Dr. Ning, Faten, Asma, Aurélien, Katarzyna, Laura.

Finally, I'm much thankful to all my family, my mother, my brothers and my sisters for their support.

Signature

Soliman Soliman

List of abbreviation

Monomers

Ac GGM	O-acetyl galactoglucomannan
DMAC	Dimethylacetamide
2EHA	2-ethylhexyl acrylate
EMA	ethyl methacrylate
*i*BA	*i*-butyl acrylate
LA	lauryl acrylate
MA	Methyl acrylate
2MEA	2-methoxy ethyl acrylate
MMA	Methyl methacrylate
nBA	n-butyl acrylate
NBA	o-nitrobenzyl acrylate
NIPAM	N-isopropyl acrylamide
NMP	N-Methylpyrrolidone
VC	Vinyl chloride
TFE	2,2,2-trifluoroethanol

Polymers

Dex	Dextran
mPEG-b-P(HEMAm-Lacn)	methoxy poly(ethylene glycol)-b-poly(N-(2-hydroxyethyl)methacrylamide)-oligolactates
PAzoMA	polymethacrylate containing azobenzene groups
PEG	poly(ethylene glycol)
PEG-r-CPP-r-SA	terpolymer composed of poly(ethylene glycol), 1,3-bis(carboxyphenoxy) propane and sebacic acid
PEO-b-P(MEOMA-co-CMA)	poly[2-(2-methoxyethoxy) ethyl methacrylate-co-4-methyl-[7- (methacryloyl)oxyethyloxy]coumarin]
PGA	poly(glycolic acid)
PLA	poly(lactic acid)
PLGA	poly(lactide-co-glycolide)
PmCL¯ONB	o-nitrobenzyl-substituted poly(methyl-佟caprolactone)
PMPC	poly(o-methacryloyloxyethyl phosphorylcholine)

PNBA-Br	Poly(o-nitrobenzyl acrylate) with bromide end function
PNBA-N_3	Poly(o-nitrobenzyl acrylate) with azide end function
P(NBA-r-AA)-b-PS	poly(o-nitrobenzyl acrylate-random-acrylic acid)-b-Polystyrene
PNBMA	Poly(nitrobenzyl methacrylate)
PPO	Poly(propylene oxide)
PtNEA	poly(trans-N-(2-ethoxy-1,3- dioxan-5-yl)acrylamide)
PUNB	polyurethane containing several nitrobenzyl groups
P(VDF-co-CTFE)	poly(vinylidene fluoride-co-chlorotrifluoroethylene)

Ligands

BPy	2,2˘-bipyridine
Me_6TREN	Tris(2-dimethylaminoethyl)amine
Pr-PMI	N-n-propyl-2-pyridiylmethanimine
TREN	Tris(2-aminoethyl)amine

Solvents

$CDCl_3$	Deuterated Chloroform
DCM	Dichloromethane
DMF	Dimethylformamide
DMSO	Dimethyl sulfoxide
DMSO-d_6	Deuterated dimethyl sulfoxide
EA	Ethyl acetate
EC	Ethylene carbonate
[mim][AT]	1-methylimidazolium acetate
[mim][PT]	1-methylimidazolium propionate
[mim][VT]	1-methylimidazolium valerate
THF	Tetrahydrofuran

Techniques of polymerization

AGET ATRP	Activator Generated by Electron Transfer ATRP

ARGET ATRP	Activator regenerated by electron transfer ATRP
ATRP	Atom Transfer Living Radical Polymerization
eATRP	electrochemically induced ATRP
NMP	Nitroxide- Mediated Polymerization
ICAR ATRP	Initiators for Continuous Activator Regeneration ATRP
RAFT	Reversible-Addition Fragmentation chain Transfer
RDRP	Reversible-Deactivation Radical Polymerization
SARA ATRP	Supplemental Activators and Reducing Agents
SET-DTLRP	Single-electron transfer degenerative chain transfer living radical polymerization
SET-LRP	Single Electron Transfer ¯ Living Radical Polymerization

Characterization techniques

DLS	Dynamic Light Scattering
DSC	Differential Scanning Calorimetry
FT-IR	Fourier Transform InfraRed spectroscopy
MDSC	Modulated Differential Scanning Calorimetry
NMR	Nuclear Magnetic Resonance
SEC	Size Exclusion Chromatography
SEC-MALLS	Size Exclusion Chromatography - Multi Angle Laser Light Scattering
TEM	Transmission Electron Microscopy

Characteristics of polymer and glycopolymer

CWC	Critical Water Content
dn/dC	Increment of refractive index
伋	Dispersity
$\overline{M}_n$	Number average molecular weight
$\overline{X_n}$	Degree of polymerization
x	Conversion
Tg	Glass transition temperature
F_{PNBA}	Weight fraction of PNBA in glycopolymer
	Yield of substitution= number of groups per 100 glucosidic units

LIST OF CONTENT

RESUME ETENDU DE LA THESE EN FRANÇAIS

GENERAL INTRODUCTION

Chapter (I)Bibliography

RESUME ETENDU DE LA THESE EN FRANÇAIS

I) Résumé cours de la thèse

Au cours de cette thèse, des glycopolymères dibloc et greffés (Figure 1), photosensibles et amphiphiles, à base de dextrane et de poly(acrylate d'o-nitrobenzyle) (PNBA) ont tout d'abord été préparés. Ces glycopolymères ont alors été caractérisés par différentes techniques telles que les spectroscopies RMN et FT-IR ou encore la Chromatographie d'Exclusion Stérique (SEC). Des nanoparticules ont ensuite été formulées à partir de ces glycopolymères en utilisant diverses techniques telles que la nanoprécipitation et l'émulsion / évaporation de solvant organique. Ces nanoparticules ont ensuite été analysées en utilisant diverses techniques comme la Diffusion de la Lumière Dynamique (DLS), la Microscope Electronique à Transmission (MET) ou encore par granulométrie ou zétamétrie. La stabilité de ces nanoparticules contre différentes forces ioniques a été démontrée et permet d'envisager leur emploi pour administrer des médicaments dans le corps humain où la force ionique du sang est égale à 0,15 mol / L. Enfin, la sensibilité des nanoparticules fabriquées à la lumière a été étudiée.

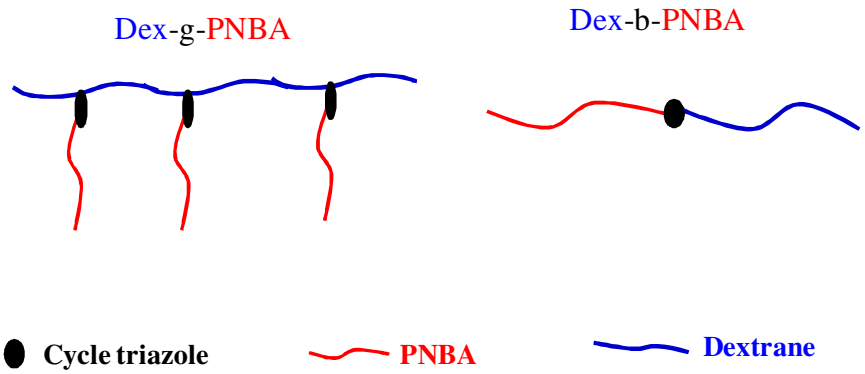

Figure 1. Représentation schématique des glycopolymères greffés et dibloc, à base de dextrane et de PNBA

II) Les systèmes de délivrance de médicaments

Les systèmes de délivrance de médicaments (DDS) permettent l'administration *in vivo* de composés pharmaceutiques pour guérir les sites de maladie. Les avantages de ces systèmes sont: 1) la protection des composés pharmaceutiques encapsulés contre leurs dégradations précoces, 2) l'amélioration de la biodisponibilité du médicament, 3) le contrôle de la libération du médicament et 4) le ciblage potentiel du médicament vers des cellules spécifiques à traiter. De nombreux DDS sont décris dans la littérature telles que les nanoparticules cˇur de polylactide / couronne de poly(éthylène glycol). Cependant, depuis

près de 15 ans, le LCPM s'est intéressé à la formation de DDS à partir de glycopolymères amphiphiles. Les glycopolymères amphiphiles sont composés d'une partie polysaccharide hydrophile et de parties polymères hydrophobes comme représentés sur la figure 1.

Après avoir réussi à encapsuler un médicament au sein des DDS et avoir injecté le tout dans le corps humain, le médicament se libère par dégradation ou "gonflage" du DDS ou par diffusion du médicament hors du DDS. Malheureusement, ces mécanismes conduisent à une libération "lente" et non contrôlée du médicament. Pour surmonter cela, les scientifiques ont développé des DDS stimulables permettant d'améliorer et surtout de contrôler la libération du médicament. Ces DDS sont obtenus à partir de copolymères amphiphiles comprenant une partie stimulable. Il existe différents types de DDS "intelligents" et leur classification dépend de la réponse du système à un stimulus environnemental, externe ou interne, tels que le pH, la température, la lumière... Certains DDS sont également doublement stimulables comme le montre la figure 2. Les DDS photosensibles sont particulièrement intéressants car tout le corps peut être exposé à une lumière contrôlée, ce qui n'est pas le cas avec d'autres stimuli tels que le pH ou la température.

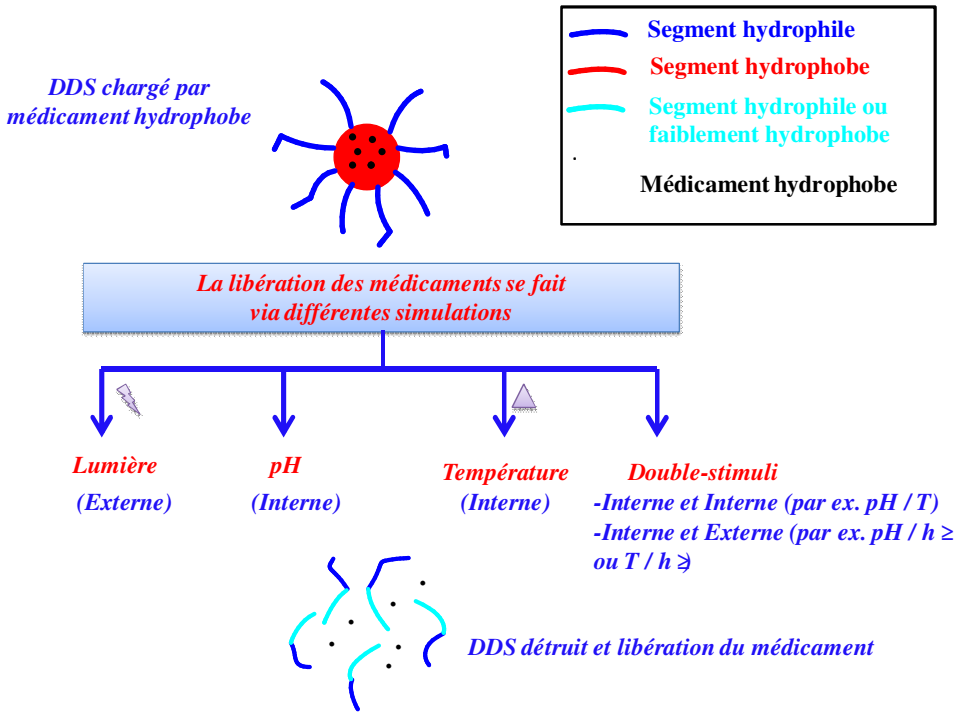

Figure 2. Représentation schématique des différentes méthodes de stimulation pour la libération du médicament hors des DDS

Il existe différents types de DDS sensibles à la lumière. Ils peuvent être classés en quatre catégories, selon les changements structurels photoinduits tel que rapporté par Zhao [1]: a)

Déplacement de la balance hydrophile-hydrophobe des copolymères dibloc amphiphiles, b) Rupture de la liaison reliant les deux blocs, c) Dégradation de la partie hydrophobe et d) Réticulation réversible du c˘ur hydrophobe du DDS, comme le montre la figure 3.

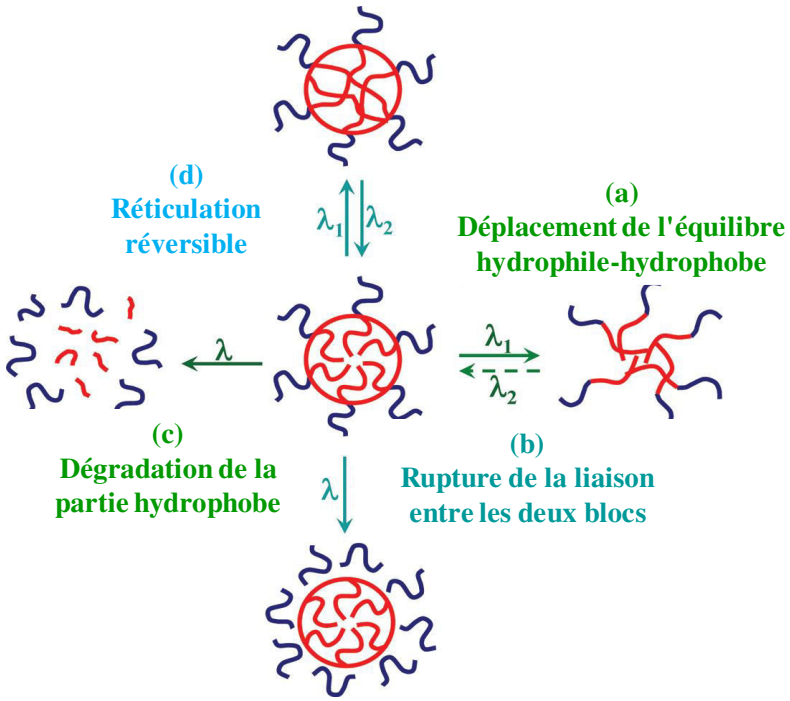

Figure 3. Représentation schématique des différents types de DDS photosensibles.

III) Démarche suivie au cours de cette thèse

Dans cette thèse, nous nous sommes intéressés à la formulation de nanoparticules photosensibles, obtenues à partir de glycopolymères greffés et dibloc, amphiphiles et photosensibles. Ces glycopolymères sont composés de deux parties :

ð Une partie polysaccharide hydrophile. Nous avons choisissons le dextrane car c'est un polysaccharide naturel, soluble dans l'eau et dans certains solvants organiques tel que le DMSO. Le dextrane est biocompatible et biodégradable *in vivo* où il est transformé en sucres de bas poids moléculaire tel que le glucose. Aussi, il a déjà été utilisé dans les industries pharmaceutiques et cosmétiques.

ð Une partie hydrophobe dérivée des polyacrylates. Plus précisément, nous avons choisi le poly(acrylate de 2-nitrobenzyle) (PNBA) qui possède des groupements 2-nitrobenzyle photolabiles. Ces groupements peuvent être clivés par absorption de photons, mais aussi par

absorption de deux photons dans le proche infrarouge (NIR) où la lumière (longueur d'ondes ~ 700 à 1000 nm) est particulièrement adaptée aux applications biomédicales.

Comme le montre le schéma 1, les glycopolymères ont été synthétisés en plusieurs étapes, par la stratégie "greffage sur". Premièrement, la polymérisation contrôlée du NBA par SET-LRP a permis d'obtenir le PNBA-Br. Celui-ci est ensuite modifié pour remplacer le brome terminal par une fonction azide et obtenir le PNBA-N_3. Deuxièmement, les dextranes (T40) et (T10) ont été modifiés pour introduire respectivement plusieurs groupes alcyne sur la chaine polysaccharide ou un seul à son extrémité réductrice. Enfin, les glycopolymères greffés et dibloc sont obtenus en réalisant une réaction de Huisgen (cycloaddition 1,3 dipolaire entre un alcyne et un azide, catalysée par le cuivre (I) - Chimie Click CuAAC) entre les PNBA-N_3 et dextranes modifiés. Les glycopolymères préparés ont ensuite été caractérisés par différentes techniques telles que les RMN ^{1}H, ^{13}C et DOSY, la spectroscopie FT-IR et la chromatographie d'exclusion stérique. Enfin, nous avons vérifié l'effet photosensible de ces glycopolymères dû à la présence de la partie PNBA.

Des nanoparticules ont ensuite été formulées à partir des glycopolymères précédemment obtenus. Pour cela nous avons employé la nanoprécipitation et nous avons également obtenu des nanoparticules par la méthode émulsion/évaporation de solvant organique en réalisant, ou non, une CuAAC *in situ*, durant l'étape de sonication. Les nanoparticules préparées ont été caractérisées par Diffusion de la Lumière Dynamique (DLS), Microscope Electronique à Transmission (MET) ou encore par granulométrie ou zétamétrie. La stabilité des nanoparticules contre différentes forces ioniques ou vis-à-vis d'un tensioactif compétitif tel que le SDS (DodécylSulfate Sodium) a été étudiée par spectrophotomètre UV-Vis.

Enfin, l'effet de la lumière UV sur les nanoparticules obtenues a été étudié par DLS ou par spectroscopie de fluorescence après y avoir encapsulé une sonde de fluorescence hydrophobe (Rouge de Nil).

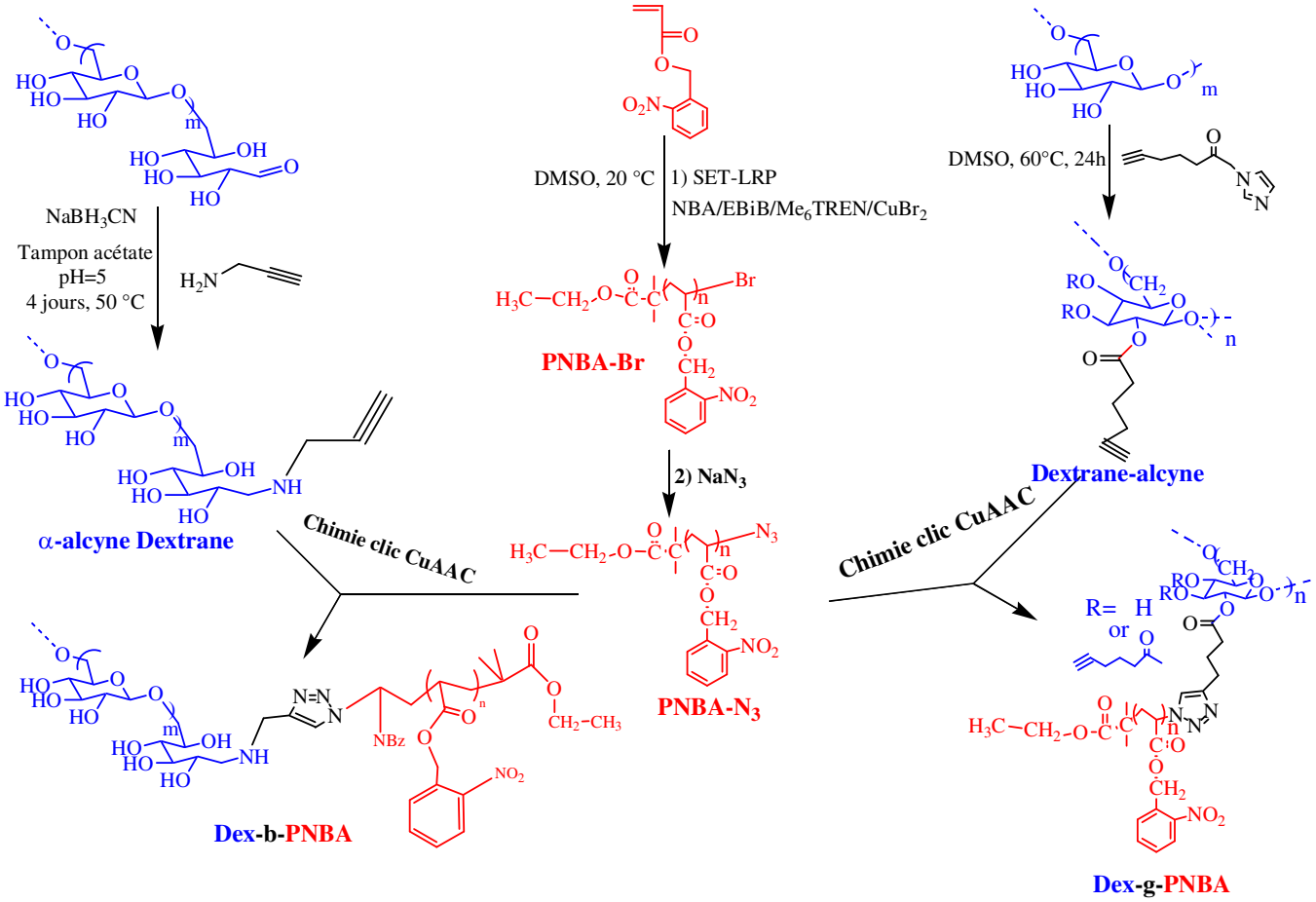

Schéma I. Stratégie de synthèse des glycopolymères greffés et dibloc, à base de dextrane et de PNBA

IV) Résultats obtenus

IV.1) Synthèse des glycopolymères

Pendant longtemps, l'acrylate d'o-nitrobenzyle a été considéré comme un monomère difficile à polymériser par des techniques de polymérisation radicalaire contrôlée telles que la RAFT, l'ATRP ou la NMP. Ce manque de contrôle a principalement été attribué à l'inhibition et au retard provoqué par les groupes nitro-aromatiques. Dans un récent article [2], nous avons montré que ce monomère pouvait être polymérisé de façon contrôlée par SET-LRP. Les PNBA-Br préparés par SET-LRP ont ensuite été modifiés à l'aide de NaN_3 et nous avons obtenu des PNBA-N_3 de M_n égale à 3500 ou 9800 g/mol.

Différents glycopolymères greffés ont été préparés en réalisant une CuAAC entre les PNBA-N_3 et le dextrane modifié par plusieurs groupes alcyne. La longueur des chaînes PNBA et le

rapport molaire fonction azide/ groupe alcyne ont été variés, ce qui a permis de synthétiser plusieurs glycopolymères greffés qui possédent diverses fractions massiques (F_{PNBA}) de la partie PNBA (de 22 à 85%), comme indiqué dans le tableau 1. Nous avons aussi fait réagir les mêmes PNBA-N_3 sur le dextrane modifié à son extrémité réductrice pour préparer deux glycopolymères dibloc dont la F_{PNBA} est de 27 ou 49%. Comme indiqué dans le tableau 1, les données estimées par diverses techniques de caractérisation sont en bon accord avec les valeurs théoriques.

Tableau 1. Caractéristiques de glycopolymères Dex-g-PNBA et Dex-b-PNBA

Glycopolymère [a)]	F_{PNBA} (%) [b)]	M_n glycopolymère (g/mol) c)		Đ [d)]	dn/dC [d)]
		Théo	SEC		
Dex(15)-g-1.5PNBA$_{3500}$	22	52 000	40 640	1.34	0.071
Dex(15)-g-14PNBA$_{3500}$	75	150 800	149 400	1.59	0.08
Dex(15)-g-1.5PNBA$_{9800}$	44	71 750	75 800	1.09	0.07
Dex(15)-g-12PNBA$_{9800}$	85	348 250	324 900	1.59	0.08
Dex-b-PNBA$_{3500}$	27	13275	13 890	1.12	0.071
Dex-b-PNBA$_{9800}$	49	19 500	18 310	1.07	0.08

a)Dex(15)-g-1.5PNBA$_{3500}$ où 15 est le taux de substitution du dextrane en groupes alcyne, 1.5 est le nombre de greffons PNBA pour 100 unités glucosidiques et 3500 est la M_n de chaque greffon PNBA.
b) Fraction massique de la partie PNBA
c) M_n du glycopolymère. Valeur prédite par la théorie (Théo) ou estimée par SEC-MALLS
d) Estimés par SEC-MALLS

IV.2) Effet de la lumière sur les glycopolymères

Selon la littérature, la photolyse des esters nitrobenzyliques produit des acides carboxyliques et le 2-nitrosobenzaldéhyde. Pour nos glycopolymères et à conversion totale, les produits de photolyse seront des glycopolymères greffés Dex-g-PAA (PAA = poly(acide acrylique)) ou dibloc Dex-b-PAA, comme indiqué dans le schéma 2. Nous avons donc étudié l'effet de la lumière sur nos glycopolymères greffés et dibloc. Pour cela, des solutions de glycopolymères blocs et greffés (0,1 mg / mL) ont été préparées puis irradiées en utilisant une lampe UV avec

une puissance égale à 1150 mW/cm^2. Après chaque irradiation, les spectres d'absorption UV des produits obtenus ont été enregistrés. Comme le montre la figure 4, au fur et à mesure de l'irradiation, la bande d'adsorption à 275 nm, caractéristique des esters nitro-aromatiques, diminue progressivement alors que l'on observe l'apparition et l'augmentation d'une bande à 325 nm liée à la formation progressive du 2- nitrosobenzaldéhyde.

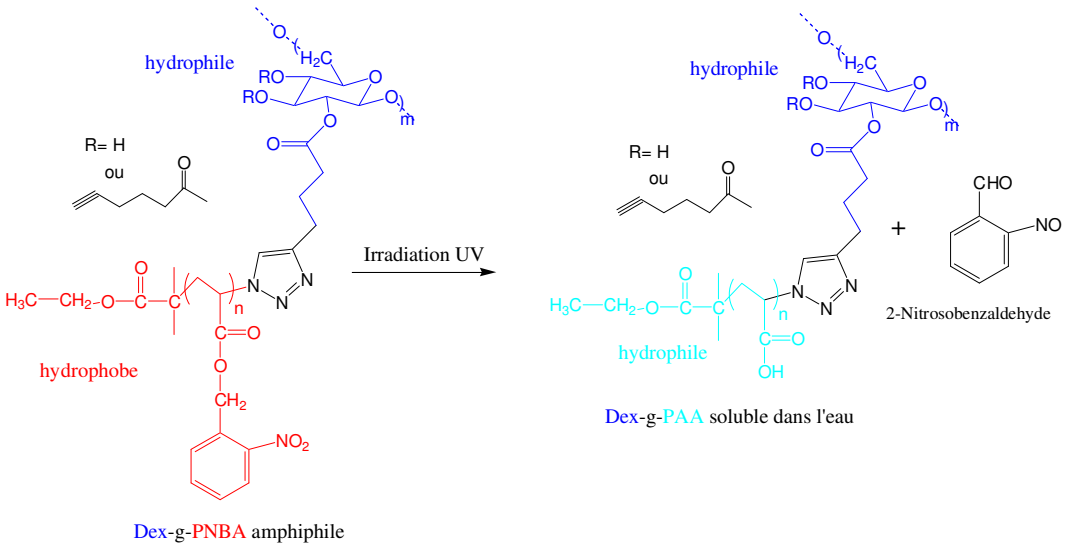

Schéma 2. Effet de l'irradiation UV sur les glycopolymères greffés amphiphiles

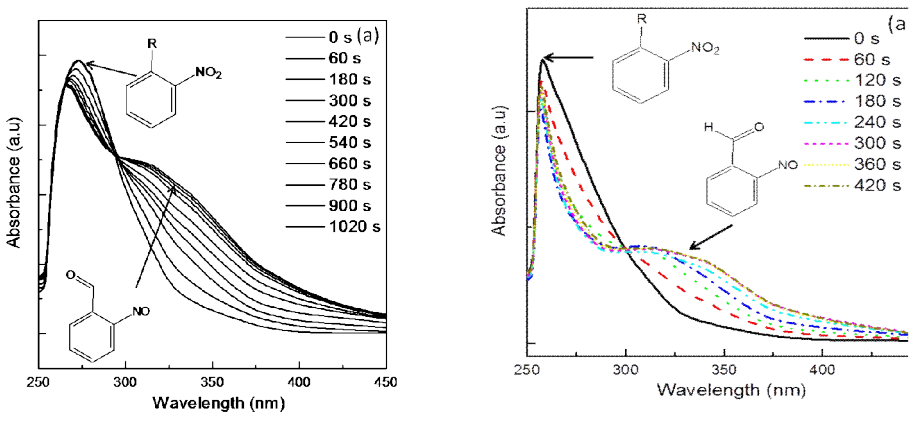

(A) **(B)**

Figure 4. Absorption UV du A) Dex-b-PNBA$_{9800}$ et B) Dex(15)-g-12PNBA$_{9800}$ pendant l'irradiation dans du DMSO (0.1mg/mL et 0.07 mg/mL, respectivement)) avec une lampe UV équipée d'un filtre de 320 -500 nm (puissance 1150 mW / cm²).

IV.3) Elaboration et caractérisation des nanoparticules

Après avoir préparé et caractérisé les différents glycopolymères greffés et dibloc, nous avons ensuite optimisé les conditions de fabrication de nanoparticules en utilisant tout d'abord la nanoprécipitation (cas des glycopolymères greffés à F_{PNBA} élevée). Les nanoparticules obtenues ont ensuite été caractérisées par DLS pour déterminer les diamètres moyens en Z et leur polydispersité, comme indiqué dans le tableau 2.

Tableau 2. Diamètre moyen en Z et polydispersité (PDI) des nanoparticules par nanoprécipitation de divers Dex-g-PNBA

Glycopolymère utilisé [a)]	F_{PNBA} (%) [b)]	Masse de dextrane (mg) par gramme de PNBA [c)]	Diamètre moyen en Z (nm) [d)]	PDI [d)]
Dex(15)-g-14PNBA$_{3500}$	75	310	118±3	0.08
Dex(15)-g-12PNBA$_{9800}$	85	153	185±2	0.04

a)Dex(15)-g-14PNBA$_{3500}$ où 15 est le taux de substitution du dextrane en groupes alcyne, 14 est le nombre de greffons PNBA pour 100 unités glucosidiques et 3500 est la $\overline{M}_n$ de chaque greffon PNBA.
b) Fraction massique de la partie PNBA dans le glycopolymère
c) Dans la nanoparticule
d) Déterminé par DLS

Nous avons aussi mis en oeuvre une autre technique pour obtenir des nanoparticules : l'émulsion / évaporation de solvant organique qui est l'une des techniques couramment utilisées. Nous avons alors d'une part utilisé les divers PNBA-Br et PNBA-N_3 précédemment synthétisés et d'autre part le dextrane modifié par de nombreux groupes alcyne. La fonction azide sur la chaîne PNBA nous permet de mener une CuAAC *in situ*, pendant l'étape de sonication. Des nanoparticules ont été formées en menant, ou non, la chimie click CuAAC et en faisant varier le rapport massique PNBA-Br/PNBA-N_3. Les caractéristiques de ces particules sont données dans le tableau 3.

Tableau 3. caractéristiques des particules formées par émulsion/évaporation de solvant organique.

Entrée	Ratio des PNBA utilisés		Masse de dextrane (mg) par gramme de PNBA [e]	Diamètre moyen en Z (nm) [f]	PDI [f]
	PNBA-Br [c]	PNBA-N_3 [d]			
[a]**1**	**1**	**0**	140	109±2	0.144
[b]**2**	**0.75**	**0.25**	174	131±3	0.107
[b]**3**	**0.5**	**0.5**	185	125±1	0.069
[b]**4**	**0.25**	**0.75**	174	117±1	0.047
[b]**5**	**0**	**1**	185	118±1	0.103
[a]**6**	**0.5**	**0.5**	109	132±2	0.124
[a]**7**	**0**	**1**	114	140±0	0.170

a) Sans CuAAC

b) Avec chimie Click CuAAC

c) M_n mesurée par SEC-MALLS = 7900 g/mol

d) M_n mesurée par SEC-MALLS = 8100 g/mol

e) Dans la nanoparticule

f) Déterminé par DLS

Quelle que soit leur méthode de préparation, la couche dextrane en surface des particules a été caractérisé notamment en terme d'épaisseur. Elle permet d'alors d'écranter la charge négative de surface des nanoparticules PNBA et permet la stabilité des suspension colloïdales de particules contre différentes forces ioniques. Nous avons également étudié la stabilité de cette surface vis-à-vis d'un tensioactif compétitif, le SDS, utilisé pour mimer l'action de certaines protéines circulantes dans le système sanguin. Cette surface dextrane est parfaitement stable lorsque des glycopolymères sont employés pour former les particules, ou encore lorsque la chimie click CuAAC est réalisée lors de l'émulsion/évaporation de solvant. Ces résultats permettent d'envisager l'emploi de ces nanoparticules comme DDS photosensibles. A l'opposé, lorsque la CuAAC n'est pas employée dans cette technique, la couche dextrane n'est pas suffisamment ancrée sur la particule et est désorbée en présence de SDS. On peut alors imaginer que ceci peut poser problème pour une utilisation des particules par voie parentérale.

IV.4) Effet de la lumière sur les nanoparticules

Pour étudier la photolyse UV des nanoparticules, nous avons tout d'abord mis au point les conditions expérimentales (milieu d'irradiation et concentration de la suspension colloïdale) pour mener les expériences. Puis, les nanoparticules à base de Dex(15)-g-14PNBA$_{3500}$ (F_{PNBA} = 75%) et contenant la sonde de fluorescence hydrophobe (Rouge de Nil) ont été irradiées sous diverses conditions de temps, mode et puissance d'irradiation par exemple.

Les résultats obtenus montrent tout d'abord que la présence de dextrane n'influence pas la cinétique de photolyse des PNBA. On observe également que ces nanoparticules photosensibles sont progressivement détruites par la lumière, avant même la photolyse totale des parties PNBA. Ceci permet de conclure que les glycopolymères Dex-g-P(NBA-r-AA) formés au cours de l'irradiation doivent se solubiliser en solution aqueuse à partir d'un certain taux de photolyse ; ce qui conduit à la destruction de la nanoparticules.

Après avoir vérifié que la sonde de fluorescence ne pouvait pas être libérée par simple diffusion hors de la particule, nous avons observé que cette sonde était libérée sous irradiation. De plus, en jouant sur les conditions expérimentales, il est possible de moduler, voire de contrôler, la libération de cette sonde fluorescente.

L'étude menée sur les nanoparticules de Dex(15)-g-14PNBA$_{3500}$ obtenues par nanoprécipitation a été répétée avec les particules formées par émulsion/évaporation de solvant organique. Des résultats similaires ont été obtenus dans chaque cas. En conclusion, ces nanoparticules présentent de fort potentiel d'utilisation comme DDS photosensibles.

IV.5) Etude de la cytotoxicité des nanoparticules

Des premiers résultats préliminaires sur la cytotoxcité des nanoparticules ont été obtenus grâce à la collaboration avec le Centre de Recherche en Automatique de Nancy (CRAN), de l'Université de Lorraine (Prof. Muriel Barberi-Heyob).

Il s'avère que les nanoparticules à base de Dex-g-PNBA ne sont pas cytotoxiques, tout comme leurs produits d'irradiation . Cependant l'irradiation doit être réalisée en milieu tampon, sans quoi le milieu aqueux devient trop acide pour les cellules, ce qui est dû à la formation des fonctions acides carboxylique.

Références

[1] ZHAO, Y., Macromolecules 2012. **45**: p. 3647Б3657.
[2] SOLIMAN, S. M. A., NOUVEL, C., BABIN, J., SIX, J.L., J. Polym. Sci., Polym. Chem. 2014, **52**: p. 2192¯2201

GENERAL INTRODUCTION

Nanomedicine is the field that studies disease treatments through nanotechnology applications. Nanotechnology has two approaches, which are nanomaterials and nanoelectronics. Firstly, nanomaterials are materials having sizes in the range of nanoscale like carbon or silicone nanotubes, and inorganic nanoparticles for instance. Secondly, nanoelectronics are diverse set of devices and materials to produce nanodevices like biosensors. Recently, nanomedicine has reached a high significant impact on economy [1]. For example and as mentioned in the last report of technical market research, `The global nanomedicine market was valued at $43 billion in 2010, and $50 billion in 2011. The market is expected to grow to $97 billion by 2016 at a compound annual growth rate of 14.1% between years 2011 and 2016_ [2]. Figure 1 shows a statistic description of nanomedicine sales by different diseases like cancer, central nervous system, inflammatories and cardiovascular.

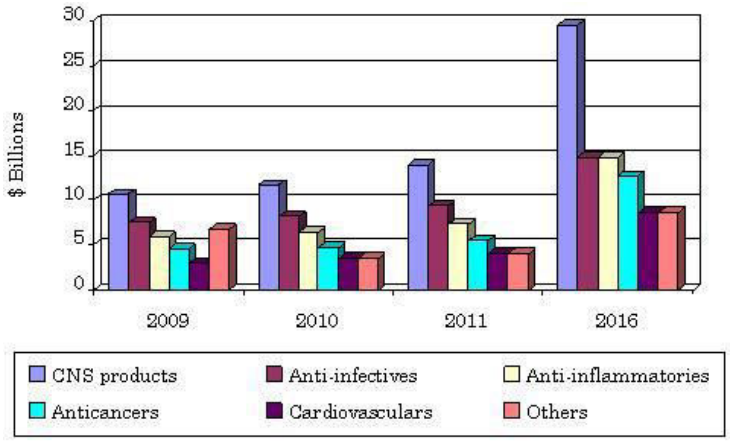

Figure 1. Nanomedical global sales by therapeutic area, 2009-2016 [2].

Many years ago, Laboratory of Physical Chemistry Macromolecules (LCPM) interested in the development of one nanomedicine approach, that is drug delivery systems (DDS) to allow the administration of pharmaceutical compounds in human body. Consequently, this general introduction will be DDS oriented. DDS has a vital role in controlling the pharmacological effect of the drug as it can influence the pharmacokinetics profile of the drug. An optimal DDS has to ensure that the pharmaceutical compound is available at specific sites (infected cells for instance). Moreover, the drug concentration at the appropriate site should be above the minimal effective concentration and below the minimal toxic concentration.

Depending on the administration route (Figure 2), different types of DDS could be used:

a) Oral is the most common route for drug delivery systems like formulations (e.g. s tablets, capsules, chewables, liquids), GI (gastrointestinal) specific hydrogels. Thin films DDS are buccally or sublingually administered.

b) Parenteral/Injection route is more rapid than oral administration. By this way, we can administrate drugs that are poorly absorbed or ineffective when orally given or drugs having short half-life. There are many types of parenteral routes depending on the site of administration into the body as intravenous, intramuscular, subcutaneous, intradermal and intraperitoneal routes. In case of intravenous delivery, we can administrate aqueous solutions or forms containing a small enough dispersed phase (solid or liquid) (e.g. smaller than 200¯ 250 nm) to avoid embolism.

c) Transdermal route in which drugs are administered via skin surface. This type includes semisolid dosage forms (like creams, ointments, gels and pastes) and liquid like emulsions.

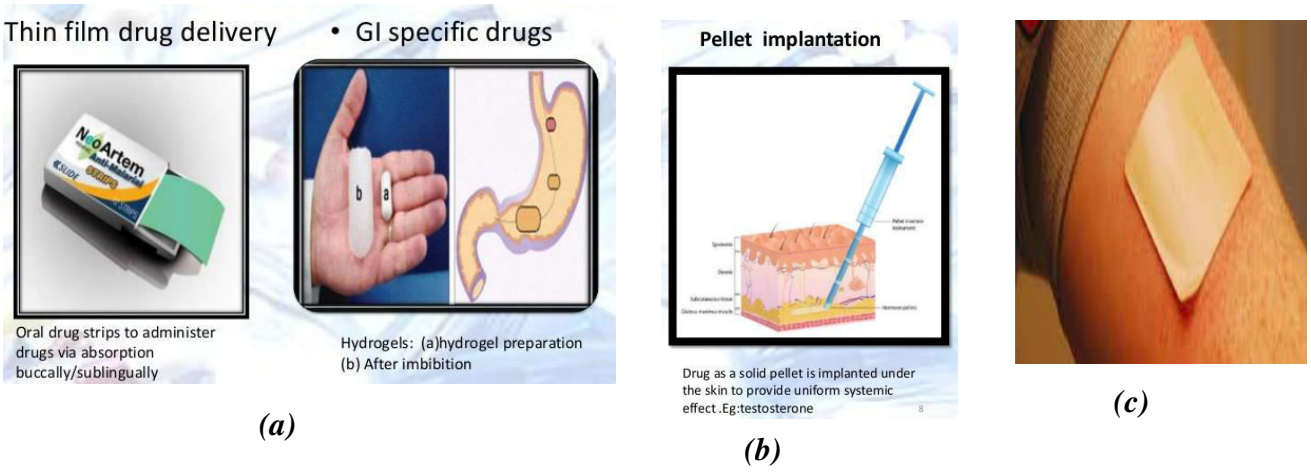

Figure 2. Different routes of drug administration into the human body as (a) Oral, (b) Injection and (c) Transdermal

Drug can be encapsulated into a specific DDS and intravenously administered. With this aim and on one hand, the scientists formulated in 90˘s first generation of DDS based on hydrophobic, biocompatible and biodegradable polymers as shown in Figure 3, A. By this way, the drug was encapsulated during polymer nanoprecipitation inside nanoparticles for instance. Unfortunately, this first generation of DDS had many drawbacks when administrated into the body. Three main drawbacks are i) trapping by the immune system (due to opsonins adsorption on the DDS surface), ii) unspecific and iii) uncontrolled drug

release. The development of second generation DDS was made to overcome these drawbacks. The surface of first generation of DDS was thus modified by introducing a hydrophilic polymeric shell (Figure 3, B) to enable a long blood circulation of DDS. These new DDS were called stealthy DDS. Poly(ethylene glycol) (PEG) is the common hydrophilic polymer used in surface modification of these DDS and this process is called PEGylation. In LCPM, scientists proved that stealthness could also be obtained using hydrophilic polysaccharide (based on dextran for instance) coverage [3]. Second generation of DDS was more recently modified to target DDS to specific cells by introducing specific groups (like antibodies, carbohydrate or peptide) onto the surface. We called them third generation DDS as shown in Figure 3, C.

In another hand, amphiphilic copolymers can be used to auto-organize themselves and produced nano-objects useful as DDS. By this way, the inner core of DDS is composed by the hydrophobic part of the block copolymer and can dissolve the poorly water-soluble drug, whereas the outer shell or corona is produced by the hydrophilic block of the copolymer. This shell stabilizes DDS colloidal suspension. Amphiphilic copolymers can form nano-objects as nanoparticles but also micelles or vesicles as shown in Figure 3, (D, and E). The structure of formed nano-objects depends on many parameters such as the ratio between hydrophobic and hydrophilic parts of copolymer.

Mechanisms of drug release are based on DDS degradation or swelling and/or drug diffusion. Unfortunately, these mechanisms lead to slow rate and poor controlled drug release. To overcome that, new DDS were developed as smart or sensitive DDS to improve and control the drug release. Fabrication of smart DDS is based on the incorporation of sensitive block into amphiphilic copolymers. Sensitive polymers undergo reversible or irreversible physical or chemical changes. These changes depend on response to internal or external stimulations. Internal stimulations may be temperature, ionic and pH stimulation while external ones are light, magnetic and electric fields.

Some examples will be given in the bibliography part of this manuscript.

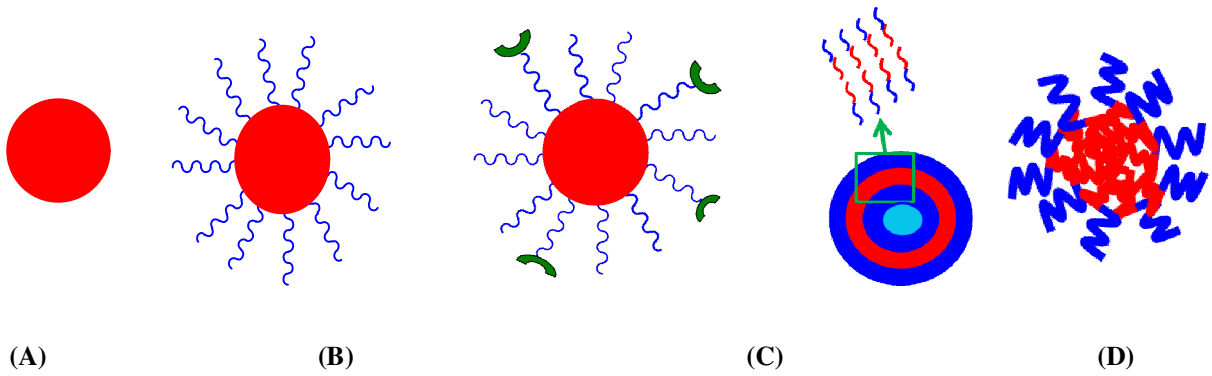

(A) **(B)** **(C)** **(D)**

Figure 3. DDS nanoparticles structures (A) First Generation (B) Second Generation (C) Third Generation. Amphiphilic copolymer-based nano-objects (D) Vesicle (E) Micelle.

(Red Color: hydrophobic polymer, Blue color: hydrophilic polymer, and Green color: targeting group).

(E)

As we already mentioned, LCPM interested in the development of drug delivery systems since more than 15 years. In the current thesis, we studied the fabrication of smart drug delivery systems that are based on light sensitive amphiphilic glycopolymers.

The amphiphilic copolymers we used to produce these smart DDS are associating hydrophilic dextran polysaccharide block and poly(2-nitrobenzyl acrylate) hydrophobic grafts or block. Because they are based on a polysaccharide, these copolymers will be named glycopolymers. We selected these materials as dextran is nontoxic, biocompatible and biodegradable. Moreover poly(2-nitrobenzyl acrylate) has a very good nitrobenzyl photolabile group that i) is non toxic and ii) can be cleaved into an hydrophilic polyacrylic acid through two-photon absorption of near infrared (NIR) light (~700¯1000 nm), that is particularly attractive for biomedical applications. We chose this stimulation because it give us more opportunity to use these smart DDS in overall the human body and because the drug release will occur by using an external source of light (external stimulation).

The current manuscript is consisting of four main chapters:

»***First chapter*** will be devoted to bibliographic studies about DDS. Firstly, we will talk about the development of first, second and third generations of DDS. The methods used to produce these DDS will be shown and some information about the techniques used to characterize DDS will be given. Secondly, smart DDS that are sensitive to pH, temperature, light or ionic strength will be exposed. Finally, we will give some information about various techniques of Reversible- Deactivation Radical Polymerization (RDRP)[a].

»***Second Chapter*** of this manuscript will show optimal conditions to control the RDRP of 2-nitrobenzyl acrylate using SET-LRP will be studied. In the second part, dextran will be modified by two different ways in order to produce grafted and diblock glycopolymers by click chemistry.

»***Third Chapter*** will describe the use of the previous amphiphilic copolymers to produce nano-objects by various techniques. Then, these nano-objects will be characterized in terms of diameter, dispersity, structure and zeta potential. Nano-objects will be irradiated by UV light and the effect of irradiation will be studied. Encapsulation of fluorescent probe and release by light irradiation will be studied. Finally, the cytotoxicity of these nano-objects before and after irradiation will be evaluated in vitro.

»***Fourth Chapter*** will expose all the experiments we carried out.

Then, a general conclusion and several perspectives will be given.

[a] *According to recent IUPAC rules, controlled Radical Polymerization (CRP) is now called Reversible-Deactivation Radical Polymerization (RDRP)*

References

1) Ruth D., Rogerio G., Nanomedicine(s) under the Microscope, Mol. Pharmaceutics 2011, 8, 2101¯2141.
2) BCC Research (Market Research), code HLC069B, 2012; http://www.bccresearch.com/market-research/healthcare/nanotechnology-medical-applications-global-market-hlc069b.html
3) C. Gavory, A. Durand, J.-L. Six, C. Nouvel, E. Marie, and M. Leonard, Polysaccharide-covered nanoparticles prepared by nanoprecipitation, Carbohyd. Polym. , 84 (2011) 133-140.

Chapter (I)

Bibliography

I) Introduction

The current thesis deals with the fabrication of photosensitive nanoparticles that may be used as smart drug delivery systems (DDS). The photosensitive nanoparticles we produced are based on amphiphilic glycopolymers composed of two parts (Figure 1). The first part is a hydrophilic polysaccharide backbone or block, which is dextran (Dex). The other part is a hydrophobic photosensitive polyacrylate grafts or block (poly(2-nitrobenzyl acrylate)- PNBA).

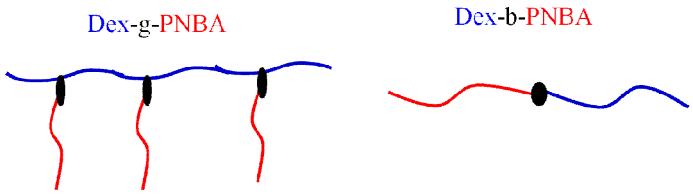

Figure 4. Schematic representation of grafted and diblock glycopolymers

After a controlled synthesis of these amphiphilic glycopolymers, nanoparticles will be prepared via several methods such as nanoprecipitation, dialysis and emulsion/organic solvent evaporation. Consequently, this bibliographic chapter is divided into two parts.

***In the Part one**, the development of drug delivery systems will be introduced and we will focus on smart or sensitive drug delivery systems. Moreover, methods of nano-objects formation and techniques to characterize them will be discussed.*

***In the Part two**, we will talk about Reversible-Deactivation Radical Polymerization techniques, which are useful to prepare polymer with controlled parameters. More precisely, we will focus on the technique used in this study that is Single Electron Transfer- Living Radical Polymerization (SET-LRP).*

II) Drug Delivery Systems

The `Drug delivery system (DDS)_ thematic approach is a very important one of nanomedicine for healthcare field. DDS allow an encapsulation and an administration of pharmaceutical compounds to cure disease sites in human body. After successful encapsulation of drug into DDS, the drug release occurs and depends on DDS degradation or swelling and/or by diffusion outside the DDS. As we will see in the following pages, DDS were developed into many forms to improve their stability in body and to increase the encapsulation capacity of drug. We will also discuss the steps of development of such DDS design. As many administration routes are offered, we have only selected parental routs hereafter.

II.1) Development of Drug Delivery Systems (DDS)

II.1.1) Three generations of DDS

The essential three generations or stages of drug delivery systems development are described as follow.

First generation of DDS groups simple nanoparticles, which are produced from biodegradable, biocompatible and hydrophobic polymers. The common hydrophobic polymers used to produce such DDS are poly(lactic acid) (PLA), poly(glycol acid) (PGA) and their copolymers as poly(lactide-co-glycolide) (PLGA) [1, 2], peptides and proteins [3-5] for instance. Polyanhydrides were also used as controlled release vehicles [6]. Whatever the polymer used to produce such DDS, these first generation DDS exhibit one main drawback that is to be trapped and removed from blood circulation by the reticuloendothelial system (RES) after the adsorption of opsonins (circulating proteins) on DDS surface.

To overcome this drawback, nanoparticles surface must be modified using a hydrophilic polymer to enhance the repulsion of proteins. This surface modification enables nanoparticles to prolong their circulation time. This type was called Second generation of DDS. The hydrophilic poly(ethylene glycol) was commonly used to produce a hydrophilic shell onto the nanoparticle and this modification is called PEGylation. In this case, hydrophilic PEG chains repulse opsonins and nanoparticles remain in the circulation of blood for a prolonged period. Such nanoparticles are called `stealthy DDS_ [7]. Nanoparticles with hydrophilic surface can also be obtained with

some other hydrophilic chains. In our lab, polysaccharidic hydrophilic dextran shell has been many times reported [8-10]

Further modifications of second generation DDS was made to produce targeting drug delivery systems. Such modifications were made by introduction of specific groups like antibodies against tumor, carbohydrates or peptides that are recognized by cells receptors. This generation is called third generation DDS.

Some DDS based on biodegradable materials were approved by Food and Drug Administration (FDA) and are on the market, as shown in Figure 2 [11].

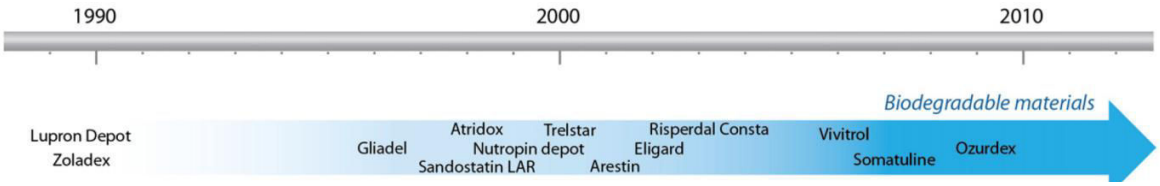

Figure 5. DDS based on biodegradable materials on the market [11].

II.1.2) DDS based on amphiphilic copolymers

Scientists were very interested to develop drug delivery systems based on block amphiphilic copolymers due to their remarkable chemical flexibility [12]. Moreover, their block constituents are generally immiscible, leading to one microphase separation. Since the different blocks are linked together by covalent bonds, the microphase separation is spatially limited and results in self-assembled structures. In the beginning of 90s, the first DDS based on A-B diblock copolymers were investigated by Kataoka˘s group [13]. These DDS were based on PEG and poly(aspartic acid) modified by 4-phenyl-1-butanol, PEG-b-poly(ethylene imine) and PEG-b-polylysine. At the same time, another independent Kabanov˘s group investigated DDS based on triblock copolymers which are poly(propylene oxide)-b-poly(ethylene oxide)-b- poly(propylene oxide) (PEO-b-PPO-b-PEO). Such DDS are actually under phase III clinical evaluation in Canada. Unfortunately, some problems occur when using such self-assembly structures in human body. For instance, after injection in blood stream, destabilization of such polymeric micelles was observed that leads to a rapid dissociation of the structure and to a burst release of drug. To tackle this problem, various innovative approaches have been tested to modify the micelle cores chemistry [14]: a) To increase the hydrophobicity of the core by attaching pendant groups to the

hydrophobic part, such as fatty acids, benzyl groups or cholesterol [15-17]. b) To introduce hydrogen-bond interactions in the core [18]. c) To promote electrostatic interactions by introducing oppositely charged groups in the core [13]. d) To post-crosslink the core via chemical, thermal or photo-induced polymerization [19].

Some examples of amphiphilic copolymers used to produce drug delivery systems and their corresponding encapsulated drugs are resumed in Table 1 [20].

Table 1. Examples of amphiphilic copolymers used and their corresponding encapsulated drug [20]

Polymer	Drug/imaging agent encapsulated
PLGA-B-PPO-B-PLGA	Doxorubicin
PEG-b-PPO	Doxorubicin
Poly(ϵ-caprolactone)-b-PEO	Pyrene (hydrophobic fluorescent probe)
Poly(lactic acid)-b-polyurethane	Gliclazide
PMPC-b-PMBA	Paclitaxel
Poly(ethylene glycol)-b-(lactide)	Taxol
Poly(lactide-b-PEG)	Paclitaxel
mPEG-b-p(HEMAm-Lac_n)	Pyrene
PEG-b-∴benzyl-l-glutamate¯N-carboxyanhydride	Adriamycin

Abbr.: mPEG-b-p(HEMAm-Lac_n), methoxy poly(ethylene glycol)-b-poly(N-(2-hydroxyethyl)methacrylamide)-oligolactates ; PMPC= poly(2-methacryloyloxyethyl phosphorylcholine)

II.2) Methods of nanoparticles formation

In the beginning, we would like to mention the definition of nanospheres that may be nanoparticles or nanocapsules (Figure 3). Nanoparticles are composed by a full solid core and nanocapsules present a liquid core. Nanospheres are colloidal objects in the range 10¯1000 nm [21, 22].

Nanoparticles can be conveniently prepared by direct polymerization of monomers using classical polymerizations [23]. But, some others methods are commonly used to prepare nanoparticles based on amphiphilic copolymers. One can mention: 1) Nanoprecipitation, 2)

Emulsion/organic solvent evaporation, 3) Dialysis methods that mainly lead to micelle-like structure and sometimes form nanoparticles depending on the copolymer nature.

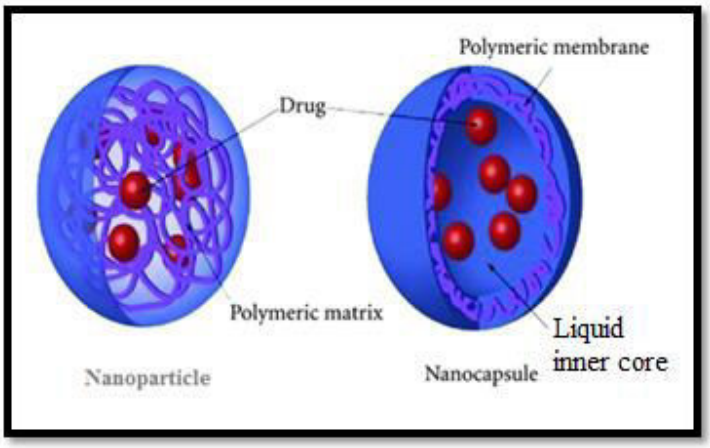

Figure 6. Nanoparticle and nanocapsule loaded by hydrophobic drug

II.2.1) Nanoprecipitation method

Nanoprecipitation method is a simple, fast and reproducible method, which is widely used for the preparation of nanoparticles. It is also called `solvent displacement method_. Fessi et. al. demonstrated nanoprecipitation since 1989 [24]. Nanoprecipitation system consists of three basic components: the polymer (synthetic, semi synthetic or natural), the solvent (usually organic phase) and the non-solvent (aqueous phase) of the polymer. Used organic solvent (i.e., ethanol, acetone, THF or dioxane) has to be miscible in water and easily removable by evaporation. Due to this reason, acetone is the most frequently employed polymer solvent [24-26]. The basic principle of this technique is based on a rapid addition of the polymer solution into the non-solvent phase resulting in the formation of small particle containing polymers chains when the organic solvent diffuses into the water phase, as shown in Figure 4 [24, 27]. After evaporation of organic solvent then centrifugation, solid nanoparticles are recovered.

Lince et al. [28] indicated that the process during nanoprecipitation comprises three stages: nucleation, growth and aggregation. The rate of each step determines the particle size and the driving force of these phenomena is the ratio of polymer concentration over the solubility of the polymer in the solvent/nonsolvent mixture. The separation between the nucleation and the growth stage is the key factor for uniform particle formation.

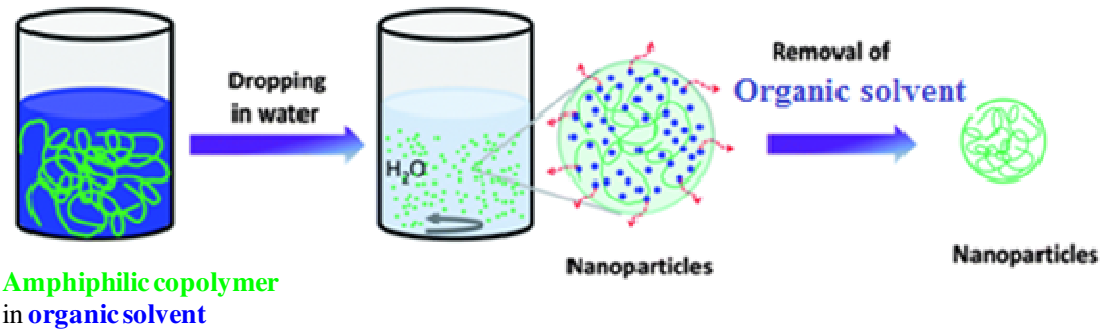

Figure 7. Basic principle of nanoprecipitation method

The key variables determining the success of this method and affecting the physicochemical properties of nanoparticles are associated with the conditions of adding the organic phase into the aqueous one: copolymer concentration, organic phase injection rate, aqueous phase agitation rate, the method of organic phase addition (position of needle of syringe during addition as inside or above the aqueous phase) and the organic/aqueous phases ratio. Likewise, recovered nanoparticles characteristics are influenced by the nature and weight fraction of blocks in copolymer [29, 30].

In our lab, dextran-g-PLA glycopolymers have been nanoprecipitated successfully [8], for instance. As shown in the Table 2, other amphiphilic copolymers have been used into nanoprecipitation[9]. As shown in Table 2, stabilizing agent may be required for some polymer during nanoprecipitation.

Table 2. Some examples of nanoparticles prepared using nanoprecipitation method [9]

Polymer	Solvent	Non-solvent	Stabilizing agent	Particle size (nm)
PLGA	Acetone	Water	PVA	95–560
PBCA	Acetone	Water	Pluronic F 68	269 ± 4
			Polysorbate 80	210 ± 5
			Dextran	238 ± 5
Allylic starch	Acetone	Water	–	270
PHB	Acetone	Water	Tween 80	100–125
Dextran ester	Acetone	Water	–	77
PLGA	Acetone/ethanol	Water	Tween 20	63–90
PCL diol	Chloroform	Water	Pluronic F 127	17.4
Eudragit L100-55	Acetone/absolute ethanol	Water	–	120
PLGA	Acetone	Water	–	165 ± 5
	Acetonitrile			164 ± 4
PCL	Acetone	Water	PVA	365 ± 5
PCA	Ethanol/water	Water	–	150
PLA	THF	Water	–	100–300
PCL	Acetone	Water	Span 20	741–924
PCL	Acetone	Water	Polysorbate 80	266 ± 11
PLA	Acetone	Water	Poloxamer 188	250 ± 50
PCL	Acetone	Water	PE/F68	308–352

II.2.2)Dialysis method

Dialysis is one another technique to produce small and narrow-distributed nanoparticles [24, 31]. Dialysis is performed against a non-solvent that is miscible with the organic solvent used to dissolve polymers (Figure 5). This method is based on osmosis where a spontaneous net movement of organic solvent molecules through the partially permeable membrane occurs. The displacement of the solvent inside the membrane is followed by the progressive aggregation of copolymer chains due to their loss of solubility. This leads to the formation of homogeneous suspensions of nanoparticles [32]. Usually, copolymers that are insoluble in volatile organic solvents like acetone, THF and DCM or that are soluble in DMF, DMSO, are dialyzed.

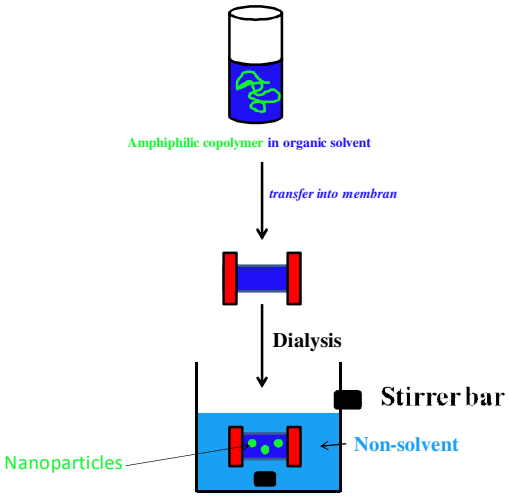

Figure 8. Schematic representation of dialysis method [32]

Many nano-objects based on different amphiphilic copolymers have been prepared by dialysis method, as shown in Table 3 [32]

Recently, scientists modified this dialysis method by dissolving copolymers in organic solvent that is miscible in water then adding dropwise this solution into water to form nanoparticles. The organic solvent was then removed by dialysis. This method is called nanoprecipitation-dialysis method. Some examples of nano-objects were fabricated by this method. For instance, dextran vesicular carriers [33] have been produced with using block copolymers based on poly(DL-lactide-co-glycolide) [34].

Table 3. ***Examples of some nanoparticles prepared by dialysis method***

Polymer	Solvent	MWCO (kg/mol)	Dialysis time (h)	Particle size (nm)
PBG-PEO	DMF	–	24	250–362
PA-CMPEG	DMAc	12	21	193.3 ± 13.5
PDLLA-P(NIPAM-MAA)	DMSO	12–14	48	84–338
PDLLA	DMF	08–15	12	321
DexEst	DMAc	03.5	96	87
TosDex	DMAc	03.5	96	345–500
PA	DMSO	02	72	50–130
mPEG-PLGA	DMF	06–08	12	42.8 ± 3.8
PLAF	DMF/DMSO	3.5	24	347
PLA-TPGS	DMF	3.5	30	327 ± 13
PCL-PVA	DMSO	12–14	45	361
PLGF	DMF/DMSO	3.5	24	285
PLGA	DMSO	10	24	635 ± 102
PHB	DMSO	10	24	53 ± 13
PMMA	DMF	12	72–96	200

Before studying the self-assembly of amphiphilic copolymers by dialysis, it is very important to estimate the Critical Water Content (CWC), that depends on the copolymer solution concentration. CWC is the critical value of water content to add into the copolymer organic solution, at which the copolymers start to self-associate. Below this CWC, copolymer chains are unassociated. When the addition of water progresses further, more and more copolymer chains associate to form micelles and the concentration of the copolymers in single-chain form decreases. In addition, Critical Micelle Concentration (CMC) of copolymers may be estimated at this CWC. Eisenberg et. al. reported one method to estimate the Critical Water Content (CWC) [35]. The method is measuring scattered light intensity as a function of added water content.

For instance, Schubert et. al. estimated CWC for amphiphilic supramolecular graft copolymers that are based on a poly(methyl methacrylate) (PMMA) backbone with PEG side chains linked to the backbone via a ruthenium(II)-terpyridine complexe (Figure 6)[36] .

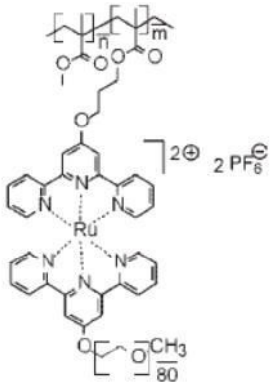

A : m=2 , n= 34

B : m=4, n= 35

C : m=5, n=51

Figure 9. **Structure of the graft copolymer used by Schubert et. al. [36]**

The authors dissolved their copolymer in DMF and determined counts per second (CPS) as a function of added water volume as shown in Figure 7. They studied the behavior of three copolymers (A, B, C see Figure 6) with different ratio of hydrophobic/hydrophilic ratio. At low added water content, CPS is low because graft copolymer chains exist as unimers. Then, an increase in CPS is observed because of the formation of aggregates, as proven by the observation of a correlation function. Finally, CPS reaches a plateau value as an indication that the aggregates are already frozen at these water contents and do not further modify their structure (grow for instance). It should however be noted that the CWC of sample A was lower than CWC for B, than CWC for C, according to the increase of hydrophilic PEG blocks weight fraction in copolymers as shown in Figure 7.

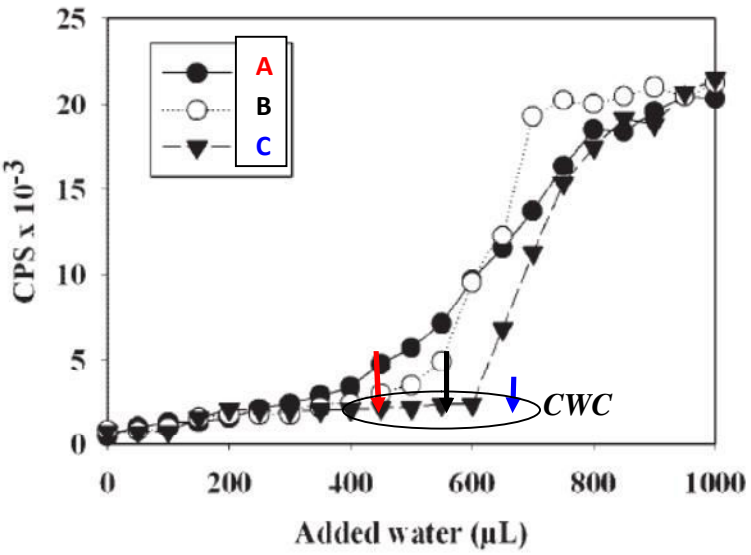

Figure 10. Scattered light intensity (counts per second CPS) as a function of the added water amount for the grafted copolymers A, B, C (see Figure 6) [36].

II.2.3) Emulsion/organic solvent evaporation method

There are two types of emulsion technique, which are single and double emulsions. First technique is one very simple nanoemulsification using sonication. On another hand, double emulsion undergoes simple pre-emulsification. Then, water aqueous or oil containing stabilizer is added. The mixture undergoes a second emulsification, as we will describe below.

II.2.3.a) Single emulsion technique

Single emulsion/ organic solvent evaporation was developed by Ogawa et al for hydrophobic drugs encapsulation [37]. The methodology of this technique is firstly to prepare a polymeric nano-dispersion wherein the polymer was dissolved in the organic phase that is not miscible with surfactant water phase. Sonication methods are required to reach submicronic diameter. Organic phase used depends on required nano-object shape i.e. nanoparticles or nanocapsules. For instance, volatile organic solvents like dichloromethane, chloroform or ethyl acetate are used to prepare nanoparticles, while non-volatile (oily) hydrophobic organic solvent are used to prepare nanocapsules. Secondly, in case of nanoparticles, the organic solvents contained in nano-droplets is gradually evaporated to generate nanoparticles [32]. If hydrophobic drugs are initially dissolved in the organic phase, this method leads to drug encapsulation. The advantages of nanoparticles or nanocapsules are the high hydrophobic drug encapsulation efficiency due to the optimized drug solubility in the nano-object cores. Due to this encapsulation the drug itself remains protected against degradation [38].

Langlois et. al. prepared nanoparticles of amphiphilic dextran-g-poly(3-hydroxybutyrateco-3-hydroxyvalerate) (Dextran-g-PHBHV) using dichloromethane as organic solvent [39], for instance. In LCPM, many researches deal with the preparation either of PLA nanoparticles using dextran-based copolymer surfactants [8] or hydrophobically modified polysaccharides [10]. Using adequate conditions, the authors got on stable nanoparticles (average diameter = 160 nm with PDI = 0.14) without additional surfactant.

II.2.3.b) Double emulsion technique

Double emulsion (W/O/W) technique requires three steps: (1) a primary emulsification between an aqueous solution of the active agent (internal waterphase, W) is emulsified into an organic solution containing the biodegradable polymer (oil phase, O) that will become the core of nanoparticles. Surfactant is used to stabilize this W/O emulsion. (2) Re-emulsification: the primary emulsion (W/O) is further emulsified with a large amount of a second aqueous phase containing a stabilizer (external water phase, W) to form a W/O/W double emulsion. (3) Solidification: the organic solvent is removed by evaporation or extraction and then solid nanoparticles are collected by centrifugation or filtration and subsequently lyophilized. The advantages of such double emulsion technique are a high hydrophilic drug entrapment efficiency,

a desired particle size and an effectively sustainable release property [40]. Double emulsion method is very important and useful with special cases as protein encapsulation for instance. Indeed, if the protein is denatured during encapsulation, it will become therapeutically inactive and may cause unpredictable side effects such as immunogenicity or toxicity [40, 41]. As example, Su et. al. prepared microparticles based on monomethoxypoly(ethylene glycol)-b-poly(DL-lactide) copolymer and reported a very efficient encapsulation of protein such as lysozyme using modified W/O/W double emulsion-solvent diffusion method [40].

Some other examples of polymers nanoparticles that were fabricated using single and double emulsion-solvent methods as shown in Table 4.

Table 4. Some examples of prepared nanoparticles via emulsion/organic solvent evaporation methods [30]

Polymer	Organic solvent	Stabilizer	Emulsion type	Particle size (nm)
POP	Acetone	Poloxamine 908	o/w	200
PLGA	Dichloromethane/acetone	PVA	o/w	60–200
PLGA	Dichloromethane	Span 40	(w/o)/w	200
PLA	Methylene chloride	PVA	(w/o)/w	200
PEG-PLA	Methylene chloride	Sodium cholate	(w/o)/w	200
mPEO-PLA	Methylene chloride	Sucrose	(w/o)/w	268 ± 4
PLGA	Chloroform	SDS	(w/o)/w	76
PEO-mPAE	Ethanol	Pluronic F-108	o/w	100–150
PS copolymer	THF	-	o/w	300
PS	THF	-	o/w	300

II.3) Smart or sensitive drug delivery systems

As shown above, drug delivery systems are usually based on amphiphilic copolymers. Since several years, scientists took interest to introduce sensitive part in the copolymer chain to reach DDS that are sensitive to internal or external stimulations. These DDS were called smart or intelligent drug delivery systems (Smart DDS). After formulation, the encapsulated drug is released according this stimulation, when and where doctors want. There are different types of smart drug delivery systems and their classification depends on the type of stimulation, as shown in Figure 8.

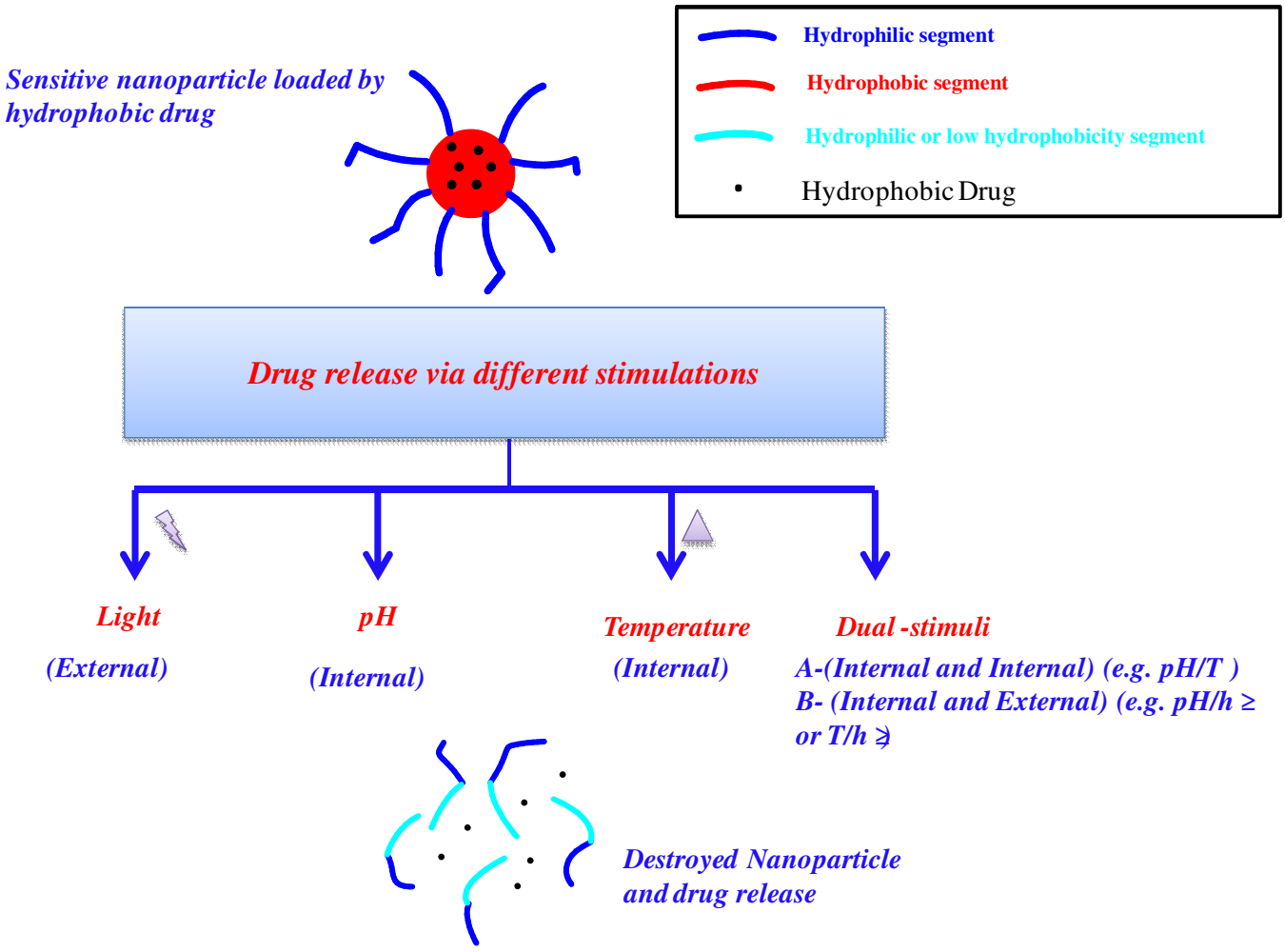

Figure 11. Schematic representation of major stimulation methods for drug release

II.3.1) pH-sensitive DDS

This type of DDS is based on amphiphilic copolymers, whose one block at least is sensitive to the pH. This block undergoes a hydrophilic- hydrophobic shift depending on the pH of environment. Consequently, the self assembly of these amphilic copolymers will be destroyed by changing the pH because amphilic copolymers became water-soluble. To illustrate that, Du et. al. fabricated pH-sensitive DDS from triblock copolymers that are composed of hydrophilic poly[2-(methacryloyloxy)ethyl phosphorylcholine] (PMPC) block and hydrophobic poly[2-(diisopropylamino)ethyl methacrylate (PDPA) and poly[2-(dimethylamino)ethyl methacrylate] (PDMA) ones (Figure 9) [42]. This copolymer is amphiphilic at pH > 6.2 but completely water soluble at pH< 5. Indeed, PMPC and PDPA have tertiary amine groups that are protonated at pH佒. Consequently, at pH<5, this amphiphilic copolymers become soluble in water. Therefore, smart DDS produced by self-assembly of this copolymer will be destroyed into infected cell (tumor) due to the inner acidic pH inside cells, leading to the drug release as shown in Figure 9.

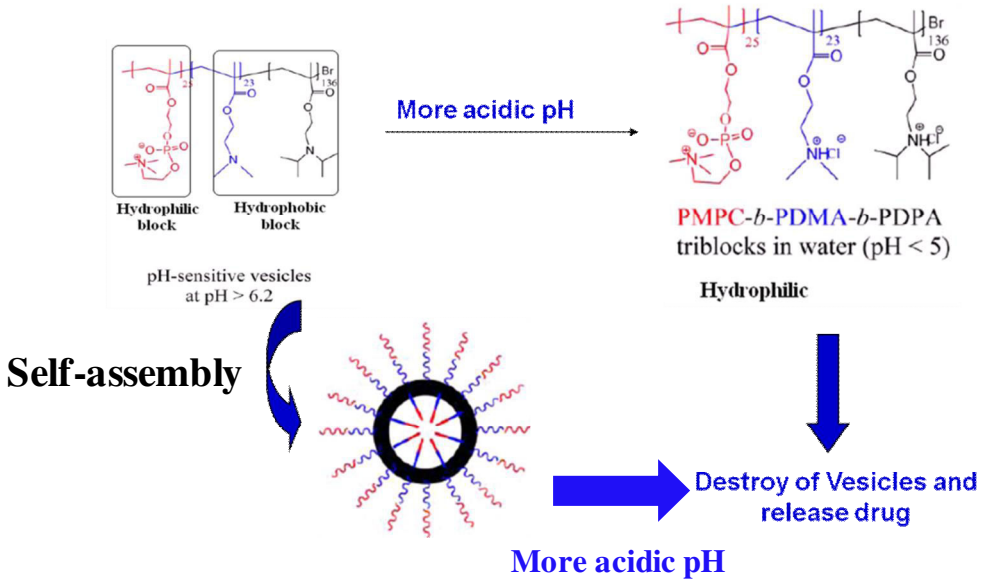

Figure 12. pH sensitive based DDS based on PMPC-b- PDMA-b-PDPA [42].

Another pH-sensitive DDS were fabricated by Zhang et. al., which used copolymer based on acetalated dextran as hydrophobic pH-sensitive block and an poly(ethylene glycol) (PEG) [43]. This copolymer is amphiphilic in basic or neutral media (pH = 6.0-6.5) as the protected dextran is

hydrophobic and self-assembles to give micelle-like structures. These DDS are destroyed in acidic medium (pH= 4.5 -5.5) as acetal groups are cleaved at acidic pH. Scheme 1 describes how hydrophobic acetalated dextran is transferred into hydrophilic dextran.

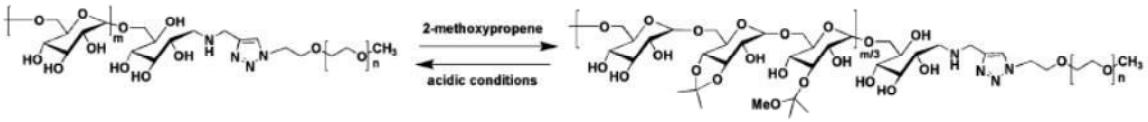

Scheme 1. Effect of acidic pH on acetalated dextran [43].

As shown in Figure 10, Doxorubicin (Dox) was encapsulated into these PEG-b-acetalated dextran based DDS. After endocytosis by tumoral cells, DDS are destroyed due to the more acidic inner pH than normal or early cells and drug is released into the cell cytoplasm.

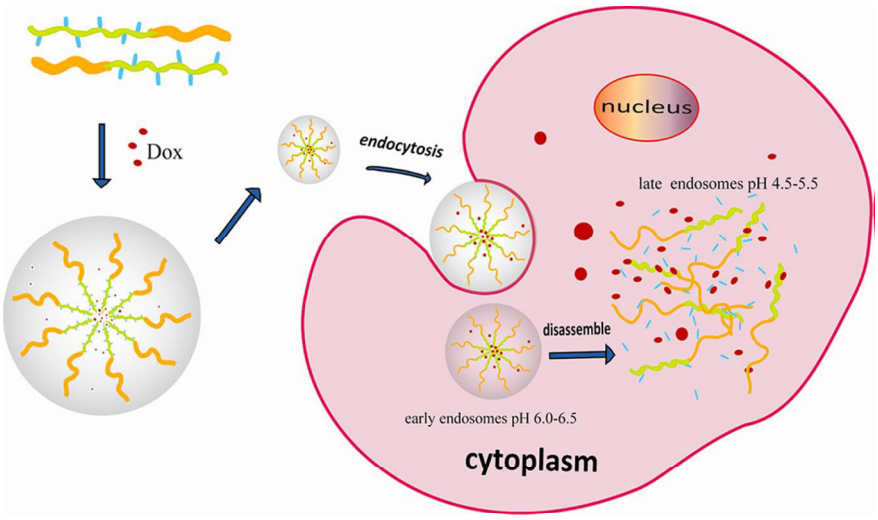

Figure 13. Schematic illustration of DOX loading and intracellular release from DOX-loaded smart DDS [43].

Many studies were done about pH-sensitive nano-objects, which may be used as drug delivery systems as shown in Table 5. As above written, the pH-sensitive drug delivery systems are very selective and effective in tumor curing because `infected cells present more acidic inner pH than healthy cells_. This property enhances the selectivity of drug release.

Table 5. Some examples of pH-sensitive copolymers

Amphiphilic Copolymers	Morphology	Refs
Heparin-g-poly(侑caprolactone)	Nanoparticle	[44]
poly(ethylene glycol)-b-poly(-caprolactone)	Micelle-like structure	[45]
[P(MMA-*co*-MAA)-*b*-PPEGMA]	Micelle-like structure	[46]
Poly(L-histidine)-b-PEG/poly(L-lactide)-b-PEG	Micelle-like structure	[47]
Cholesteryl-bearing Carboxymethylcellulose	Micelle-like structure	[48]
PEG-b-PtNEA where PtNEA = poly(trans-N-(2-ethoxy-1,3- dioxan-5-yl)acrylamide) (PtNEA)	Micelle-like structure	[49]
PEG-b-PMYM where PMYM = polymethacrylamide derivative (PMYM)-bearing orthoester side chains	Micelle-like structure	[50]
poly(N-vinylpyrrolidone)-block-poly(styrene-alt-maleic anhydride) (PVP-b-PSMA)	Micelle-like structure	[51]
urocanyl and cholesterol succinyl modified pullulan	Nanoparticle	[52]

II.3.2) Thermosensitive DDS

Thermosensitive nano-objects are based on amphiphilic copolymers having one thermosensitive part at least. Thermosensitive behavior of these nano-objects must often depends on lower critical solution temperature (LCST) of this particular part. LCST is defined as the critical temperature at which polymer solution undergoes phase separation from one phase (isotropic state) to two phases (anisotropic state) wherein the polymer is no more soluble [53]. Wei et. al. obtained thermosensitive biotinylated diblock copolymers (biotin-PEG-*b*-P(NIPAAm-*co*-HMAAm)) [54],

where LCST is equal to 36.7 °C. P(NIPAAm-*co*-HMAAm) block become hydrophobic (insoluble) at temperature higher than LCST (=36.7 °C) and then will constitute the DDS core when the PEG block becomes the shell of the micelle-like structure. At temperature lower than LCST, P(NIPAAm-*co*-HMAAm) becomes completely miscible in water that leads to reversibly destroy the DDS, as shown in the Figure 11.

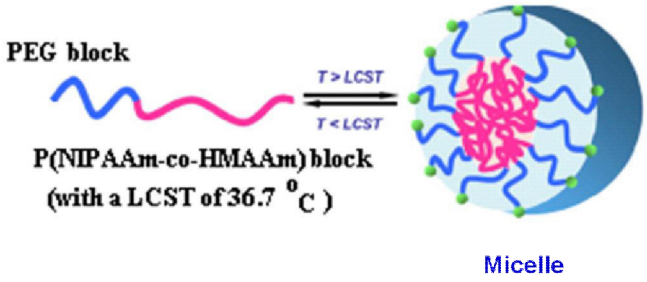

Figure 14. Thermosensitive PEG-b- P(NIPAAm-*co*-HMAAm) copolymer behavior [54].

Tan et. al. obtained thermosensitive grafted copolymer (called DgP) based on dextran as backbone (hydrophilic segment) and an poly(N-isopropylacrylamide) (PNIPAAm) thermosensitive grafts, as shown in Figure 12 [55]. PNIPAAm is a common thermosensitive polymer used as its LCST is approximately 32 °C [56]. The authors found that this copolymer forms loose aggregates of unimers in aqueous solution below the LCST, while compact nanoparticles appear above the LCST, because of the phase transition of the PNIPAAm grafts. When they tried to load indomethacin (IMC, Figure 12, b) into these nano-objects, they observed that uniform nanoparticles were formed even below the PNIPAAm LCST.

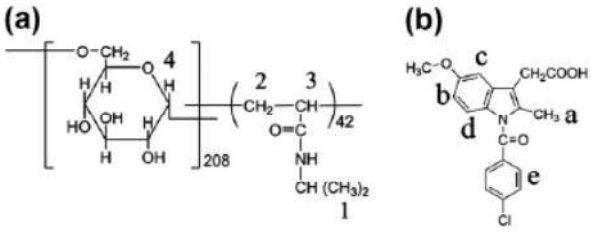

Figure 15. Chemical structures of a) (Dex-g- PNIPAAm) and b) Indomethacine (IMC) [55].

The authors explained that by the formation of hydrogen bonding between IMC and the PNIPAAm side chains as the driving force for the aggregation as shown in Figure 13. The IMC release rate increases with the temperature because of the dissociation of the hydrogen bonds.

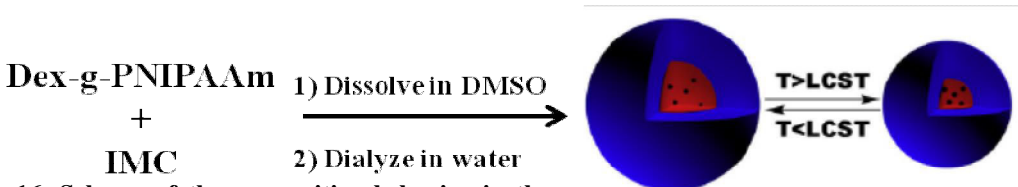

Figure 16. Scheme of thermosensitive behavior in the presence of IMC (blue shell: dextran, red core: PNIPAAm; black dot: IMC) [55].

Some other different thermosensitive amphiphilic copolymers were studied, as shown in Table 6.

Table 6. Some examples of thermosensitive copolymers

Amphiphilic Copolymers	Morphology	Refs
cholesteryl-modified hydroxypropyl cellulose	Micelle-like structure	[57]
PEG-b- (polyacrylate of PNIPAAm)	Micelle-like structure	[58]
PEG-b- poly(*N*-(*N*-Boc-ethylenediamine)methacryloylglycylglycylamide))	Micelle-like structure	[59]
poly(*N*-isopropylacrylamide)-*b*-poly(-caprolactone) and poly(ethylene glycol)-*b*-poly(-caprolactone)	Mixed nanoparticles	[60]
(PEG:CPP:SA) terpolymer composed of poly(ethylene glycol) (PEG), 1,3-bis(carboxyphenoxy) propane (CPP) and sebacic acid (SA)	Micelle-like structure	[61]
poly(N-vinylcaprolactam)-b-poly(ε-caprolactone)	Micelle-like structure	[62]
poly(*N*-isopropylacrylamide)-*b*-poly(*D,L*-lactide)	Micelle-like structure	[63]
PNIPAAm-b-PPG-b-PNIPAAm	vesicle	[64]

II.3.3) Light sensitive DDS

This is another type of sensitive copolymers that can be used to obtain smart DDS. These copolymers include photosensitive part. Photosensitive group shows definite response when exposure to light and this response depends on the nature of photosensitive group. Recently, scientists focused on this DDS type because all the body may be exposed to a controlled light, that it˘s not the case with pH and thermo sensitive DDS (internal stimulations). Photosensitive DDS are classified into four types and this classification is based on their photoinduced structural changes [65]: a) Shifting the hydrophilic-hydrophobic balance of the amphiphilic block copolymers, b) Breaking the junction between the two blocks c) Main degradation of the DDS

and d) Reversible cross-linking of the DDS core, as shown in Figure 14. In this section, we will talk about each type of photo-responsive DDS in details.

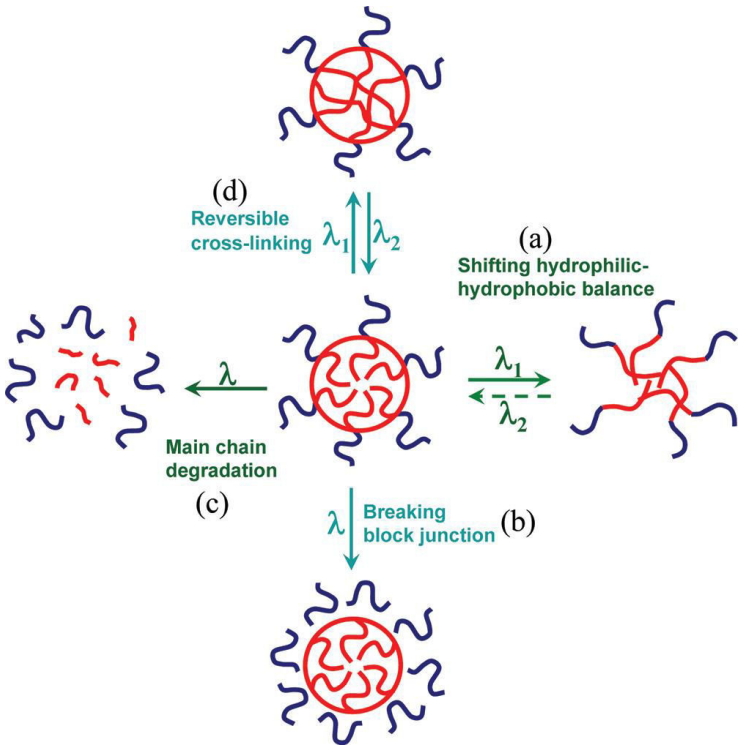

Figure 17. Schematic illustration of various types of light responsive DDS [65].

II.3.3.a) Shifting the hydrophilic-hydrophobic balance

To observe this behavior, the used amphiphilic copolymers have to possess photochromic moieties into their hydrophobic block. By exposing the DDS to light, the polarity of the hydrophobic block significantly increases or simply converts it into hydrophilic ones. Consequently, the hydrophobic block is no longer hydrophobic enough to retain the micellar association and the disassembly happens. This design strategy can be further divided into two types of photoreactions leading to reversible or irreversible disassembly.

I.3.3.a.1) Reversible shifting hydrophilic-hydrophobic balance

The reversible photoinduced shifting of the hydrophilicБhydrophobic balance occurs without the removal of photochromic moieties as shown in Figure 15.

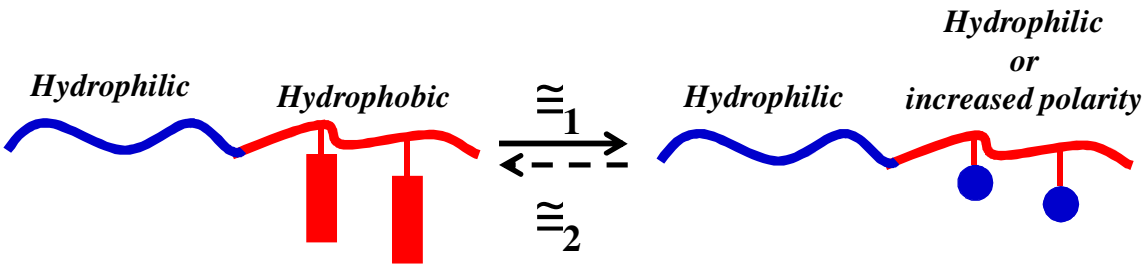

Figure 18. Schematic illustration of photoinduced shifting of the hydrophilicБhydrophobic balance of copolymer without removal of photochromic moieties [65].

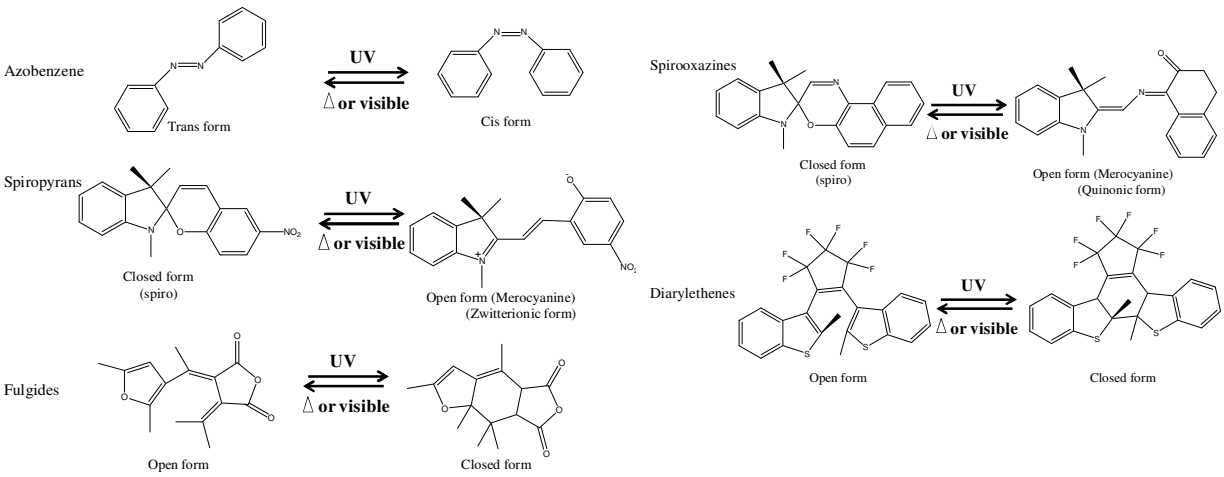

Figure 19. Families of photochromic compounds commonly used in polymeric sensitive systems [66]

To observe this reversible behavior, block copolymers must have photosensitive groups that exhibit reversible behavior when exposure to light. Some examples of such photosensitive groups are azobenzene, spiropyran, diarylethene, fulgides and spirooxazoine as shown in Figure 16 [66].

Tong et al. synthesized amphiphilic azobenzene-based block copolymers P(tBA-co-AA)-b-PAzoMA), as shown in Figure 17 [67]. The hydrophobized block is based on polymethacrylate containing azobenzene as side-chain liquid crystalline polymer (PAzoMA), while the hydrophilic block is poly(tert-butyl acrylate-co-acrylic acid) as shown in Figure 17, A. Azobenzene groups adopt `trans_ form under visible light but, when exposed to UV- irradiation, they immediately convert to `cis_ form. This isomerization modifies the polarity of copolymer leading to the

disassembly of the micelle-like structure. Indeed, the dipole moment of trans isomer equal to zero, while cis isomer exhibits dipole moment approximately equal to 4.4 D due to bend structure formed as shown in Figure 17. B.

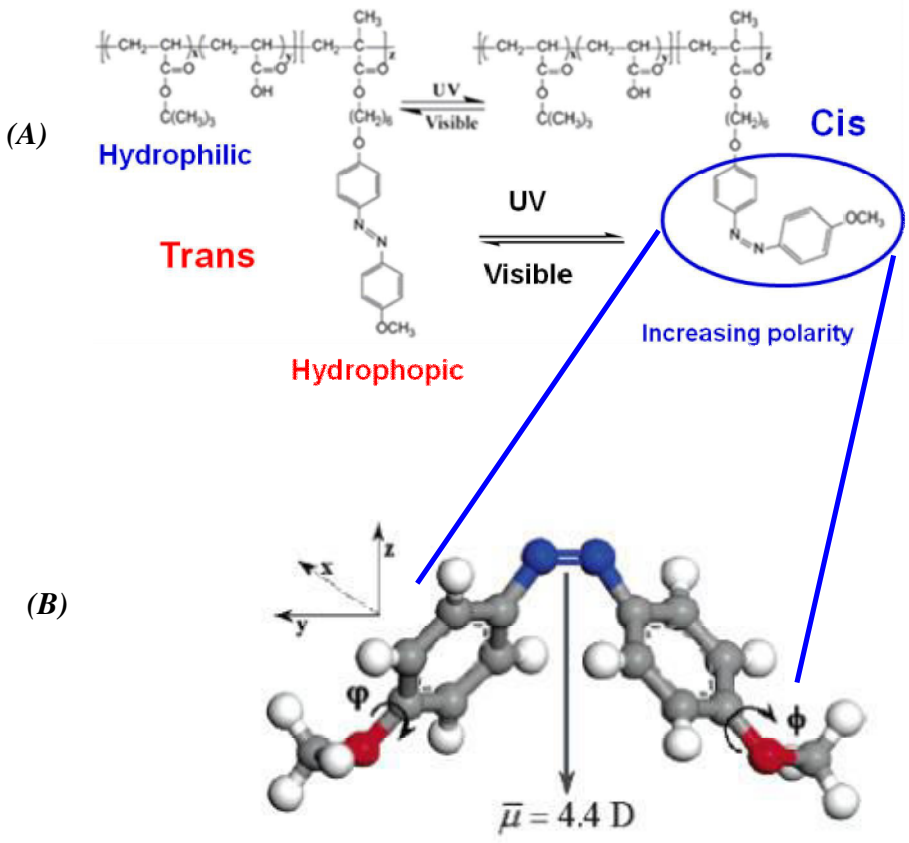

Figure 20. A) Chemical structure of diblock copolymer P(tBA-co-AA)-b-PAzoMA) and B) resulting dipole moment of 4,4-dimethoxyazobenzene in the cis form (N blue, O red, C gray, H white). (⍰ is the dipole moment) [67].

Several other copolymers based on azobenzene, spiropyran or diarylethane have been used to produce such light sensitive DDS. Some of these copolymers have been grouped in Table 7.

Table 7. Some examples of photoinduced reversible shifting of the hydrophilic-hydrophobic balance

Photochromic	Structure	Ref
Spiropyran	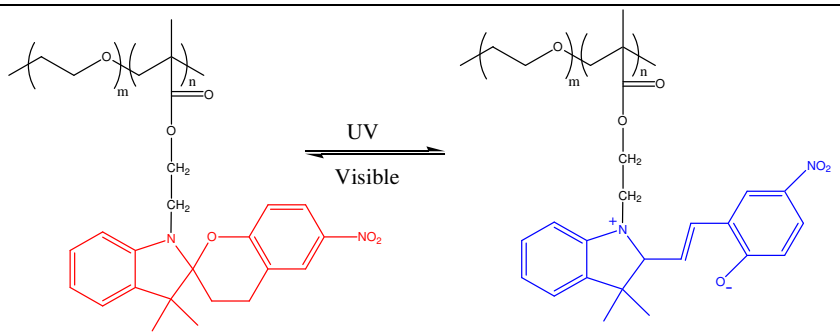	[68]
Diarylethene	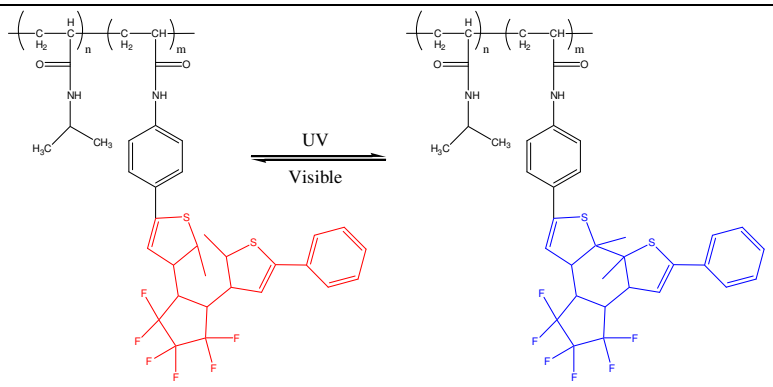	[69]
Azobenzene	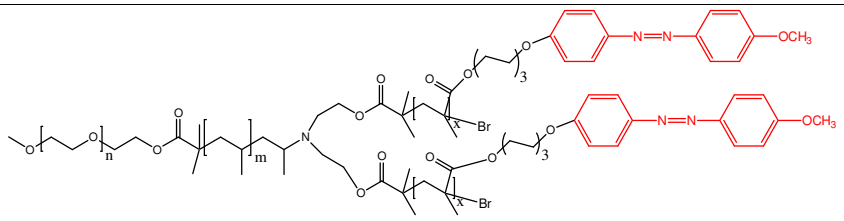	[70]

II.3.3.a.2) Irreversible shifting hydrophilic hydrophobic balance

Irreversible shifting of the hydrophilic-hydrophobic balance of amphiphilic copolymers undergoes via hydrophobic photochromic moieties that are completely removed from the copolymer as shown in Figure 18, A. To realize this irreversible shifting, copolymers must be have several very good photolabile groups like the common chromophores: pyrene, o-nitrobenzyl, and coumarin groups. Main concept of such design is based on hydrophobic blocks possessing an aryl methylester group linked to the chain backbone. In all cases, the irradiation cleaves the photochromic moieties and converts the initial hydrophobic block into a hydrophilic one by producing carboxylic acid functions in hydrophilic block. Nevertheless, there is some differences in photoreactions undergone by each photochromic group. Pyrene undergoes a photosolvolysis reaction requiring the presence of water or a protonic solvent [71]. While o-nitrobenzyl group undergoes an intramolecular rearrangement reaction that don't need the presence of water [72]. O-nitrobenzyl and coumarin groups are commonly used because they can be activated by near-infrared (NIR) light through two-photons absorption, that is very favorable in biomedical applications [73, 74]. For instance, Theato et. al. reported that o-nitrobenzyl group enables to make different designs as shown in Figure 18, B [75].

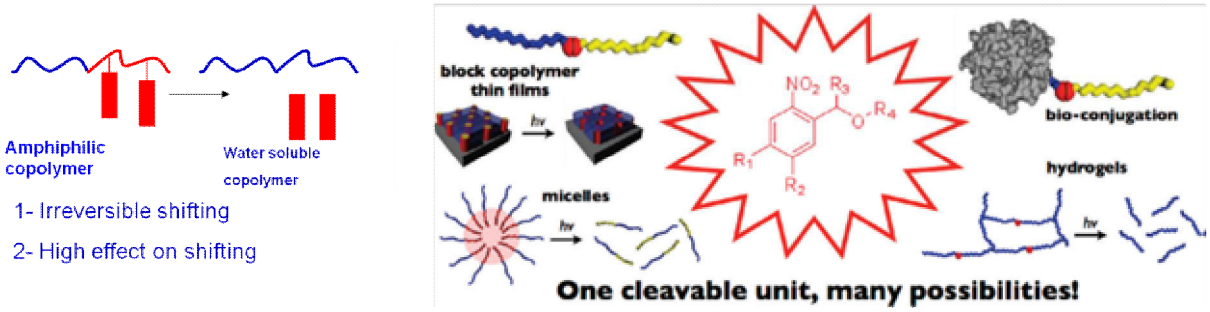

Figure 21. A) Schematic illustration of irreversible photoinduced shifting of the hydrophilicЬhydrophobic balance B) Different designs using o-nitrobenzyl moieties (in red) [75].

Because an o-nitrobenzyl-based acrylate has been studied in this thesis, we will focus from this point the bibliography on copolymers containing o-nitrobenzyl groups.

Gu et. al. prepared near-infrared light-breakable amphiphilic chitosan (N-succinyl-N˘-4-(2-nitrobenzyloxy)-succinyl-chitosan) as shown in Figure 19 [76]. Then, authors used dialysis method to obtain N-succinyl-N˘-4-(2-nitrobenzyloxy)-succinyl-chitosan-based micelle-like structure. To investigate the NIR-induced drugs release profiles from these DDS, fluorescein and cypate have been used as hydrophobic drug models and were encapsulated during dialysis. For instance, micelles loaded by the cypate were Near IR irradiated as shown in Figure 20, A at different excitation wavelengths and excitation powers. They observed that fluorescent intensity of cypate decreased under NIR light irradiation. These results indicate the release of cypate from the inner core of micelles into hydrophilic (water) environment because the hydrophobic o-nitrobenzyl groups are photo-cleaved (Figure 20 A). This release occurs with the micelle-destruction as hydrophobic blocks convert to hydrophilic blocks carrying carboxylic groups as shown in Figure 20, B.

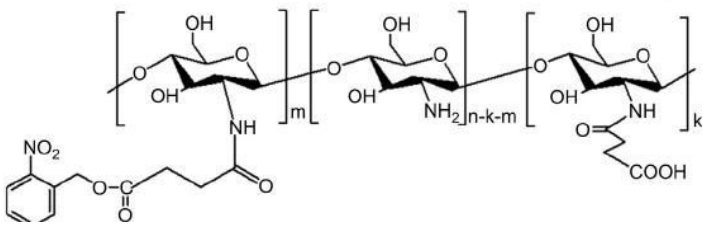

Figure 23. Chemical structure of N-succinyl-N˘-4-(2-nitrobenzyloxy)-succinyl-chitosan [76]

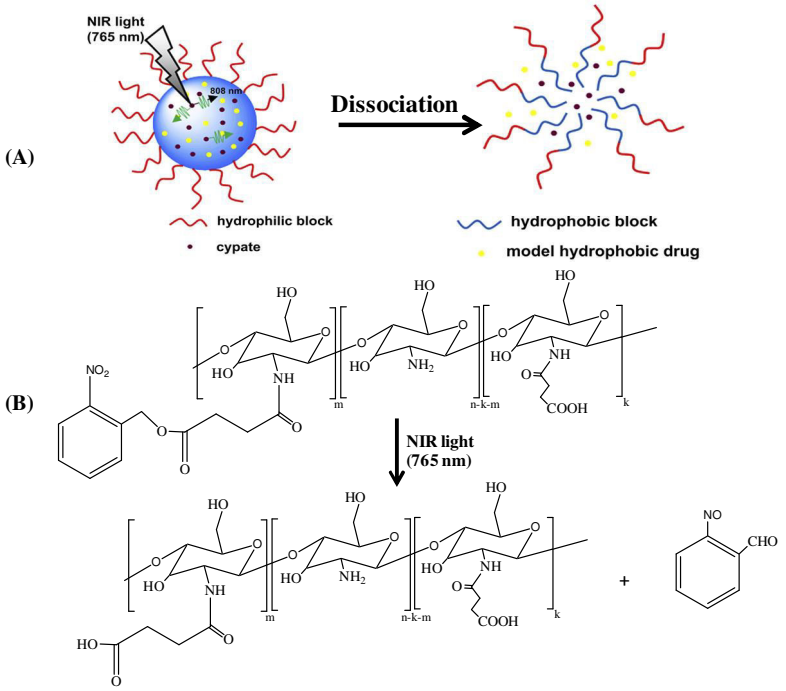

Figure 22. (A) Schematic illustration of using NIR light excitation to trigger dissociation of DDS and (B) NIR light-triggered photoreaction [76].

The dissociation time of micelles could be accelerated depending the NIR light, while the content of cypate remaining in the micelles depends on the wavelength. For instance, after 1 h illumination, the cypate contents in the micelles decreased by about 85.6%, 74.1% and 29.5% with excitation of 765 nm, 808 nm and 980 nm, respectively. The authors also studied the effect of different powers with fixed wavelength (765 nm) on the kinetic of cypate- loaded micelle degradation, as shown in Figure 21 B. For instance after 10 min of irradiation 20, 36 and 50% of cypate were released with power equal to 400, 800 and 1200 mW, respectively.

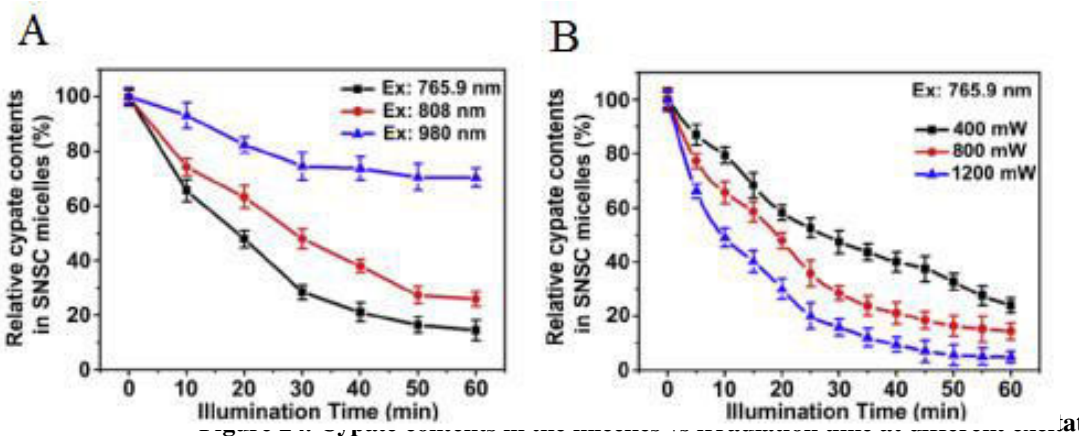

ation wavelength (A) different excitation power at 765 nm (B) [76].

During this photo-cleavage 2-nitrosobenzaldehyde was also released under irradiation. This photoreaction occurs through a free radical mechanism as shown in Scheme 2 [75]

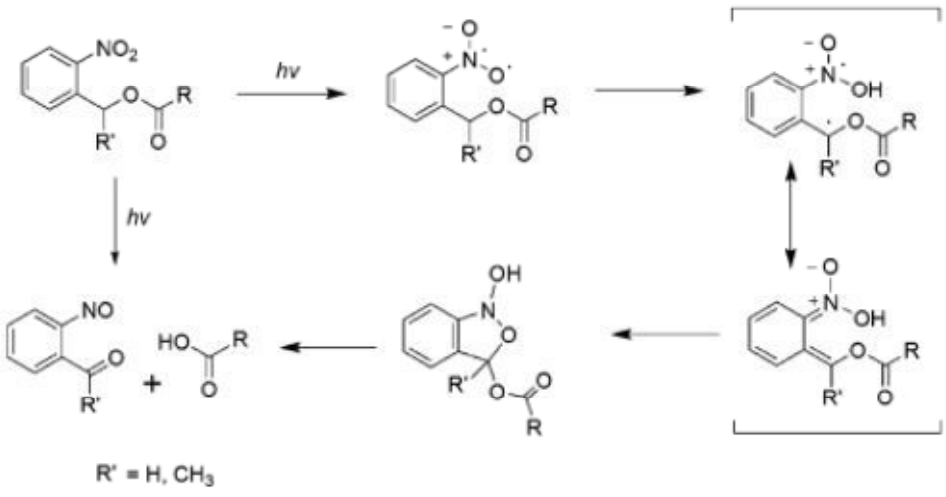

Scheme 2. Photoisomerization mechanism of o-nitrobenzyl Alcohol derivatives into an o-nitrosobenzaldehyde [75].

Gohy et. al. formulated light sensitive micelles that are based on poly(2-nitrobenzyl acrylate-random-acrylic acid)-block-polystyrene (P(NBA-r-AA)-b-PS) [77]. This block copolymer was synthesized through many steps 1) ATRP of tert-butyl acrylate, 2) PtBA-Br was used as macroinitiator in ATRP of styrene and 3) complete hydrolysis of butyl acrylate units to acrylic acid. 4) Post modification of poly(acrylic acid)-block-polystyrene by o-nitrobenzyl bromide in the presence of non-nucleophilic base, as shown in Figure 22.

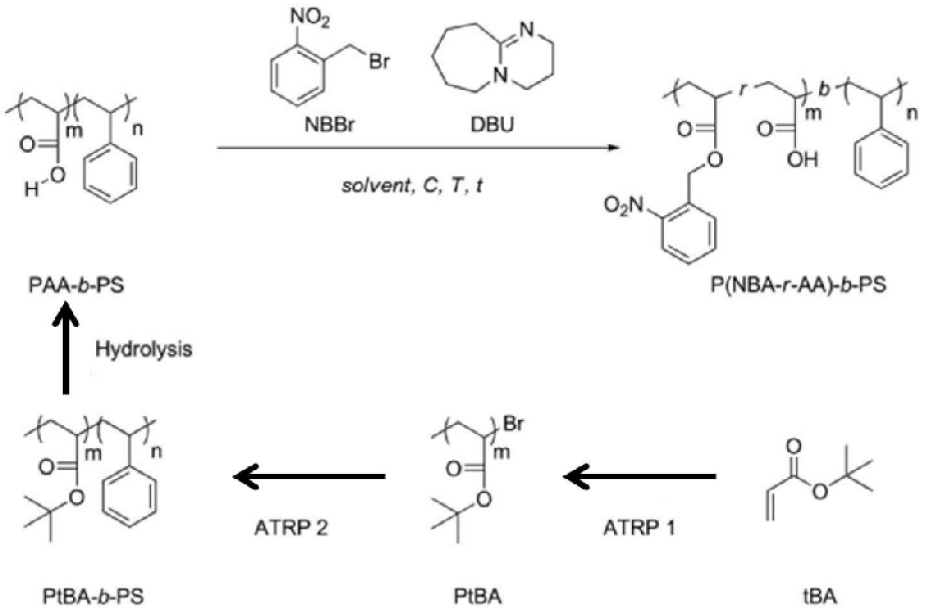

Figure 25. Synthesis of P(NBA-r-AA)-b-PS block copolymers [77].

Micelles and thin films based on PAA-b-PS were photo-induced in one selective solvent for PS block. In aqueous phase, the hydrophobic-hydrophilic shift leads to the micelle destruction because the fraction of hydrophobic block decreases and become not enough to stabilize the micelle. In this present case, self-assembly of copolymer occurred by irradiation in THF, which is a nonsolvent for PAA. Consequently, PAA core/ PS shell micelle like structures are produced, as shown in Figure 23.

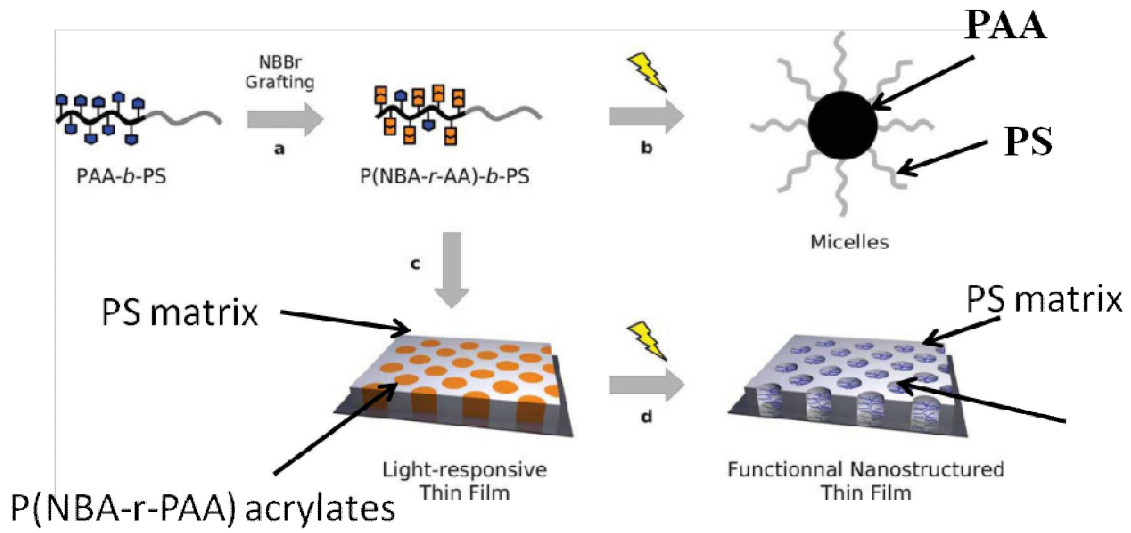

Figure 26. Schematic representation of the synthesis, self-assembly and light-responsive behavior of P(NBA-r-AA)-b-PS photocleavable block copolymers: (a) grafting of 2-nitrobenzyl bromide (NBBr) on a PAA-b-PS precursor, (b) light-induced micellization in a selective solvent of PS, (c) self-assembly in thin film with a cylindrical morphology, and (d) light exposure leading to functional and nanostructured thin films [77].

Many other light sensitive nano-objects were fabricated, which include different chromogroups. We present some examples of these copolymers in Table 8.

II.3.3.b) Breaking block junction (Figure 14-b)

In this case, one photosensitive group acts as linker between hydrophobic and hydrophilic blocks. The link is broken by exposure to irradiation that leads to separate the two blocks as shown in Figure 24. There are two types of breaking junction (reversible and irreversible). The most popular irreversible photocleavable junction is o-nitrobenzyl-based moiety. Other photochromic moieties including truxillic acid derivatives [78] and inclusion complex of azobenzene with cyclodextrin [79] have also been investigated as reversible photocleavable linkages.

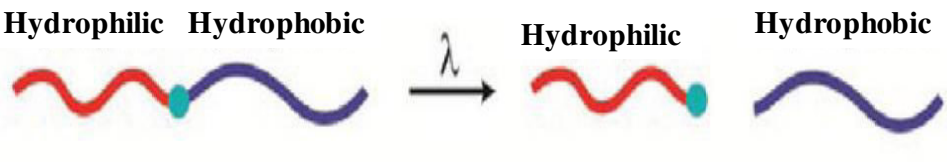

Figure 27. Schematic illustration of photoinduced breaking of the junction between the hydrophilic and hydrophobic blocks [65].

Table 8. Some examples of copolymers having different chromophore moieties like o-nitrobenzyl groups, pyrene and Coumarin.

Chromophores	Copolymers structure	Morphology	Ref
O-Nitrobenzyl	poly(N-isopropylacrylamide-co-2-nitrobenzylacrylate ester) 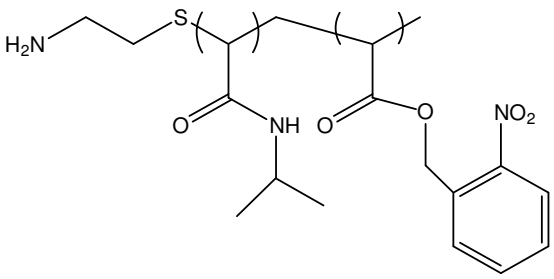	Nanoparticle	[80]
	poly(dimethoxynitrobenzyl acrylate)-block-polystyrene 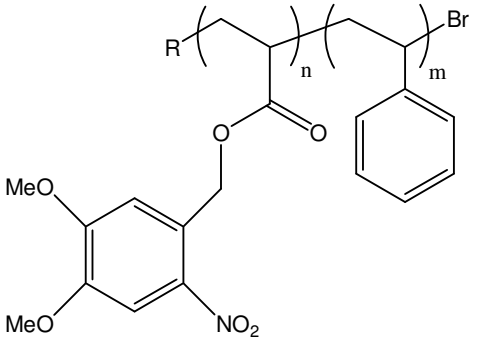	Micelle-like structure	[81]
	PEO-b-PNBM Poly(nitrobenzyl methacrylate)= PNBM 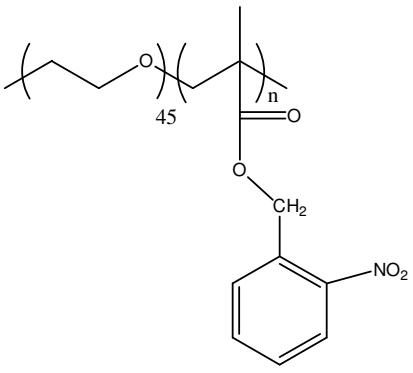	Micelle-like structure	[82]

Pyrene	4-oxo-4-(pyren-4-ylmethoxy) butanoic acid and chitosan hydrochloride complex 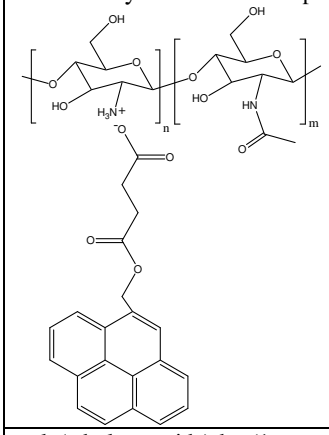	Nanoparticle	[83]
	poly(ethylene oxide)-b-p(1-pyrenemethyl Methacrylate) 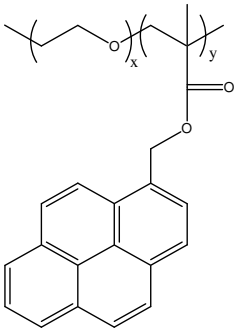	Micelle-like structure	[84]
Coumarin	poly(ethylene oxide) ¯b- poly- ([7-(diethylamino)coumarin-4-yl]methyl methacrylate) 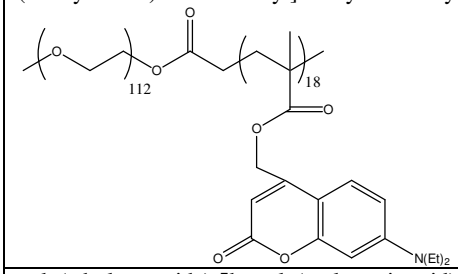	Micelle-like structure	[85]
	poly(ethylene oxide) ¯b- poly(L-glutamic acid) bearing a number of 6-bromo-7-hydroxycoumarin-4-ylmethyl groups 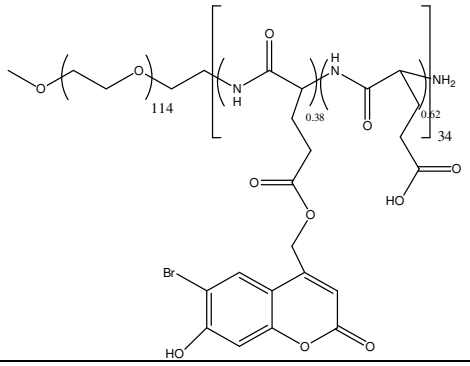	Micelle-like structure	[86]

II.3.3.b.1) Irreversible Breaking Junction

Moon et. al. prepared photosensitive thin films based on PS-b-PEO copolymers [87]. These two blocks were linked via one o-nitrobenzyl group (ONB) light sensitive group. The authors studied the effect of UV irradiation on the block copolymers by exposing the copolymer solution to UV light. Similarly that above written, o-nitrobenzyl group as linker is converted to o-nitrosobenzaldehyde and carboxylic acid after irradiation (***Scheme 2)***. The authors suppose the effect of UV irradiation as shown in Figure 25.

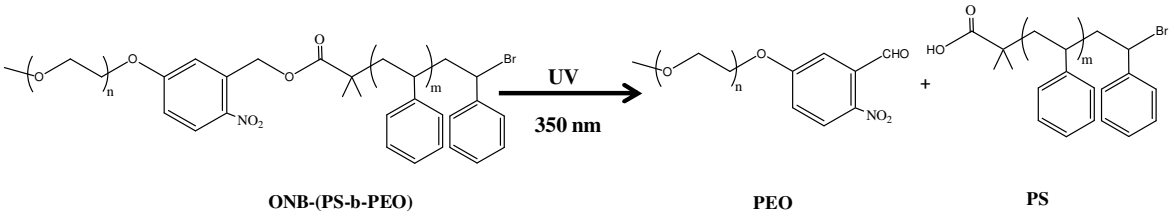

Figure 28. Effect of UV irradiation on block copolymer (polystyrene-b-poly(ethylene oxide)) [87].

After UV, PEO block was removed by precipitation and irradiated product was characterized by Size Exclusion Chromatography in THF as eluent. They observed that intensity of block copolymer peak (high molecular weight) was decreasing with increasing time of irradiation. In the same time, new peak appeared indicating polystyrene block (low molecular weight) formation as shown in Figure 26.

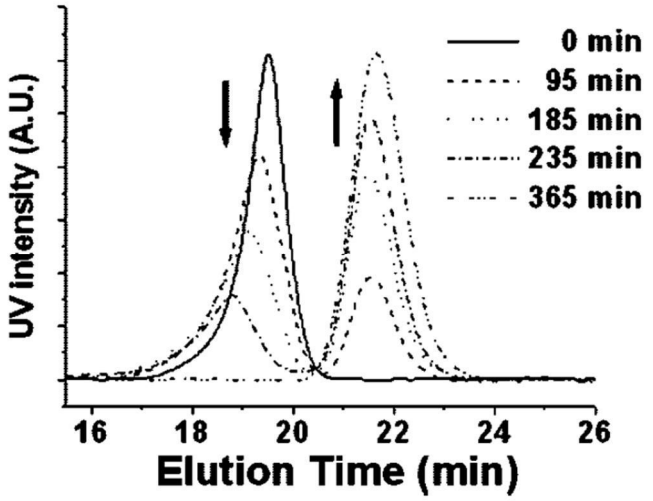

Figure 29. Monitoring of the photocleavage reaction of ONB-(PS-b-PEO) (23.7-b-5.0 K) in THF by SEC [87].

Some examples of breaking block junctions are represented as shown in Table 9.

Table 9. Some examples of irreversible breaking block junction block copolymers

Copolymer	Structure	Ref
PmCL¯ONB¯ PAA Poly(methyl caprolactone)	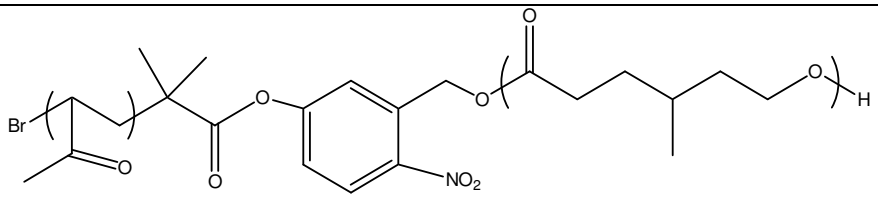	[88]
poly(ethylene glycol)-b-poly(acrylate), bearing truxillic acid derivative linkage	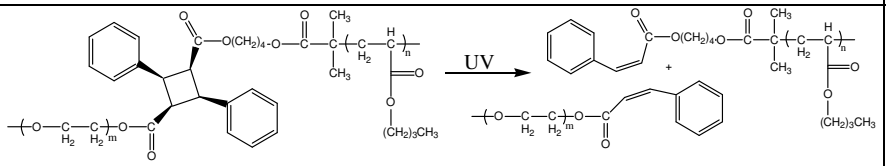	[78]
PEO-b-PS	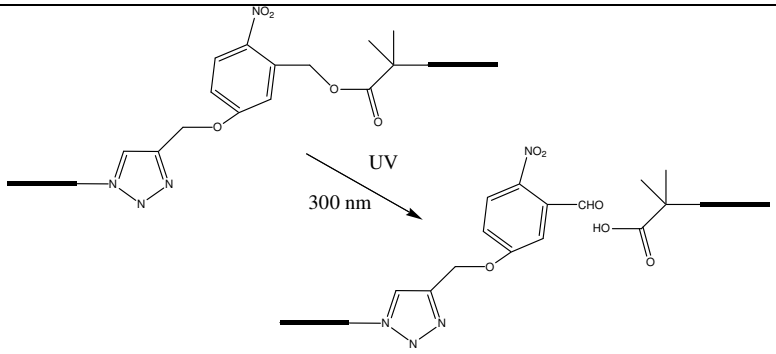	[89]
PCL-b-PEG	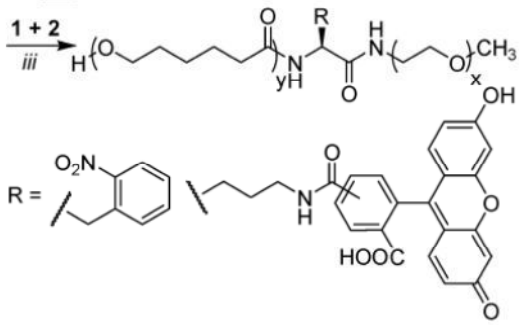	[90]

II.3.3.b.2) Reversible Breaking block junction

Yuan et. al. studied the breaking of block junction based on azobenzene/cyclodextrin (inclusion complex) as shown in Figure 27 [79]. In this study, the two blocks of the copolymer are not linked by chemical bond but by an inclusion complex. Inclusion complex is attained when one compound (host) forms a cavity in which other molecules of a second compound (guest) are located.

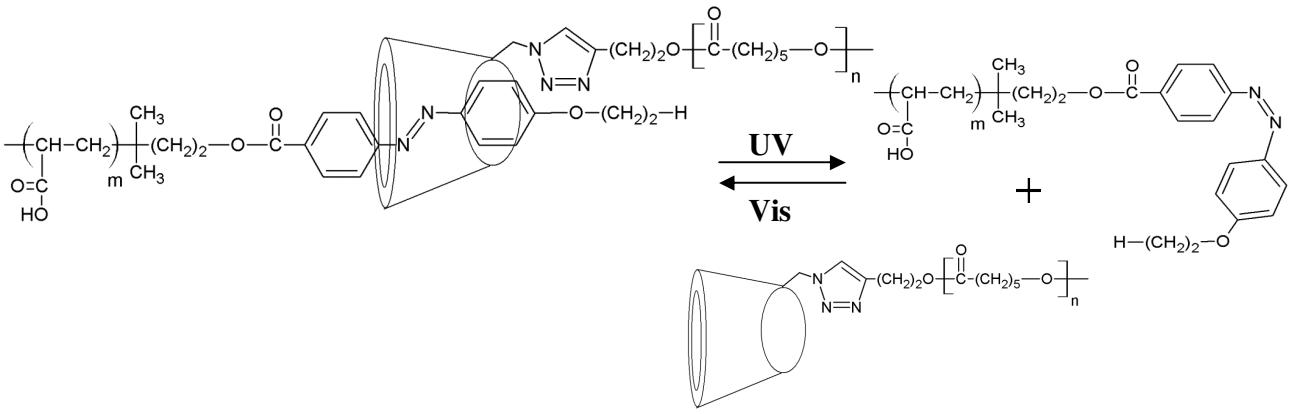

Figure 30. Inclusion complex of azobenzene and cyclodextrin [79].

As shown in Figure 27, cyclodextrin carrying PEG-block acts as a host compound for azobenzene molecule in `*trans*_ form located at the extremity of the second block. After irradiation, trans-cis azobenzene isomerization undergoes and azobenzene adopts `*cis*_ form. Thus, the inclusion complex is broken because the bent cis isomer of azobenzene. Consequently, azobenzene is released from the cyclodextrin cavity, while the junction can be formed again upon visible light irradiation that induces the reverse cisБtrans isomerization of azobenzene.

II.3.3.c) Main degradation (Figure 14-c)

Design of this type of photo-responsive copolymers is based on photobreakable junction that was inserted repeatedly into the main hydrophobic block as shown in the Figure 28, a. After copolymer exposure to UV irradiation, the hydrophobic block was irreversibly converted to low molecular weight species, leading to the destruction of the smart DDS.

Zhao et. al. demonstrated the difference between breaking block junction and main degradation against UV irradiation as shown in Figure 28 b, c, respectively [91]

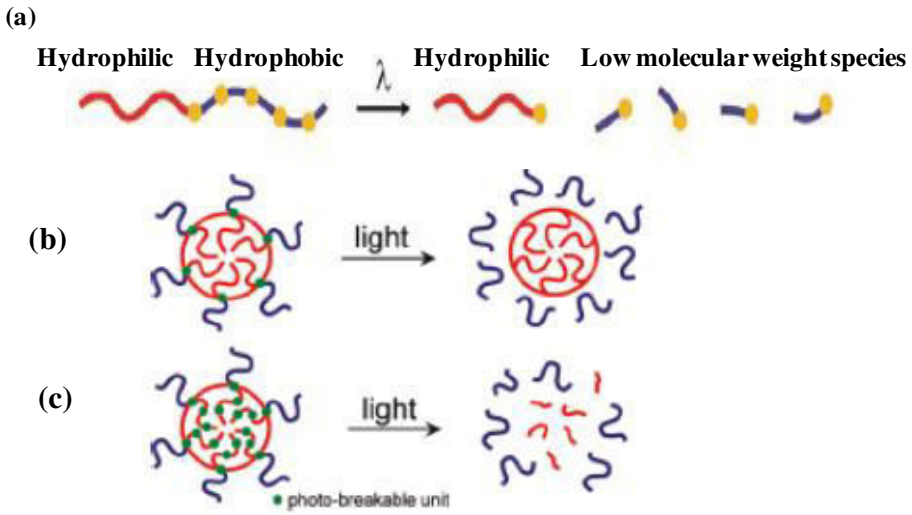

Figure 31. (a) Schematic illustration of photoinduced main chain degradation. Schematic illustration of the difference between placing (b) a photobreakable unit at only the block junction and (c) repeatedly on the hydrophobic block [65].

They fabricated photodegradable micelles based on PEO-b-PUNB-b-PEO, where PUNB is a hydrophobic polyurethane containing several nitrobenzyl groups as monomer units, as shown in Figure 29 [91]

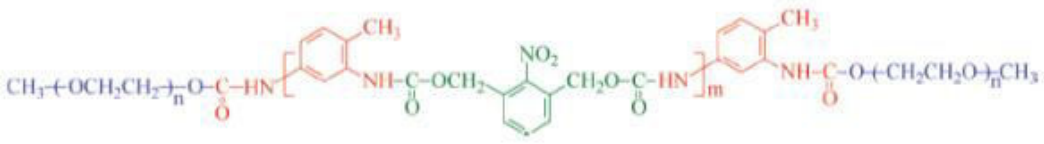

Figure 32. Chemical structure of PEO-b-PUNB-b-PEO triblock copolymer [91].

This triblock copolymer was exposed to irradiation leading to all o-nitrobenzyl groups cleavage. Consequently, the inner hydrophobic block of the self-assembly converts to low molecular weight species and leads to the destruction of the DDS. The authors proofed this destruction by using hydrophobic drug models like Nile red dye. They followed the destruction of the DDS by Nile Red fluorescence intensity against time of irradiation. Size Exclusion Chromatography was also used. Authors observed after applying UV irradiation that peak characteristic to high molecular weight disappears, while a new peak indicated on low PEO molecular weight appeared.

In another article, Zhao et. al. fabricated other micelles based on PEO-b-poly(disulfide-alt-nitrobenzene)-b-PEO, as shown in Figure 30 [92]. In this case, o-nitrobenzyl group was repeated into main chain. The degradation of the inner hydrophobic block was followed by SEC during light exposure.

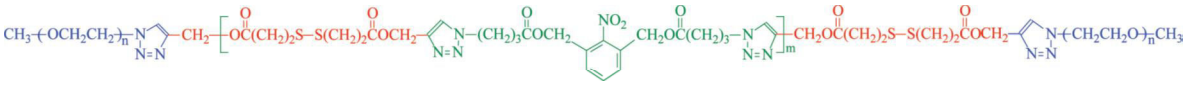

Figure 33. Chemical structure of triblock copolymer PEO-b-poly(disulfide-alt-nitrobenzene)-b-PEO [92].

II.3.3.d) Reversible cross-linking (Figure 14-d)

To increase the stability of polymeric micelle-like structures while prolonging the encapsulation time after injection in the body, scientists supported structure of micelles by chemically cross-linking core or shell [93, 94]. Unfortunately, a more stable drug encapsulation may render its release more difficult. To overcome that, development of reversible photocontrolable crosslinking has been studied.

This type of photosensitive micelle is based on copolymers carrying photosensitive groups that can undergo dimerization through cycloaddition under visible light. In an opposite way, cleavage of formed linkage occurs under UV irradiation as shown in Figure 31. The most used reversible photo-cross-linking reaction is the photodimerization through cycloaddition of coumarin groups under UV light at > 310 nm. The subsequent cleavage of obtained cyclobutane bridges occurs under UV light at < 260 nm [95].

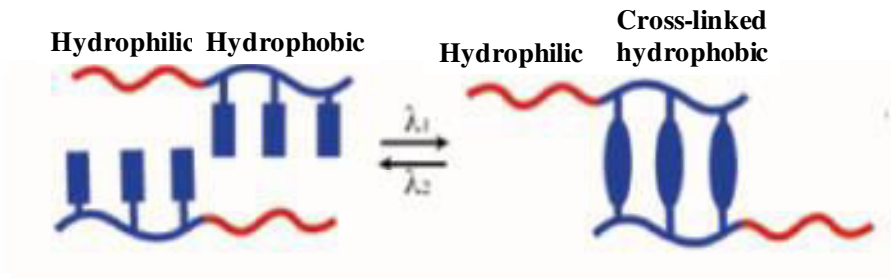

Figure 34. Schematic illustration of reversible photoinduced cross-linking and de-cross-linking of block copolymers using a reversible photoreaction at two different wavelengths [65].

Zhao et. al. synthesized diblock copolymer composed by poly(ethylene oxide) (PEO) as the hydrophilic block and poly(coumarin methacrylate-random-methyl methacrylate) as hydrophobic block, as shown in Figure 32 [96]. At visible light >310 nm, coumarin groups undergo cycloaddition and form cross-linking between several copolymer chains. This cross-linking was broken using wavelength less than 260 nm, as shown in Figure 32.

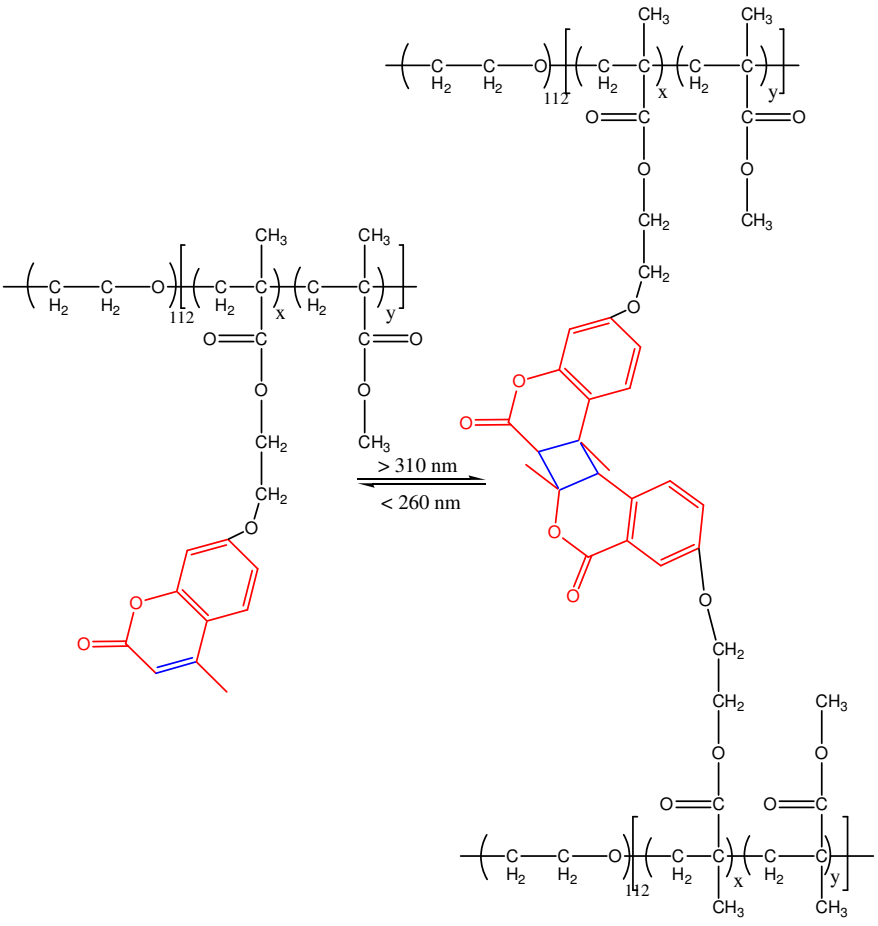

Figure 35. Chemical structure of the diblock copolymers and photodimerization/photocleavage of coumarin side groups [96].

Several other copolymers carrying coumarins acting as reversible photocontrolable crosslinkers are resumed in Table 10.

Table 10. Some examples of reversible cross-linking copolymer based on coumarin moieties

Copolymer	Structure	Ref
(PEO-b-P(MEOMA-co-CMA)), where poly[2-(2-methoxyethoxy) ethyl methacrylate-co-4-methyl-[7-(methacryloyl)oxyethyloxy]coumarin]	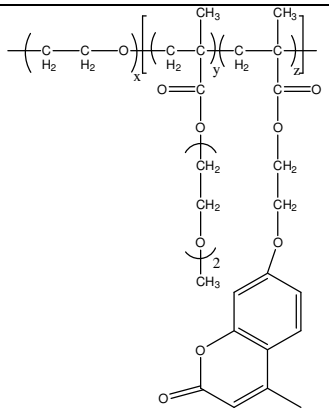	[97]
Poly(2-(N,N˘-dimethyamine)ethyl methacrylate-co-coumarin methacrylate)-b- Poly(N-isopropyl acrylamide) P(DMAEMA-co-CMA)-b-PNIPAM	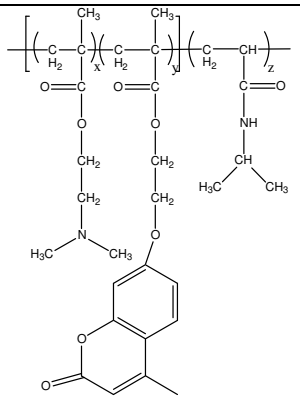	[97]
Poly(vinyl-coumarin-b-2-acrylamido-2-methyl-1-propanesulfonic acid)	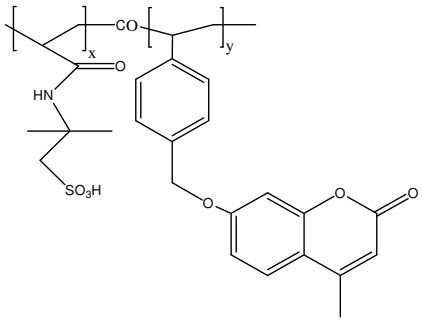	[98]
Poly((methoxyethoxyethylvinyl ether)-b-(4-methyl-7-(2-vinyloxyethoxy) coumarin))	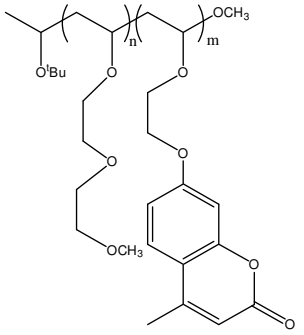	[99]

II.3.4) Dual-Stimuli responsive DDS

Recently, sensitive DDS were developed to be dual or multi responsive. This means that micelle-like structure are sensitive in same time to internal stimulation like pH, temperature redox medium, ŭ etc. and external stimulation like light, ultrasound, ŭ etc., for instance.

The final part of this first bibliographic chapter is devoted to these dual/multi- responsive DDS. As we can show in Table 11, some examples of copolymers form micelles were sensitive for pH and temperature of the environment [100].

Table 11. Some examples of pH/Thermo sensitive nanocarriers [100]

Stimuli	Copolymers
pH/Thermo	P(NIPAAm-co-DMAAm-co-UA) P(NIPAAm-co-DMAAm-co-UA)-g-cholesterol P(NIPAAm-co-AA)-b-PCL mPEG-b-P(HPMA-Lac-co-His), mPEG-b-PLA and cy5.5-PEG-PLA mixed micelles PLA-g-P(NIPAAm-co-MAA) P(NIPAAm-co-DMAAm)-b-PCL/PLA PNIPAAm and PAA hollow nanogels Polyaminoester-based dendrimer Poly(ionic liquid-co-NIPAAm) with deoxycholic acid ionically mPEG-g-P(AA-co-MEA)-g-PNIPAAm

For instance, Yang and co. synthesized tercopolymers (P(NIPAAm-co-DMAAm-co-UA) based on N-isopropylacrylamide, dimethylacrylamide (DMAAm) and 10-undecenoic acid (UA), in which UA was used as hydrophobic pH-sensitive units when DMAAm was employed to ajust the LCST of the copolymer [101].

II.3.4.a) Photo- and pH-Responsive Micelles

Yan et. al. fabricated pH and light dual responsive micelles that can be used as anticancer DDS [102]. These micelles are based on hydrophobized chitosan, which was obtained by grafting hydrophobic o-Nitrobenzyl Succinate (NBSC) onto the hydrophilic glycolized Chitosan (GC).

This hydrophobized chitosan produces micelle-like structures encapsulating comptotheain (CPT, anticancer drug). The cross-linking of the chitosan shell was carried out with glutaraldehyde by reaction with the free NH_2 functions, leading to imine linkages between several chitosan chains. Consequently, micelles exhibit photosensitive groups (o-nitrobenzyl groups) and pH sensitive imine linkers as shown in the Figure 33.

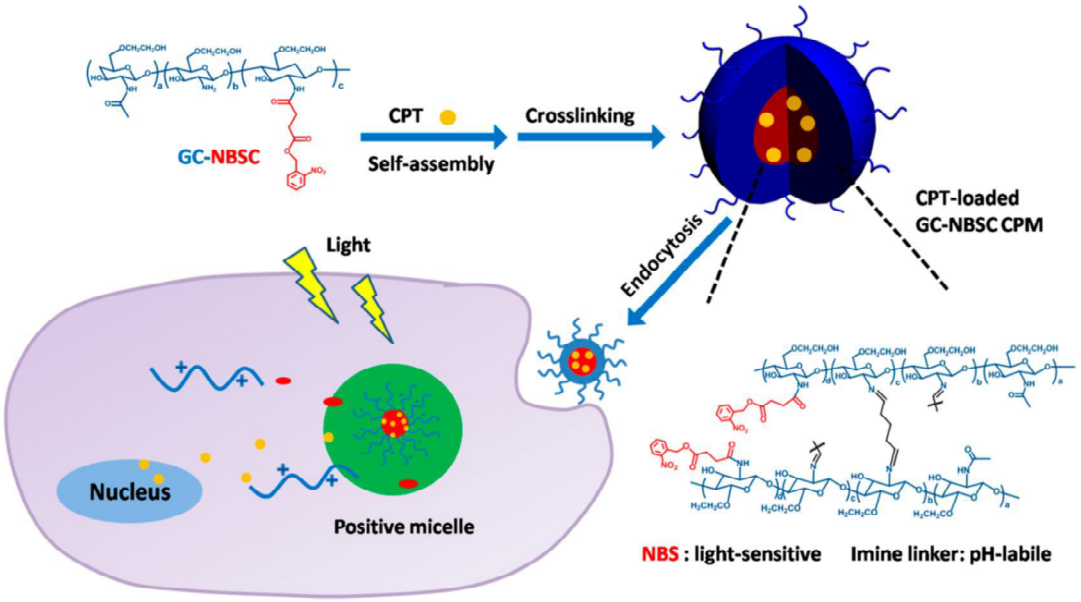

Figure 36. Preparation of CPT-loaded chitosan-based micelles and intracellular drug release triggered by pH and UV Light [102].

The advantage of pH sensitive moieties is to be very selective for infected cells that exhibit a more acidic medium than healthy cells. In the same time, light enhances the destroying of micelles leading to the fast release of the drug. Other examples of copolymers forming micelles that are pH and light dual sensitive are shown in Table 12.

Table 12. Some examples of pH/light-sensitive nanocarriers

Stimuli	Copolymers	Ref
pH/h ≥	poly(ethylene oxide)-b-poly(2-(diethylamino) ethyl methacrylate-co-6-(4-phenylazo phenoxy)hexyl methacrylate)	[103]
	poly(ethylene oxide) and polymethacrylate with photochromic azopyridine	[104, 105]

II.3.4.b) Photo- and Thermo-Responsive Micelles

Blasco et. al. synthesized dual thermo- and photo-responsive micelles based on miktoarm star polymers, as shown in Figure 34 [106]. These star polymers are composed of an `azopolymer_ (azobenzene-derivative polymethacrylate, photosensitive group) and three identical arms of poly(N,N-diethylacrylamide) (PDEAA) featuring thermo-responsive properties.

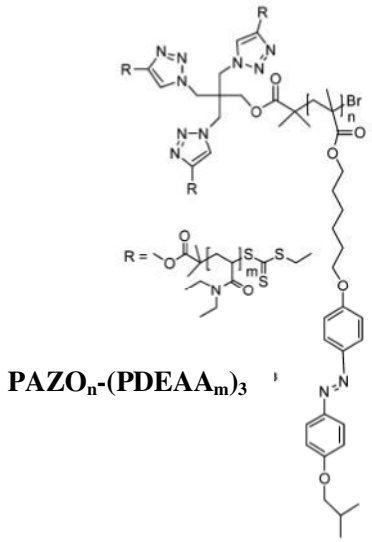

$PAZO_n$-$(PDEAA_m)_3$

Figure 37. Chemical structure of miktoarm star polymers [106].

During the self-assembly of such miktoarm star polymers, the authors encapsulated hydrophobic Nile Red as drug model to study the effect of temperature and light for instance. At 40 °C, they observed that the fluorescence intensity of Nile red increased. That indicates the collapse of copolymers in micelles and that Nile Red was loaded into their hydrophobic core (Figure 35, b). At temperature less than the low critical solution temperature of PDEAA block (LCST equal to 20 °C) authors observed the decrease of Nile Red fluorescence intensity according to the decrease of hydrophobicity around Nile Red dye (Figure 35, a). On another hand, the decrease of Nile Red fluorescence intensity was also observed after UV irradiation. This indicates that the environment of the probe becomes more hydrophilic due to the micelles destruction (Figure 35, c).

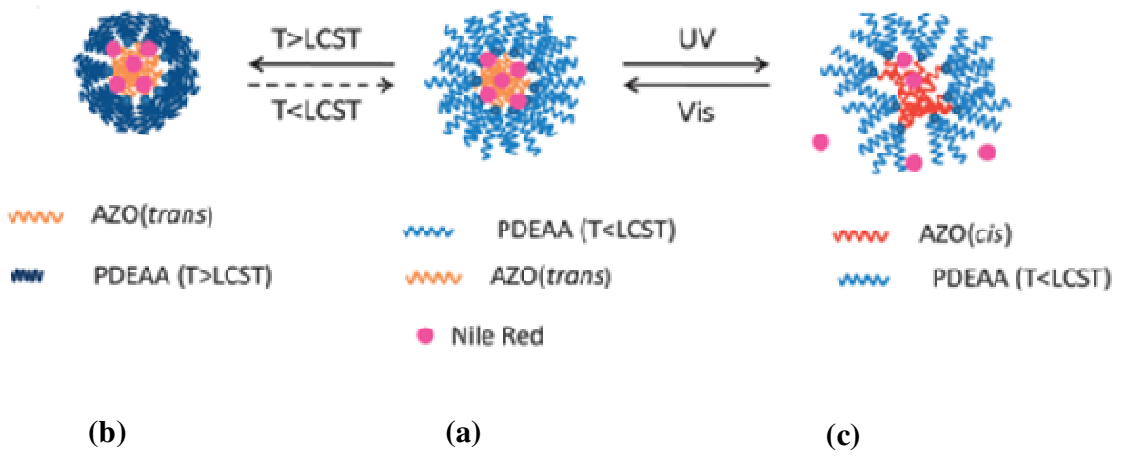

Figure 38. Schematic representation of the proposed thermo- and photo-induced Nile Red release [106].

As shown in Table 13, we presented some other examples of micelles based on thermo and light sensitive copolymers

Table 13. Some examples of Thermo/light-sensitive nanocarriers

Stimuli	Copolymers	Ref
Thermo/ h ≥	triblock copolymer containing azobenzene (AZO) and N-isopropylacrylamide (NIPAM)	[107]
	poly(4˘-(6-(4-vinylbenzyloxy)hexyloxy)-2-(4-methoxyl) azobenzene)-b-Poly(*N*-isopropylacrylamide)	[108]

II.3.4.c) Multi-Responsive Micelle

At the moment, multi-responsive micelles that are reported in literature are based on amphiphilic copolymers containing pH-sensitive groups. Some copolymers contain also thermosensitive and photosensitive groups. Recently, Yuan et. al. fabricated multi-response micelles that are based on poly(2-(N,N-dimethylamino)ethylmethacrylate)-b-poly{6-[4-(4-pyridyazo)phenoxy] hexylmethacrylate} copolymers [109]. Poly(2-(N,N-dimethylamino)ethyl methacrylate) (PDMAEMA) block is both pH and temperature sensitive as it exhibits a lower critical solution temperature (LCST) in the range of 32˘ 46 °C and has a pKa of 7.0˘7.8, depending on its molar

mass. The other block based on azopyridine group acts as photosensitive block as azopridine undergoes trans¯cis photoisomerization in response to UV and visible light (Figure 36).

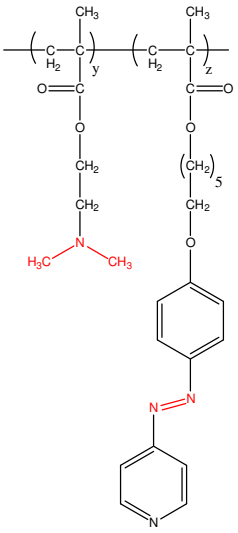

Figure 39. Chemical structure of multi-responsive copolymer poly(2-(N,N-dimethylamino)ethylmethacrylate)-b-poly{6-[4-(4-pyridyazo)phenoxy]hexylmethacrylate} [109].

II.4) Conclusion

As exposed in the first part of bibliography, different types of sensitive nano-objects could be used as drug delivery systems. In the present thesis, we focused on the fabrication of photosensitive nanoparticles that can be used as drug delivery systems, because of its high controllable release of encapsulated drug that depends on one external stimulation: the light. These light sensitive DDS differ to pH and thermo-sensitive ones, which depend on internal stimulations. Light sensitive nanoparticles may be useful for encapsulation of many hydrophobic drugs like anticancer drugs for instance. Moreover, photosensitive nanoparticles can be administrated into body via parenteral route. Through the results and discussion part of this manuscript, we will try to study and cover areas required for the fabrication of such smart DDS such as the nanoparticles formation and characterization and the study of encapsulation then release of hydrophobic fluorescence probe with irradiation.

As indicated in the introduction of this bibliography chapter, the second part is devoted to Reversible-Deactivation Radical Polymerization.

III) Reversible-Deactivation Radical Polymerization techniques

Conventional free radical polymerization (RP) is one technique used to polymerize vinyl monomers. This polymerization is one of the chain-growth polymerizations and is very efficient for synthesizing numerous numbers of polymers. Consequently, `United States polymer sales are over $250 billion (~2% of gross domestic product)_, half of this is based on copolymers prepared by radical polymerization . As all the chain-growth polymerizations, RP is consisting of three steps: 1) Initiation, 2) Propagation, and 3) Termination. Unfortunately, side reactions called transfer also occurred during the process. Firstly, initiators form radicals by homolytical cleavage that is induced by temperature, light,ŭ .etc. Each radical reacts with the double bond of olefin, then propagation step occurs and many monomer units inserted in the growing radical chain. Due to their high reactivity, as the same time, active radical chains convert to dead chains through two mechanisms as 1) chains coupling or 2) disproportionation. Moreover, the radical center could be transferred to another molecule. Consequently, transfer produces dead chains and new radical that can initiate a new propagation step. Conventional free radical polymerization has many drawbacks as it gives uncontrolled high molecular weight polymer with a high value of dispersity (Đ), without controlled end functionality, so the chain extension is impossible. At the end of twentieth century, researchers studied how to better control such RP. The main idea was to decrease the radical active species concentration in the medium in order to promote propagation ($R_p = k_p[RM_{•}][M]$) *versus* termination ($R_t = k_t[RM_{•}]^2$). On the first hand, the use of initiators that produce very slowly radicals didn˘t allow to control chains length. On contrary, higher dispersity than that observed in RP was obtained. On the second hand, other people thought than increasing the radical life can lead to the control of RP. To reach that, the Controlled Radical Polymerization (CRP) concept appeared in 90˘s. This polymerization is now recommended to be called `Reversible-Deactivation Radical Polymerization (RDRP) by IUPAC, since 2010. RDRP concept exhibits a slightly different mechanism than conventional RP. Otsu was the first to describe RDRP concept taking advantage of reversible dissociation of dithiocarbamate [110, 111]. Then Solomon developed the reversible deactivaton of growing chain by using a persistant radical [112]. Georges applied it to polymerize styrene in a controlled way [113]. RDRP mechanism is based on a dynamic equilibrium between dormant species that are activated (with a rate constant k_{act}) thermally, via photolysis or with an appropriate catalyst to form the radical growing centers (active species). Active species will react with monomer (propagation step) but will deactivated

into dormant species. Due to this equilibrium, dormant species are in majority (deactivation step is predominant than activation one) as shown in Figure 37. Consequently, the active species concentration is lower than in case of RP, and termination steps are limited.

Moreover, if this equilibrium is as fast as propagation step, a good control of [illegible] and 仔 is obtained. Dynamic equilibrium was established by one of two processes 1) reversible

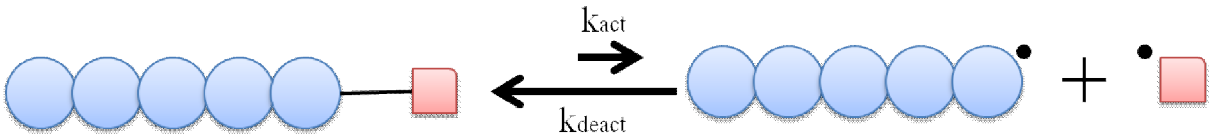

Figure 40. ***Dynamic activation/deactivation process equilibrium***

deactivation/activation process or 2) degenerative exchange process (where the transfer agent plays role of dormant specie) that is established using thiocarbonylthio compounds for instance (polymerization known as Reversible-Addition Fragmentation chain Transfer (RAFT)). Reversible deactivation/activation process can be established using nitroxide agent (polymerization known as Nitroxide Mediated radical Polymerization (NMP)) or a halogen (polymerization known as Atom Transfer Living Radical Polymerization (ATRP)).

III.1) Reversible-Addition Fragmentation chain Transfer (RAFT)

RAFT polymerization is mediated by thiocarbonylthio compounds as transfer agents and these compounds play an important role in the control of reversible deactivation radical polymerization. RAFT polymerization is different from the other controlled radical polymerizations in the initiation step, as RAFT polymerization is initiated with initiator used in conventional RP. The common initiators used are azoïque derivatives like azobisisobutyronitrile (ABIN) [114] and 2,2˘-azobis(2-methylbutyronitrile) (AMBN) [115].

In the first step, initiator creates radicals that react with monomer and the propagation step occurs. The dynamic equilibrium is established with a thiocarbonylthio agent as shown in Scheme 3. This agent reacts with growing chain reversibly leading to an intermediate (k_{add}) that can either give back the growing chain (k_{-add}) or produce dormant species and a new radical [illegible]·. The [illegible]· can then re-initiate the polymerization by reacting with the monomer and starts a new polymer chain, which will propagate (k_p) as shown in Scheme 3 [116].

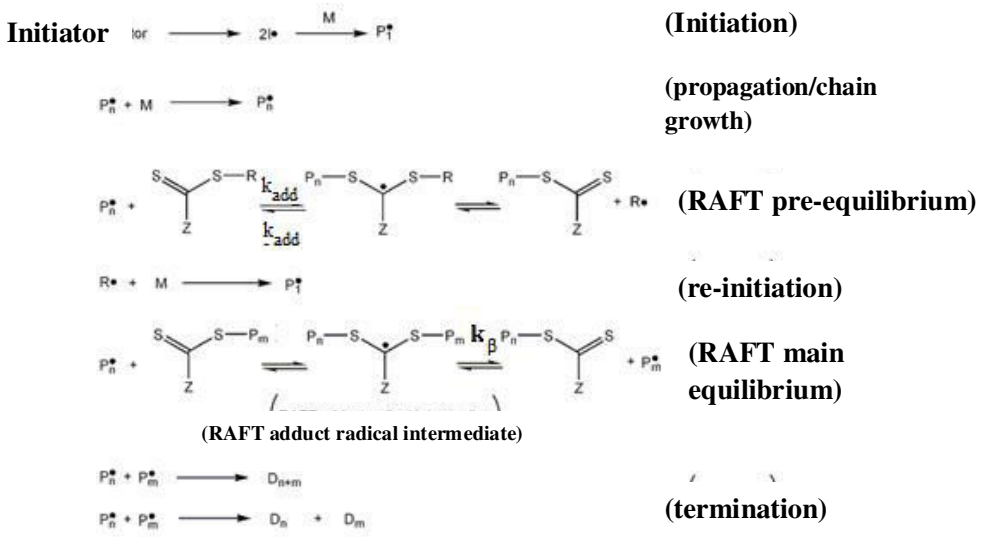

Scheme 3. Mechanism of RAFT [116].

The key for controlling the RAFT polymerization is to choose an efficient and suitable chain transfer agent (CTA) that depends on the monomer. The efficiency of the chain transfer agent depends on its R and Z groups. Perrier et. al. reported the order of R and Z groups due to the capacity of R group to act as leaving group and Z group to generate more stable intermediate as shown in the Figure 38 [116]. The authors used different vinyl monomers in this study as methyl mathacrylate, vinylacetate, acrylamide and styrene. MADIX (macomolecular design by Interchange of Xanthates) polymerization is called when the chain transfer agent is one xanthates [117].

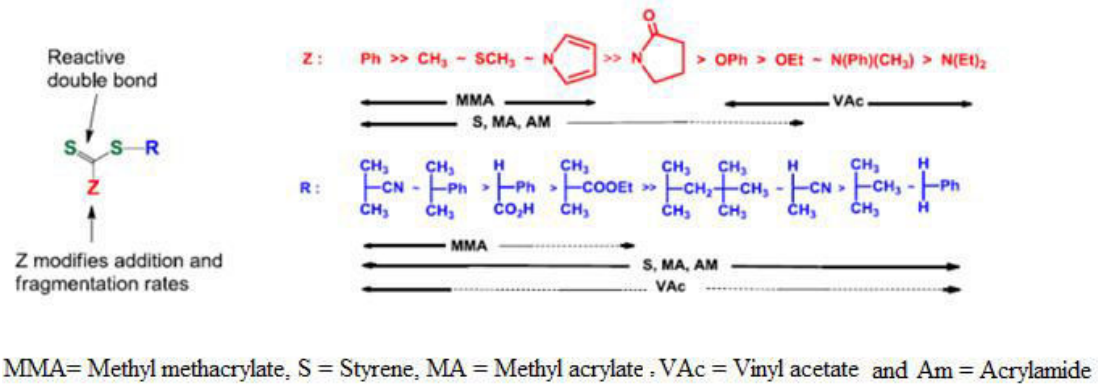

Figure 41. ***CTA classification for various monomers [116].***

The equilibrium between dormant and active species is characterized by the chain transfer constant (k_{tr}), according to following equation (1) [118]:

$$k_{tr} = k_{add}\left[{}^{k_\beta}\!/\!_{\left(k_{\ add} + k_\beta\right)}\right] \qquad \textbf{Equation (1)}$$

Where, $k_{add}, k_{\ add}$ *and* k_β *are the rate constants of the addition of the growth chain to the transfer agent, of the reverse reaction and of the intermediate scission into dormant species, respectively.*

There are many advantages of RAFT polymerization. RAFT can be used to polymerize monomers having polar group (e.g. hydroxyl, amine ŭ .. etc.) and ionic group without pre-protection. In addition, we can produce polymers with specific architectures such as block, gradient, statistical, comb, brush, star, hyperbranched and network copolymers. Some examples of monomers were already polymerized using RAFT (Figure 39). In the following pages, as this thesis will talk about photosensitive poly(nitrobenzyl acrylate), we will show examples of RAFT of acrylates and, if published, of o-nitrobenzyl (meth)acrylate.

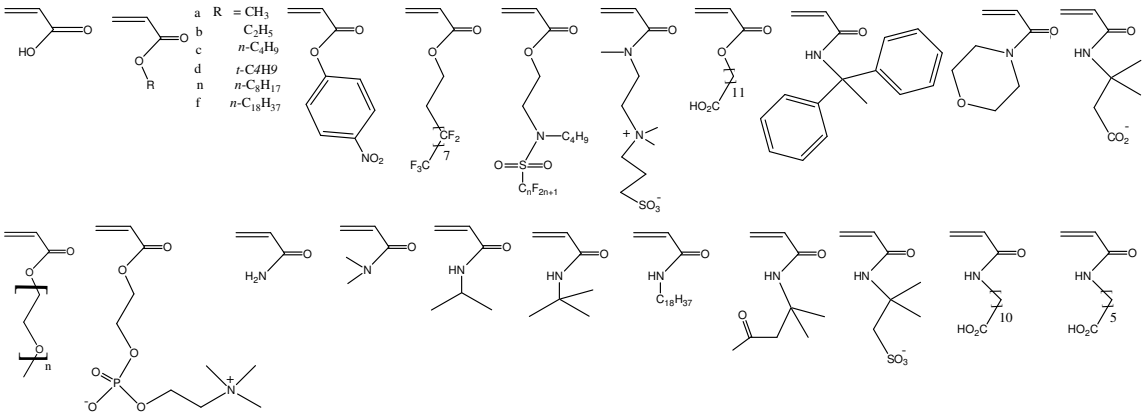

Figure 42. ***Examples of Monomers that are polymerized via RAFT [117].***

Schumers et. al. unsuccessfully tried to polymerize o-nitrobenzyl acrylate by RAFT using 2-cyano-2-butyl dithiobenzoate and cumylphenyldithioacetate as CTA and Azobis(isobutyronitrile) as initiators in DMF at 70 °C [119]. The authors suggest that acrylate radicals undergo side reactions with the o-nitrobenzyl group in agreement with literature. Actually, nitro-aromatic compounds are known to act as inhibitors/retardators in radical polymerizations and to produce radicals when heated. Two complementary mechanisms describing the inhibition by nitro-aromatic compounds have been proposed. The first one, proposed by Price and Durham in 1943,

involves the attack of the propagating radical onto the aromatic ring on the para position(a few attack on ortho position is also possible) [120]. Afterward, hydrogen abstraction by another propagating radical occurs leading to the death of both two active species, as shown in Scheme 4.

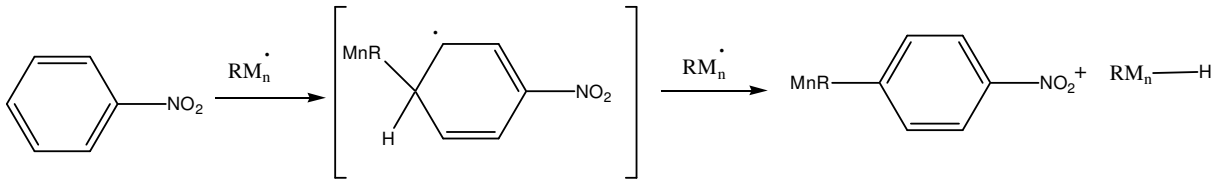

Scheme 4. First mechanism of polymerization inhibition was suggested by Price and Durham [120]

A few years later, a complementary mechanism implying the direct attack of the propagating radical onto the nitro function, and consequently leading to modify the chemistry of the active species (from RMnð to RMnOð), has been suggested by Hammond and Bartlett (Scheme 5) [121]

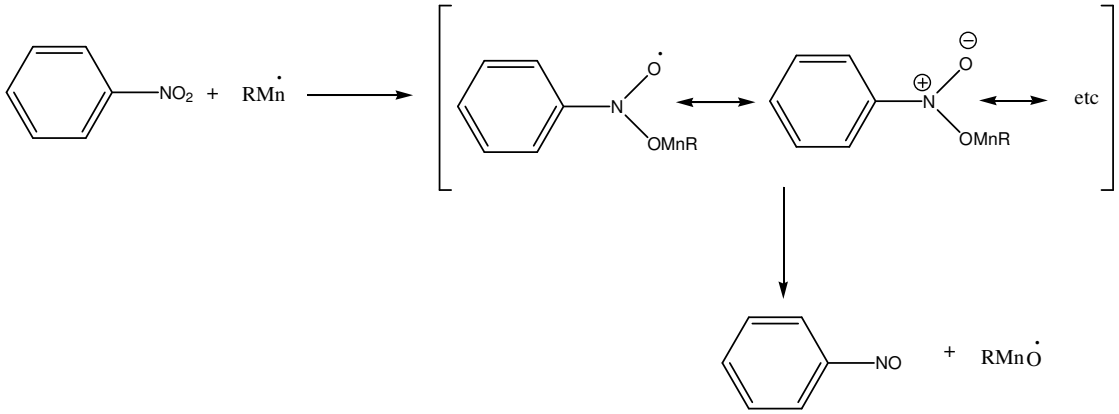

Scheme 5. Second mechanism of polymerization inhibition was suggested by Hammond and Bartlett [121]

III.2) Nitroxide Mediated radical Polymerization (NMP)

Nitroxides and alkoxyamine couples can be used to control radical polymerizations. These species are establishing one dynamic equilibrium by activation deactivation process as shown in Scheme 6 [122].

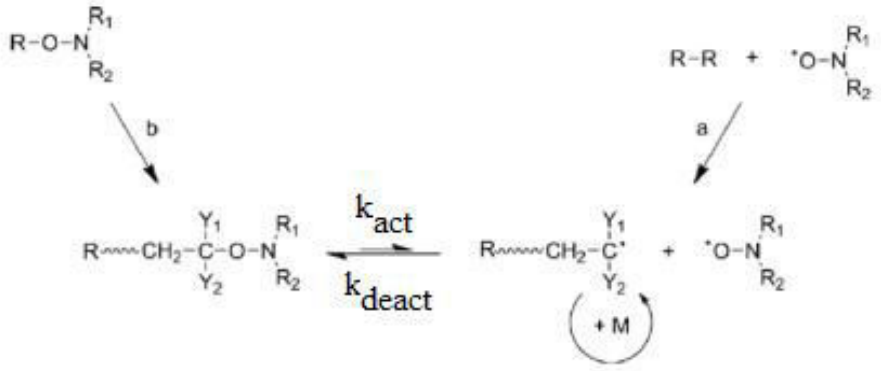

Scheme 6. Activation-deactivation equilibrium of nitroxide-mediated polymerization bicomponent initiating system (a) and monocomponent initiating system (b) [122].

Alkoxyamines are thermally dissociated in two radicals (activation step): one nitroxide that is to stable to react with the monomer, while the other radical initiates the propagation of the polymerization. Nevertheless, nitroxide can react with others radicals (deactivation step) to produce a new stable alkoxyamine (Scheme 6, way b). Sometimes, researchers prefer to add nitoxide and classical initiator (R-R) in the medium (Scheme 6, way a). This R-R initiator is thermally dissociated and the control of the RP is ensured by the presence of nitroxide.

The first trials of acrylates polymerization via NMP have been carried out in the presence of TEMPO and unfortunately shown uncontrolled polymerization. More precisely, polymerizations proceeded to low conversions in the first hour and then stop [123]. Consequently, scientists worked to find other nitroxides that might be give controlled acrylates polymerization [124, 125] and discovered a number of acyclic nitroxides that work very well for acrylates. In 2004, Georges et. al. reported controlled NMP of butyl acrylate mediated by TEMPO in the presence of reducing agents as ascorbic acid under miniemulsion conditions [126]. The role of this reducing agent is to react with excess TEMPO and to shift equilibrium to the right according to Scheme 7.

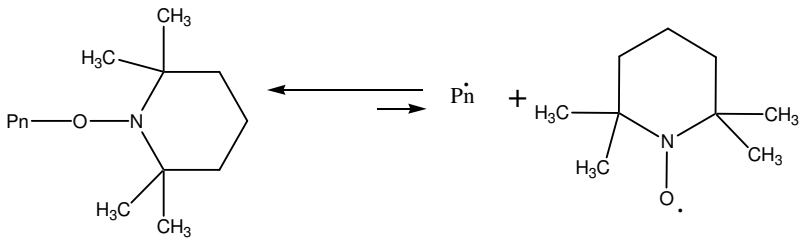

Scheme 7. Equilibrium between active and dormant polymer chains under SFRP conditions where Pn· is a polymer chain and T is a terminating agent, in this case TEMPO.

Schumers et. al. studied NMP of o-nitrobenzyl acrylate mediated by the SG1 nitroxide and N-(tert-butyl)-N-(1-diethylphosphono-2,2-dimethylpropyl)-O-(2-carboxylprop-2-yl)hydroxylamine (MAMASG1) BlocBuilder^{TM} as initiator (Figure 40) [119]. Unfortunately, no polymerization has been observed in the tested conditions, which were previously optimized for many acrylates. The authors explained that by the high temperature used, which favors the degradation of the o-nitrobenzyl moiety and thus the important generation of side radicals inhibiting the NBA polymerization. Same reasons were already mentioned with RAFT.

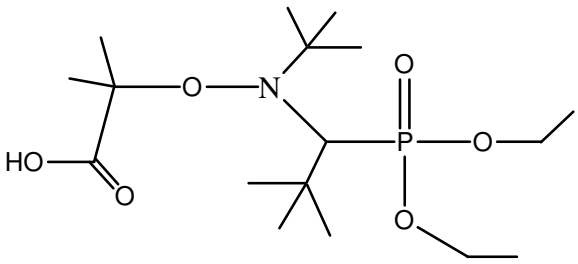

Figure 43. Structure of the water-soluble SG1-based alkoxyamine, MAMA (BlocBuilder^{TM}).

Other monomers were polymerized by NMP as acrylonitrile, acrylamide, their derivatives and acrylic acid as shown in (Figure 41) [122]. For instance, acrylic acid was polymerized without pre-protection and its polymerization was mediated by methyl 2-[N-tertiobutyl-N-(1-diethoxyphosphoryl-2,2-dimethylpropyl) aminoxy] propionate (MONAMS) SG1-based alkoxyamine in 1,4-dioxane solution at 120 °C [127].

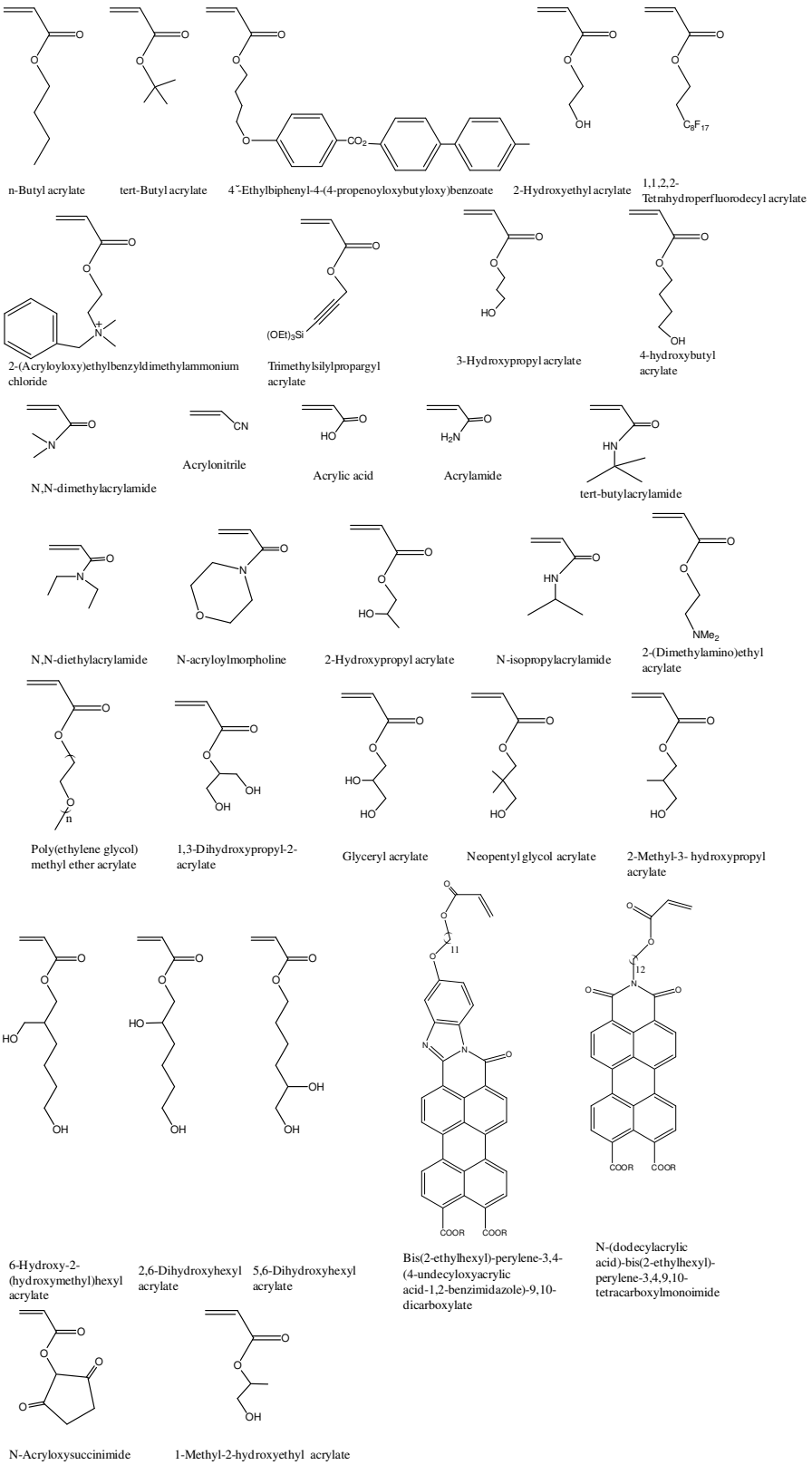

Figure 44. ***Some acrylates, acrylamide and their derivatives polymerized via NMP [122].***

III.3) Atom transfer radical polymerization

III.3.1) Mechanism of ATRP

This polymerization is completely different from RAFT as dynamic equilibrium between dormant and active species is established via a reversible exchange of one halogen. This exchange is easier due to the presence of a metallic catalyst complex. Propagating radicals rapidly trapped a halogen atom from the catalyst in the deactivation process (with a rate constant of deactivation, k_{deact}) shifting the equilibrium towards the dormant species Pn-X (Scheme 8).

The efficient ATRP catalyst complex consists of a transition metal species (Mt^n), which can expand its coordination sphere and increase its oxidation number, complexing ligands (L) and a counter ion (X) that can form a covalent or ionic bond with the metal center. The transition metal complex (Mt^n/L) is responsible for the homolytic cleavage of the alkyl halogen bond (RX), which generates the corresponding higher oxidation state metal halide complex Mt^{n+1}X/L (with a rate constant k_{act}) and an organic radical R^{δ} [68, 128]. R^{δ} can propagate the polymerization (k_p), terminate as in conventional free radical polymerization by either coupling or disproportionation (with a termination rate k_t), or be reversibly deactivated (k_{deact}) by Mt^{n+1}X/L to form a halid-capped dormant polymer chain as shown in Scheme 8.

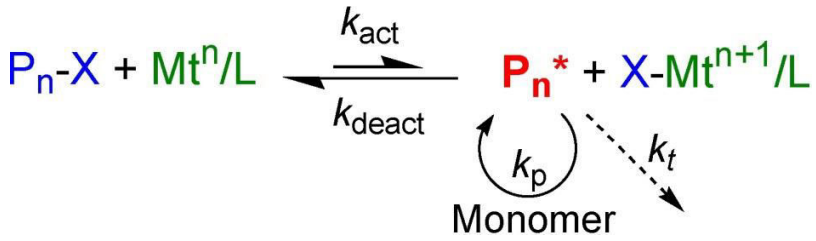

Scheme 8. Mechanism of `Atom Transfer Living Radical Polymerization_. (*http://www.cmu.edu/maty/development-atrp/index.html*).

For each monomer, the success ATRP depends on various parameters such as the transition metal complex, the alkyl halide used as initiator and the solvent. In brief, we will discuss these parameters in following pages.

III.3.2) Effect of transition metal

ATRP has been successfully mediated by a variety of metals including Ti [129], Mo[130, 131], Re[132], Fe[133], Ru[134], Os[135], Rh[136], Co[137], Ni[138], Pd[139], and Cu [140] (Figure 42). Nevertheless, complexes of Cu have been found to be the most efficient catalysts in the ATRP of a broad range of monomers, in diverse media [141].

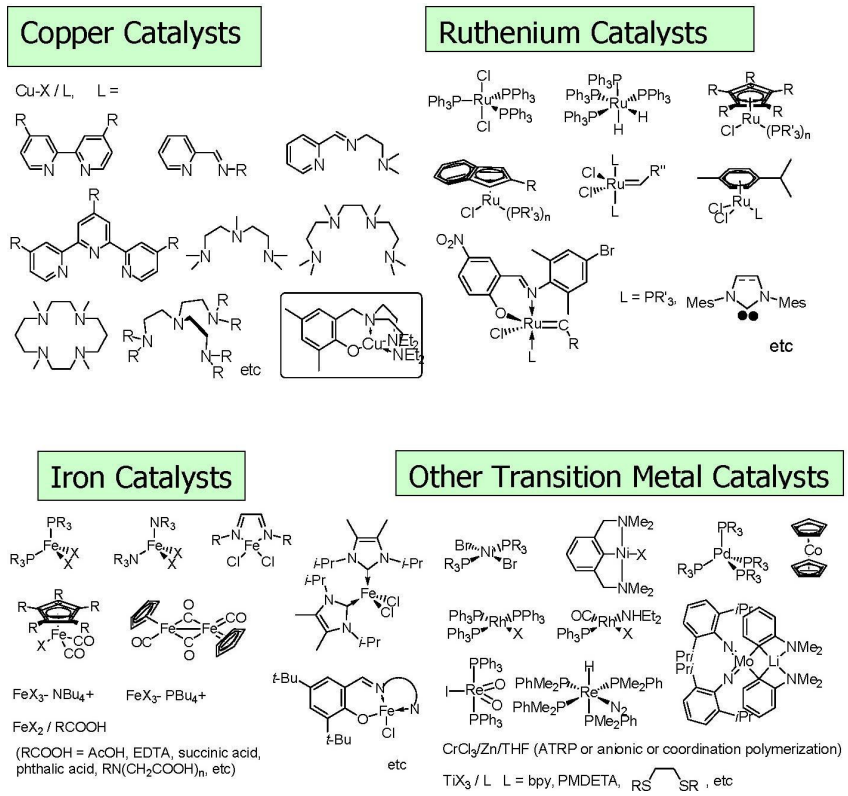

Figure 45. ***Examples of transition metal catalysts based on Copper, Iron, Ruthenium, Nickel, Cobalt, Palladium and Molybdenum. (http://www.cmu.edu/maty/chem/catalyst-development/solvent-effects-and-selection-of-a-catalyst-for-aqueous-media.html)***

III.3.3) Effect of Ligand

Ligand influences the reactivity of the catalyst system and consequently the equilibrium between dormant and active species. There are several rules that determine the reactivity of the catalyst complex: (1) distance between N atoms (C4佣C3佣C2) and/or the coordination angle. (2) Topology of the ligand (cyclic~ linear佣branched). (3) Nature of the N-ligand (aryl amine佣aryl imine佣alkyl imine佣alkyl amine~pyridine). (4) Steric bulk created around the metal center (after

complexation with ligand that can affect the rate of activation/deactivation (e.g., the Me_6TREN complex is ~1000 times more active than Et_6TREN) [142].

Activation rate constants for different ligands were determined via the trapping method of the produced Rð from the homolytic cleavage of R-X using 2,2,6,6-tetramethylpiperidinyl-1-oxy (TEMPO) [143], that gives stable alkoxyamine after reaction as shown in Scheme 9. In this case, TEMPO was used in a large excess (~10-fold) with respect to alkyl halides to prevent reversible dissociation of the formed alkoxyamine into active species as shown in Scheme 9.

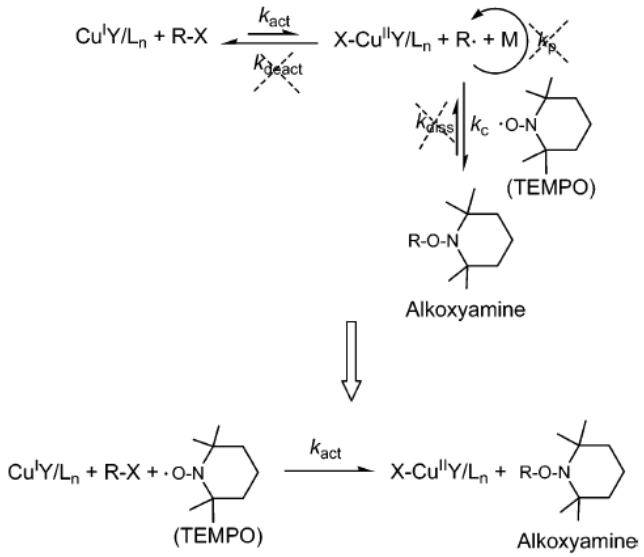

Scheme 9. Trapping of alky radical by TEMPO [143].

By this way, one can sort ligands depending the activation rate of the metallic system as shown in Figure 43 [143].

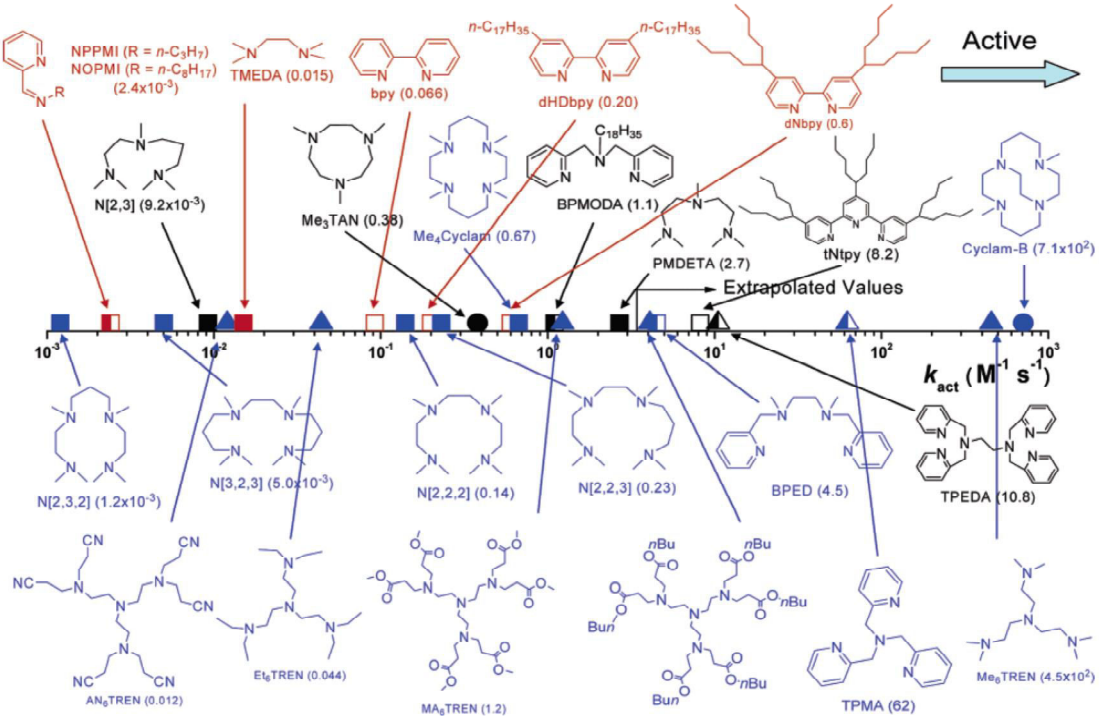

Figure 46. ***ATRP activation rate constants for various ligands with EtBriB as initiator in the presence of $Cu^{I}Y$ (Y= Br or Cl) in MeCN at 35 °C: N2, red; N3, black; N4, blue; amine/imine, solid; pyridine, open. Mixed, left-half solid; linear □; branched▲; cyclic, ○[143].***

III.3.4) Effect of Initiator case of (alkyl halide)

The alkyl halid reactivity was affected by three parameters such as degree of substitution of the carbon that is linked to the halide, the nature of transferable atom (halogen atom) and groups attached to the carbon. As shown in the Figure 44, the arrangement of initiators having different structures has been realized after carrying ATRP runs with $Cu^{I}X$/TPMA in MeCN at 22 °C[144].

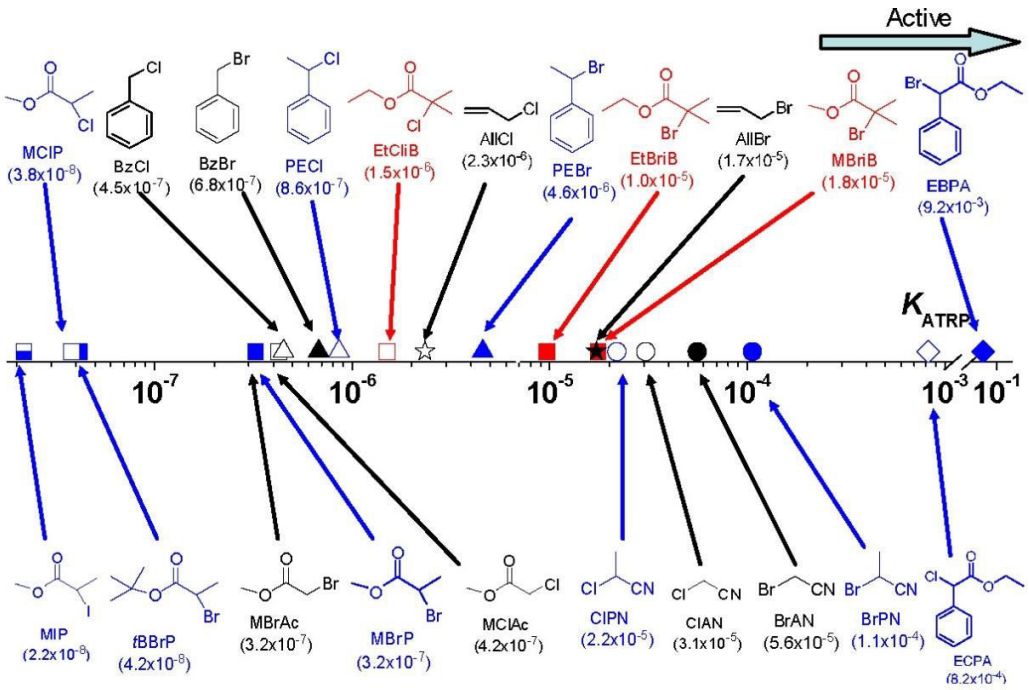

Figure 47. ***ATRP equilibrium constants for various initiators with $Cu^{I}X$/TPMA (X= Br or Cl) in MeCN at 22 °C [144].***

III.3.5) Development of ATRP technique

Controlled Atom Transfer Radical Polymerization enables to obtain polymers with controlled average molecular weight($\bar{M}_n$), with very narrow range of dispersity ($\bar{D}$ is very close to 1.00) and chain end functionality is approximately 100%. Unfortunately, large amount of copper to catalyze ATRP is required, and the completely removing of the copper from crude polymers may be difficult. Some researcher teams were working on easily removable catalyst systems with more or less success.

Matyjaszewski's team modified ATRP to develop some new techniques in order to decrease copper concentration, while still controlling the ATRP. These techniques are known as Activator Generated by Electron Transfer (AGET ATRP), Initiators for Continuous Activator Regeneration (ICAR ATRP), Activator ReGenerated by Electron Transfer (ARGET) ATRP, Supplemental Activators and Reducing Agents (SARA) in ATRP, Electrochemically induced ATRP (eATRP), and Photochemically induced ATRP ($h\nu$ATRP. All these techniques run with the same mechanism of normal ATRP, but produce the reductive agent (Cu^{I} in case of copper catalyst) by different ways. Reducing agent Cu^{I} plays an important role in reduction of Cu^{II} that accumulates

at the beginning of the polymerization before establishing the activation/deactivation equilibrium. This is called Persistent Radical Effect (PRE) and generates Cu^{I} ATRP activator as shown in Scheme 10.

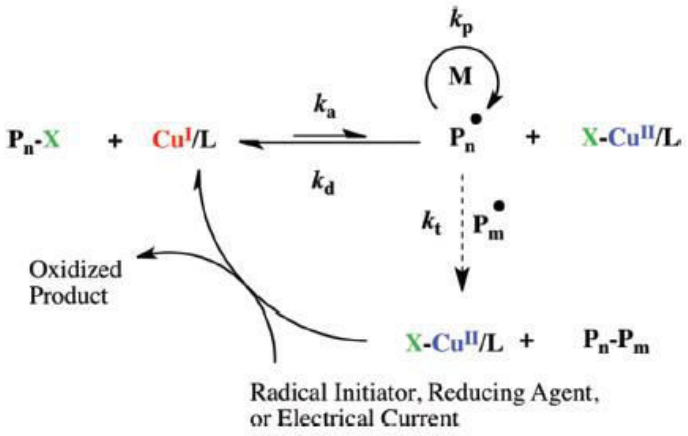

Scheme 10. General mechanism of modified ATRP techniques (such as AGET, ARGET, ICAR, SARA, electrochemically and photochemically).

III.3.5.a) Activator Generated by Electron Transfer (AGET ATRP)

In this case, reducing agent that can be used is tin^{II}2-ethylhexanoate [145], ascorbic acid [146] or triethylamine [147]. The role of reducing agent is to reduce accumulated Cu (II) species during PRE to establish the activation/deactivation equilibrium and regenerate Cu(I) species.

III.3.5.b) Activator ReGenerated by Electron Transfer (ARGET-ATRP)

Same reducing agents already mentioned in AGET-ATRP can be used with this technique but in addition, organic derivatives like hydrazine, phenol, sugar, or inorganic species such as Sn^{II} or Cu^{0} can be used [148, 149]. Contrary to AGET, ARGET can be run in presence of air and by introducing Cu^{II} complex (Cu^{II}X/L) instead of (Cu^{I}X/L) at the beginning. For that, ARGET needs a large excess of reducing agent and/or strong reducing agent for a continuous regeneration of Cu^{I} from Cu^{II}.

III.3.5.c) Initiators for Continuous Activator Regeneration (ICAR) ATRP

Classical organic initiators used with conventional radical polymerization, like azobis(isobutyronitrile) AIBN [150] and 2,2'-azobis[2-(2-imidazolin-2-yl)propane] dihydrochloride [151], can be used in this case as shown in the Scheme 11. Radicals produced from these initiators react with Cu^{II} to regenerate Cu^{I}.

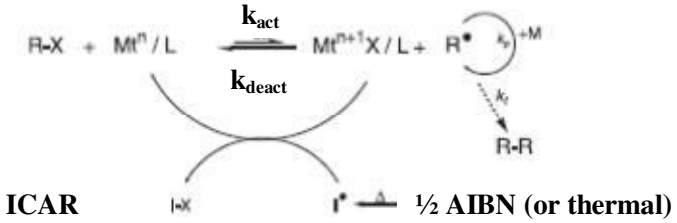

Scheme 11. Mechanism of ICAR ATRP.

III.3.5.d) Supplemental Activators and Reducing Agents (SARA ATRP)

Zero-valent metal (e.g. Zn°, Mg°, Fe°[152] and Cu°[153]) is used as activator, which activates alkyl halid into active radical species. On other hand, the zero-valent metal reduces accumulated $Cu^{II}X_2$ species, which resulted from bimolecular termination or which is established by persistent radical effect (PRE) as shown in Scheme 12.

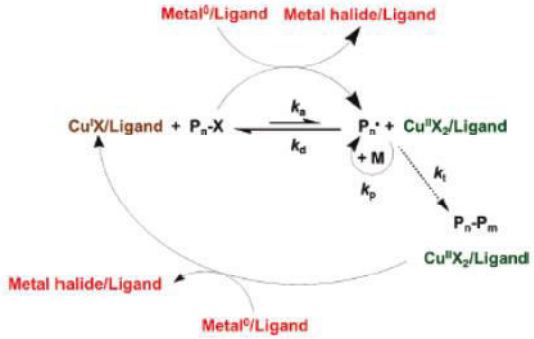

Scheme 12. Mechanism of SARA ATRP.

III.3.5.e) Electrochemically induced ATRP (*e*ATRP)

Reduction of Cu^{II} into Cu^{I} can be established via electrochemical reaction. Cell of polymerization was setup by Matyjaszewski as shown in the Figure 45. The Cu^{II} species were reduced to Cu^{I} species at the cathode surface [154, 155].

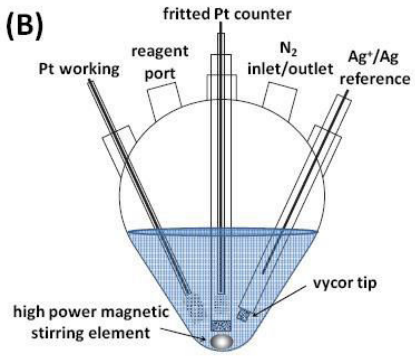

Figure 48. ***Five necked flask with three electrodes used for e-ATRP: the working electrode (Pt working), the counter electrode (fitted Pt counter), and the reference electrode which were a 3 mm Pt disk (Gamry Instruments), a Pt mesh, and an Ag\Ag+ (cathode), which contained a 0.1 M $AgNO_3$ and TBAPF6 filling solution in MeCN separated from the working solutions by a porous Vycor tip, respectively (http://www.cmu.edu/maty/atrp-how/procedures-for-initiation-of-ATRP/eatrp.html).***

III.3.5.f) Photochemically induced ATRP (h ≥ATRP)

Reduction of Cu^{II} species can also be mediated by the light (h ≥ATRP). It can be done by visible light (392 and 450 nm), sunlight[156] and UV irradiation[157]. For example, Zhou et. al. studied gold surface-initiated ATRP of different monomers (e.g. 3-sulfopropyl methacrylate potassium salt (SPMA), 2-(dimethylamino)ethyl methacrylate (DMAEMA), N-isopropylacrylamide (NIPM) and oligo(ethylene glycol) methacrylate (OEGMA)). Firstly, thiol initiator is linked to the gold surface as shown in Figure 46, a [157]. Then, the polymerization activators, Cu(I)Бligand, was continuously generated from Cu^{II} by an indirect photochemical UV reduction process. TiO_2 nanoparticles were used here as the photosensitive material that adsorb UV light, then promote the production of excited electrons that react with Cu^{II} as shown in Figure 46, b.

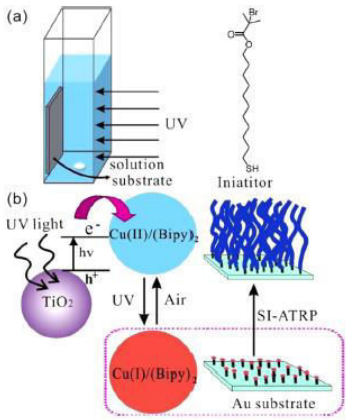

Figure 49. ***(a) Schematic setup to perform UV-ATRP and structure of the Thiol initiator and (b) Mechanism of UV light ¯induced surface-initiated atom transfer radical polymerization [157].***

III.4) RDRP via outer Sphere Electron Transfer (SET) mechanism

III.4.1) How did Percec discover RDRP via outer Sphere Electron Transfer mechanism?

ATRP and modified ATRP techniques undergo inner sphere electron transfer mechanism as we described in the previous chapter through a homolytic cleavage of alkyl halide by Cu^{I} catalyst complex and a halide transfer to Cu^{II} complex. However, this mechanism needs high activation energy. Due to that, side reactions (chain or monomer transfer) may happen during the polymerization. In these cases, polymerization has to be stopped at low conversion in order to keep the controlled character of RDRP, nevertheless resulted polymer chains have wide range of dipersity (Đ). In 1998, Percec et. al. discovered new catalyst of RDRP, which are Cu^{0}/bpy (Cu° powder, wire, films, coins), Cu_2O/bpy and mixtures. They inspired that from previous work made by Minisci, which reported the $FeCl_2$-catalyzed Karasch addition of alkyl halides [158, 159]. In addition, Hajek and Silhavy were publishing the role of zero-valent metals and metal oxides as redox catalysts for radical additions to olefins [160]. Consequently, Percec et. al. tested the ability of Cu° metal to form radical from arenesulfonyl chlorides during a heterogeneous self-regulated phase-transfer catalyzed of butyl methacrylate (BMA) in presence of $Cu^{I}Cl$/bpy. They chose sulfonyl halides due to their ability to form stable radical-anion intermediates [161] and observed high rates of polymerization. This highlights that all initiations with sulfonyl halides / Cu^{0} or Cu_2O systems undergo through a heterogeneous outer-sphere single electron transfer mechanism. Some examples of sulfonyl chlorides, bromides, and iodide already used in RDRP as drawn in Figure 47 [160].

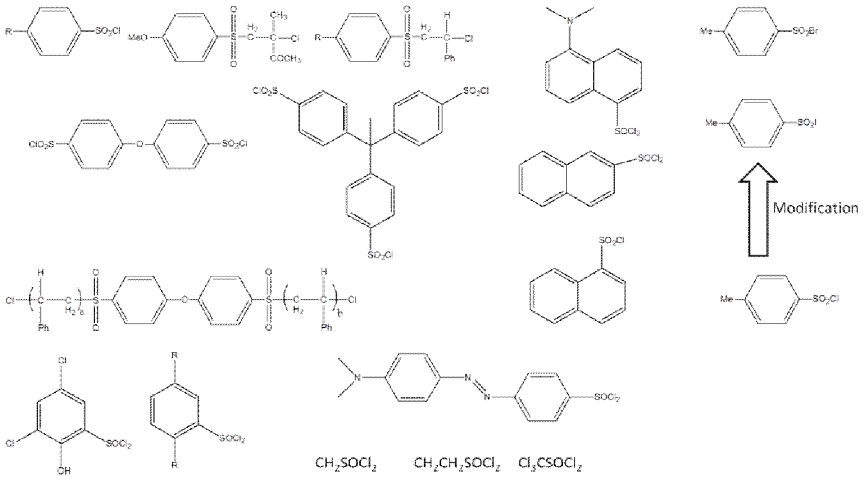

Figure 50. ***Structures of sulphonyl chlorides, bromide and iodide used as initiators in the $Cu^{I}Cl$, Cu°, and Cu_2O/bpy-catalyzed RDRP [160].***

III.4.2) Various types of SET

Since their previous studies, Percec et. al. demonstrated new techniques based on zero-valent transition metal that undergo via outer sphere electron transfer mechanism. These techniques are called Single-Electron Transfer Degenerative chain Transfer Living Radical Polymerization (SET-DTLRP) and Single-Electron Transfer Living Radical Polymerization (SET-LRP).

*III.4.2.*1) Single-electron transfer degenerative chain transfer living radical polymerization *(SET-DTLRP)*

Common initiator used in SET-DTLRP is iodoform and there are two methods for activation of Chain Transfer (CT):

a) Cu° or Cu_2Y (Y= O, S, Te or Se) can be used in case of Cu°-catalyzed RDRP of vinyl chloride in aqueous medium carried out at room temperature (scheme 13) [162]. This was the first controlled radical polymerization of vinyl chloride, contrary to general case where vinyl chloride based radicals (active species) prefer to undergo side reactions like dimerization or disproportioantion and lead to alkane and alkene.

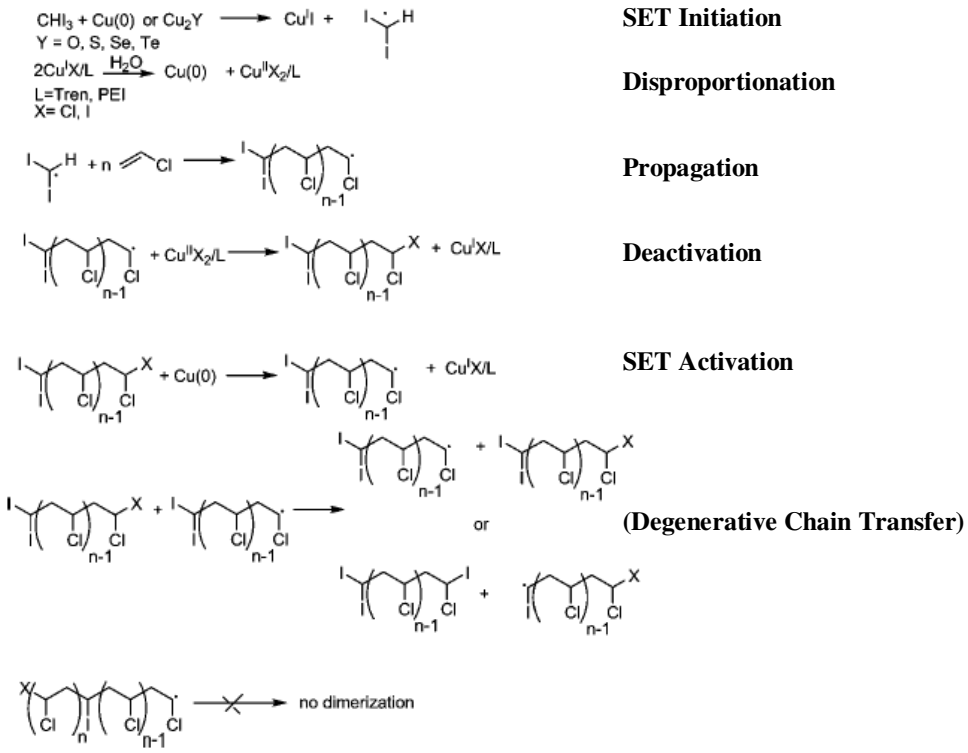

Scheme 13. Mechanism of transition metal mediated SET-DTLRP of vinyl chloride [162].

b) Sodium dithionite can activate iodoforme initiator used in SET-DTLRP at room temperature as shown in Scheme 14. This type of mechanism is called `***Non-Transition Metal Mediated SET-DTLRP***_ [163].

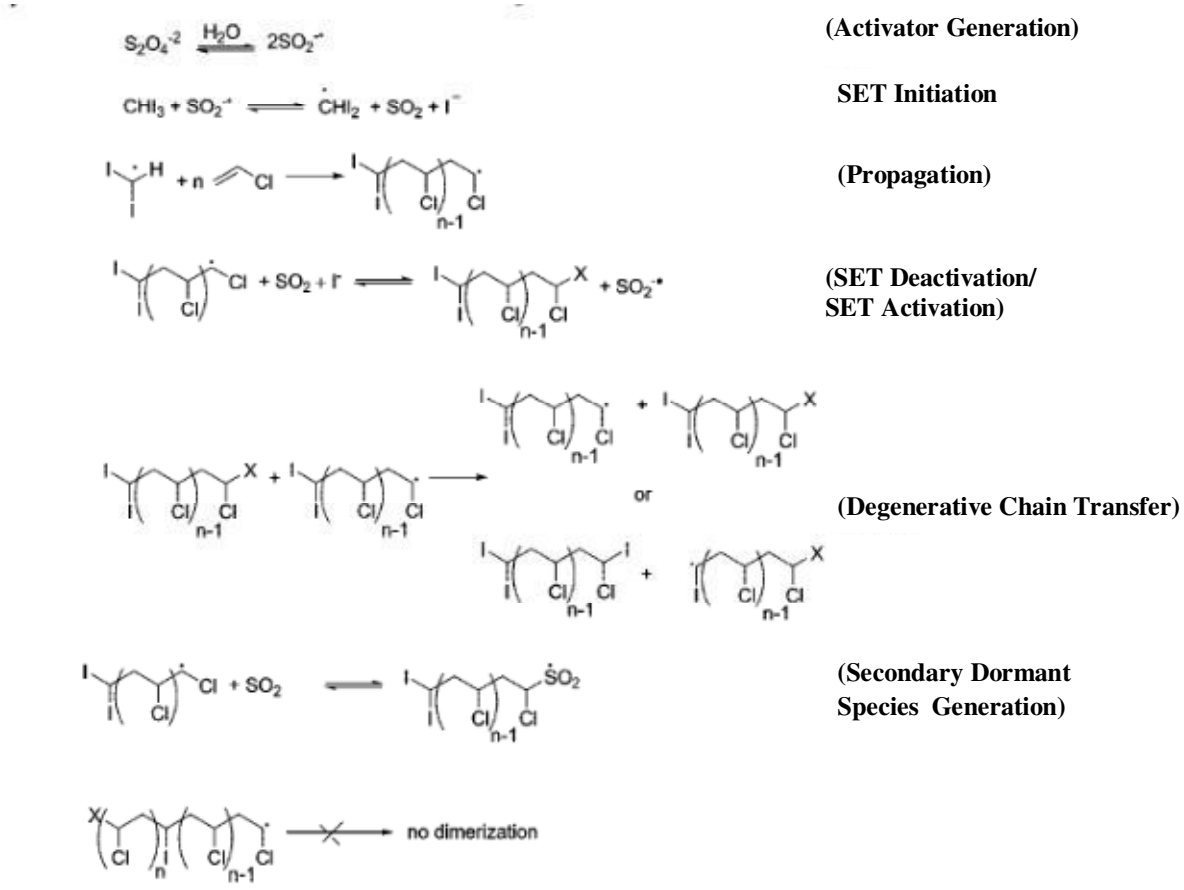

Scheme 14. Mechanism of non-transition metal mediated SET-DTLRP of vinyl chloride [163].

SET-DTLRP allows to get on different structures of polymers such as telechelic, four-armed star and bifunctional polymers. The topology of polymer can be controlled by choosing suitable initiator as shown in Table 14.

Table 14. *Examples of monomers polymerized via SET-DTLRP.*

Monomers	Initiators	Resulted polymers	Ref
(a) Non-Transition Metal Mediated (activator $Na_2S_2O_4$*)*			
Vinyl chloride (VC), ethyl acrylate (EA) *n*-butyl acrylate(BA) *i*-butyl acrylate (*i*BA), *t*-butyl acrylate (*t*BA), lauryl acrylate (LA), 2-ethylhexyl acrylate (2EHA), 2-methoxy ethyl acrylate (2MEA)	CHI_3	-telechelic polymer	[164] [165, 166] [166] [166, 167] [168] [167] [169]
Vinyl chloride (VC)	CH_2I_2	-telechelic polymer	[170]
Vinyl chloride	bis(2-iodopropionyloxy)ethane, 2,5-diiodohexanediothoate, bis(2-methoxyethyl) 2,5-diiodohexanedioate	,≪ telechelic polymer	[171]
PVC and PBA	Pentaerythritol tetrakis(2-iodopropionoate)	four-armed star	[171]
Vinyl chloride (VC)	,≪di(iodo)-poly(hydroxypropyl acrylate)	triblock copolymer poly(vinyl chloride)-b-poly(hydroxypropyl acrylate)-b-poly(vinyl chloride)	[172]
(b) ***Transition Metal Mediated***			
Methyl methacrylate (MMA)	,≪di(iodo)PVC/ CuCl/bpy	PMMA-*b*-PVC-*b*-PMMA	[173]
	2-iodo-2-methylpropionitrile/Cu°-without ligand	PMMA with iodide end functionlity (~96%)	[174]

*III.4.2.*2) Single-Electron Transfer Living Radical Polymerization *(SET-LRP)*

Single-electron transfer living radical polymerization (SET-LRP) was demonstrated after SET-DTLRP. In SET-LRP, degenerative transfer agent was removed and replaced by adjusting polymerization conditions. More precisely, in SET-LRP, a dynamic equilibrium between dormant and active species is established via an activation/deactivation between Cu° surface and $Cu^{II}X_2$/L.

III.4.2.2.1) Comparing SET-LRP and ATRP mechanisms

SET-LRP techniques are based on the full disproportionation of $Cu^{I}X$ to Cu° and $Cu^{II}X_2$ that is controlled by the extremely high constant of disproportionation (k_{dis}) (Scheme 15). Before talking about SET-LRP technique in details, we would like to show the difference between ATRP and SET-LRP mechanisms [175]. SET-LRP and ATRP activation steps process via Cu°/L (outer-sphere electron) [176] and Cu(I)X/L (inner-shpere electron) [177], respectively. During propagation step, generated Cu(I) species directly undergo full disproportionation and give nascent Cu°(very active) and Cu(II) species through SET-LRP. On contrary, disproportionation step doesn˘t exist in ATRP as shown in Scheme 15. Consequently, present $Cu^{I}X$ catalyzes the polymerization and that need high energy to homolytic cleavage.

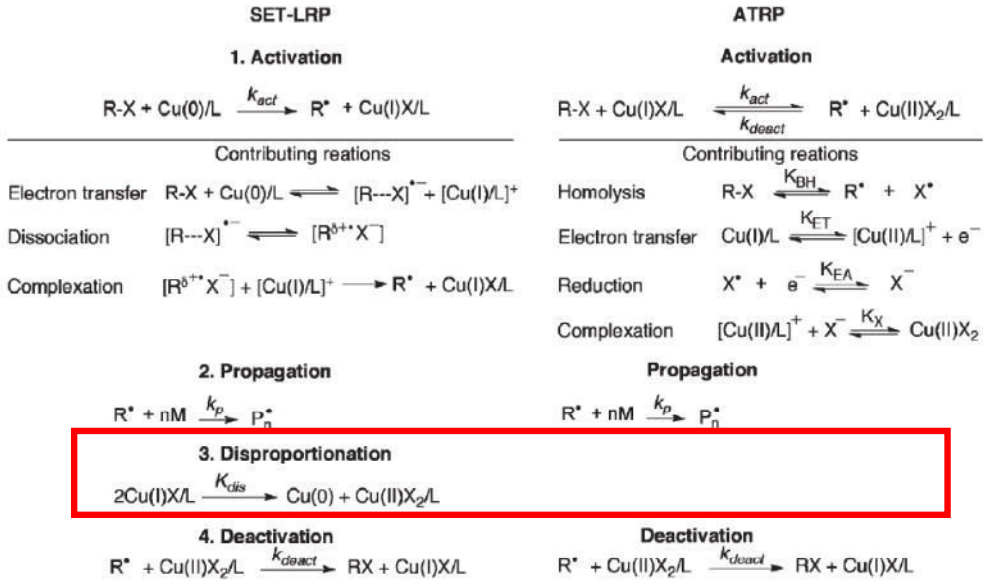

Scheme 15. Contributing reactions involved in SET-LRP (left side) and ATRP (right side) [175].

There are many factors affecting the rate constant of SET-LRP such as zero-valent metal, solvent, initiator, ligand, adding external $CuBr_2$ and inhibitor. We will explain each influence in the following chapter.

III.4.2.2.2) Factors affecting SET-LRP

III.4.2.2.2.1) Effect of zero-valent metal

We must take in consideration two parameters to study the effect of zero-valent metal such as the chemistry and the shape of the metal

1) Chemistry of the zero-valent metal

The rate of SET-LRP polymerization is depending on the zero-valent metal used as studied by Liu et. al [178]. More precisely, they studied the polymerization of methyl methacrylate in presence of EBiB and PMDETA as initiator and ligand, respectively. They studied different metal such as Zn(0), Ni(0), Mg(0), Fe(0). Runs were established with same (monomer/ligand/initiator) molar ratio in DMSO at 25 °C with adding external $CuBr_2$. For each run they observed a good agreement between theoretical and SEC values of M_n. Zn(0) and Ni(0) give higher conversion than other metals. They observed that Zn(0) give higher conversion than Ni(0) with lower time, while Ni(0) give polymers with lower dispersity ($Đ$= 1.04) than Zn(0) ($Đ$=1.66). Finally, the authors found that the more efficient zero-valent metal is Ni(0) and highlighed that the magnetic properties of nickel powder facilitates its recycling.

Controlled SET-LRP of different acrylates and vinyl monomers were reported by different zero-valent metals such as Fe, Sm, Yb, Sn, Ln and Cu as shown in Table 15.

Table 15. ***Different Zero-valent metals mediated SET-LRP runs***

Zero-valent metals	***Monomers***	***Ref***
Fe	*Acrylonitrile,*	*[179]*
	Styrene and MMA	*[180]*
Sm	*Acrylonitrile*	*[181]*
Yb	*Methyl methacrylate*	*[182]*
Sn	*Acrylonitrile*	*[183]*
Ln	*Acrylonitrile /Vinyl chloride*	*[184]*
Cu	*(MMA, N-isopropyl acrylamide(NIPAM), and acrylamide)*	*[185]*
	(N,N-Dimethylacrylamide and N-Isopropylacrylamide)	*[186]*
	Vinyl chloride	*[187]*
	cyclohexyl methacrylate	*[188]*
	(MMA-co-MAA)	*[189]*
	other acrylates	*[160]*

2) Activation and shape of Metal

Three shapes of zero-valent metal can be used to mediate SET-LRP such as wire, plate and powder. Before we discuss the effect of surface area, one important step is the activation of metal surface. Indeed, Cu(0) undergoes spontaneous oxidation to Cu_2O in air and the presence of Cu_2O will delay the initiation of SET-LRP and consequently will produce an induction period of polymerization. There are many methods to activate Cu° surface.

2.a) Activation using hydrazine hydrate

Cu_2O can be reduced to copper metal by the introduction of an excess of hydrazine monohydrate under refluxing conditions. The reaction is carried out in an inert atmosphere of N_2 in order to prevent the reoxidation of the copper metal by atmospheric oxygen [79]. Percec et. al. used this method to activate Cu° wire and used it rapidly in SET-LRP of methyl acrylate in DMSO at 25 °C [190].

2.b) Activation using organic or inorganic acid

Another method to remove copper oxide layer onto the surface is the treatment of copper wire with concentrated acid. Copper oxide reacts with acid to give corresponding copper salt. Many acids were reported for the activation of copper wire like inorganic acids such as HNO_3 [191], HCl and H_2SO_4 [191, 192] or organic acids such as citric acid [193]. Nguyen et. al. studied SET-LRP of MA in DMSO using Cu° wire, that was activated using different acid such as CH_3COOH, HNO_3 and HCl [194].

2.c) Increasing the surface

Percec et. al. studied the effect of surface area of Cu° on SET-LRP of methyl acrylate in DMSO using Cu° wire or Cu° powder. They found that Cu° powder lead to a fast polymerization indicating a rapid surface-mediated SET activation process [195]. In other experiments, they used different surface area of Cu° wire such as 1.39, 2.65, 6.05 and 110 cm² and determined the corresponding apparent rate constant of propagation k_{app} equal to 0.045, 0.058, 0.073 and 0.114 min^{-1}, respectively. From these results, k_{app} has proved to be in a linear relationship with the surface area of Cu° wire. Moreover, the lower polydispersity of Cu° wire allows an easy prediction of reaction rates from wire dimensions. Authors mention also other advantages of Cu° wire than powder: a) a greater control and prediction of molecular weight b) an easy

preparation/removal/ recycling of catalyst, c) the lack of need of purification of the resulting polymers.

III.4.2.2.2.2) Effect of solvent

Disproportionation step of Cu^{I} is one of the most important steps in SET-LRP as shown in Scheme 15. Therefore, solvents used in SET-LRP must have the ability to promote thus disproportionation via an electron transfer in substitution radical-nucleophilic unimolecular ($S_{RN}1$) reactions. These solvents are called Disproportionating Solvents.

1) Effect of DMSO on SET-LRP

DMSO is one common solvent used in SET-LRP because its properties: a) DMSO dissolves most of monomers at room temperature. b) DMSO is one coordinating solvent that stabilizes $Cu^{II}X_2$ [196] and thereby promotes disproportionation by shifting the K_{dis} further to high value. Monge et. al. demonstrated the effect of DMSO by comparing SET-LRP runs of MMA and BMA using N-(n-propyl)-2-pyridylmethanimine as a ligand in DMSO or in toluene, under the same conditions [196]. The authors observed that MMA SET-LRP was faster in DMSO (27% conversion in toluene, k_p^{app} = 9.76 X 10^{-4} min^{-1}, while 51% in DMSO, k_p^{app} = 20.4 X 10^{-4} min^{-1}). The same result was noticed for BMA polymerization: after 6 h, 32% conversion was reached in toluene (k_p^{app} = 10.8 X 10^{-4} min^{-1}) whereas it was 58% in DMSO (k_p^{app}= 24.9 X 10^{-4} min^{-1}). All results provide that DMSO played a crucial catalytic role on the rate of polymerization. Increasing the polarity of the medium by using DMSO instead of toluene enhances the stability of the polymerization intermediates. Moreover, the authors proved the interaction between DMSO and Cu species by running various experiments with different ratio from [DMSO]/[ligand] ratios from zero to $2.6X10^{4}$, as shown in Figure 48. More precisely, authors studied firstly the UV absorbance spectra of CuBr/L complex in toluene and observed one band at 380 nm. Then, they increased the concentration of DMSO and noticed both the disappearance of the band at 380 nm and the appearance of a new band at 490 nm. This new band was attributed to the formation of a new copper complex CuBr(L)n(DMSO), wherein DMSO ligands CuBr.

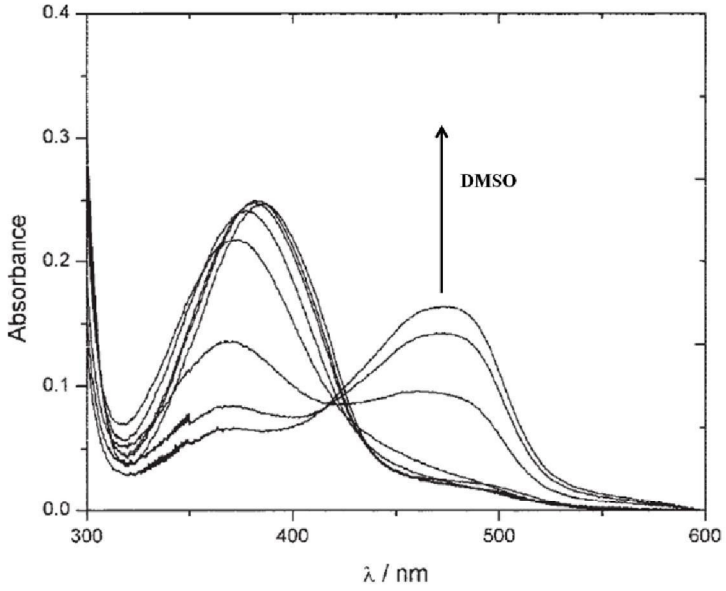

Figure 51. ***UV titration of CuBr/ligand (ligand=4.1 X10^{-4} M) in presence of Cu(I)Br in toluene with small amount of DMSO. Ratio ([DMSO] / [Ligand]) X10^{-4} = 0.0, 2.3 X 10^{-2}, 4.6 X 10^{-2}, 1.1 X 10^{-1}, 3.4 X 10^{-1}, 9.2 X 10^{-1}, 1.5, 2.1, 2.6 [196].***

In addition to DMSO, there are some other disproportionating solvents e.g. DMF, Dimethylacetamide (DMAC), Ethylene carbonate (EC), Propylene carbonate, ethanol, methanol, methoxyethanol, N-Methylpyrrolidone (NMP), acetone and their binary mixtures with H_2O [197]. Binary mixture of alcohols is sometimes important to be used because the increase of hydrophobic character of the alcohol leads to decrease k_p^{app} and consequently lead to control the molecular weight distribution. Actually, increasing the hydrophobic character of the solvent decreases its polarity and diminishes the stabilization of charge separation, thereby reduces the rate of activation and also the extent and rate of disproportionation of Cu^I/N-ligand. Consequently, binary mixture with water can be used to increase the polarity of alcohol and enhance disproportionation of Cu^I/N-ligand (low level of water was mixed with alcohol). Nguyen et. al. studied the effect of disproportionating and non disproportionating solvents as well as binary mixture on SET-LRP of MA at room temperature [175]. They estimated the apparent rate constants of propagation k_p^{app}. As one can see in Table 16, runs were made in disproportionating solvents exhibit higher k_p^{app} than nondisproportionating solvents. In addition, low amount of water addition in the medium may enhance k_p^{app}.

Table 16. ***Apparent rate constant of propagation values*** (k_p^{app}) ***of SET-LRP of MMA in Disproportionating and Nondisproportionating solvents, and Binary mixture (blue color).***

Runs	Solvents	k_p^{app} (min^{-1})
	Disproportionating solvents	
1	DMSO	0.131
2	MeOH	0.072
3	MeOH + 10% H_2O	0.089
4	Ethylene carbonate	0.117
	Nondisproportionating solvents	
5	Ethylacetate	0.005
6	CH_2Cl_2	0.009
7	Acetone	0.011
8	Acetone +10% H_2O	0.055
9	Methyl Ethyl Ketone	0.013
10	MeCN	0.038
11	MeCN + 10% H_2O	0.136

** SET-LRP runs of MA were carried out at same conditions (initiator MBP and Catalyzed with Cu(0) wire at 25 °C).*

Fluorinated alcohols as 2,2,2-trifluoroethanol (TFE) and 2,2,3,3-tetrafluoropropanol (TFP) were studied as medium of SET-LRP by Percec et. al. [198]. SET-LRP of methyl methacrylate (MMA), ethyl methacrylate (EMA) and n-butyl methacrylate (BMA) were carried out with Cu° wire, initiated with tosyl chloride (TsCl). They observed as excellent evolution of molecular weight with a narrow molecular weight distribution until almost complete monomer conversion. The rate of polymerization may be enhanced using binary mixture as we already mentioned.

Percec et. al. also studied SET-LRP of n-butyl acrylate (nBA) and 2-ethylhexyl acrylate (EHA) mediated by Cu° wire in different solvents such as 2,2,2-trifluoroethanol, DMSO and their binary mixtures (e.g. 30% , 50 % and 70% DMSO in TFE). The authors observed a higher k_p^{app} value in case of binary mixture than in TFE only according to the disproportionation effect of DMSO [199].

Recently, Haddleton et. al. studied SET-LRP of N-isopropyl acrylamide (NIPAM) in commercial alcohol solutions (e.g. beer/wine/cider/spirit) [200]. Authors didn˜t introduce Cu° wire directly in the medium but introduced Cu(I)Br in the alcohol solution and waited for 30 min to reach a full disproportionation of Cu(I)Br to nascent Cu° as shown in Figure 49.

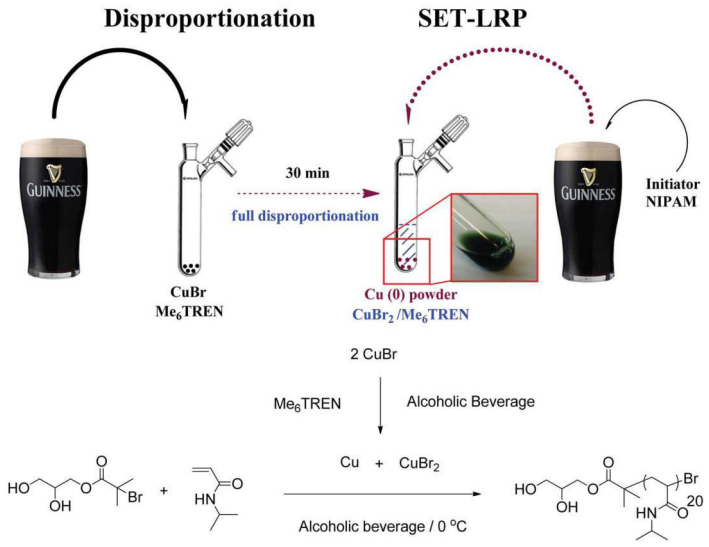

Figure 52. ***Typical polymerization procedure. Disproportionation of [Cu(I)(Me$_6$-TREN)Br] into Cu(0) and Cu(II) is first conducted in deoxygenated commercial beer/wine/cider/spirit followed by addition of a separate deoxygenated monomer/initiator solution [200].***

This study was done by cooperation between lots of chemists from different countries. They got on efficient SET-LRP in different commercial solutions as shown in the Table 17.

Table 17. ***SET-LRP of NIPAM in a range of commercial water ¯ alcohol mixtures***

Country	"Solvent"	% Alc.	Chemist(s)	% Conv. (min)	M_n[a] (g mol^{-1})	$Đ$
England	Banks's Bitter	3.8	PW, CS, DMH	99 (30)	3900	1.06
England	Banks's Mild	3.5	PW	99 (30)	4000	1.08
England	Burrow Hill Cider	6.0	JC	63 (30)	2300	1.08
England	Kingston Black Apple Apperitif	18.0	JC	87 (30)	1900	1.09
England	Pimm's	25.0	JC	99 (15)	3900	1.06
Ireland	Guinness	4.2	RM	99 (22)	3600	1.08
China	Tsingtao	4.7	RR, QZ, ZL	99 (104)	3600	1.20
China	Tsingtao	4.7	DJL, JAB	99 (30)	3500	1.09[b]
France	Verveine Verte	55	AS, MG	62 (30) phase separation	1600	1.05
France	Chateau Laubes Bordeaux 2009	12.5	AS	87 (90)	2600	1.16
France	Napoleon Brandy Bordeaux 1973	40.0	CW	83 (60) phase separation	3900	1.05
Germany	Krombacher	4.7	CH	70 (90)	3000	1.28
Thailand	Singha	5.0	NR	99 (10)	3300	1.12
Belgium	Leffe	6.6	MD	93 (40)	3000	1.10
Wales	Brains Rev. James	4.5	JG	99 (45)	3200	1.10
Greece	Ouzo	38.0	AA	67 (60)	3800	1.07
Greece	Alpha Beer	5.0	VN	96 (9)	3200	1.06
Greece	Tsipouro	40.0	VN	94 (30) phase separation	3200	1.06
Romania	Homemade Brandy	??	AH	97 (60)	3000	1.07
Scotland	McEwan's Champion	7.3	KM	99 (30)	3400	1.09
Scotland	A'Bunadh Single Malt	59.0	JG	99 (60) phase separation	2800	1.08
Finland	Karhu	4.6	JK	99 (45)	3600	1.07
Switzerland	Morand Abricotine	43.0	AS	96 (30)	2800	1.14
Turkey	Yeni Raki	45.0	GY, RB	99 (60) phase separation	5000	1.06
Russia/Poland	Imperial Vodka	37.5	ML	99 (30) phase separation	4000	1.05
Sweden	Absolut Elyx Vodka	40.0	CW	83 (60)	3000	1.08
Sweden	Absolut Elyx Vodka[b]	40.0	CW	—	—	—[c]

[a] M_n measured *versus* PMMA standards; $M_{n,theo.}$ = 2504 g mol^{-1}. [b] Repeated on reviewer request. [c] Reaction performed in the absence of CuBr.

2) Solvents that stabilize Cu(I)X/ L complex

Some solvents do not mediate disproportionation of Cu^IX such as THF and toluene. Percec et. al. overcome this defect by adding a low amount of disproportionating solvent like phenol to promote the disproportionation of Cu^IX. By adding 10% PhOH into THF medium, they observed a rapid disproportionation of Cu^IBr/Me_6-TREN [176].

3) Ionic liquids

Some SET-LRP have been run in ionic liquid medium. Ionic liquids are organic salts and remain liquid over a wide temperature range. They have been used as green solvents for many polymerizations as they dissolve many organic and inorganic compounds. Percec et. al. demonstrated a dramatic acceleration of the controlled radical polymerization of MMA initiated with arenesulfonyl chlorides and catalyzed by the self-regulated Cu_2O/2,2ˇ-bipyridine catalyst in the presence of 1-butyl-3-methylimidazolium hexafluorophosphate [C4mim][PF6] as solvent [160, 201]. The ionic liquid exhibits the catalytic effect of the Cu_2O/2,2ˇ-bipyridine complex and makes disproportionation of Cu^I/bpy feasible. At the same time, Jing et. al. carried out SET-LRP of acrylonitrile without ligand in ionic liquids as 1-methylimidazolium acetate ([mim][AT]), 1-methylimidazolium propionate ([mim][PT]) and 1-methylimidazolium valerate ([mim][VT]) [202]. The authors gave the sequence of the apparent polymerization rate constants k_p^{app} ([mim][AT]) > k_p^{app} ([mim][PT]) > k_p^{app} ([mim][VT]) according to the length of substituent groups into the counter ions as shown in Figure 50 [201]. These substituent groups were hydrophobic and their length related to increase the hydrophobic character.

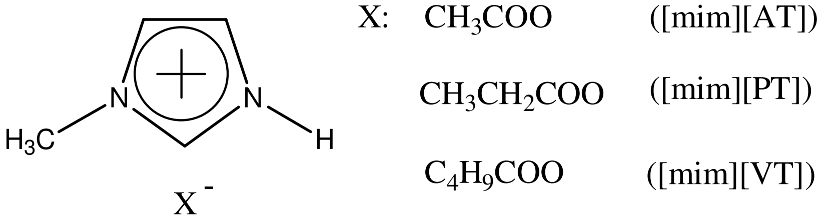

Figure 53. ***Structures of different ionic liquid such as 1-methylimidazolium acetate ([mim][AT]), 1-methylimidazolium propionate ([mim][PT]), and 1-methylimidazolium valerate ([mim][VT]).***

III.4.2.2.2.3) Effect of Initiator

SET-LRP can be initiated with same initiators that were used in ATRP (e.g. monofunctional initiators, bifunctional initiators, multifunctional initiators and macroinitiators). In ATRP, K_{ATRP} values depend on the nature of halide (e.g. bromide, chloride or iodide) due to the inner-sphere electron-transfer process, and the ratio $k_{R\text{-}Br}/k_{R\text{-}Cl}$ can be between 5×10^2 and 9×10^4. In case of SET-LRP, the ratios of apparent rate propagation constant for iodide, bromide or chloride compounds are $k_{R\text{-}I}/k_{R\text{-}Br}$ ū $k_{R\text{-}Br}/k_{R\text{-}Cl}$ ū 1-10, in good agreement with an outer-sphere electron-transfer process [160]. Percec et. al. presented energy diagrams of homolytic C-halide bond dissociation and formation and decomposition of anion-radicals formed during a SET process (Scheme 16) [176]. That could be explained by the crucial step of SET-LRP is the disproportionation of Cu(I) to ::nascent ˘˘ Cu(0) and Cu(II).

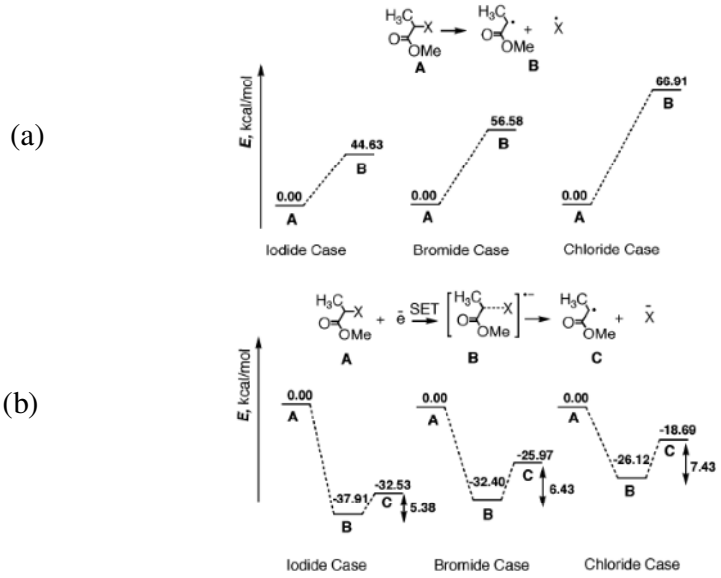

Scheme 16. Relative C-X bond dissociation energies in methyl 2-halopropionates, a) Homolytic bond dissociation and b) formation and decomposition of anion-radicals formed by an SET process [176].

The type of carbon attached to halogen (such as primary, secondary or tertiary carbon) is another factor that can affect the rate of initiation. Sundaram et. al. studied SET-LRP of tBA using different initiators such as benzyl bromide and ethyl 2-bromopropionate, which generate primary and secondary radical, respectively, as shown in Figure 51 [203]. The authors observed that the rate of initiation and consequently the rate of polymerization were faster with the secondary initiator than primary initiator. Moreover, primary initiator shows an induction period.

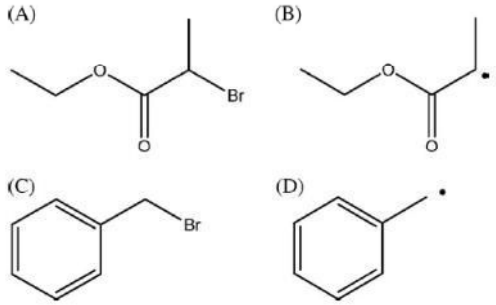

Figure 54. ***Initiators used for SET-LRP of tBA and the corresponding radicals formed during the initiation A= ethyl2-bromopropionate with the formed radical B and C= benzyl bromide with radical D [203].***

Different types of initiators were used in SET-LRP runs such as -haloesters, sulfonyl halides, -haloamides and other initiators as shown in Figure 52 [97, 160, 179]. In addition, macroinitiators produced by ATRP and carrying a halide at one chain extremity can also be used to initiate SET-LRP. For example SET-LRP of MMA mediated by copper zero wire can be carried out using poly(vinylidene fluoride-co-chlorotrifluoroethylene) (P(VDF-co-CTFE)) as initiator [204].

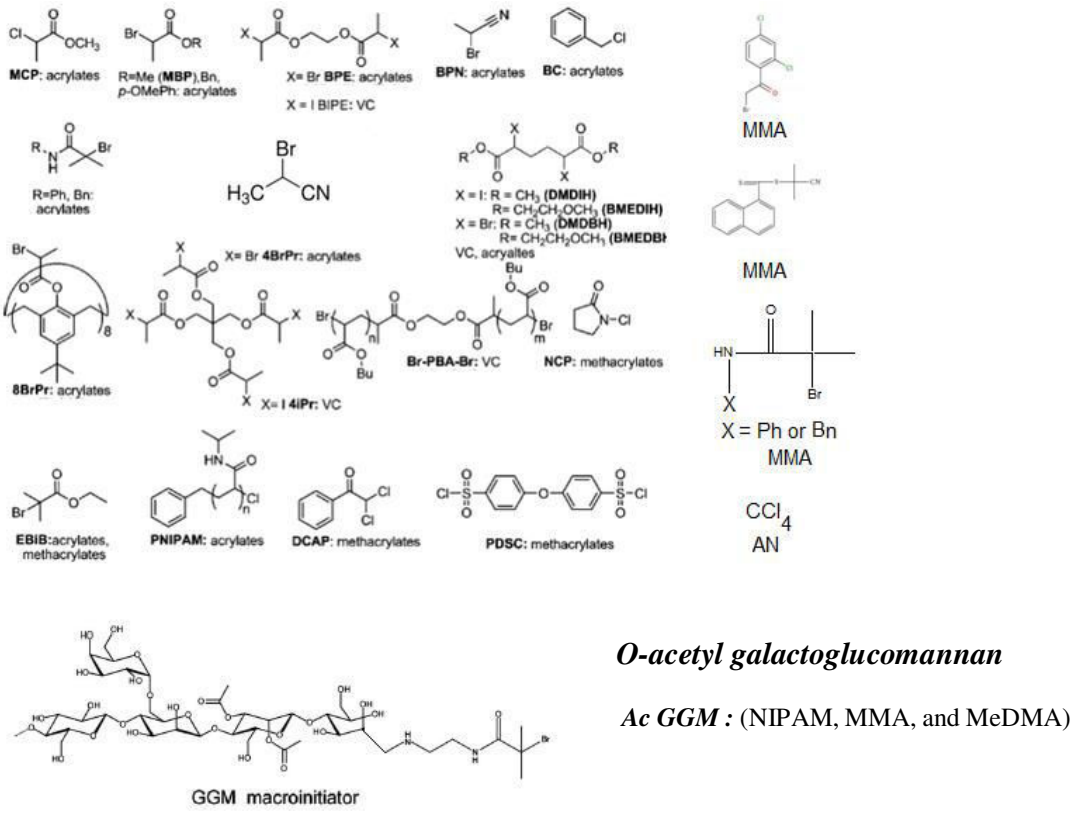

Figure 55. ***Initiators were used in SET-LRP and corresponding monomers that were polymerized***

III.4.2.2.2.4) The effect of ligand

Successful SET-LRP process is achieved through a fast disproportionation of $Cu^{I}X$ to Cu° and $Cu^{II}X_2$. Ligand has importance to enhance this diproportionation process because the presence of ligands can disrupt the disproportionation equilibrium depending on its relative binding energy with Cu^{I} and Cu^{II} species [205]. Consequently, the nature and concentration of ligand both affect the efficiency and the rate of polymerization of SET-LRP.

1) The nature of ligand

Percec et. al. studied the effect of different ligands on the diproportionation using UV-vis measurements [206]. The authors made different experiments using different ligands, to study the effect of ligand on disproportionation of CuBr into $CuBr_2$. The experiments were done with each ligand with CuBr or with $CuBr_2$ in DMSO. The solutions CuBr/L and $CuBr_2$/L were leaved for 10 min before UV-Vis measurements. Without ligand, UV-Vis spectrum of CuBr in DMSO shows absorbance at 500 nm, while $CuBr_2$ spectrum without ligand shows one band at 1000 nm (Figure 53, a).

Firstly, with Bpy and Pr-PMI as ligands, UV-Vis spectra of runs with $CuBr_2$ in DMSO show peaks around 750 nm. The Cu(I)Br species spectra recovered after 10 min show a slightly absorbance at 400-450 nm characteristic of Cu(I)Br/Bpy or Cu(I)Br/Pr-PMI, as shown in Figure 53, b, c. The both spectra didn't show any peaks characteristic of the Cu(II)Br/L formation. In conclusion, ligands such as Bpy and Pr-PMI preferentially bind Cu^{I} cation leading to a slow disproportionation.

Secondly, Me_6TREN and TREN were studied as ligands. Experiments were carried out with Cu(I)Br in DMSO exhibit UV-Vis spectra characteristic of the formation of ($CuBr_2$/Me_6TREN) and ($CuBr_2$/TREN) complexes (band at 750-950 nm) as proved with the experiments carried out with $CuBr_2$ (Figure 53, d, e). They concluded on these results that disproportionation process of Cu(I)Br into $CuBr_2$ were enhanced in presence of Me_6TREN and TREN. Consequently, Me_6TREN and TREN were very effective for outer sphere electron mechanism than Bpy and Pr-PMI.

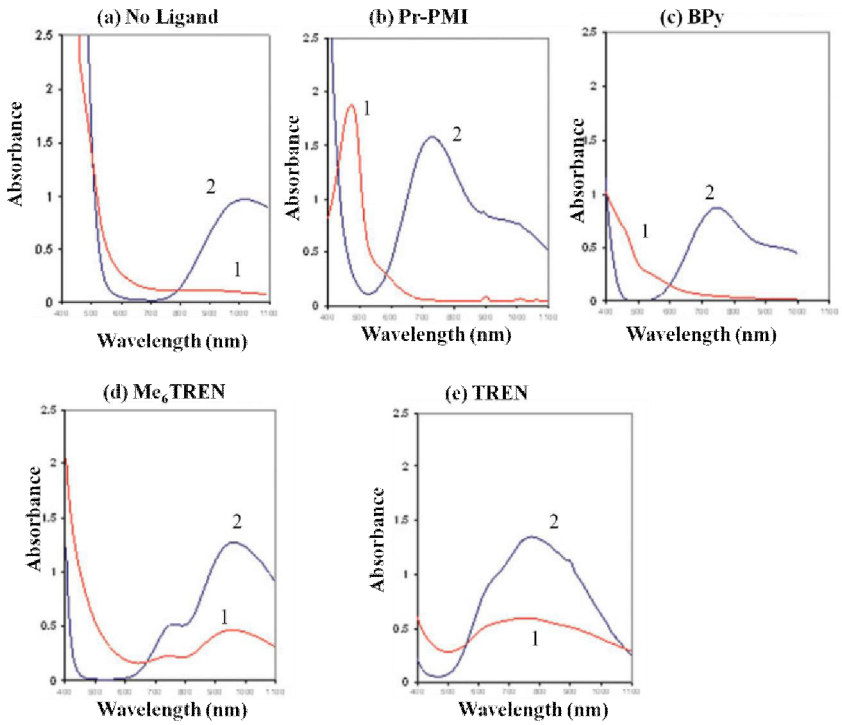

Figure 56. ***Effect of several ligands. SET-LRP were carried out with 0.01 mmol of Cu^{I} or Cu^{II} in 0.01 ml of DMSO, (1) CuBr (2) $CuBr_2$. The UV studies were observed after 10 min at 25 °C [206].***

Other ligands were also tested in DMSO using UV-vis measurements. Some are promoting a rapid diproportionation such as *N*,*N*,*N*′,*N*″,*N*″-pentamethyldiethylenetriamine (PMDETA), 1,1,4,7,10,10-hexamethyltriethylenetetraamine (HMTETA) and PEI [176].

2) Concentration of the ligand

The concentration of ligand should be incorporated into the equilibrium expression of disproportionation according to equations 2 and 3 [207]. If the ligand strongly stabilizes Cu^{II} species versus Cu^{I} species, a maximum disproportionation should occur when only half of the amount of ligand is present, by comparison with the required amount of ligand that stabilize Cu^{I}. Consequently, excess of ligand would drive the reaction in the reverse direction, while low amount of ligand would provide insufficient stabilization of the resultant $Cu^{II}X_2$.

$$Cu^{I}X/L + Cu^{I}X/L \overset{K^{*}_{disp}}{\rightleftharpoons} Cu^{0} + Cu^{II}X_2/L + L \qquad \textit{Equation (2)}$$

$$K^{*}_{disp} = [Cu^{II}X_2/L][L]/[Cu^{I}X/L]^2 \qquad \textit{Equation (3)}$$

III.4.2.2.2.5) The effect of adding external $CuBr_2$

Dan et. al. studied the effect of the quantity of external Cu(II) deactivator on the SET-LRP [208]. In their study, SET-LRP of tBA were carried out in absence and in presence of $CuBr_2$ with different ratio to Cu° ($[CuBr_2]_0/[Cu(0)]_0$) using methyl 2-bromopropionate (MBP) as initiator in DMSO. They observed that polymerization is out of control in absence of external $CuBr_2$. In presence of external $CuBr_2$, the rate of polymerization increases with increasing $[CuBr_2]_0$. However, at higher concentration of external $CuBr_2$ the polymerization shows a decrease of [illegible]. These results are in agreement with SET-LRP results of methyl acrylate, that was initiated with ethyl 2-bromoisobutyrate in DMSO as reported by Haddleton et. al. [209]. Moreover, Haddleton et. al. observed another effect of adding external $CuBr_2$, as it is preventing the formation of high molecular weight contaminants (Figure 54). These contaminants are produced during the period of slow rate in the beginning of SET-LRP.

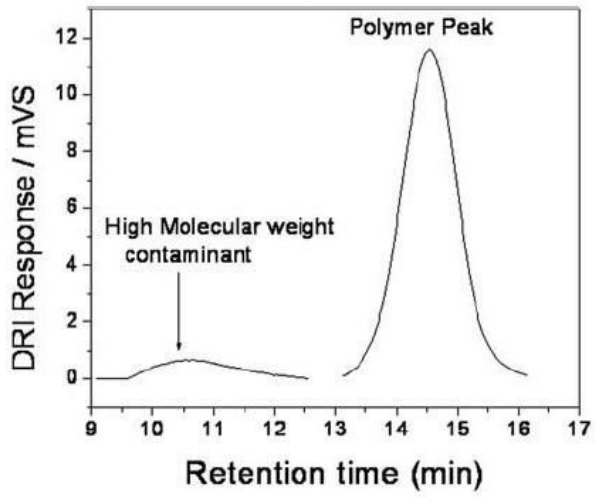

Figure 57. ***DRI chromatogram of SET-LRP of MA using EtBriB in DMSO without $CuBr_2$ [208].***

III.4.2.2.2.6) The effect of inhibitor

Usually, monomers that are polymerized using free radical polymerization have to be purified before polymerization, in order to remove free radical inhibitor added to prevent its polymerization during storage. In case of SET-LRP, this purification step is not necessary. Percec et. al. proved that by running SET-LRP of methyl acrylate in presence of one classical free radical inhibitor, which is 4-methoxyphenol (MEHQ) [210]. Authors studied the tolerance of

SET-LRP toward inhibitors by adding different amounts of solid MEHQ to the polymerization medium. They observed one small induction period due to the addition of solid MEHQ that could bring oxygen in the polymerization system. Of course, the length of this induction period depends on the amount of the inhibitor added. Moreover, they observed slight decrease in $\overline{M}_n$ value. One can compare SET-LRP of MA with MMA ATRP both made in presence of inhibitor MEHQ with by Haddleton et. al., as shown in Table 18 [211]. The both studies were did using different monomers, but we know from literature that MMA is more reactive than MA. Haddleton et. al. concluded on mechanism of MMA ATRP in presence inhibitor as the propagation step undergoes via carbon-bromine bond not by carbon center free radical. Whatever mechanism of ATRP, by comparing the results of SET-LRP and ATRP we observed that SET-LRP show high tolerance of radical inhibitor than ATRP.

Table 18. The results of MMA ATRP and MA SET-LRP in presence of inhibitor

Technique	monomer	[Phenol/Initiator]	solvent	Temperature °C	Time (min)	Conversion %
ATRP	MMA	10	Xylene	90	30	31
SET-LRP	MA	10	DMSO	25	30	70

III.4.2.2.3) Monomers

Variety of monomers has been used in SET-LRP such as acrylates, methacrylate, vinyl halide and other monomers as shown in Figure 55 [160]. Recently, Dax et. al. published SET-LRP of different monomers like [2-(methacryloyloxy) ethyl]trimethylammonium chloride, methyl methacrylate (MMA) and N-isopropylacrylamide (NIPAM) mediated by Cu° wire [97]. The authors used modified O-acetyl galactoglucomannan (Ac GGM-Br) with bromide end function as macroinitiator. They observed controlled radical polymerizations with low dispersity.

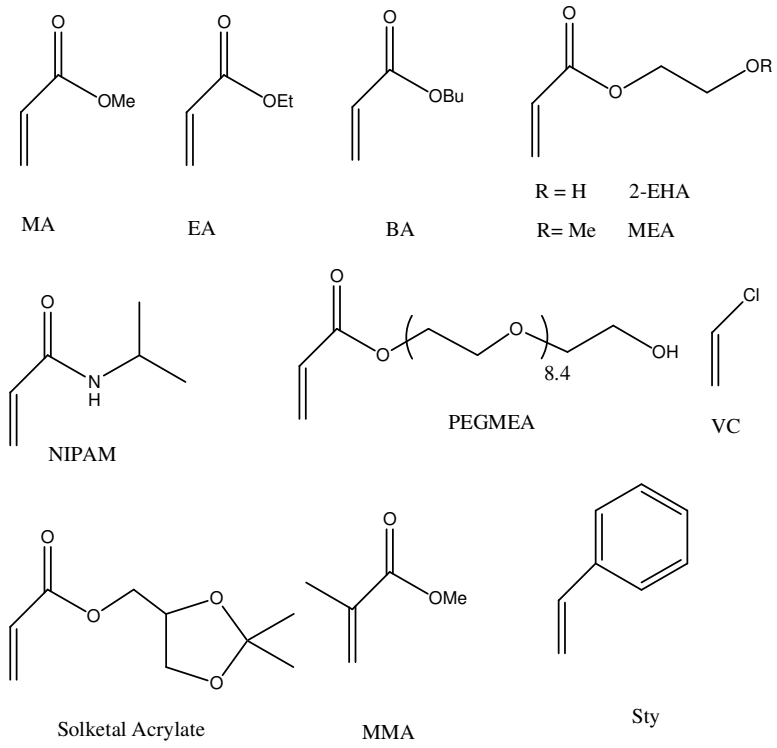

Figure 58. ***Examples of monomers were polymerized by SET-LRP [160].***

III.5) Conclusion

In this second part of bibliography, different controlled radical polymerization techniques such as RAFT, NMP, ATRP and SET-LRP were discussed. We focused on SET-LRP technique and chose it for various reasons: 1) SET-LRP needs low activation energy in contrast with other techniques, where initiation step undergoes via heterolytic cleavage. Actually, SET-LRP can be established at low temperature such as 20 °C. 2) SET-LRP shows high tolerance of radical inhibitors as reported in literature. Radical polymerization of NBA was reported as uncontrolled via different RDRP techniques due to retardation and inhibition effect of nitrobenzyl group. Therefore, we expected that SET-LRP would be very useful to control the radical polymerization of 2-nitrobenzyl acrylate (NBA). 3) SET-LRP provides polymer with high end functionality, 4) SET-LRP uses less amount of Copper than ATRP, more precisely, we can use wire copper and 5) SET-LRP is easy to carried out, even in presence of high amount of O_2.

References

[1] R. Jain, N.H. Shah, A.W. Malick, and C.T. Rhodes, Controlled drug delivery by biodegradable poly(ester) devices: different preparative approaches, Drug Dev. Ind. Pharm., 24 (1998) 703¯727.

[2] R.A. Jain, The manufacturing techniques of various drug loaded biodegradable poly(lactide-co-glycolide) (PLGA) devices, Biomaterials, 21 (2000) 2475-2490.

[3] G.P. Carino, J.S. Jacob, and E. Mathiowitz, Nanosphere based oral insulin delivery, J. Control. Release, 65 (2000) 261-269.

[4] J. Panyam, M.M. Dali, S.K. Sahoo, W.Ma, S.S. Chakravarthi, G.L. Amidon, R.J. Levy, and V. Labhasetwar, Polymer degradation and in vitro release of a model protein from poly(D, L-lactide-co-glycolide) nano- and microparticles, J. Control. Release, 92 (2003) 173-187.

[5] M. van de Weert, W.E. Hennink, and W. Jiskoot, Protein instability in poly(lacticco-glycolic acid) microparticles, Pharm. Res. , 17 (2000) 1159-1167.

[6] H.C. Lawson, P. Sampath, E. Bohan, M.C. Park, N. Hussain, A. Olivi, J. Weingart, L. Kleinberg, and H. Brem, Interstitial chemotherapy for malignant gliomas: the Johns Hopkins experience, J. Neurooncol. , 83 (2007) 61-70.

[7] D. Chognot, J.-L. Six, M. Leonard, E. Dellacherie, B. Faivre, F. Bonneaux, and C. Vigneron, Synthesis and in vivo studies of protein C-loaded nanoparticles with PEO modified surfaces, J. Bioact. Compat. Pol. , 23 (2008) 49-68.

[8] C. Nouvel, J. Raynaud, E. Marie, E. Dellacherie, J.-L. Six, and A. Durand, Biodegradable nanoparticles made from polylactide-grafted dextran copolymers, J. Colloid Interf. Sci. , 330 (2009) 337-343.

[9] C. Gavory, A. Durand, J.-L. Six, C. Nouvel, E. Marie, and M. Leonard, Polysaccharide-covered nanoparticles prepared by nanoprecipitation, Carbohyd. Polym. , 84 (2011) 133-140.

[10] M. Laville, J. Babin, I. Londono, M. Legros, C. Nouvel, A. Durand, R. Vanderesse, M. Leonard, and J.-L. Six, Polysaccharide-covered nanoparticles with improved shell stability using click-chemistry strategies, Carbohyd. Polym. , 93 (2013) 537- 546.

[11] T.M. Allen and P.R. Cullis, Drug delivery systems: entering the mainstream, Sci., 303 (2004) 1818-1822.

[12] A.S. Hoffman, The origins and evolution of `controlled_ drug delivery systems, J. Control. Release, 132 (2008) 153-163.

[13] A. Harada, K. Kataoka, Formation of polyion complex micelles in an aqueousmilieu from a pair of oppositely-charged block-copolymers with poly(ethylene glycol) segments, Macromolecules, 28 (1995) 5294-5299.

[14] Y. Zhang, H. F. Chan, and K.W. Leong, Advanced materials and processing for drug delivery: The past and the future, Adv. Drug Deliv. Rev., 65 (2013) 104-120.

[15] A. Lavasanifar, J. Samuel, S. Sattari and G.S. Kwon, Block copolymer micelles for the encapsulation and delivery of amphotericin B, Pharm. Res., 19 (2002) 418-422.

[16] A. Falamarzian and A. Lavasanifar, Chemical modification of hydrophobic block in poly(ethylene oxide) poly(caprolactone) based nanocarriers: effect on the solubilization and hemolytic activity of amphotericin B, , Macromol. Biosci., 10 (2010) 648-656.

[17] A. Falamarzian and A. Lavasanifar, Optimization of the hydrophobic domain in poly(ethylene oxide)-poly(varepsilon-caprolactone) based nano-carriers for the solubilization and delivery of Amphotericin B, Colloids Surf. B Biointerfaces, 81 (2010) 313-320.

[18] S.H. Kim, J.P. Tan, F. Nederberg, K. Fukushima, J. Colson, C. Yang, A. Nelson, Y.Y. Yang, and J.L. Hedrick, Hydrogen bonding-enhanced micelle assemblies for drug delivery, Biomaterials, 31 (2010) 8063-8071.

[19] J.H. Kim, K. Emoto, M. Iijima, Y. Nagasaki, T. Aoyagi, T. Okano, Y. Sakurai, and K. Kataoka, Core-stabilized polymeric micelle as potential drug carrier: Increased solubilization of taxol, Polym. Adv. Technol., 10 (1999) 647-654.

[20] U. Kedar, P. Phutane, S. Shidhaye, and V. Kadam, Advances in polymeric micelles for drug delivery and tumor targeting, Nanomedicine: Nanotechnology, Biology, and Medicine 6(2010) 714-729.

[21] J. Kreuter, Nanoparticles. In: Kreuter J, editor. Colloidal drug delivery systems, New York: Marcel Dekker, 66 (1994) 219-342.

[22] P. Couvreur, Polyalkylcyanoacrylates as colloidal drug carriers, Crit. Rev. Ther. Drug Carrier Syst., 5 (1988) 1-20.

[23] K.E. Geckeler and J. Stirn, Polyreaktionen - Mechanismen, Systematik, Relevanz, Naturwissenschaften, 80 (1993) 487-500.

[24] H. Fessi , F. Puisieux, J.P. Devissaguet, N. Ammoury, and S. Benita, Nanocapsule formation by interfacial polymer deposition following solvent displacement, Int. J. Pharm., (1989) 55:R1-4.

[25] A. Dalpiaz, E. Vighi, B. Pavan, and E. Leo, Fabrication via a nonaqueous nanoprecipitation method, characterization and in vitro biological behavior of N6-cyclopentyladenosine-loaded nanoparticles, J. Pharm. Sci., 98 (2009) 4272-4284.

[26] C. Fong-Yu , W. Saprina Ping-Hsien , S. Chio-Hao , T. Tsung-Liu , W. Ping-Ching , S. Dar-Bin , C. Jyh-Horng , H. Patrick Ching-Ho , and Y. Chen-Sheng, Stabilizer-free poly(lactide-co-glycolide) nanoparticles for multimodal biomedical probes, Biomaterials, 29 (2008) 2104-2112.

[27] B. Mishra, B.B. Patel, and S. Tiwari, Colloidal nanocarriers: a review on formulation technology, types and applications toward targeted drug delivery, Nanomedicine: NBM, 6 (2010) 9-24.

[28] F. Lince, D.L. Marchisio, and A.A. Barresi, Strategies to control the particle size distribution of poly-仿caprolactone nanoparticles for pharmaceutical applications, J. Colloid. Interface Sci. 322 (2008) 505-515.

[29] I. Limayem, C. Charcosset , S. Sfar, and H. Fessi, Preparation and characterization of spironolactone-loaded nanocapsules for paediatric use., Int J Pharm, 325 (2006) 124-131.

[30] V. Ferranti, H. Marchais, C. Chabenat , A.M. Orecchioni, and O. Lafont, Primidone-loaded poly-仿caprolactone nanocapsules: incorporation efficiency and in vitro release profiles, Int. J. Pharm., 193 (1999) 107-111.

[31] Y.-l. Jeong, C.-S. Cho, S.-H. Kim, K.-S. Ko, S.-l. Kim, Y.-H. Shim, and J.-W. Nah., Preparation of poly(dl-lactide-co-glycolide) nanoparticles without surfactant, J. Appl. Polym. Sci., 80 (2001) 2228-2236.

[32] J. P. Raoa and K.E. Geckelera, Polymer nanoparticles: Preparation techniques and size-control parameters, Prog. Polym. Sci., 36 (2011) 887-913.

[33] P. S. Pramod, K. Takamura, S. Chaphekar, N. Balasubramanian, and M. Jayakannan, Dextran Vesicular Carriers for Dual Encapsulation of Hydrophilic and Hydrophobic Molecules and Delivery into Cells, Biomacromolecules, 13 (2012) 3627Б3640.

[34] D. H. Kim, M.-D. Kim, C.-W. Choi, C.-W. Chung, S. H. Ha, C. H. Kim, Y.-H. Shim, Y.-I. Jeong, and D.H. Kang, Antitumor activity of sorafenib-incorporated nanoparticles of dextran/poly(dl-lactide-co-glycolide) block copolymer, Nanoscale res. Lett., 7 (2012) 91- 97.

[35] L. Zhang, H. Shen, and A. Eisenberg, Phase Separation Behavior and Crew-Cut Micelle Formation of Polystyrene-b-poly(acrylic acid) Copolymers in Solutions, Macromolecules, 30 (1997) 1001-1011.

[36] J.-F. Gohy, H. Hofmeier, A. Alexeev, and U.S. Schubert, Aqueous Micelles from Supramolecular Graft Copolymers, Macromol. Chem. Phys., 204 (2003) 1524-1530.

[37] Y . Ogawa, M. Yamamoto, H. Okada, T. Yashiki and T.Shimamoto, A new technique of efficiently entrapped leuprolide acetate into microcapsules of polylactic acid or copoly(lactic / glycolic) acid Chem. Pharm. Bull., 36 (1988) 1095¯1103.

[38] N. Anton, J.-P. Benoit, and P. Saulnier, Design and production of nanoparticles formulated from nano-emulsion templates´ A review, J. Control. Release, 128 (2008) 185-199.

[39] P. Lemechko, E. Renard, J. Guezennec , C. Simon-Colin , and V. Langlois, Synthesis of dextran-graft-PHBHV amphiphilic copolymer using click chemistry approach, React. Funct. Polym. , 72 (2012) 487-494.

[40] F. T. Meng, G. H. Ma, W. Qiu and Z. G. Su, W /O/W double emulsion technique using ethyl acetate as organic solvent: effects of its diffusion rate on the characteristics of microparticles, J. Control Release, 91 (2003) 407-416.

[41] J .L. Cleland, M.F. Powell, and S.J. Shire, The development of stable protein formulation: A close look at protein aggregation, deamidation, and oxidation, Crit. Rev. Ther. Drug Carrier. Syst., 10 (1993) 307-377.

[42] J. Du, L. Fan, and Q. Liu, pH-Sensitive Block Copolymer Vesicles with Variable Trigger Points for Drug Delivery, Macromolecules, 45 (2012) 8275Б8283

[43] Z. Zhang, X. Chen, L. Chen, S. Yu, Y. Cao, C. He, and X. Chen, Intracellular pH-Sensitive PEG-block-Acetalated-Dextrans as Efficient Drug Delivery Platforms, Appl. Mater. Interfaces 5(2013) 10760Б10766.

[44] L. Ye, Z. Gao, Y. Zhou, X. Yin, X. Zhang, A. Zhang, and Z. Feng, A pH-sensitive binary drug delivery system based on poly(caprolactone)¯heparin conjugates, J. Biomed. Mater. Res. A, 102 (2014) 880-889.

[45] X. Guo, C. Shi, J. Wang, S. Di, and S. Zhou, pH-triggered intracellular release from actively targeting polymer micelles, Biomaterials, 34 (2013) 4544-4554.

[46] Y. Q. Yang, L.S. Zheng, X.D. Guo, Y. Qian, and L.J. Zhang, pH-Sensitive Micelles Self-Assembled from Amphiphilic Copolymer Brush for Delivery of Poorly Water-Soluble Drugs, Biomacromolecules, 12 (2011) 116-122.

[47] G. Chang, L. Yu, and J. Ding, A smart polymer for drug delivery sensitive to tumor extracellular pH, J. Control Release, 152 (2011) 1-132.

[48] L. Yang, J. Kuang, J. Wang, Z. Li, and L.M. Zhang, Loading and in vitro controlled release of indomethacin using amphiphilic cholesteryl-bearing carboxymethylcellulose derivatives, Macromol. Biosci., 8 (2008) 279-286.

[49] X. Huang, F. Du, J. Cheng, Y. Dong, D. Liang, S. Ji, S.-S. Lin and Z. Li, Acid-sensitive polymeric micelles based on thermoresponsive block copolymers with pendent cyclic orthoester groups, Macromolecules, 42 (2009) 783-790.

[50] R.P. Tang, W.H. Ji, and C. Wang, Amphiphilic block copolymers bearing ortho ester side-chains: pH-dependent hydrolysis and self-assembly in water, Macromol. Biosci., 10 (2010) 192-201.

[51] Y. Luo, A. Wang, J. Yuan, and Q. Gao, Preparation, characterization and drug release behavior of polyion complex micelles, Int. J. pharmaceut., 374 (2009) 139-144.

[52] Y. Wang, Y. Liu, Y. Liu, Y. Wang, J. Wu, R. Li, J. Yang, and N. Zhang, pH-sensitive pullulan-based nanoparticles for intracellular drug delivery, Polym. Chem., 5 (2014) 423.
[53] E. S. Gil and S.M. Hudson, Stimuli-reponsive polymers and their bioconjugates, Prog. Polym. Sci., 29 (2004) 1173-1222.
[54] H. Wei, S.-X. Cheng, X.-Z. Zhang, and R.-X. Zhuo, Thermo-sensitive polymeric micelles based on poly(N-isopropylacrylamide) as drug carriers, Prog. Polym. Sci., 34 (2009) 893-910.
[55] S. Tan, D. Zhao, D. Yuan, H. Wang, K. Tu, and L.-Q. Wanga, Influence of indomethacin-loading on the micellization and drug release of thermosensitive dextran-graft-poly(N-isopropylacrylamide), React. Funct. Polym., 71 (2011) 820-827.
[56] H.G. Schild, Poly(N-isopropylacrylamide): experiment, theory and application, Prog. Polym. Sci., 17 (1992) 163-249.
[57] M. Bagheri and S. Shateri, Thermosensitive nanosized micelles from cholesteryl-modified hydroxypropyl cellulose as a novel carrier of hydrophobic drugs, Iranian Polymer Journal, 21 (2012) 365-373.
[58] X.-L. Yang, Y.-L. Luo, F. Xu, and Y.-S. Chen, ThermosensitivemPEG-b-PA-g-PNIPAMComb Block Copolymer Micelles: Effect of Hydrophilic Chain Length and Camptothecin Release Behavior, Pharm. Res., 31 (2014) 291-304.
[59] Z. Wei, Q. Yu, and Z. Gan, Thermosensitive block copolymers PEG-b-PBEMAGG containing functional pendant amino groups, Macromol. Res., 20 (2012) 313-318.
[60] C. Choi, M.-K. Jang, and J.-W. Nah, Preparation and characterization of nanoparticles using poly(N-isopropylacrylamide)-poly(-caprolactone) and poly(ethylene glycol)-poly(-caprolactone) block copolymers with thermosensitive function, Macromol. Res., 15 (2007) 623-632.
[61] A. Zhao, S. Zhou, Q. Zhou, and T. Chen, Thermosensitive Micelles from PEG-Based Ether-anhydride Triblock Copolymers, Pharm. Res., 27 (2010) 1627-1643.
[62] Q. Wu, L. Wang, X. Fu, X. Song, Q. Yang, and G. Zhang, Synthesis and self-assembly of a new amphiphilic thermosensitive poly(N-vinylcaprolactam)/poly(e-caprolactone) block copolymer, Polym. Bull., 71 (2014) 1-18.
[63] F. Xu, T.-T. Yan, and Y.-L. Luo, Synthesis and micellization of thermosensitive PNIPAAm-b-PLA amphiphilic block copolymers based on a bifunctional initiator, Macromol. Res., 19 (2011) 1287-1295.
[64] X. Chen, X. Ding, Z. Zheng, and Y. Peng, Thermosensitive polymeric vesicles self-assembled by PNIPAAm-b-PPG-b-PNIPAAm triblock copolymers, Colloid. Polym. Sci., 283 (2005) 452-455.
[65] Y. Zhao, Light-Responsive Block Copolymer Micelles, Macromolecules, 45 (2012) 3647Б3657.
[66] F. Ercole, T. P. Davis, and R.A. Evans, Photo-responsive systems and biomaterials: photochromic polymers, light-triggered self-assembly, surface modification, fluorescence modulation and beyond, Polym. Chem., 1 (2010) 37-54.
[67] X. Tong, G. Wang, A. Soldera, and Y. Zhao, How Can Azobenzene Block Copolymer Vesicles Be Dissociated and Reformed by Light?, J. Phys. Chem. B, 109 (2005) 20281-20287.
[68] H. Lee, W. Wu, J. K. Oh, L. Mueller, G. Sherwood, L. Peteanu, T. Kowalewski, and K. Matyjaszewski, Light-Induced Reversible Formation of Polymeric Micelles, Angew. Chem., Int. Ed., 46 (2007) 2453Б2457.
[69] S.-J. Lim, C.-J. Carling, C. C. Warford, D. Hsiao, B. D. Gates, and N.R. Branda, Multifunctional photo- and thermo-responsive copolymer nanoparticles, Dyes Pigm., 89 (2011) 230Б235.

[70] Y. Wang, S. Lin, M. Zang, Y. Xing, X. He, J. Lin, and T. Chen, Self-assembly and photo-responsive behavior of novel ABC2-type block copolymers containing azobenzene moieties, Soft Matter., 8(2012) 3131¯3138.

[71] J. A. Pincock, Photochemistry of Arylmethyl Esters in Nucleophilic Solvents: Radical Pair and Ion Pair Intermediates, Acc. Chem. Res., 30 (1997) 43Б49.

[72] J. E. Beecher, J. F. Cameron, and J.M.J. Frechet, Photogeneration of polymeric amines: synthesis, photocrosslinking and photoimaging of copolymers containing photoactive carbamate pendant groups, J. Mater. Chem., 2 (1992) 811Б816.

[73] I. Aujard, C. Benbrahim, M. Gouget, O. Ruel, J.-B. Baudin, P. Neveu, and L. Jullien, o-Nitrobenzyl Photolabile Protecting Groups with Red-Shifted Absorption: Syntheses and Uncaging Cross-Sections for One- and Two-Photon Excitation, Chem.-Eur. J., 12 (2006) 6865Б6879.

[74] T. Furuta, S. S.-H. Wang, J. L. Dantzker, T. M. Dore, W. Bybee, E.M. Callaway, W. Denk, and R.Y. Tsien, Proc. Natl. Acad. Sci. U. S. A., 96 (1999) 1193Б1120.

[75] H. Zhao, E. S. Sterner, E. B. Coughlin, and P. Theato, o-Nitrobenzyl Alcohol Derivatives: Opportunities in Polymer and Materials Science, Macromolecules, 45 (2012) 1723Б1736.

[76] J. Cao, S. Huang, Y. Chen, S. Li, X. Li, D. Deng, Z. Qian, L. Tang, and Y. Gu, Near-infrared light-triggered micelles for fast controlled drug release in deep tissue, Biomaterials 34 (2013) 6272-6283.

[77] J.-M. Schumers, O. Bertrand, C.-A. Fustin, and J.-F. Gohy, Synthesis and Self-Assembly of Diblock Copolymers Bearing 2-Nitrobenzyl Photocleavable Side Groups, J. Polym. Sci. A: Polym. Chem., 50 (2012) 599-608.

[78] H. Yang, L. Jia, Z. Wang, A. Di-Cicco, D. Levy, and P. Keller, Novel Photolabile Diblock Copolymers Bearing Truxillic Acid Derivative Junctions, Macromolecules 44 (2011) 159-165.

[79] H. H. Huang, F. Q. Yan, Y. M. Kek, C. H. Chew, G. Q. Xu, W. Ji, P. S. Oh, and S.H. Tang, Synthesis, Characterization, and Nonlinear Optical Properties of Copper Nanoparticles, Langmuir, 13 (1997) 172-175.

[80] J. Lai, X. Mu, Y. Xu, X. Wu, C. Wu, C. Li, J. Chen, and Y. Zhao, Light-Responsive Nanogated Ensemble Based on Polymer Grafted Mesoporous Silica Hybrid Nanoparticles, Chem. Commun., 46 (2010) 7370-7372.

[81] O. Bertrand, J.-M. Schumers, C. Kuppan, J. Marchand-Brynaert, C.-A. Fustin, and J.-F. Gohy, Photo-induced micellization of block copolymers bearing 4,5-dimethoxy-2-nitrobenzyl side groups, Soft Matter, 7 (2011) 6891-6896.

[82] J. Jiang, X. Tong, D. Morris, and Y. Zhao, Toward Photocontrolled Release Using Light-Dissociable Block Copolymer Micelles, Macromolecules, 39 (2006) 4633-4640.

[83] W. Cui, X. Lu, K. Cui, J. Wu, Y. Wei, and Q. Lu, Photosensitive nanoparticles of chitosan complex for controlled release of dye molecules, Nanotechnology, 22 (2011) 65702-65711.

[84] J. Jiang, X. Tong, and Y. Zhao, A New Design for Light-Breakable Polymer Micelles, J. Am. Chem. Soc. , 127 (2005) 8290-8291.

[85] J. Babin, M. Pelletier, M. Lepage, J. F. Allard, D. Morris, and Y. Zhao, A New Two-Photon-Sensitive Block Copolymer Nanocarrier, Angew. Chem., Int. Ed., 48 (2009) 3329Б3332.

[86] S. Kumar, J.-F. Allard, D. Morris, Y. L. Dory, M. Lepage, and Y. Zhao, Near-infrared light sensitive polypeptide block copolymer micelles for drug delivery, J. Mater. Chem., 22 (2012) 7252-7257.

[87] M. Kang and B. Moon, Synthesis of Photocleavable Poly(styrene-block-ethylene oxide) and Its Self-Assembly into Nanoporous Thin Films, Macromolecules, 42 (2009) 455-458.

[88] E. Cabane, V. Malinova, and W. Meier, Synthesis of Photocleavable Amphiphilic Block Copolymers: Toward the Design of Photosensitive Nanocarriers, Macromol. Chem. Phys., 211 (2010) 1847-1856.

[89] J.-M. Schumers, J.-F. Gohy, and C.-A. Fustin, A versatile strategy for the synthesis of block copolymers bearing a photocleavable junction, Polym. Chem., 1 (2010) 161-163.

[90] J. S. Katz, S. Zhong, B. G. Ricart, D. J. Pochan, D. A. Hammer, and J.A. Burdick, Modular Synthesis of Biodegradable Diblock Copolymers for Designing Functional Polymersomes, J. Am. Chem. Soc. , 132 (2010) 3654-3655.

[91] D. Han, X. Tong, and Y. Zhao, Fast Photodegradable Block Copolymer Micelles for Burst Release, Macromolecules, 44 (2011) 437-439.

[92] D. Han, X. Tong, and Y. Zhao, Block Copolymer Micelles with a Dual-Stimuli-Responsive Core for Fast or Slow Degradation, Langmuir, 28 (2012) 2327Б2331.

[93] A. Guo, G. Liu, and J. Tao, Star Polymers and Nanospheres from Cross-Linkable Diblock Copolymers, Macromolecules, 29 (1996) 2487-2493.

[94] K. B. Thurmond II, T. Kowalewski, and K.L. Wooley, Water-Soluble Knedel-like Structures: The Preparation of Shell-Cross-Linked Small Particles, J. Am. Chem. Soc. , 118 (1996) 7239-7240.

[95] S. R. Trenor, A. R. Shultz, B. J. Love, and T.E. Long, Coumarins in Polymers: From Light Harvesting to Photo-Cross-Linkable Tissue Scaffolds, Chem. Rev. , 104 (2004) 3059-3077.

[96] J. Jiang, B. Qi, M. Lepage, and Y. Zhao, Polymer Micelles Stabilization on Demand through Reversible Photo-Cross-Linking, Macromolecules, 40 (2007) 790-792.

[97] D. Dax, C. Xu, O. Langvik, J. Hemming, P. Backman, and S. Willfor, Synthesis of SET¯LRP-Induced Galactoglucomannan-Diblock Copolymers, J. Polym. Sci. A Polym. Chem., 51 (2013) 5100-5110.

[98] J. Luo, Q. Zhou, J. Sun, J. Jiang, X. Zhou, H. Zhang, and X. Liu, Photoresponsive Water-Dispersible Polyaniline Nanoparticles Through Template Synthesis with Copolymer Micelle Containing Coumarin Groups, J. Polym. Sci. A Polym. Chem., 50 (2012) 4037-4045.

[99] J. Motoyanagi, I. Nishimura, and M. Minoda, Living Cationic Polymerization of a Coumarin-Substituted Vinyl Ether and Reversible Photoinduced Crosslinking of the Resulting Homopolymers and Amphiphilic Block Copolymers, J. Polym. Sci. A Polym. Chem., 49 (2011) 4701-4707.

[100] R. Cheng , F. Meng , C. Deng , H.-A. Klok, and Z. Zhong, Dual and multi-stimuli responsive polymeric nanoparticles for programmed site-specific drug delivery, Biomaterials, 34 (2013) 3647-3657.

[101] K.S. Soppimath, D.C.W. Tan, and Y.Y. Yang, pH-triggered thermally responsive polymer core-shell nanoparticles for drug delivery, Adv. Mater., 17 (2005) 318-323.

[102] L. Meng, W. Huang, D. Wang, X. Huang, X. Zhu, and D. Yan, Chitosan-Based Nanocarriers with pH and Light Dual Response for Anticancer Drug Delivery, Biomacromolecules, 14 (2013) 2601Б2610.

[103] Q. Jin, C. Luy, J. Ji, and S. Agarwal, Design and Proof of Reversible Micelle-To-Vesicle Multistimuli-Responsive Morphological Regulations, J. Polym. Sci. A Polym. Chem., 50 (2012) 451-457.

[104] L. Lin, Z. Yan, J. Gu, Y. Zhang, Z. Feng, and Y. Yu, UV-Responsive Behavior of Azopyridine-Containing Diblock Copolymeric Vesicles: Photoinduced Fusion, Disintegration and Rearrangement, Macromol. Rapid Commun., 30 (2009) 1089-1093.
[105] J. Wei, Z. Yan, L. Lin, J. Gu, Z. Feng, and Y. Yu, Photo/pH dual-responsive behavior of azopyridine-containing copolymer vesicles, React. Funct. Polym., 73 (2013) 1009-1014.
[106] E. Blasco, B. V. K. J. Schmidt, C. Barner-Kowollik, M. Pinol, and L. Oriol, Dual thermo- and photo-responsive micelles based on miktoarm star polymers, Polym. Chem., 4 (2013) 4506¯4514.
[107] G.X. Pan, Z. Feng, J. Wei, and Y.L. Yu, Synthesis and Self-assembly Behavior of a Thermo-/photo-dual Responsive Triblock Copolymer, Acta Chimica Sinica, 71 (2013) 733-738.
[108] G. Huang, J. Zhu, Z. Zhang, W. Zhang, N. Zhou, and X. Zhu, Reversible Photo- and Thermo-Responsive Block Copolymer Micelles Functionalized by NIPAM and Azobenzene, J. Macromol. Sci., A 50 (2013) 193-199.
[109] W. Yuan, W. Guo, H. Zou, and J. Ren, Tunable thermo-, pH- and light-responsive copolymer micelles, Polym. Chem., 4 (2013) 3934-3937.
[110] T. Otsu and M. Yoshida, Role of initiator-transfer agent-terminator (iniferter) in radical polymerizations: Polymer design by organic disulfides as iniferters, Die Makromolekulare Chemie, Rapid Communications, 3 (1982) 127-132.
[111] T. Otsu, M. Yoshida, and T. Tazaki, A model for living radical polymerization, Die Makromolekulare Chemie, Rapid Communications, 3 (1982) 133-140.
[112] S. David H, R. Ezio, and C. Paul, Patent US 4581429 (1986).
[113] M. K. Georges, R. P. N. Veregin , P. M. Kazmaier, and G.K. Hamer, Narrow molecular weight resins by a free-radical polymerization process, Macromolecules 26 (1993) 2987-2988.
[114] J. F. Quinn, R. P. Chaplin, and T.P. Davis, Facile Synthesis of Comb, Star, and Graft Polymers via Reversible Addition¯Fragmentation Chain Transfer (RAFT) Polymerization, J. Polym. Sci. A Polym. Chem., 40 (2002) 2956¯2966
[115] A. Vora, K. Singh, and D.C. Webster, A new approach to 3-miktoarm star polymers using a combination of reversible addition¯fragmentation chain transfer (RAFT) and ring opening polymerization (ROP) via ::Click˜˜ chemistry, polymer, 50 (2009) 2768¯2774.
[116] S. Perrier and P. Takolpuckdee, Macromolecular Design via Reversible Addition¯Fragmentation Chain Transfer (RAFT)/Xanthates (MADIX) Polymerization, J. Polym. Sci. A Polym. Chem., 43 (2005) 5347¯5393.
[117] Rhodia Chimie invs., P. Corpart, D. Charmot , T. Biadatti, S. Z. Zard, and D. Michelet, WO. 9858974, (1998).
[118] J. Chiefari, R. T. A. Mayadunne, C. L. Moad, G. Moad, E. Rizzardo, A. Postma, M. A. Skidmore, and S.H. Thang, Thiocarbonylthio Compounds (SdC(Z)S-R) in Free Radical Polymerization with Reversible Addition-Fragmentation Chain Transfer (RAFT Polymerization). Effect of the Activating Group Z, Macromolecules, 36 (2003) 2273-2283.
[119] J. Schumers, C. Fustin, A. Can, R. Hoogenboom, U.S. Schubert, and J.-F. Gohy, Are o-Nitrobenzyl (Meth)acrylate Monomers Polymerizable by Controlled-Radical Polymerization?, J. Polym. Sci. A Polym. Chem., 47 (2009) 6504-6513.
[120] C. C. Price and D.A. Durham, The Polymerization of Styrene in the Presence of Nitrobenzene, 2,4-Dinitrochlorobenzene and Nitromethane, J. Am. Chem. Soc., 65 (1943) 757-759.
[121] G. S. Hammond and P. D. Bartlett, Polymerization of allyl compounds. V. Inhibition by nitro compounds, J. Polym. Sci. Part A: Polym. Chem., 6 (1951) 617-624.

[122] J. Nicolasa, Y. Guillaneufb, C. Lefayb, D. Bertinb, D. Gigmesb, and B. Charleuxc, Nitroxide-mediated polymerization, Prog. Polym. Sci., 38 (2013) 63˜235.
[123] M. K. Georges, P. G. Odell, N. A. Listigovers, and M.H. Quinlan, Solvent-Free Stable Free Radical Polymerization: Understanding and Applications, ACS Symp. Ser., 713 (1998) 80-95.
[124] D. Benoit, V. Chaplinski, R. Braslau, and C. Hawker, Development of a universal alkoxyamine for "living" free radical polymerizations, J. Am. Chem. Soc., 121 (1999) 3904-3920.
[125] D. Benoit, S. Grimaldi, S. Robin, J. P. Finet, P.G. Tordo and Y. nanou, Kinetics and mechanism of controlled free-radical polymerization of styrene and n-butyl acrylate in the presence of an acyclic beta-phosphonylated nitroxide, J. Am. Chem. Soc., 122 (2000) 5929-5939.
[126] M. K. Georges, J. L. Lukkarila, A. R. Szkurhan, TEMPO-Mediated n-Butyl Acrylate Polymerizations, Macromolecules, 37 (2004) 1297-1303.
[127] L. Couvreur, C. Lefay, J. Belleney, B. Charleux, O. Guerret and S. Magnet, First nitroxide-mediated controlled free-radical polymerization of acrylic acid, Macromolecules, 36 (2003) 8260-8267.
[128] M. Kamigaito, T. Ando and M. Sawamoto, Metal-catalyzed living radical polymerization, Chem. Rev., 101 (2001) 3689-3745.
[129] Y. Kabachii , S. Kochev , L. Bronstein , I. Blagodatskikh and P. Valetsky, Atom transfer radical polymerization with Ti(III) halides and alkoxides, Polym. Bull., 50 (2003) 271˜278.
[130] J. Brandts , P. van de Geijn , E. van Faassen , J. Boersma and G. Van Koten Controlled radical polymerization of styrene in the presence of lithium molybdate(v) complexes and benzylic halides, J. Organomet. Chem., 584 (1999) 246˜253.
[131] S. Maria, F. Stoffelbach, J. Mata , J.C. Daran , P. Richard , and R. Poli, The radical trap in atom transfer radical polymerization need not be thermodynamically stable. A study of the $MoX_3(PMe_3)_3$ catalysts , J. Am. Chem. Soc., 127 (2005) 5946˜5956.
[132] Y. Kotani , M. Kamigaito and M. Sawamoto Re(V)-mediated living radical polymerization of styrene:1 $ReO_2I(PPh_3)_2$/R-I initiating systems., Macromolecules, 32 (1999) 2420˜2424.
[133] K. Matyjaszewski, M. Wei, J. Xia, and N. McDermott, Controlled/::living˘˘ radical polymerization of styrene and methyl methacrylate catalyzed by iron complexes., Macromolecules, 30 (1997) 8161˜8164.
[134] M. Kato, M. Kamigaito, M. Sawamoto, and T. Higashimura, Polymerization of methyl methacrylate with the carbon tetrachloride/dichlorotris- (triphenylphosphine) ruthenium(II)/methylaluminum bis(2,6-di-tert-butylphenoxide) initiating system: possibility of living radical polymerization., Macromolecules, 28 (1995) 1721˜1723.
[135] W. Braunecker, Y. Itami and K. Matyjaszewski, Osmium mediated radical polymerization, Macromolecules, 38 (2005) 9402˜9404.
[136] V. Percec, B. Barboiu , A. Neumann , J. Ronda and M. Zhao, Metal-catalyzed ::living˘˘ radical polymerization of styrene initiated with arenesulfonyl chlorides. From heterogeneousto homogeneous catalysis, Macromolecules, 29 (1996) 3665˜3668.
[137] B. Wang , Y. Zhuang , X. Luo , S. Xu , and X. Zhou, Controlled/ ::living˘˘ radical polymerization of MMA catalyzed by cobaltocene, Macromolecules, 36 (2003) 9684˜9686.
[138] H. Uegaki, Y. Kotani, M. Kamigaito and M. Sawamoto Nickel-mediated living radical polymerization of methyl methacrylate, Macromolecules, 30 (1997) 2249˜2253.

[139] P. Lecomte , I. Drapier, P. Dubois , P. Teyssie , and R. Jerome, Controlled radical polymerization of methyl methacrylate in the presence of palladium acetate, triphenylphosphine, and carbon tetrachloride, Macromolecules, 30 (1997) 7631¯7633.
[140] J.S. Wang and K. Matyjaszewski, Controlled/::living˘˘ radical polymerization. atom transfer radical polymerization in the presence of transition-metal complexes., J. Am. Chem. Soc., 117 (1995) 5614¯5.
[141] W. A. Braunecker and K. Matyjaszewski, Controlled/living radical polymerization: Features, developments, and perspectives, Prog. Polym. Sci., 32 (2007) 93¯146.
[142] Y. Inoue and K. Matyjaszewski, New amine-based tripodal copper catalysts for atom transfer radical polymerization., Macromolecules, 37 (2004) 4014¯4021.
[143] W. Tang and K. Matyjaszewski, Effect of Ligand Structure on Activation Rate Constants in ATRP, Macromolecules, 39 (2006) 4953-4959.
[144] W. Tang and K. Matyjaszewski, Effects of Initiator Structure on Activation Rate Constants in ATRP, Macromolecules, 40 (2007) 1858-1863.
[145] W. Jakubowski and K. Matyjaszewski, Activator generated by electron transfer for atom transfer radical polymerization., Macromolecules, 38 (2005) 4139¯4146.
[146] K. Min, H. Gao and K. Matyjaszewski, Preparation of homopolymers and block copolymers in miniemulsion by ATRP using activators generated by electron transfer (AGET). J. Am. Chem. Soc., 127 (2005) 3825¯3830.
[147] H. Tang, M. Radosz, and Y. Shen, CuBr2/N,N,N0,N0-tetra[(2-pyridal)methyl] ethylenediamine/tertiary amine as a highly active and versatile catalyst for atom-transfer radical polymerization via activator generated by electron transfer, Macromol. Rapid Commun., 27 (2006) 1127¯1131.
[148] A. Simakova, S. E. Averick, D. Konkolewicz, and K. Matyjaszewski, Aqueous ARGET ATRP, Macromolecules, 45 (2012) 6371Б6379.
[149] H. Dong and K. Matyjaszewski, ARGET ATRP of 2-(Dimethylamino)ethyl Methacrylate as an Intrinsic Reducing Agent, Macromolecules, 41 (2008) 6868-6870.
[150] X.h. Liu, J. Wang, F.j. Z., S.l. An, Y.l. Ren, Y.h. Yu, P. Chen, and S. Xie, Copper-Mediated Initiators for Continuous Activator Regeneration Atom Transfer Radical Polymerization of Acrylonitrile, J. Polym. Sci. A Polym. Chem., 50 (2012) 4358¯4364.
[151] D. Konkolewicz, A. J. D. Magenau, S. E. Averick, A. Simakova, H. He, and K. Matyjaszewski, ICAR ATRP with ppm Cu Catalyst in Water, Macromolecules, 45 (2012) 4461Б4468.
[152] Y. Zhang, Y. Wang and K. Matyjaszewski, ATRP of Methyl Acrylate with Metallic Zinc, Magnesium, and Iron as Reducing Agents and Supplemental Activators, Macromolecules, 44 (2011) 683¯685.
[153] Y. Zhang, Y. Wang, C. Peng, M. Zhong, W. Zhu, D. Konkolewicz, and K. Matyjaszewski, Copper-Mediated CRP of Methyl Acrylate in the Presence of Metallic Copper: Effect of Ligand Structure on Reaction Kinetics, Macromolecules, 45 (2012) 78Б86.
[154] A. J. D. Magenau, N. Bortolamei, E. Frick, S. Park, A. Gennaro, and K. Matyjaszewski, Investigation of Electrochemically Mediated Atom Transfer Radical Polymerization, Macromolecules, 46 (2013) 4346Б4353.
[155] S. Park, H. Y. Cho, K. B. Wegner, J. B. Andrew, J. D. Magenau, H.j. Paik, S. Jurga and K. Matyjaszewski, Star Synthesis Using Macroinitiators via Electrochemically Mediated Atom Transfer Radical Polymerization, Macromolecules, 46 (2013) 5856Б5860.

[156] D. Konkolewicz, K. Schröder, J. Buback, S. Bernhard, and K. Matyjaszewski, Visible Light and Sunlight Photoinduced ATRP with ppm of Cu Catalyst, ACS Macro Lett., 1 (2012) 1219Б1223.

[157] J. Yan, B. Li, F. Zhou, and W. Liu, Ultraviolet Light-Induced Surface-Initiated Atom-Transfer Radical Polymerization, ACS Macro Lett., 2 (2013) 592Б596.

[158] F. Minisci, Free-radical additions to olefins in the presence of redox systems, Acc. Chem. Res., 8 (1975) 165-171.

[159] A. E. Feiring, E. R. Wonchoba, F. Davidson, V. Percec, and B. Barboiu, The phenomena reported by Minisci were later observed in attempts to perform the Cu(0) catalyzed living radical copolymerization tetrafluoroethylene (TFE) and hexafluoropropylene (HFP) initiated with perfluoroalkylsulfonyl halides in steel reactors., J. Polym. Sci. A Polym. Chem., 38 (2000) 3313.

[160] B. M. Rosen and V. Percec, Single-Electron Transfer and Single-Electron Transfer Degenerative Chain Transfer Living Radical Polymerization, Chem. Rev., 109 (2009) 5069¯5119.

[161] M. Tamba, K. Dajka, C. Ferrerri, K. D. Asmus, and C. Chatgiliaoglu, One-Electron Reduction of Methanesulfonyl Chloride. The Fate of $MeSO_2Cl^{\cdot-}$ and $MeSO_2^{\cdot}$ Intermediates in Oxygenated Solutions and Their Role in the Cis-Trans Isomerization of Mono-unsaturated Fatty Acids, J. Am. Chem. Soc., 129 (2007) 8716.

[162] V. Percec, A. V. Popov, E. Ramirez-Castillo and O. Weichold, Living Radical Polymerization of Vinyl Chloride Initiated with Iodoform and Catalyzed by Nascent Cu0/Tris(2-aminoethyl)amine or Polyethyleneimine in Water at 25 °C Proceeds by a New Competing Pathways Mechanism, J. Polym. Sci. A Polym. Chem., 41 (2003) 3283-3299.

[163] V. Percec, A. V. Popov, E. Ramirez-Castillo, and O. Weichold, Acceleration of the Single Electron Transfer¯Degenerative Chain Transfer Mediated Living Radical Polymerization (SET¯DTLRP) of Vinyl Chloride in Water at 25 °C, J. Polym. Sci. A Polym. Chem., 42 (2004) 6364-6374

[164] J. F. J. Coelho, E. Y. Carvalho, D. S.Marques, A. V. Popov, V. Percec, P. M. F. O. Gonçalves, and M.H. Gil, Synthesis of Poly(ethyl acrylate) by Single Electron Transfer-Degenerative Chain Transfer Living Radical Polymerization in Water Catalyzed by $Na_2S_2O_4$, J. Polym. Sci., A: Polym. Chem., 46 (2008) 421.

[165] J. F. J. Coelho, A. M. F. P. Silva, A. V. Popov, V. Percec, M. V. Abreu, P. M. O. F. Gonçalves, and M. H. Gil, Single Electron Transfer¯Degenerative Chain Transfer Living Radical Polymerization of N-Butyl Acrylate Catalyzed by $Na_2S_2O_4$ in Water Media, J. Polym. Sci., A: Polym. Chem., 44 (2006) 2809.

[166] J. F. J. Coelho, E. Y. Carvalho, D. S.Marques, A. V. Popov, V. Percec, and M.H. Gil, InZuence of the Isomeric Structures of Butyl Acrylate on Its Single-Electron Transfer-Degenerative Chain Transfer Living Radical Polymerization in Water Catalyzed by $Na_2S_2O_4$, J. Polym. Sci., A.: Polym. Chem., 46 (2008) 6542-6551.

[167] V. Percec, E. Ramierez-Castillo, A. V. Popov, L. A. Hinojosa-Falcon and T. Guliashvili, Ultrafast Single-Electron-Transfer/Degenerative-Chain- Transfer Mediated Living Radical Polymerization of Acrylates Initiated with Iodoform in Water at Room Temperature and Catalyzed by Sodium Dithionite, J. Polym. Sci., A: Polym. Chem., 43 (2005) 2178-2184.

[168] J. F. J. Coelho, E. Y. Carvalho, D. S.Marques, A. V. Popov, V. Percec, and M.H. Gil, Synthesis of Poly(lauryl acrylate) by Single-Electron Transfer/Degenerative Chain Transfer Living Radical Polymerization Catalyzed by $Na_2S_2O_4$ in Water, Macromol. Chem. Phys., 208 (2007) 1218-1227.

[169] J. F. J.Coelho, J. Gois, A. C. Fonseca, R. A. Carvalho, A. V. Popov, V. Percec, and M.H. Gil, Synthesis of Poly(2-methoxyethyl acrylate) by Single Electron Transfer´ Degenerative Transfer Living Radical Polymerization Catalyzed by $Na_2S_2O_4$ in Water, J. Polym. Sci., A: Polym. Chem., 47 (2009) 4454.

[170] V. Percec, A. V. Popov, E. Ramierez-Castillo, and J.F.J. Coelho, Single Electron Transfer¯ Degenerative Chain Transfer Mediated Living Radical Polymerization (SET¯DTLRP) of Vinyl Chloride Initiated with Methylene Iodide and Catalyzed by Sodium Dithionite, J. Polym. Sci., A: Polym. Chem., 43 (2005) 773-778.

[171] M. J. Sienkowska and V. Percec, Synthesis of ,≪Di(iodo)PVC and of Four-Arm Star PVC with Identical Active Chain Ends by SET-DTLRP of VC Initiated with Bifunctional and Tetrafunctional Initiators J. Polym. Sci., A: Poylm. Chem. , 47 (2009) 635-652.

[172] J.F.J. Nuno Rocha, P. M.L. Coelho, B.B. Cardoso, M. G. Pedro , M.H. Gil, and J.T. Guthrie, Synthesis of Amphiphilic PVC-b-Poly(hydroxypropyl acrylate) (PHPA)-b-PVC Block Copolymers With Low PHPA Contents and Different Molecular Weights by (Single Electron Transfer)´ (Degenerative Chain Transfer) Living Radical Polymerization, J. Vinyl Addit. Technol., (2013) 158-167.

[173] V. Percec, T. Guliashvili, A. V. Popov and E. Ramirez-Castillo, Synthesis of Poly(methyl methacrylate)-b-Poly(vinyl chloride)-b-Poly(methyl methacrylate) Block Copolymers by CuCl/2,2-Bipyridine-Catalyzed Living Radical Block Copolymerization Initiated from Di(iodo)poly(vinyl chloride) Prepared by Single-Electron-Transfer/Degenerative-Chain-Transfer Mediated Living Radical Polymerization, J. Polym. Sci., A: Polym. Chem., 43 (2005) 1478-1486.

[174] W. Wang, J. Zhao, W. Zhang, J. Zhu, Z. Zhang, and X. Zhu, Ligand-Free SET-DTLRP of MMA at Room Temperature, J. Polym. Sci. A Polym. Chem., 51 (2013) 1872¯1879.

[175] N. H. Nguyen and V. Percec, Disproportionating Versus Nondisproportionating Solvent Effect in the SET-LRP of Methyl Acrylate During Catalysis with Nonactivated and Activated Cu(0) Wire, J. Polym. Sci. A Polym. Chem., 49 (2011) 4227¯4240.

[176] V. Percec, T. Guliashvili, J. S. Ladislaw, A. Wistrand, A. Stjerndahl, M. J. Sienkowska, M. J. Monteiro, and S. Sahoo, Ultrafast Synthesis of Ultrahigh Molar Mass Polymers by Metal-Catalyzed Living Radical Polymerization of Acrylates, Methacrylates, and Vinyl Chloride Mediated by SET at 25 °C, J. Am. Chem. Soc., 128 (2006) 14156-14165.

[177] T. Pintauer, B. McKenzie, and K. Matyjaszewski, In Advances in Controlled/Living Radical Polymerization, Am. Chem. Soc. , (2003) 130¯147.

[178] X.H. Liu, Y.H. Y., D. Jia, B.W. C., F.J. Zhang, H.N. Li, P. C., and S. Xie, In Situ Cu(0)-Mediated Single Electron Transfer Living Radical Polymerization of Methyl Methacrylate Using Nickel Powder, J. Polym. Sci. A Polym. Chem., 51 (2013) 1559¯1564.

[179] D. Liu, H. Chen, P. Yin, N. Ji, G. Zong, and R. Qu, Synthesis of Polyacrylonitrile by Single-Electron Transfer-Living Radical Polymerization Using Fe(0) as Catalyst and Its Adsorption Properties after Modification, J. Polym. Sci. A Polym. Chem., 49 (2011) 2916-2923

[180] G. Wang and M. Lu, Fe-mediated SET-LRP of MMA and St in the presence of air, Polym Int 61 (2012) 1279¯1283.

[181] H. Chen, G. Zong, L. Chen, M. Zhang, C. Wang, and R. Qu, Samarium Powder as Catalyst for SET-LRP of Acrylonitrile in 1,1,1,3,3,3-Hexafluoro-2-propanol for Control of Molecular Weight and Tacticity, J. Polym. Sci. A Polym. Chem., 49 (2011) 2924-2930.

[182] D. Liu, J. Ma, H. Chen, P. Yin, N. Ji, and G. Zong, Single Electron Transfer-Living Radical Polymerization of Methyl Methacrylate Catalyzed by Ytterbium Powder, J. Polym. Sci. A Polym. Chem., 49 (2011) 5109¯5115.

[183] Z. Hao, H. Chen, D. Liu, and L. Fan, SET-LRP of Acrylonitrile Catalyzed by Tin Powder, J. Polym. Sci. A Polym. Chem., 50 (2012) 4995-4999.

[184] Z. Hao, J. Zhang, H. Chen, D. Liu, D. Wang, H. Qu, and J. Lang, Preparation of Polyacrylonitrile via SET-LRP Catalyzed by Lanthanum Powder in the Presence of VC, J. Polym. Sci. A Polym. Chem., 51 (2013) 4088-4094.

[185] J. Voepel, U. Edlund, and A.C. Albertsson, A Versatile Single-Electron-Transfer Mediated Living Radical Polymerization Route to Galactoglucomannan Graft-Copolymers with Tunable Hydrophilicity, J. Polym. Sci. A Polym. Chem., 49 (2011) 2366-2372.

[186] N. H. Nguyen, B. M. Rosen, and V. Percec, SET-LRP of N,N-Dimethylacrylamide and of N-Isopropylacrylamide at 25 °C in Protic and in Dipolar Aprotic Solvents, J. Polym. Sci. A Polym. Chem., 48 (2010) 1752-1763.

[187] T. Hatano, B. M. Rosen, and V. Percec, SET-LRP of Vinyl Chloride Initiated with CHBr3 and Catalyzed by Cu(0)-Wire/TREN in DMSO at 25 °C, J. Polym. Sci. A Polym. Chem., 48 (2010) 164-172.

[188] N. Haridharan, K. Ponnusamy, and R. Dhamodharan, Controlled Polymerization of Methacrylates at Ambient Temperature Using Trithiocarbonate Chain Transfer Agents via SET-RAFT¯ Cyclohexyl Methacrylate: A Model Study, J. Polym. Sci. A Polym. Chem., 48 (2010) 5329-5338.

[189] S. Fleischmann and V. Percec, Copolymerization of Methacrylic Acid with Methyl Methacrylate by SET-LRP, J. Polym. Sci. A Polym. Chem., 48 (2010) 4884-4888.

[190] N.H. Nguyen and V. Percec, Dramatic Acceleration of SET-LRP of Methyl Acrylate During Catalysis with Activated Cu(0) Wire, J. Polym. Sci. A Polym. Chem., 48 (2010) 5109-5119.

[191] H. W. Richardson, Copper Compounds; Wiley-VCH Verlag GmbH & Co. KGaA: Weinheim, Germany, (2000).

[192] D. P. Gregory and A.C. Riddiford, Dissolution of Copper in Sulfuric Acid Solutions J Electrochem Soc, 107 (1960) 950-956.

[193] C. K. Ko and W.G. Lee, Effects of pH variation in aqueous solutions on dissolution of copper oxide, Surf Interface Anal 42 (2010) 1128-1130.

[194] N. H. Nguyen and V. Percec, Acid Dissolution of Copper Oxides as a Method for the Activation of Cu(0) Wire Catalyst for SET-LRP, J. Polym. Sci. A Polym. Chem., 49 (2011) 4241-4252.

[195] N. H. Nguyen, B. M. Rosen, G. Lligadas, and V. Percec, Surface-Dependent Kinetics of Cu(0)-Wire-Catalyzed Single-Electron Transfer Living Radical Polymerization of Methyl Acrylate in DMSO at 25 °C, Macromolecules, 42 (2009) 2379-2386.

[196] S. Monge, V. Darcos, and D.M. Haddleton, Effect of DMSO Used as Solvent in Copper Mediated Living Radical Polymerization, J. Polym. Sci. A Polym. Chem., 42 (2004) 6299 - 6308.

[197] N. H. Nguyen, B. M. Rosen, X. Jiang, S. Fleischmann, and V. Percec, New Efficient Reaction Media for SET-LRP Produced from Binary Mixtures of Organic Solvents and H_2O, J. Polym. Sci. A Polym. Chem., 47 (2009) 5577-5590.

[198] S.R. Samanta, A. Anastasaki, C. Waldron, D.M. Haddleton, and V. Percec, SET-LRP of methacrylates in fluorinated alcohols, Polym. Chem., 4 (2013) 5563-5569.

[199] S. R. Samanta and V. Percec, Synthesis of high molar mass poly(n-butyl acrylate) and poly(2-ethylhexyl acrylate) by SET-LRP in mixtures of fluorinated alcohols with DMSO, Polym. Chem., 5 (2014) 169¯174.

[200] C. Waldron, Q. Zhang, Z. Li, V. Nikolaou, G. Nurumbetov, J. Godfrey, R. McHale, G. Yilmaz, R. K. Randev, M. Girault, K. McEwan, D. M. Haddleton, M. Droesbeke, A. J. Haddleton, P. Wilson, A. Simula, J. Collins, D. J. Lloyd, J. A. Burns, C. Summers, C. Houben, A. Anastasaki, M. Li, C. R. Becer, J. K. Kiviaho, and N. Risangud, Absolut `copper catalyzation perfected_; robust living polymerization of NIPAM: Guinness is good for SET-LRP, Polym. Chem., 5 (2014) 57-61.

[201] V. Percec and C. Grigoras, Catalytic Effect of Ionic Liquids in the Cu_2O/2,2-bipyridine Catalyzed Living Radical Polymerization of Methyl Methacrylate Initiated with Arenesulfonyl Chlorides, J. Polym. Sci. A Polym. Chem., 43 (2005) 5609-5619.

[202] J. Ma, H. Chen, M. Zhang and M. Yu, SET-LRP of Acrylonitrile in Ionic Liquids Without Any Ligand, J. Polym. Sci. A Polym. Chem., 50 (2012) 609-613.

[203] H. S. Sundaram and D. Raghavachari, Controlled Radical Polymerization of tert-Butyl Acrylate at Ambient Temperature: Effect of Initiator Structure and Synthesis of Amphiphilic Block Copolymers, J. Polym. Sci. A Polym. Chem., 50 (2012) 996-1007.

[204] X. Hu, J. Li, H. Li, and Z. Zhang, Cu(0)/2,6-Bis(imino)pyridines Catalyzed Single-Electron Transfer-Living Radical Polymerization of Methyl Methacrylate Initiated with Poly(vinylidene fluoride-co-chlorotrifluoroethylene), J. Polym. Sci. A Polym. Chem., 51 (2013) 4378-4388.

[205] F. A. Cotton and G. Wilkinson, Advanced Inorganic Chemistry, 3rd ed.; John Wiley & Sons: New York (1970) p 905.

[206] B. M. Rosen and V. Percec, A Density Functional Theory Computational Study of the Role of Ligand on the Stability of CuI and CuII Species Associated with ATRP and SET-LRP, J. Polym. Sci. A Polym. Chem., 45 (2007) 4950-4964.

[207] B. M. Rosen, C. X. Jiang, J. Wilson, N. H. Nguyen, M. J. Monteiro, and V. Percec, The Disproportionation of Cu(I)X Mediated by Ligand and Solvent into Cu(0) and $Cu(II)X_2$ and Its Implications for SET-LRP, J. Polym. Sci. A Polym. Chem., 47 (2009) 5606-5628.

[208] W. Ren, L. Jiang, W. Wang, and Y. Dan, The Application of Copper(II) Deactivator on the Single-Electron Transfer Living Radical Polymerization of tert-Butyl Acrylate, J. Polym. Sci. A Polym. Chem., 48 (2010) 2793-2797

[209] M. E. Levere, I. Willoughby, S. O¯Donohue, A. de Cuendias, A. J. Grice, C. Fidge, C. R. Becera, and D.M. Haddleton, Assessment of SET-LRP in DMSO using online monitoring and Rapid GPC, Polym. Chem., 1 (2010) 1086-1094.

[210] G. Lligadas and V. Percec, SET-LRP of Acrylates in the Presence of Radical Inhibitors, J. Polym. Sci. A Polym. Chem., 46 (2008) 3174-3181.

[211] D. M. Haddleton, A. J. Clark, M. C. Crossman, D. J. Duncalf, A. M. Heming, S. R. Morsley, and A.J. Shooter, Atom transfer radical polymerisation (ATRP) of methyl methacrylate in the presence of radical inhibitors, Chem. Commun., 13 (1997) 1173-1174.

Chapter (II)

Light-sensitive amphiphilic glycopolymers

I. Introduction

Through this chapter, we will discuss the synthesis of light-sensitive grafted and diblock amphiphilic glycopolymers. These light-sensitive glycopolymers will be obtained by the `grafting onto_ approach developed recently at LCPM[1-6]. More precisely, in the framework of this Ph.D., such glycopolymers are composed from two parts:

(a) Hydrophilic polysaccharide part. We chose dextran because it is one natural polysaccharide that is soluble in water and some organic solvents like DMSO. Moreover, dextran is biodegradable and biocompatible and it can be transformed in vivo by dextranase into sugars of low molecular weight as glucose [7].

(b) Hydrophobic polyacrylate part. More precisely, we selected poly(2-nitrobenzyl acrylate) (PNBA) having photolabile 2-nitrobenzyl groups. These groups can be photo-cleaved by one photon absorption and also through two-photon absorption of near infrared (NIR) light (~700¯ 1000 nm), that is particularly attractive for biomedical applications.

As shown in Scheme 1, formation of such amphiphilic grafted and diblock glycopolymers involves many steps. In the first step, we optimized the conditions to control the radical polymerization of 2-nitrobenzyl acrylate (NBA) to produce PNBA-Br. Then, the bromide end-function will be modified by introducing azide group (synthesis of PNBA-N_3). In the second step, we carried out the modification of dextran by introducing several alkyne groups all long the dextran chain. In a parallel way, dextran was modified to introduce only one group at its reducing-end. In the third step, a Huisgen-type Copper(I) catalyzed Azide-Alkyne Cycloaddition (CuAAC click chemistry) was carried out between the dextran derivatives and PNBA-N_3. By this scheme, grafted (Dex-g-PNBA) and diblock (Dex-b-PNBA) glycopolymers were produced.

In the first part of this chapter II, we will show how to control the RDRP of NBA. Then, the syntheses of grafted and diblock copolymers will be exposed.

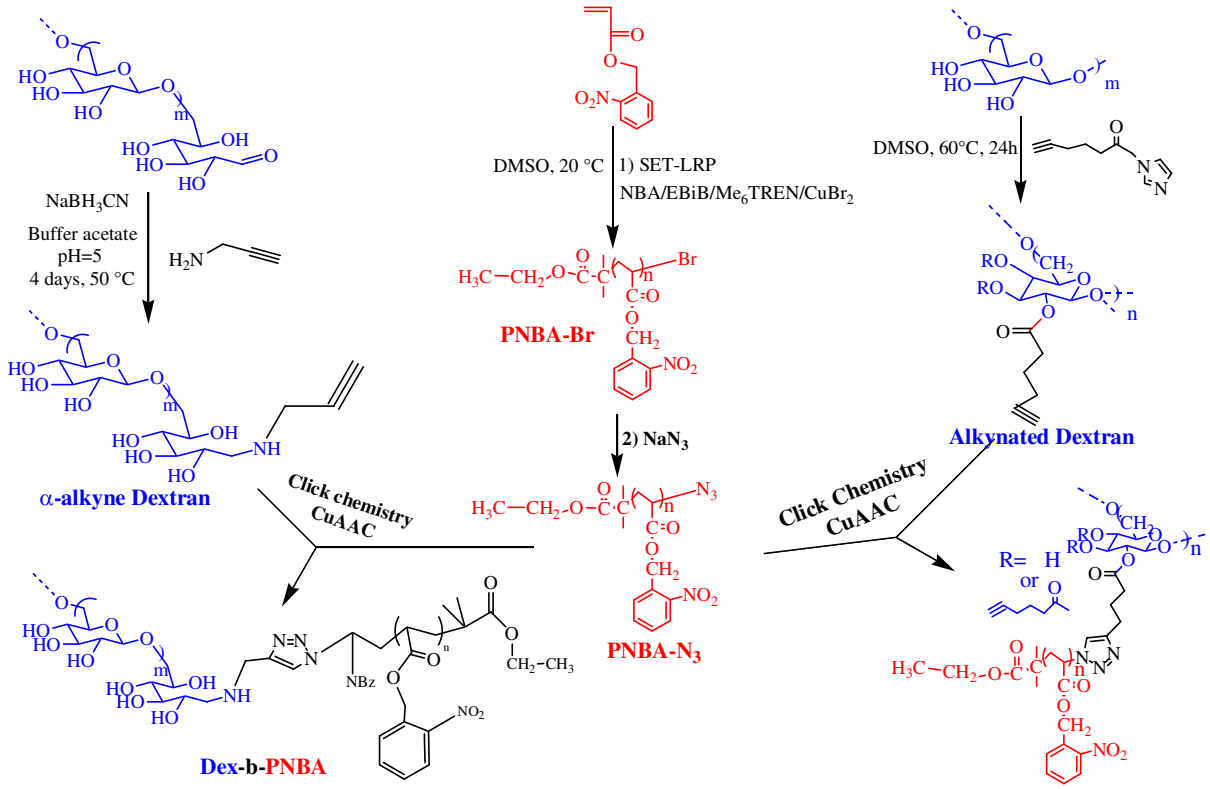

Scheme 1. Strategies to produce grafted and diblock glycopolymers based on dextran and PNBA

References

[1] C. Nouvel, P. Dubois, E. Dellacherie, and J.-L. Six, Controlled synthesis of amphiphilic biodegradable polylactide-grafted dextran copolymers, J. Polym. Sci., Polym. Chem. , 42 (2004) 2577¯2588.

[2] L. Dupayage, M. Save, E. Dellacherie, C. Nouvel, and J.-L. Six, PMMA-grafted dextran glycopolymers by atom transfer radical polymerization, J. Polym. Sci., Polym. Chem. , 46 (2008) 7606-7620.

[3] L. Dupayage, C. Nouvel, and J.-L. Six, Protected versus unprotected dextran macroinitiators for ATRP synthesis of Dex-g-PMMA, J. Polym. Sci., Polym. Chem. , 49 (2011) 35-46.

[4] K. Ferji, C. Nouvel, J. Babin, P.-A. Albouy, M.-H. Li, and J.-L. Six, Controlled synthesis of new amphiphilic glycopolymers with liquid crystal grafts, J. Polym. Sci., Polym. Chem. , 51 (2013) 3829-3839.

[5] C. Nouvel, C. Frochot, V. Sadtler, P. Dubois, E. Dellacherie, and J.-L. Six, Polylactide-Grafted Dextrans: Synthesis and Properties at Interfaces and in Solution, Macromolecules 37 (2004) 4981-4988.

[6] L. Dupayage, C. Nouvel, and J.-L. Six, Copper-mediated ATRP of MMA in DMSO from unprotected dextran macroinitiators, Polym. Bull. , 68 (2012) 647-655.

[7] C. Nouvel, J. Raynaud, E. Marie, E. Dellacherie, J.-L. Six, and A. Durand, Biodegradable nanoparticles made from polylactide-grafted dextran copolymers, J. Colloïd Interf. Sci. , 330 (2009) 337-343.

II. Homopolymerization of NBA

The radical polymerization of NBA was already reported in literature but ATRP, RAFT or NMP of NBA has never been controlled [1]. Firstly, we tried to improve the ATRP of NBA by studying several ligands as PMDETA, 2,2'-bipyridyl and HMTETA. As shown below, uncontrolled ATRP of NBA was obtained whatever the experimental conditions we used. Consequently, SET-LRP was investigated in the second time. Results obtained in case of NBA SET-LRP were published in Journal of polymer Science, Polymer Chemistry.

II.1) ATRP of NBA using PMDETA as ligand

Bulk polymerization of NBA was made using following molar ratio NBA/ EBiB/ PMDETA/ CuBr = 100/ 1/ 1/ 1. NBA, EBiB and PMDETA were successively added and freezing- thawing cycle was made and repeated for three times. Then, CuBr was introduced and freezing- thawing cycle was duplicated. Polymerization was started by putting schlenk tubes in oil-bath at 80 °C, and stopped after 15, 30 and 75 min. For each tube, conversion was estimated from ^{1}H NMR spectrum of crude product. The relation $Ln([M]_o/[M]_t)$ *versus* time was drawn (Figure 1) and the linear relation ($R^2 = 0.99$) means the active centers were constant overall polymerization.

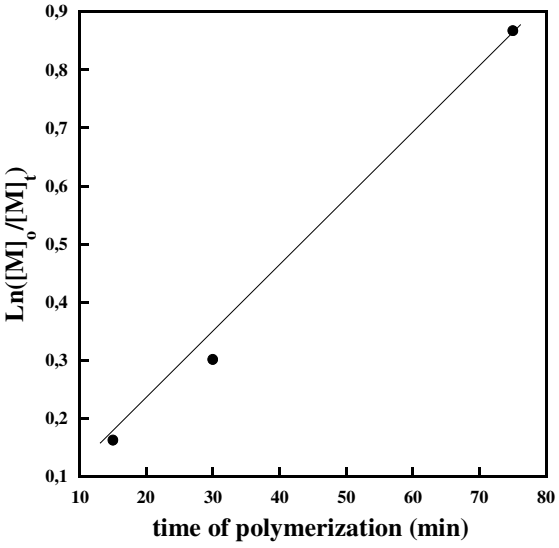

Figure 59. Plot of Ln ($[M]_0/[M]_t$) *versus* time. Bulk ATRP at 80°C, with NBA/EBiB/PMDETA/CuBr: 100/ 1/ 1/ 1.

After purification, polymers were characterized using Size Exclusion Chromatography (SEC). From LS detector, SEC traces show two populations (Figure 2). Moreover, $\bar{M}_n$ values estimated from SEC were lower than those estimated from ^{1}H NMR. All these results could be explained by chain transfer.

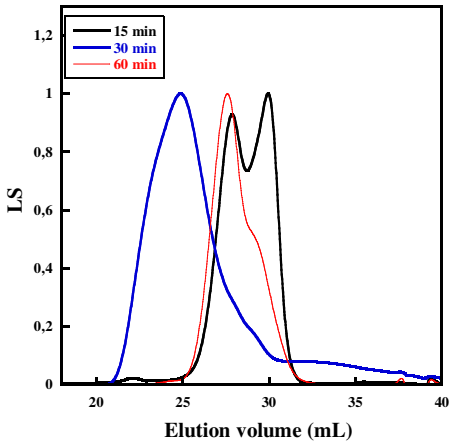

Figure 60. SEC trace (LS detector, eluent THF, 40°C). Bulk ATRP at 80°C, with NBA/ EBiB/ PMDETA/ CuBr: 100/ 1/ 1/ 1

II.2) ATRP of NBA using 2, 2˘-bipyridyl as ligand

Another bulk ATRP run was established by using 2, 2˘-bipyridyl as ligand with molar equivalents as follow : NBA/ EBiB/2,2˘-bipyridyl/CuBr = 100/ 1/ 2/ 1. NBA, 2,2˘-bipyridyl and CuBr were added and freezing- thawing cycle was made for four times. Then, EBiB was added and freezing-thawing cycle was repeated. Polymerization was started by putting schlenk tube in oil-bath at 80 ^{o}C, and polymerization was stopped after 60 min. From ^{1}H NMR, we calculated conversion equal to 25 %. But by SEC analysis, we observed two populations as shown on Figure 3. Moreover, $\bar{M}_n$ estimated by SEC was lower than that predicted from theory, due to chain transfer.

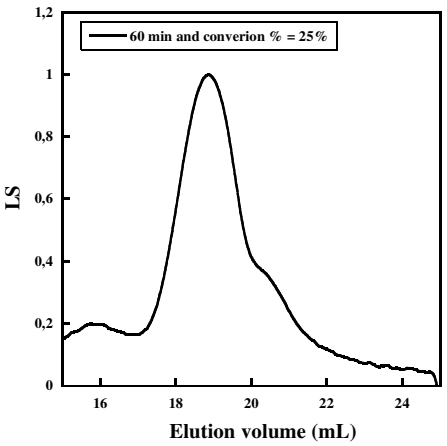

Figure 61. SEC trace (LS detector, eluent THF, 40°C). Bulk ATRP at 80°C, with NBA/EBiB/2,2˘-bipyridyl/CuBr: 100/ 1/ 2/ 1

II.3) ATRP of NBA using HMTETA as ligand

Finally, ATRP of NBA was carried out in methanol at 40 °C using hexamethyltriethylenetetramine (HMTETA) as ligand with molar ratio NBA/EBiB/HMTETA/CuBr = 100/1/1/1. Polymerization was followed by ^{1}H NMR and SEC at different times (15, 30 and 60 min). As shown in Figure 4, after 15 min, we observed a new peak at 4.9 ppm that is characteristic of CH_2OH group of 2-nitrobenzyl alcohol. Indeed, 2-nitrobenzyl group is known to be a good leaving group. In presence of methanol, nucleophilic substitution may occur as shown in Scheme 2.

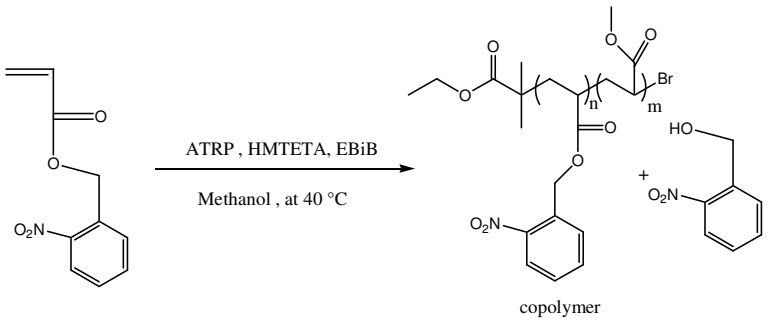

Scheme 2. Supposed nucleophilic reaction that may occur during ATRP of NBA in methanol.

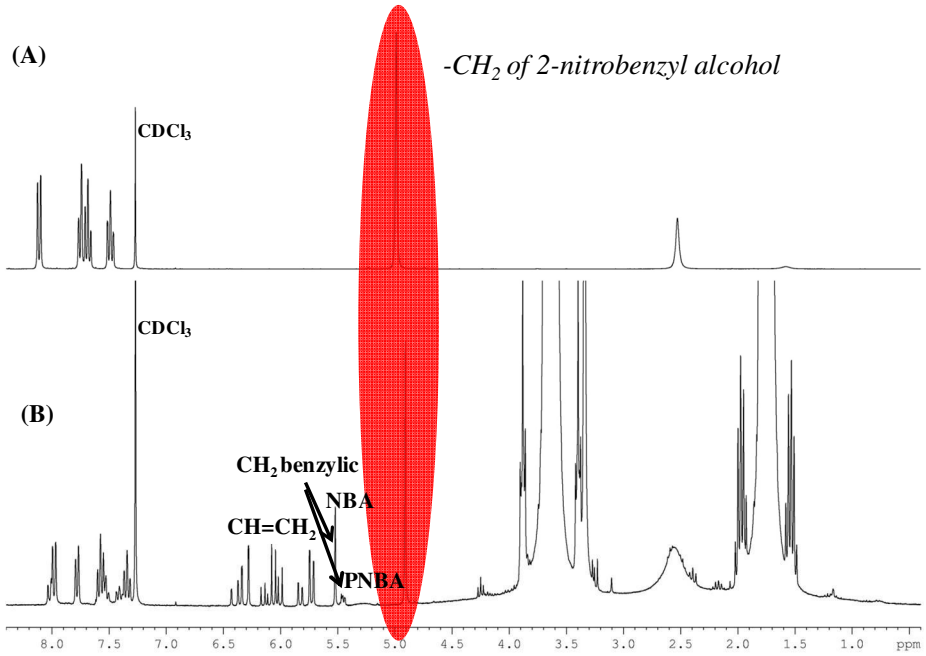

Figure 62. ^{1}H NMR spectra of (A) 2-nitrobenzyl alcohol and (B) sample withdrawn from polymerization solution after 15 min.

By following the polymerization using SEC, we observed that peak was shifted to higher elution volume with increasing time of polymerization, according to a decrease of molar mass with increasing time (Figure 5). That could be due to the nucleophilic substitution of 2-nitrobenzyl groups by methanol.

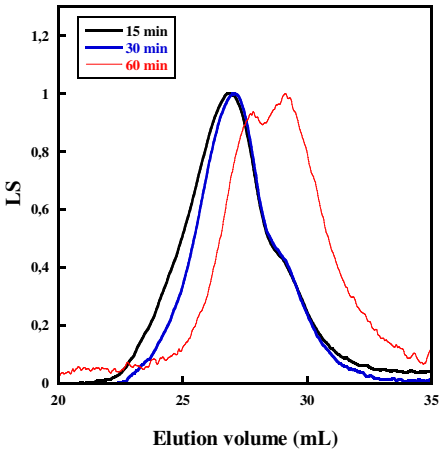

Figure 63. SEC trace (LS detector, eluent THF, 40°C). ATRP in methanol at 40°C, with NBA/ EBiB/ HMTETA/CuBr: 100/ 1/ 1/ 1.

After precipitation and drying, pure polymer was analyzed by ^{1}H NMR spectroscopy. As shown in Figure 6, the characteristic peak of methyl ester group appeared at 3.52 ppm. In other words, we have obtained copolymer of NBA and methyl acrylate (MA).

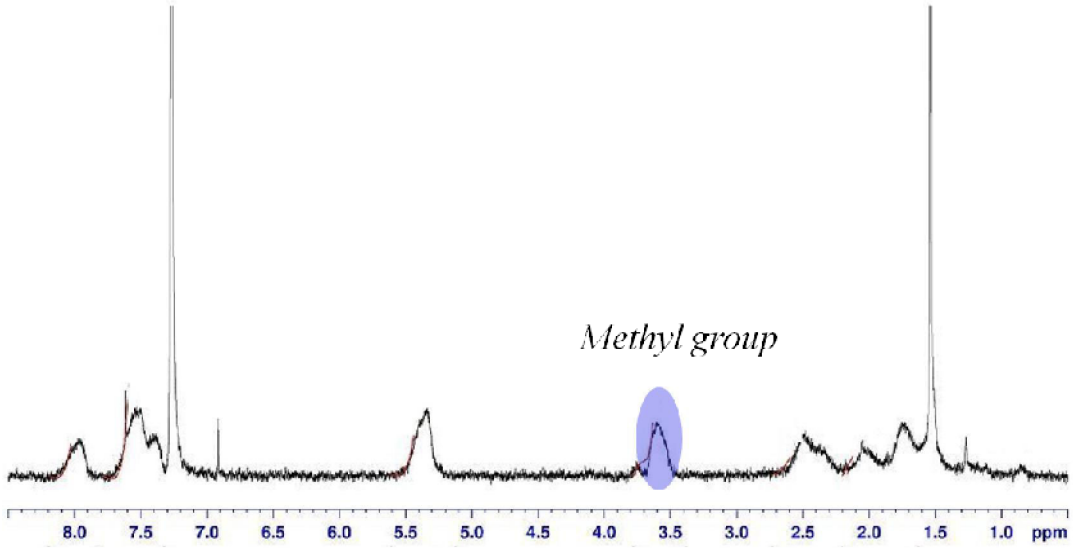

Figure 64. ^{1}H NMR spectrun of pure poly(NBA-co-MA).

II.4) Conclusions on ATRP of NBA

Whatever the ligands and experimental conditions we tested, the results of NBA ATRP are in agreement with literature and we were not able to observe a controlled ATRP.

The second technique we tested was the Single Electron Transfer- Living Radical Polymerization (SET-LRP). This technique can be used at 20 °C and we expected that may restrict the chain transfer that occurs during the polymerization. Results we obtained are published in J. Polym. Sci., Polym. Chem. 2014, 52, 2192-2201, as shown in the following pages.

Reference

[1] J. Schumers, C. Fustin, A. Can, R. Hoogenboom, U.S. Schubert, and J.-F. Gohy, Are o-Nitrobenzyl (Meth)acrylate Monomers Polymerizable by Controlled-Radical Polymerization?, J. Polym. Sci. A Polym. Chem., 47 (2009) 6504-6513.

Part (I)

Synthesis of Photo-sensitive Homopolymer PNBA

ARTICLE WWW.POLYMERCHEMISTRY.ORG JOURNAL OF POLYMER SCIENCE Polymer Chemistry

o-Nitrobenzyl Acrylate is Polymerizable by Single Electron Transfer-Living Radical Polymerization

Soliman Mehawed Abdellatif Soliman,[1,2] Cécile Nouvel,[1,2] Jérôme Babin,[1,2] Jean-Luc Six[1,2]

[1]Université de Lorraine, Laboratoire de Chimie Physique Macromoléculaire LCPM, FRE 3564, Nancy F-54000, France
[2]CNRS, Laboratoire de Chimie Physique Macromoléculaire LCPM, FRE 3564, Nancy F-54000, France
Correspondence to: J.-L. Six (E-mail: jean-luc.six@univ-lorraine.fr)

Received 9 April 2014; accepted 29 April 2014; published online 20 May 2014
DOI: 10.1002/pola.27232

ABSTRACT: Polymers containing *o*-nitrobenzyl esters are promising for preparation of light sensitive materials. *o*-Nitrobenzyl methacrylate has already been polymerized by controlled ATRP or RAFT. Unfortunately, the radical polymerization of *o*-nitrobenzyl acrylate (NBA) was not controlled until now due to inhibition and retardation effects coming from the nitro-aromatic groups. Recent developments in the Single Electron Transfer–Living Radical Polymerization (SET–LRP) provide us an access to control this NBA polymerization and living character of this NBA SET–LRP is demonstrated. Effects of $CuBr_2$ and ligand concentrations, as well as Cu(0) wire length on SET–LRP kinetics are shown presently. A first-order kinetics with respect to the NBA concentration is observed after one induction period. SET–LRP proceeds with a linear evolution of molecular weight and a narrow distribution. High initiation efficiency close to 1 and high chain-end functionality (~93%) are reached. Chain extension of poly(*o*-nitrobenzyl acrylate) is realized with methyl acrylate (MA) to obtain well defined poly(*o*-nitrobenzyl acrylate)-b-poly(methyl acrylate) (PNBA-*b*-PMA). Finally, light-sensitive properties of PNBA are checked upon UV irradiation. © 2014 Wiley Periodicals, Inc. J. Polym. Sci., Part A: Polym. Chem. **2014**, *52*, 2192–2201

KEYWORDS: biodegradable; copper; light-responsive polymer; living radical polymerization; stimuli-sensitive polymers

INTRODUCTION Since last decade, light-responsive polymers have attracted much attention in several fields like three dimensional lithography,[1] sensors,[2,3] or biomedical[4] applications for instance. Beside azobenzene,[5] *o*-nitrobenzyl alcohol[6] photosensitive derivatives are today the most studied in polymer science, among all others photochromics groups like coumarin,[7,8] spiropyran,[9] pyrene,[10] or cinnamic derivatives.[11] For instance, *o*-nitrobenzyl esters have been used as photocleavable junction between blocks in copolymer[12,13] or as polymer-drug linkage in bioconjugates.[14,15] They can also be used as photolabile protecting groups for carboxylic acid functions distributed along macromolecular chains.[16–21] In this last case, *o*-nitrobenzyl ester bonds are cleaved by UV or two-photon adsorptions, yielding highly hydrophilic carboxylic acid functions and leading to a strong increase of the polymer polarity, consequently. The strength of this polarity switch depends on the composition of the *o*-nitrobenzyl containing comonomer units. For instance, *o*-nitrobenzyl acrylate (NBA) monomer units develop higher hydrophilicity after light irradiation than the corresponding methacrylate.[22]

Unfortunately, while Gohy and coworkers[23] have demonstrated the homopolymerization of *o*-nitrobenzyl methacrylate in a controlled manner by Atom Transfer Radical Polymerization (ATRP) or by Reversible Addition–Fragmentation chain Transfer (RAFT), the acrylate homologue monomer does not homopolymerize, whatever the controlled radical polymerization used. This lack of control was mainly attributed to inhibition and retardation effects coming from the nitro-aromatic groups.[23–26] However, despite the difficulties to be homopolymerized under controlled conditions, few NBA-based block copolymers were described. For instance, diblock[18] and triblock[20] copolymers based on poly(ethylene oxide) (PEO) and poly(ethoxytri(ethylene glycol) acrylate-*co*-*o*-nitrobenzyl acrylate) P(TEGEA-*co*-NBA) were prepared through acrylates copolymerization by ATRP using PEO-Br and Br-PEO-Br macroinitiators, respectively. However, the final molar contents of NBA units in P(TEGEA-*co*-NBA) blocks remain low (11% and 17% in the diblock and triblock, respectively). More recently, poly(*o*-nitrobenzyl acrylate-*co*-acrylic acid)-*b*-polystyrene (P(NBA-*co*-AA)-*b*-PS) diblock copolymers were described[19] via a chemical modification of PAA-*b*-PS with 2-nitrobenzyl bromide,[16] due to the

Additional Supporting Information may be found in the online version of this article.

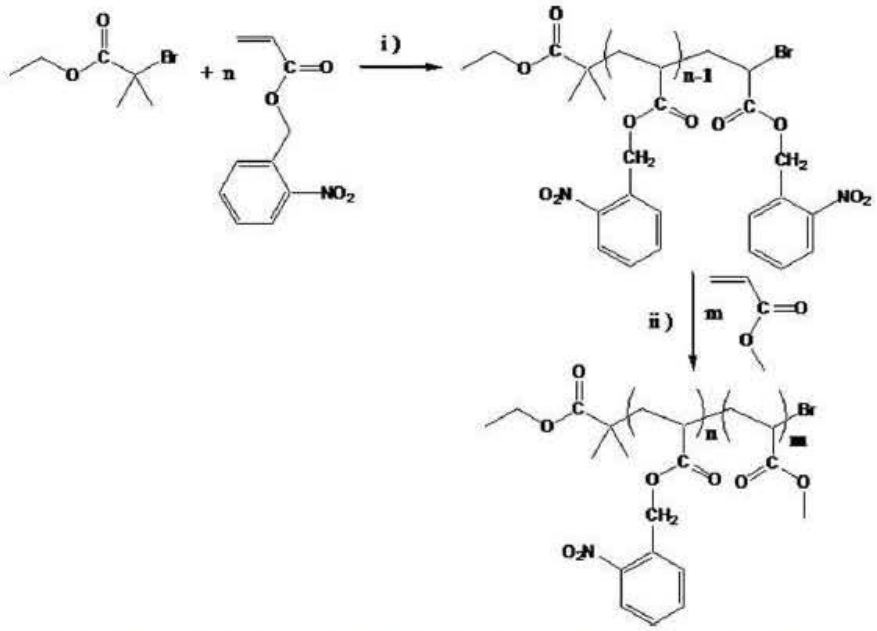

SCHEME 1 (i) SET–LRP of *o*-nitrobenzyl acrylate (NBA) and (ii) chain extension with methyl acrylate (MA). (i) and (ii) = Cu(0)/Me_6TREN/$Cu^{II}Br_2$/DMSO/20 °C.

difficulty of NBA polymerization. Recent developments in the Single Electron Transfer–Living Radical Polymerization (SET–LRP) provide an access to the very straightforward preparation of well-defined functional polymers.[27,28] For example, SET–LRP is effective for a large panel of monomers such as acrylates,[27,29,30] methacrylates,[31–34] acrylamides,[35] acrylonitrile,[36] and vinyl chloride.[37,38] This polymerization technique allows high halogen functionality at the chain end,[39] even at high monomer conversion, and is compatible with numerous polar solvents such as dimethyl sulfoxide (DMSO),[26,40] water,[41] alcohols,[42,43] beers,[44] acetic acid,[45] and nonpolar solvent/additives mixtures.[46] More remarkably, Percec and coworkers[47] have demonstrated the controlled polymerization of methyl acrylate (MA) by SET–LRP in the presence of various amount of 4-methoxyphenol, which is a frequently used stabilizer.

In this study, we investigated the homopolymerization of NBA by SET–LRP (Scheme 1). Effects of [$CuBr_2$], [ligand], and Cu(0) wire length on SET–LRP kinetics will be presented. Accessibility to low and high molecular weights PNBA as well as living character of SET–LRP will be demonstrated.

EXPERIMENTAL

Materials

Tris(2-aminoethyl)amine (TREN, 96%), formaldehyde solution (36.5–38.0% wt), formic acid solution (49–51% wt), Cu(II)Br_2 (99%), Cu(I)Br (99.999%), triethylamine (>99%), and 4-dimethylaminopyridine (>99%) were obtained from Aldrich and used without any further purification. Ethyl 2-bromoisobutyrate (EBiB, Aldrich, 98%) was dried on CaH_2 overnight and vacuum distillated at 70 °C. NBA synthesis was adapted from literature[48] (see Supporting Information). Tris(2-(dimethylamino)ethyl)amine (Me_6TREN) was synthesized as previously reported.[49] Surface of Cu(0) wire (0.25 mm diameter) was polished. Then Cu(0) was immersed in concentrated H_2SO_4 (Aldrich, 95–98%) for 20 min, washed with ethanol, and finally dried.

General Procedure for SET–LRP of *o*-Nitrobenzyl Acrylate

Schlenk tube was evacuated and filled by nitrogen. NBA (1 g, 48.3 mmol, 26 equiv), EBiB (27 μL, 0.185 mmol, 1 equiv), Me_6TREN (8 μL, 0.033 mmol, 0.16 equiv), $CuBr_2$/Me_6TREN solution in DMSO (0.11 mol L^{-1}, 33.75 μL, 0.0037 mmol, 0.02 equiv of $CuBr_2$ and of Me_6TREN) and 4 mL DMSO were successively added under N_2 flow (Entry 2, Table 1). Consequently, the final equivalent of 0.18 equiv of Me_6TREN has to be taken in consideration. Then, medium was purged with N_2 gas for 10 min. Metallic Cu(0) wire (length = 1.7 cm) was added under nitrogen to initiate the polymerization at 20 °C. Samples were withdrawn under nitrogen atmosphere from the polymerization mixture at various time intervals and quenched by cooling with liquid nitrogen. One part of each sample was used to determine the monomer conversion from ^{1}H NMR spectrum in $CDCl_3$. Conversion was estimated by comparing the peaks areas of the aromatic protons of both the monomer NBA and the polymer PNBA (7.3–8.2 ppm; Fig. 1 and Supporting Information Fig. S1) with those of the ethylenic protons of the monomer (5.9, 6.2, and 6.3 ppm). The other part of the sample was diluted using THF and was analyzed by SEC–MALLS to determine $\overline{M_n}_{(SEC)}$ and

TABLE 1 SET–LRP of NBA

Entry	$[NBA]_0/[EBiB]_0/[Me_6TREN]_0/[CuBr_2]_0$	Cu(0) wire length (cm)	Time (min)	Conversion (%)[a]	$\overline{M_{n(SEC)}}$ (g mol^{-1})[b]	Đ[b]
1	(26/1/0.18/–)	1.7	270	45	3,100	1.16[c]
2	(26/1/0.18/0.2)	1.7	360	66	4,500	1.07
3	(100/1/1/–)	1.7	360	74	18,450	1.20[c]
4	(100/1/1/0.1)	1.7	300	71	18,700	1.20
5	(100/1/1/0.2)	1.7	300	68	16,700	1.15
6	(100/1/1/0.1)	0.8	300	40	8,600	1.08
7	(100/1/1/0.1)	3.4	240	71	16,250	1.17
8	(100/1/0.5/0.1)	1.7	300	50	10,950	1.10
9	(100/1/2/0.1)	1.7	240	74	16,300	1.19
10	(200/1/1/0.1)	1.7	300	62	28,600	1.20
11[d]	(100/1/1/0.1)	6.8	180	25	5,250	1.12

[a] Estimated from ^{1}H NMR spectrum of crude product.
[b] $\overline{M_{n(SEC)}}$ and Đ are evaluated from SEC–MALLS analysis.
[c] Estimated on the peak at high elution time.
[d] Using 4 g of PNBA in 4 mL of DMSO.

dispersity Đ. $\overline{M_n}$ was also estimated from ^{1}H NMR ($\overline{M_{n(NMR)}}$) taking account the peaks (a,c,d) and (i).

Chain Extension of Poly(*o*-nitrobenzyl acrylate) with Methyl Acrylate

PNBA-Br macroinitiator (Entry 11, Table 1) was synthesized according the general procedure above described wherein polymerization was stopped after 25% conversion by cooling with liquid nitrogen. Sample of the medium was diluted with THF, passed through an activated alumina column, then PNBA-Br was precipitated twice from cold methanol, and dried under vacuum. $\overline{M_{n(NMR)}} = 5{,}500$ g mol^{-1} (Supporting Information Fig. S2), $\overline{M_{n(SEC)}} = 5{,}250$ g mol^{-1}, and Đ = 1.12.

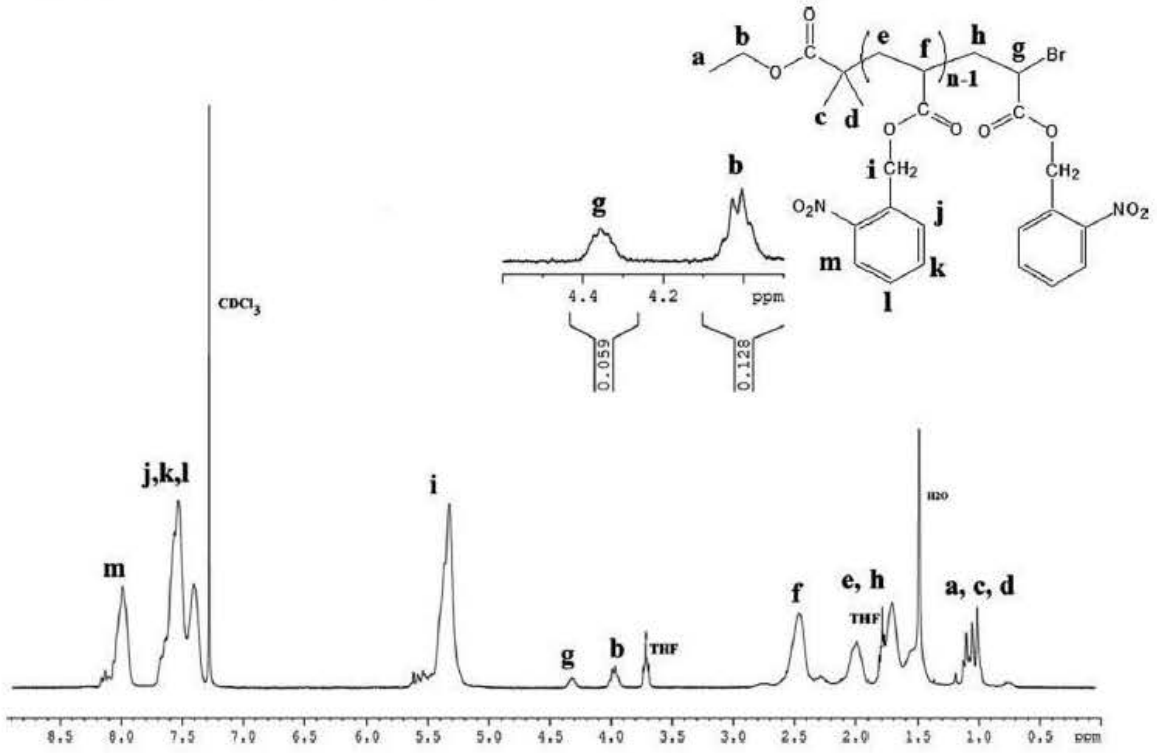

FIGURE 1 ^{1}H NMR spectrum of PNBA ($\overline{M_{n(SEC)}} = 4{,}500$ g mol^{-1} and Đ= 1.07) (Entry 2, Table 1) in $CDCl_3$.

TABLE 2 Chain Extension from PNBA-Br ($\overline{M_n}_{(SEC)}$ = 5,250 g mol^{-1} and Đ = 1.12) by SET–LRP of MA Carried Out in DMSO at 20 °C

Entry	Time (min)	Conversion (%)[a]	$\overline{M_n}_{(theo)}$ (g mol^{-1})[b]	$\overline{M_n}_{(SEC)}$ (g mol^{-1})[c]	Đ[c]
12	15	12	9,300	11,450	1.07
13	45	39	18,600	22,100	1.06

$[MA]_0/[PNBA\text{-}Br]_0/[Me_6TREN]_0/[CuBr_2]_0$ = 400/1/1/0.1 and Cu(0) wire length = 1.7 cm.
[a] Estimated from ^{1}H NMR spectrum of crude product.
[b] $\overline{M_n}_{(theo)} = \overline{M_n}_{(PNBA\text{-}Br)} + (conv. \times ([MA]_0/[PNBA\text{-}Br]_0) \times M_{MA})$ with M_{MA} = 86 g mol^{-1}.
[c] $\overline{M_n}_{(SEC)}$ and Đ are evaluated from SEC–MALLS analysis.

SET–LRP of MA was initiated from this PNBA-Br in DMSO at 20 °C with a molar ratio $[MA]_0/[PNBA\text{-}Br]_0/[Me_6TREN]_0/[CuBr_2]_0$ equal to 400/1/1/0.1. PNBA-Br macroinitiator (150 mg, 0.029 mmol), MA (1.05 mL, 11.6 mmol), Me_6TREN (7.0 µL, 0.0261 mmol), and $CuBr_2$/Me_6TREN solution in DMSO (26 µL, 0.0029 mmol) were dissolved in 1.0 mL of DMSO. The medium was then purged with N_2 gas for 10 min and SET–LRP was initiated by adding a 1.7 cm Cu(0) wire. Samples were withdrawn under nitrogen atmosphere from the polymerization mixture after 15 and 45 min, then quenched by cooling with liquid nitrogen (Table 2). One part of each sample was used to determine the MA conversion from ^{1}H NMR spectrum in $CDCl_3$. The other part of the sample was diluted using THF and was analyzed by SEC–MALLS. PNBA-*b*-PMA diblock copolymers were precipitated from cold methanol, dried by vacuum oven, and then characterized by ^{1}H NMR spectroscopy in $CDCl_3$ (Supporting Information Fig. S3).

Irradiation of Poly(*o*-nitrobenzyl acrylate)

Solution of PNBA ($\overline{M_n}_{(SEC)}$ = 7,900 g mol^{-1}, Đ = 1.12) was prepared in DMSO with concentration 0.1 mg mL^{-1}. About 3 mL of stirred solution was irradiated in 1 × 1 cm^2 quartz cuvette with a OmniCure® S1000 UV spot cure lamp at 1150 mW cm^{-2} power. A light guide of 8 mm diameter equipped with a 320–500 nm filter was used. UV–visible absorbance spectra of solution were measured before and after every 60 s of irradiation.

Characterization Techniques

^{1}H NMR spectra were recorded on a Bruker Avance 300 apparatus (300,13 MHz, 25 °C) in $CDCl_3$.

Size exclusion chromatography (SEC) was performed at 40 °C with THF as eluent. Multiangle laser light scattering detector (MALLS; Mini Dawn Treos, Wyatt), differential refractometer detector (OPTILab rex, Wyatt), HPLC pump (Waters 515), degazer AF (waters In-Line), and three PLgel 5µl (10^5, 10^3, and 100 A°) columns (300 × 7.5 mm^2) were used. Elution rate was 0.7 mL min^{-1}. Solutions (10 mg mL^{-1}) were prepared by dissolution in THF and left under vigorous stirring for 24 h. Filtration of solutions was carried out right before injection. Refractive index increments (dn/dc) of 0.137 and 0.086 mL g^{-1} (for PNBA and poly(methyl acrylate), respectively) were measured in THF at 40 °C with a differential refractometer (Waters 410). dn/dc of PNBA-*b*-PMA diblock copolymers were estimated by calculation using the dn/dc of each homopolymer weighted by the weight fractions of each block in the copolymers.

UV–visible spectra of PNBA and its photolysis product were measured using Uvikon-XL Bio-Tek Spectrophotometer. The absorbance was recorded in the 250–450 nm range.

RESULTS AND DISCUSSION

SET–LRP of *o*-Nitrobenzyl Acrylate

NBA SET–LRP runs were carried out in DMSO at 20 °C with EBiB as initiator and Me_6TREN as ligand (Scheme 1). In the first experiments we carried out (Entries 1–2, Table 1), the molar ratio of $[NBA]_0/[EBiB]_0/[Me_6TREN]_0$ was equal to 26/1/0.18 and the volume/weight ratio of DMSO/NBA was fixed at 1/1. These polymerizations were performed in the presence or not of $CuBr_2$ and kinetics were studied (Fig. 2). Without $CuBr_2$ (Entry 1), SEC analysis of polymer samples revealed the presence of two populations as shown in Figure 2(a). The first one at high elution time is evolving with monomer conversion and corresponds to the desired PNBA. The second one, at low elution time, is stationary whatever the monomer conversion and corresponds to an uncontrolled high molecular weight PNBA formed in the early stages of the reaction. Similar results have been described by Haddleton and coworkers studying SET–LRP of MA in similar conditions.[46,50] An addition of 0.2 equiv of $CuBr_2$ (Entry 2) prevented the formation of this high molecular weight contaminant as shown on the SEC chromatograms overlay [Fig. 2(b)] where only one peak corresponding to the expected PNBA is present, even at low monomer conversion. Moreover, as conversion increases, the elution volume of this population decreases. Linear evolution of $\ln([M]_0/[M]_t)$ *versus* time is observed but an apparent induction period around 120 min occurred at the beginning of the reaction [Fig. 2(c)]. After this period, the polymerization showed a typical first-order kinetics with respect to the monomer concentration, up to 66% conversion. This indicates a constant concentration in radical species during this period. $\overline{M_n}$ determined by SEC increase linearly with conversion and are slightly above than the theoretical $\overline{M_n}$ [Fig. 2(d)] accordingly an initiation efficiency equal to 84%. Dispersity (Đ) decreases with conversion to stabilize to 1.07 confirming the good control of the NBA polymerization [Fig. 2(d)]. PNBA sample obtained at 66% conversion ($\overline{M_n}_{(SEC)}$ = 4,500 g mol^{-1}, Đ = 1.07) was purified and analyzed by ^{1}H NMR spectroscopy (Fig. 1). The areas of signal (b) corresponding to the methylene initiator group and that of signal (g) corresponding to the chain end -CHBr are close to a 2/1 ratio that indicates a high bromine chain end functionality (93%).

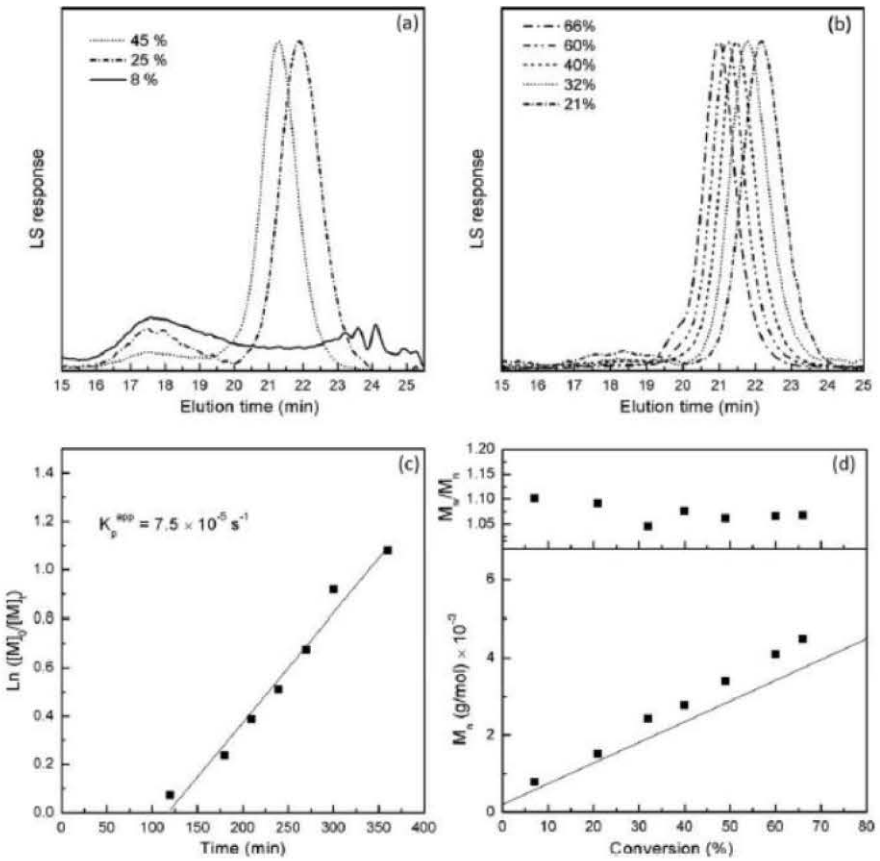

FIGURE 2 SET–LRP of NBA with $[NBA]_0/[EBiB]_0/[Me_6TREN]_0/[CuBr_2]_0 = 26/1/0.18/R$ in DMSO at 20 °C. (a) Evolution of the SEC traces (light scattering detection) at various conversion ($R = 0$, Entry 1, Table 1). (b) Evolution of the SEC traces (light scattering detection) at various conversion ($R = 0.2$, Entry 2, Table 1). (c) Plots of $\ln([M]_0/[M]_t)$ *versus* time (Entry 2, Table 1). K_p^{app} is the slope. (d) Plots of $\overline{M_{n(SEC)}}$ (square), theoretical $\overline{M_n}$ (line), and dispersity Đ *versus* conversion (Entry 2, Table 1).

As described in the experimental part, metallic copper wire surface was activated with a sulfuric acid treatment before use to improve the polymerization rate and to decrease the induction period as previously related.[51] But despite of careful activation we still observed one induction period. The same behavior was described by Lligadas and Percec[47] studying the SET-LRP of MA in the presence of high concentration of 4-methoxyphenol that is a free radical inhibitor. Indeed, they observed the appearance of an induction period of 5 min when the concentration of inhibitor was 0.33 mol L^{-1}. In our work, NBA must be also considered as an inhibitor due to the nitro-aromatic groups.[23–26] Thus, as these experiments (Entries 1 and 2) were carried out with 2.6 mol L^{-1} of NBA, this large concentration of inhibitor moiety explains the experimental long induction period [Fig. 2(c)].

Effect of $[CuBr_2]_0$ on SET–LRP of *o*-Nitrobenzyl Acrylate

One way to reduce the induction period is the addition of Cu(II) species at the beginning of the polymerization as related by Haddleton and coworkers.[46,50] Following this advice, we investigated the effect of $[CuBr_2]_0$ on the polymerization of NBA. The initial molar ratio we used in experiments (Entries 3–5, Table 1) was $[NBA]_0/[EBiB]_0/[Me_6TREN]_0$ equal to 100/1/1 and the volume/weight ratio of DMSO/NBA was fixed at 1/1. Figure 3(a) presents the kinetics plots of $\ln([M]_0/[M]_t)$ *versus* time for different molar ratio $[CuBr_2]_0/[EBiB]$. As shown, an induction period of 95 min was observed when no $CuBr_2$ was initially added. This period was reduced to 39 min using a molar ratio $[CuBr_2]_0/[EBiB]$ equal to 0.1. Surprisingly, an additional increase in the ratio $[CuBr_2]_0/[EBiB]$ to 0.2 was accompanied by a small increase (15 min) of the induction period. After the induction period, all polymerization present a first-order kinetic with respect to the monomer concentration. The apparent polymerization rate constants (K_p^{app}) extracted from the kinetic plots were 8.7×10^{-15}, 8×10^{-15}, and 7.8×10^{-15} s^{-1} for the ratios $[CuBr_2]_0/[EBiB]$ equal to 0, 0.1, and 0.2, respectively. The more initial Cu(II) concentration is high, the more polymerization rate is slow. Indeed, it is well established that Cu(II) species act as deactivator of radicals in

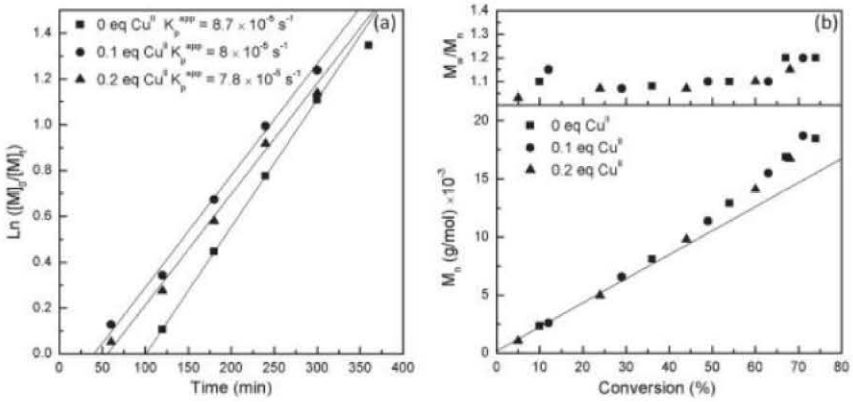

FIGURE 3 SET–LRP of NBA with $[NBA]_0/[EBiB]_0/[Me_6TREN]_0 = 100/1/1/$ in DMSO at 20 °C using different ratios $y = [CuBr_2]_0/[EBiB]_0$. $y = 0$ (Entry 3, Table 1, square), $y = 0.1$ (Entry 4, Table 1, circle), and $y = 0.2$ (Entry 5, Table 1, triangle). (a) Kinetics plots of $\ln([M]_0/[M]_t)$ *versus* time. K_p^{app} is the slope. (b) Plots of $\overline{M_{n\,(SEC)}}$ (square, circle, and triangle), theoretical $\overline{M_n}$ (line), and dispersity Đ *versus* conversion

ATRP and SET–LRP reactions, thus decreasing the active species concentration and consequently the polymerization rate. Whatever the $[CuBr_2]_0$ and below 50% conversion, $\overline{M_n}$ determined by SEC increase linearly with the conversion and are in good agreement with the theoretical $\overline{M_n}$, denoting a high initiation efficiency close to 1. Similarly, in the same conversion range, the dispersity (Đ) remains lower than 1.1 confirming the good control of the NBA polymerization [Fig. 3(b)]. However, for all polymerizations and above 50% conversion, a small shoulder at lower elution volume was observed on SEC traces (Supporting Information Fig. S4). This shoulder may be due to the bimolecular coupling as the molecular weight estimated for this shoulder is the double of that for the peak. This bimolecular coupling leads to a positive deviation of $\overline{M_{n\,(SEC)}}$ *versus* theoretical ones and to an increase of Đ. Nevertheless, this bimolecular coupling remains low and poly(*o*-nitrobenzyl acrylate) (PNBA) with narrow dispersity ($Đ < 1.2$) were obtained for conversions up to 70%.

Effect of Copper Wire Length on SET–LRP of *o*-Nitrobenzyl Acrylate

Another way to reduce the induction period is to extend the copper(0) surface area as previously reported.[50] In SET–LRP, Cu(0) is described to catalyze the polymerization through an outer sphere electron transfer where halide from the initiators or from the propagating end chains reacts with Cu(0) to produce active radicals. Thus, increasing the metallic copper surface must afford a greater activation rate, leading to a higher propagating radical concentration. Fixing the molar ratio of $[NBA]_0/[EBiB]_0/[Me_6TREN]_0/[CuBr_2]_0$ to 100/1/1/0.1 and the volume/weight ratio of DMSO/NBA to 1/1, the effect of the copper wire length on the kinetics was studied (Entries 4, 6, and 7; Table 1). Induction period durations of 97, 39, and 23 min and $K_p^{app} = 4.2 \times 10^{-15}$, 8×10^{-15}, and 1×10^{-14} s^{-1} for copper wire lengths equal to 0.8, 1.7, and 3.4 cm, respectively, were estimated from the kinetics plots of $\ln([M]_0/[M]_t)$ *versus* time [Fig. 4(a)]. Clearly, polymerization carried out using a larger area of Cu(0) wire shown a shorter induction period and a faster polymerization rate as expected. Whatever the Cu(0) wire length and below 50% monomer conversion, $\overline{M_n}$ determined by SEC increase linearly with the conversion and are in good agreement with the theoretical $\overline{M_n}$. Again, when the monomer conversion exceeded 50%, a small shoulder at lower elution time corresponding to the bimolecular coupling was observed on SEC chromatograms.

Effect of $[Me_6TREN]_0$ on SET–LRP of *o*-Nitrobenzyl Acrylate

To discuss the effect of ligand concentration on SET–LRP of NBA, polymerization were carried out at 20 °C with varied $[Me_6TREN]_0$. The molar ratio $[NBA]_0/[EBiB]_0/[CuBr_2]_0$ equal to 100/1/0.1 was used, the volume/weight ratio of DMSO/NBA was fixed at 1/1 and a 1.7 cm copper wire length was added (Entries 4, 8, and 9; Table 1). The induction period duration decreases from 114 to 27 min when the $[Me_6TREN]_0/[EBiB]_0$ molar ratio increases from 0.5 to 2 [Fig. 5(a)]. After the induction period, each polymerization present a first-order kinetic with respect to the monomer concentration. The apparent polymerization rate constants (K_p^{app}) extracted from the kinetic plots were 6.2×10^{-15}, 8×10^{-15}, and 1.11×10^{-14} s^{-1} for molar ratios $[Me_6TREN]_0/[EBiB]_0 = 0.5$, 1, and 2, respectively. In SET–LRP, Cu(I)X moieties are generated during the heterolytic C-X bond dissociation via a Cu(0)-catalyzed outer sphere electron transfer process (activation) and during the reversible radical deactivation provided by $Cu(II)X_2$/ligand. It is assumed that in appropriate solvent such as DMSO and in combination with N-donor ligands like Me_6TREN, Cu(I)X species are readily converted into Cu(0) and $Cu(II)X_2$ through disproportionation.[52] Cu(0) acts as activator and $Cu(II)X_2$ as deactivator in SET–LRP polymerization. Increasing the ligand concentration promotes the disproportionation of Cu(I)X/N-

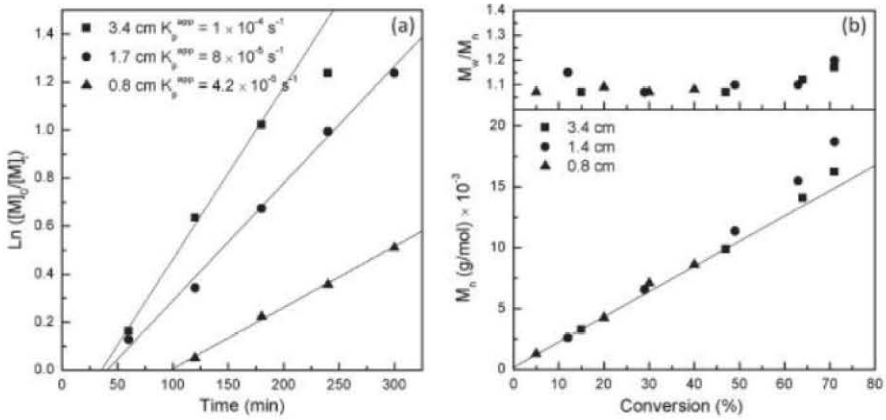

FIGURE 4 SET–LRP of NBA using $[NBA]_0/[EBiB]_0/[Me_6TREN]_0/[CuBr_2]_0 = 100/1/1/0.1$ in DMSO at 20 °C with different copper wire lengths: 3.4 cm (Entry 7, Table 1, square), 1.7 cm (Entry 4, Table 1, circle), and 0.8 cm (Entry 6, Table 1, triangle). (a) Kinetics plots of $\ln([M]_0/[M]_t)$ *versus* time. K_p^{app} is the slope. (b) Plots of $\overline{M_{n\,(SEC)}}$ (square, circle, and triangle), theoretical $\overline{M_n}$ (line), and dispersity Đ *versus* conversion.

ligand complex into highly active "nascent" Cu(0), which goes with a decrease of the induction period and an increase of the polymerization rate. For all polymerizations, theoretical $\overline{M_n}$ and $\overline{M_{n\,(SEC)}}$ were in good agreement below 50% monomer conversion. From this conversion, differences were observed as shown in Figure 5(b), coming from the bimolecular coupling already presented. However, the gap was reduced in the case of a molar ratio $[Me_6TREN]_0/[EBiB]_0 = 2$. In this case, the accordance of theoretical $\overline{M_n}$ and $\overline{M_{n\,(SEC)}}$ is good up to 75% conversion (Đ = 1.2 at 75% conversion).

Poly(*o*-nitrobenzyl acrylate) with Higher Molecular Weight

To obtain higher molecular weight PNBA, one experiment was carried out using a molar ratio $[NBA]_0/[EBiB]_0/[Me_6TREN]_0/[CuBr_2]_0 = 200/1/1/0.1$ in DMSO at 20 °C (Entry 10; Table 1). The volume/weight ratio of DMSO/NBA was maintained equal to 1/1. Consequently, Entries 4 and 10 (Table 1) were carried out with the same initial monomer concentration when the initiator one was divided by 2 in case of Entry 10. By comparison with Entry 4, decreasing the initiator concentration increases the apparent induction period (from 39 to 100 min) as observed in Figures 6(a) and 4(a); then the polymerization evolve and show a typical first-order kinetics with respect to the monomer concentration, up to 62% conversion after 300 min (71% for the same time in case of Entry 4). $\overline{M_{n\,(SEC)}}$ increase linearly with the conversion and are in good accordance with the theoretical $\overline{M_n}$. An initiation efficiency equal to 99% was calculated. Dispersities (Đ) remain lower than 1.2, confirming the good control of the NBA polymerization [Fig. 6(b)]. Due to the inhibitor character of *o*-nitrobenzyl groups, increasing $[NBA]_0$ leads to a longer induction period. As

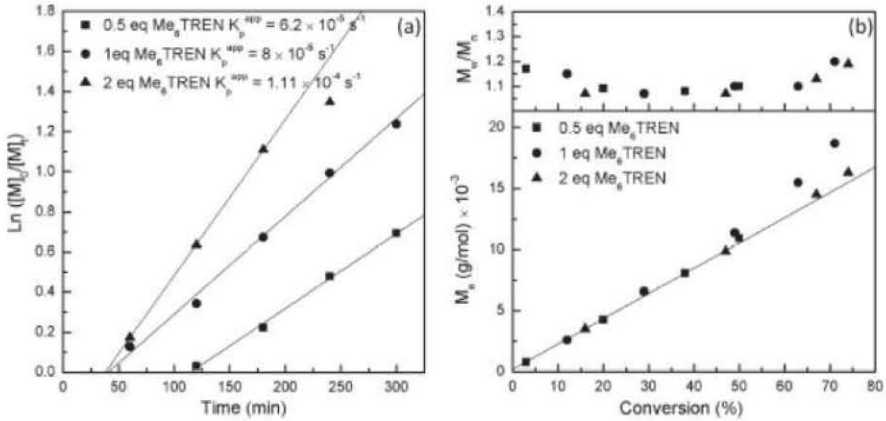

FIGURE 5 SET–LRP of NBA using $[NBA]_0/[EBiB]_0/[CuBr_2]_0 = 100/1/0.1$ in DMSO at 20 °C with different molar ratios $x = [Me_6TREN]_0/[EBiB]_0$. x = 0.5 (Entry 8, Table 1, square), x = 1 (Entry 4, Table 1, circle), and x = 2 (Entry 9, Table 1, triangle). (a) Kinetics plots of $\ln([M]_0/[M]_t)$ *versus* time. K_p^{app} is the slope. (b) Plots of $\overline{M_{n\,(SEC)}}$ (square, circle, and triangle), theoretical $\overline{M_n}$ (line), and dispersity Đ *versus* conversion.

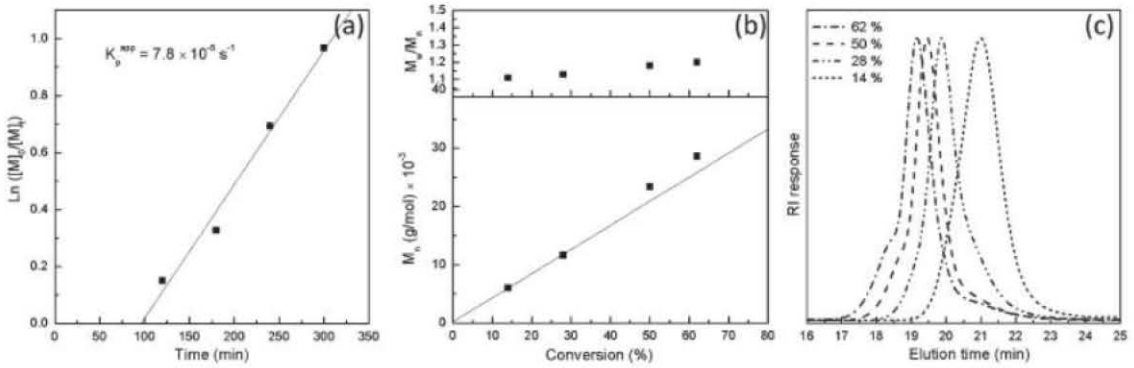

FIGURE 6 SET–LRP of NBA (Entry 10, Table 1) with $[NBA]_0/[EBiB]_0/[Me_6TREN]_0/[CuBr_2]_0 = 200/1/1/0.1$ in DMSO at 20 °C. (a) Kinetics plots of $\ln([M]_0/[M]_t)$ *versus* time. K_p^{app} is the slope. (b) Plots of $\overline{M_{n\,(SEC)}}$, theoretical $\overline{M_n}$ (line), and dispersity Đ *versus* conversion and (c) Evolution of the SEC traces (differential refractive index detection) at various conversions given on figure.

previously related, an addition of $CuBr_2$ at the beginning of the polymerization prevents the significant formation of the high molecular weight contaminant (at low elution volume) as shown on the overlay of SEC chromatograms [Fig. 6(c)]. Indeed, only one population corresponding to the expected polymer is present, even at low monomer conversion. PNBA sample isolated at 62% conversion presented a high molecular weight ($\overline{M_{n\,(SEC)}} = 28{,}600$ g mol^{-1}) and a low dispersity (Đ = 1.2). However, at this conversion, a small shoulder at low elution time corresponding to the bimolecular coupling was observed on SEC chromatogram.

Chain Extension of PNBA-Br by SET-LRP of Methyl Acrylate

To check the living character of one polymerization, chain extension is commonly studied.[53] In our case, we studied PNBA chain extension by carrying out SET–LRP of MA in DMSO at 20 °C, initiated with one PNBA-Br as macroinitiator and Me_6TREN as ligand (Scheme 1). The molar ratio $[MA]_0/[PNBA\text{-}Br]_0/[Me_6TREN]_0/[CuBr_2]_0$ was 400/1/1/0.1 and the volume/weight ratio of DMSO/MA was equal to 1/1. Consequently $[PNBA\text{-}Br]_0$ was decreased by comparison with Entry 4 (Table 1) for instance.

The PNBA-Br macroinitiator was first prepared in DMSO at 20 °C by SET–LRP of NBA using the molar ratio $[NBA]_0/[EBiB]_0/[Me_6TREN]_0/[CuBr_2]_0 = 100/1/1/0.1$ and the polymerization was stopped at 25% conversion (Entry 11, Table 1). After purification, $\overline{M_n}$ of PNBA-Br was estimated by ^{1}H NMR (Supporting Information Fig. S2) and SEC analyses (Fig. 7). A really good agreement was obtained between the theoretical $\overline{M_n}$ estimated from the conversion ($\overline{M_{n\,(theo)}} = 5{,}175$ g mol^{-1}), those calculated by ^{1}H NMR ($\overline{M_{n\,(NMR)}} = 5{,}500$ g mol^{-1}) and by SEC ($\overline{M_{n\,(SEC)}} = 5{,}250$ g mol^{-1}). From these data, an initiation efficiency equal to 98% was calculated, that is in perfect agreement with the previously determined value in same experimental conditions.

Chain extension was studied at two different MA conversions (Entries 12 and 13; Table 2). After purification, diblock copolymers were analyzed by ^{1}H NMR and SEC (Fig. 7). Both ^{1}H NMR spectra show the characteristic methoxy signal of MA monomer unit (-OCH_3 at 3.6 ppm) jointly with the typical signals of PNBA (Supporting Information Fig. S3). SEC chromatograms overlay of crude copolymers shows narrow peaks evolving to lower elution time with the increase of MA conversion. This shift clearly demonstrates the chain extension from the macroinitiator. Nevertheless, one can observe a small PNBA-Br residual signal according to the 93% bromide chain end functionality previously mentioned. $\overline{M_{n\,(SEC)}}$ were in good agreement with the theoretical $\overline{M_n}$ calculated from conversion (Table 2). Low dispersities extracted from SEC

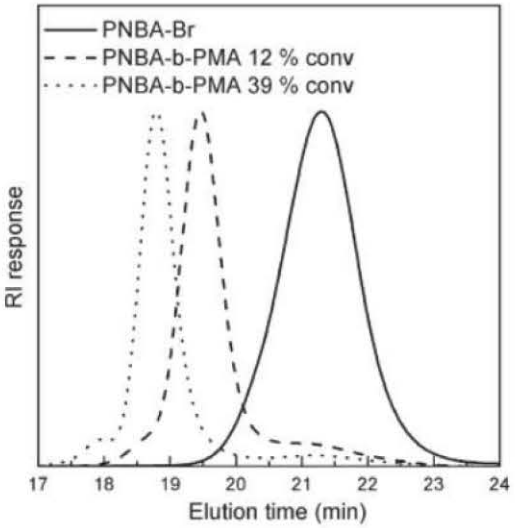

FIGURE 7 Evolution of SEC traces (differential refractive index detection) during the chain extension of PNBA-Br ($\overline{M_{n\,(SEC)}} = 5{,}250$ g mol^{-1} and Đ = 1.12) by SET–LRP of MA. SET–LRP was carried out in DMSO at 20 °C with $[MA]_0/[PNBA\text{-}Br]_0/[Me_6TREN]_0/[CuBr_2]_0 = 400/1/1/0.1$. Conversions are given on figure.

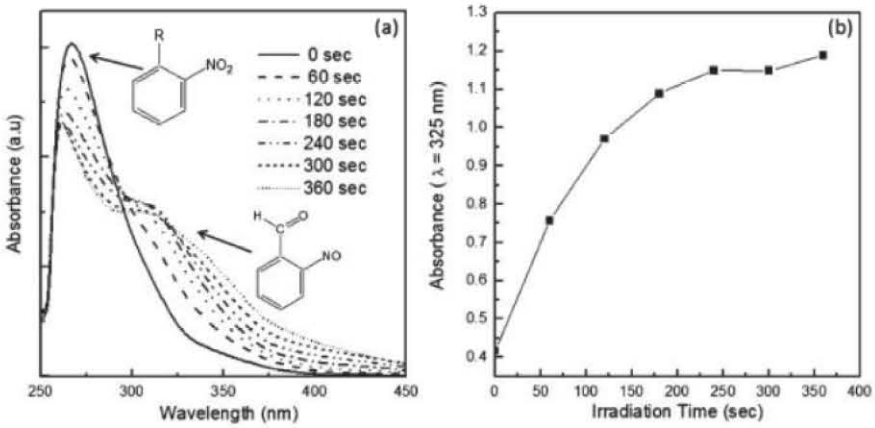

FIGURE 8 Light irradiation of PNBA ($\overline{M_{n\,(SEC)}}$ = 7,900 g mol^{-1}, Đ=1.12) in DMSO (0.1 mg mL^{-1}) with a UV lamp equipped with a 320–500 nm filter (power 1150 mw cm^{-2}). (a) UV–vis spectra after various irradiation time. (b) Absorbance at 325 nm *versus* irradiation time

chromatograms (Đ < 1.07) demonstrated that diblock copolymers are well defined.

Light Irradiation of Poly(*o*-nitrobenzyl acrylate)

Photosensitive properties of PNBA were checked with a light irradiation experiment. Upon one photon irradiation, 2-nitrobenzyl esters are known to be cleaved liberating carboxylic acid groups and 2-nitrosobenzaldehyde byproduct.[6] This photocleavage can be easily followed on UV–visible absorption spectra, where 2-nitrobenzyl ester and 2-nitrosobenzaldehyde present two different bands [Fig. 8(a)]. Light irradiation of PNBA ($\overline{M_{n\,(SEC)}}$ = 7,900 g mol^{-1}, Đ = 1.12) was carried out in DMSO (0.1 mg mL^{-1}) with a UV light (spectra range from 250 to 450 nm and a 1150 mW cm^{-2} power). UV–visible absorbance spectra of solution were measured before and after every 60 s of irradiation [Fig. 8(a)]. Before irradiation, a band at 275 nm was detected corresponding to the absorption of 2-nitrobenzyl ester. After UV irradiation, the intensity of this band decreased while another band appeared at 325 nm that is characteristic of the formation of 2-nitrosobenzaldhyde. Plot of the absorbance at 325 nm *versus* irradiation time shows a fast photocleavage that evolves no more after 350 s [Fig. 8(b)].

CONCLUSIONS

Until now, NBA was considered as one capricious monomer that is difficult to polymerize by controlled radical polymerization techniques such as RAFT, ATRP or NMP. In this study, we demonstrated that NBA could be polymerized by controlled SET–LRP. A first-order kinetics with respect to the NBA concentration are observed. Moreover, up to 50% conversion, the SET-LRP proceeds with a linear evolution of molecular weight and a narrow distribution (dispersity < 1.2). High initiation efficiency close to 1 and high chain-end functionality (~93%) are reached. A small amount of bimolecular coupling is detected by SEC (light ccattering detector) for NBA conversion higher than 50%.

Significant and expected effect of $[CuBr_2]_0$, $[ligand]_0$, and Cu(0) wire length on SET–LRP kinetics are demonstrated. Indeed, induction period duration and rate of the polymerization decrease with a higher $[CuBr_2]_0$. On contrary, the more $[Me_6TREN]_0$ and Cu(0) wire length are high, the more apparent rate constant of polymerization is high and the more induction period is small.

PNBA chains, up to $\overline{M_n}$ = 28,600 g mol^{-1} could be prepared with a good control and the living character of such NBA SET–LRP is further verified by chain extension with MA. By this way, well-defined PNBA-*b*-PMA diblock copolymers are thus elaborated.

In the very next future, such controlled PNBA-Br chains will be used to obtain amphiphilic copolymers that will produce micelle-like structures.

ACKNOWLEDGMENT

The authors express their highest gratitude to Marie-Christine Grassiot for help in SEC measurements and Olivier Fabre for NMR measurements. S.M.A. Soliman gratefully acknowledges support from an Erasmus Mundus External Cooperation Windows – Flow by Flow EU-Egypt Bridge Building (FFEEBB) Graduate Research Fellowship.

REFERENCES AND NOTES

1 D. H. Kang, S. H. Kim, B. Lee, H. Yoon, K. Y. Suh, *Analyst* **2013**, *138*, 6230–6242.

2 Y. Fuchs, O. Soppera, K. Haupt, *Anal. Chim. Acta* **2012**, *717*, 7–20.

3 X. Wang, J. Luo, C. Yi, X. Liu, *Electroanalysis* **2013**, *25*, 1907–1916.

4 J.-F. Gohy, Y. Zhao, *Chem. Soc. Rev.* **2013**, *42*, 7117–7129.

5 Y. Zhao, T. Ikeda, Smart Light-Responsive Materials: Azobenzene-Containing Polymers and Liquid Crystals; Wiley: New Jersey, **2009**.

6 H. Zhao, E. S. Sterner, E. B. Coughlin, P. Theato, *Macromolecules* **2012**, *45*, 1723–1736.

7 J. Babin, M. Lepage, Y. Zhao, *Macromolecules* **2008**, *41*, 1246–1253.

8 J. Babin, M. Pelletier, M. Lepage, J.-F. Allard, D. Morris, Y. Zhao, *Angew. Chem. Int. Ed.* **2009**, *48*, 3329–3332.

9 L. Florea, D. Diamond, F. Benito-Lopez, *Macromol. Mater. Eng.* **2012**, *297*, 1148–1159.

10 J. Jiang, X. Tong, Y. Zhao, *J. Am. Chem. Soc.* **2005**, *127*, 8290-.

11 A. Ravve, In Light-Associated Reactions of Synthetic Polymers; A. Ravve, Ed.; Springer New York: New York, **2006**; chapter 4, pp 199–245.

12 M. Kang, B. Moon, *Macromolecules* **2009**, *42*, 455–458.

13 J.-M. Schumers, J.-F. Gohy, C.-A. Fustin, *Polym. Chem.* **2010**, *1*, 161–163.

14 W. E. Georgianna, H. Lusic, A. L. McIver, A. Deiters, *Bioconjugate Chem.* **2010**, *21*, 1404–1407.

15 D. Saran, D. H. Burke, *Bioconjugate Chem.* **2007**, *18*, 275–279.

16 O. Bertrand, J.-M. Schumers, C. Kuppan, J. Marchand-Brynaert, C.-A. Fustin, J.-F. Gohy, *Soft Matter* **2011**, *7*, 6891–6896.

17 J. Jiang, X. Tong, D. Morris, Y. Zhao, *Macromolecules* **2006**, *39*, 4633–4640.

18 X. Jiang, C. A. Lavender, J. W. Woodcock, B. Zhao, *Macromolecules* **2008**, *41*, 2632–2643.

19 J.-M. Schumers, O. Bertrand, C.-A. Fustin, J.-F. Gohy, *J. Polym. Sci. Part A: Polym. Chem.* **2012**, *50*, 599–608.

20 J. W. Woodcock, R. A. E. Wright, X. Jiang, T. G. O'Lenick, B. Zhao, *Soft Matter* **2010**, *6*, 3325–3336.

21 M. Lepage, J. Jiang, B. Qi, L. Tremblay, Y. Zhao, *Phys. Med. Biol.* **2007**, *52*, N249–N255.

22 B. Adnadjevic, J. Jovanovic, *Colloids Surf. B: Biointerfaces* **2009**, *69* 31–42.

23 J.-M. Schumers, C.-A. Fustin, A. Can, R. Hoogenboom, U. Schubert, J.-F. Gohy, *J. Polym. Sci. Part A: Polym. Chem.* **2009**, *47*, 6504–6513.

24 G. S. Hammond, P. D. Bartlett, *J. Polym. Sci.* **1951**, *6*, 617–624.

25 G. Odian, *Principles of Polymerization*, 4th ed; Wiley: New York, **2004**.

26 C. C. Price, D. A. Durham, *J. Am. Chem. Soc.* **1943**, *65*, 757–759.

27 V. Percec, T. Guliashvili, J. S. Ladislaw, A. Wistrand, A. Stjerndahl, M. J. Sienkowska, M. Monteiro, S. Sahoo, *J. Am. Chem. Soc.* **2006**, *128*, 14156–14165.

28 B. M. Rosen, V. Percec, *Chem. Rev.* **2009**, *109*, 5069–5119.

29 C. Feng, Z. Shen, Y. Li, L. Gu, Y. Zhang, G. Lu, X. Huang, *J. Polym. Sci. Part A: Polym. Chem.* **2009**, *47*, 1811–1824.

30 S. Zhai, B. Wang, C. Feng, Y. Li, Y. Dong, J. Hu, G. Lu, X. Huang, *J. Polym. Sci. Part A: Polym. Chem.* **2010**, *48*, 647–655.

31 S. Ding, J. A. Floyd, K. B. Walters, *J. Polym. Sci. Part A: Polym. Chem.* **2009**, *47*, 6552–6560.

32 W. Wang, Z. Zhang, J. Zhu, N. Zhou, X. Zhu, *J. Polym. Sci. Part A: Polym. Chem.* **2009**, *47*, 6316–6327.

33 Z. Zhang, W. Wang, H. Xia, J. Zhu, W. Zhang, X. Zhu, *Macromolecules* **2009**, *42*, 7360–7366.

34 S. Fleischmann, V. Percec, *J. Polym. Sci. Part A: Polym. Chem.* **2010**, *48*, 2251–2255.

35 N. H. Nguyen, B. M. Rosen, V. Percec, *J. Polym. Sci. Part A: Polym. Chem.* **2010**, *48*, 1752–1763.

36 Z. Hao, H. Chen, D. Liu, L. Fan, *J. Polym. Sci. Part A: Polym. Chem.* **2012**, *50*, 4995–4999.

37 M. J. Sienkowska, B. M. Rosen, V. Percec, *J. Polym. Sci. Part A: Polym. Chem.* **2009**, *47*, 4130–4140.

38 T. Hatano, B. M. Rosen, V. Percec, *J. Polym. Sci. Part A: Polym. Chem.* **2010**, *48*, 164–172.

39 F. Nyström, A. H. Soeriyadi, C. Boyer, P. B. Zetterlund, M. R. Whittaker, *J. Polym. Sci. Part A: Polym. Chem.* **2011**, *49*, 5313–5321.

40 C. Boyer, A. Atme, C. Waldron, A. Anastasaki, P. Wilson, P. B. Zetterlund, D. Haddleton, M. R. Whittaker, *Polym. Chem.* **2013**, *4*, 106–112.

41 Q. Zhang, P. Wilson, Z. Li, R. McHale, J. Godfrey, A. Anastasaki, C. Waldron, D. M. Haddleton, *J. Am. Chem. Soc.* **2013**, *135*, 7355–7363.

42 G. Lligadas, V. Percec, *J. Polym. Sci. Part A: Polym. Chem.* **2008**, *46*, 2745–2754.

43 N. H. Nguyen, B. M. Rosen, X. Jiang, S. Fleischmann, V. Percec, *J. Polym. Sci. Part A: Polym. Chem.* **2009**, *47*, 5577–5590.

44 C. Waldron, Q. zhang, Z. Li, V. Nikolaou, G. Nurumbetov, J. Godfrey, R. McHale, G. Yilmaz, R. K. Randev, M. Girault, K. McEwan, D. M. Haddleton, M. Droesbeke, A. J. Haddleton, P. Wilson, A. Simula, J. Collins, D. J. Lloyd, J. A. Burns, C. Summers, C. Houben, A. Anastasaki, M. Li, C. R. Becer, J. K. Kiviaho, N. Risanqud, *Polym. Chem.* **2014**, *5*, 57–61.

45 S. Fleischmann, V. Percec, *J. Polym. Sci. Part A: Polym. Chem.* **2010**, *48*, 4889–4893.

46 M. E. Levere, I. Willoughby, S. O'Donohue, P. M. Wright, A. J. Grice, C. Fidge, C. R. Becer, D. M. Haddleton, *J. Polym. Sci. Part A: Polym. Chem.* **2011**, *49*, 1753–1763.

47 G. Lligadas, V. Percec, *J. Polym. Sci. Part A: Polym. Chem.* **2008**, *46*, 3174–3181.

48 V. V. Ramanan, J. S. Katz, M. Guvendiren, E. R. Cohen, R. A. Marklien, J. A. Burdick, *J. Mater. Chem.* **2010**, *20*, 8920–8926.

49 M. Ciampolini, N. Nardi, *Inorg. Chem.* **1966**, *5*, 41–44.

50 M. E. Levere, I. Willoughby, S. O'Donohue, A. de Cuendias, A. J. Grice, C. Fidge, C. R. Becer, A. J. Haddleton, *Polym. Chem.* **2010**, *1*, 1086–1094.

51 N. H. Nguyen, V. Percec, *J. Polym. Sci. Part A: Polym. Chem.* **2010**, *48*, 5109–5119.

52 B. M. Rosen, X. Jiang, C. J. Wilson, N. H. Nguyen, M. Monteiro, V. Percec, *J. Polym. Sci. Part A: Polym. Chem.* **2009**, *47*, 5606–5628.

53 A. H. Soeriyadi, C. Boyer, F. Nyström, P. B. Zetterlund, M. R. Whittaker, *J. Am. Chem. Soc.* **2011**, *133*, 11128–11131.

SUPPORTING INFORMATIONS FOR

o-Nitrobenzyl Acrylate is Polymerizable by SET-LRP

Soliman Mehawed Abdellatif SOLIMAN[1,2], *Cécile NOUVEL*[1,2], *Jérôme BABIN*[1,2], *Jean-Luc SIX*[1,2]*

1) Université de Lorraine, Laboratoire de Chimie Physique Macromoléculaire LCPM, FRE 3564, Nancy F-54000, France

2) CNRS, Laboratoire de Chimie Physique Macromoléculaire LCPM, FRE 3564, Nancy F-54000, France

KEYWORDS

o-nitrobenzyl acrylate, SET-LRP, chain extension, living radical polymerization, copper, light-responsive polymer.

Synthesis of *o*-Nitrobenzyl Acrylate

2-nitrobenzyl alcohol (65.3 mmole), triethylamine (130.6 mmole) and 4-N, N-dimethylamino pyridine (3.435 mmole) were dissolved in 70 mL of anhydrous dichloromethane and stirred in ice bath under nitrogen flow. Acryloyl chloride (78.4 mmole) was diluted in 30 mL of anhydrous dichloromethane then was added drop wise. After complete addition of acryloyl chloride, mixture was leaved stirring at room temperature and the reaction was followed by thin layer chromatography (TLC). Finally, ammonium salts were filtrated and washed with tetrahydrofuran (THF). Organic phase was neutralized by solution of K_2CO_3 (0.065 M) till having a basic medium. The organic phase was washed with distilled water and dried with $MgSO_4$. After filtration, the solution was concentrated and NBA was purified by column chromatography (petrolum ether/ethyl acetate) (8/2; v:v). Finally, monomer was dried to obtained 9.23 g of oily *o*-nitrobenzyl acrylate with 69 % yield.

Pure monomer was analyzed by ^1H NMR spectroscopy (Fig. S1) and size exclusion chromatography (SEC). SEC was used to confirm the absence of free homopolymer, which could be formed during storage or purification steps of monomer.

Figure S1. ^{1}H NMR spectrum of *o*-nitrobenzyl acrylate in $CDCl_3$

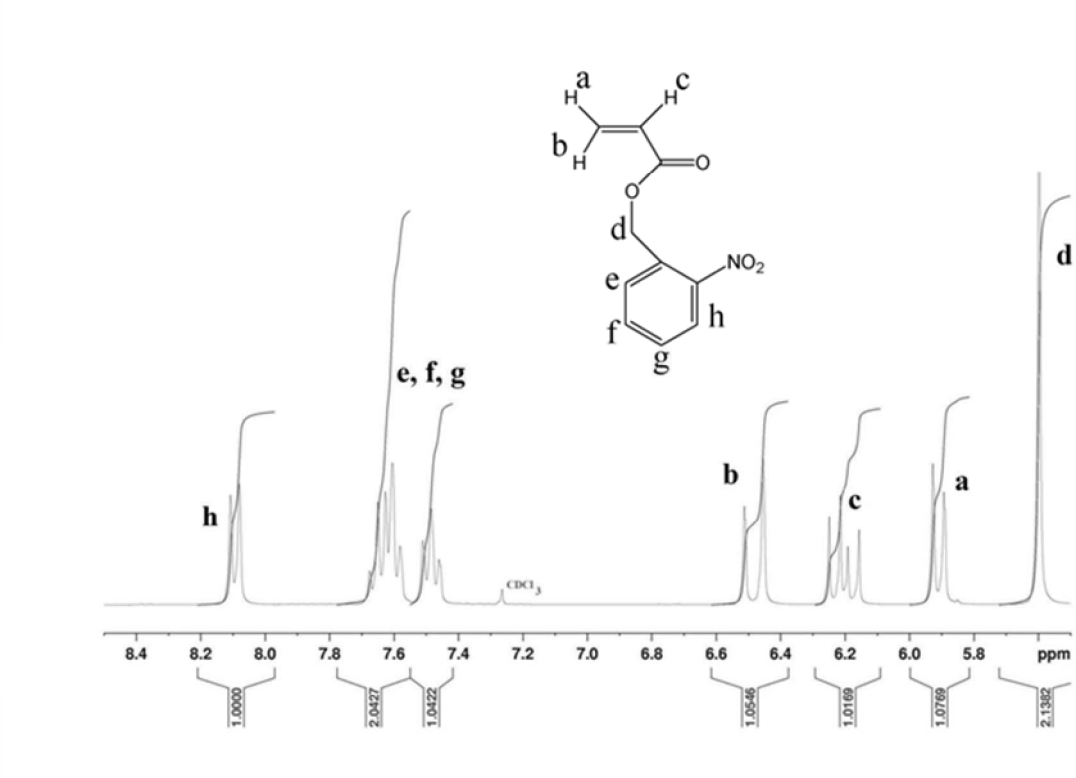

Figure S2. ^{1}H NMR spectrum ($CDCl_3$) of PNBA-Br Macroinitiator ($M_{n,(NMR)}$ = 5,250 g/mol and $Đ$ = 1.12) obtained with $[NBA]_0/[EBiB]_0/[Me_6TREN]_0/[CuBr_2]_0$ = 100/1/1/0.1 (Entry 11, Table 1) (25 % conversion)

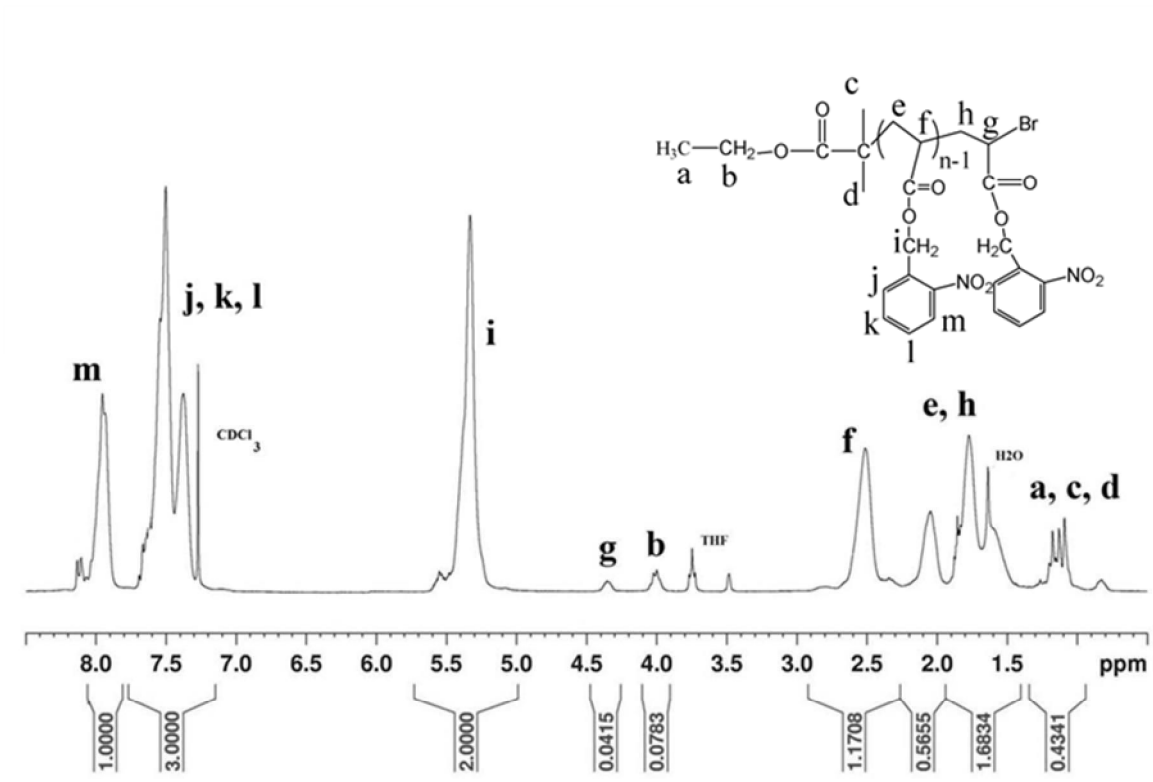

Figure S3. ^{1}H NMR spectrum of PNBA-*b*-PMA diblock copolymer ($M_{n(NMR)}$ = 22,100 g/mol, $Đ$ = 1.06, Entry 13, Table 2) in $CDCl_3$

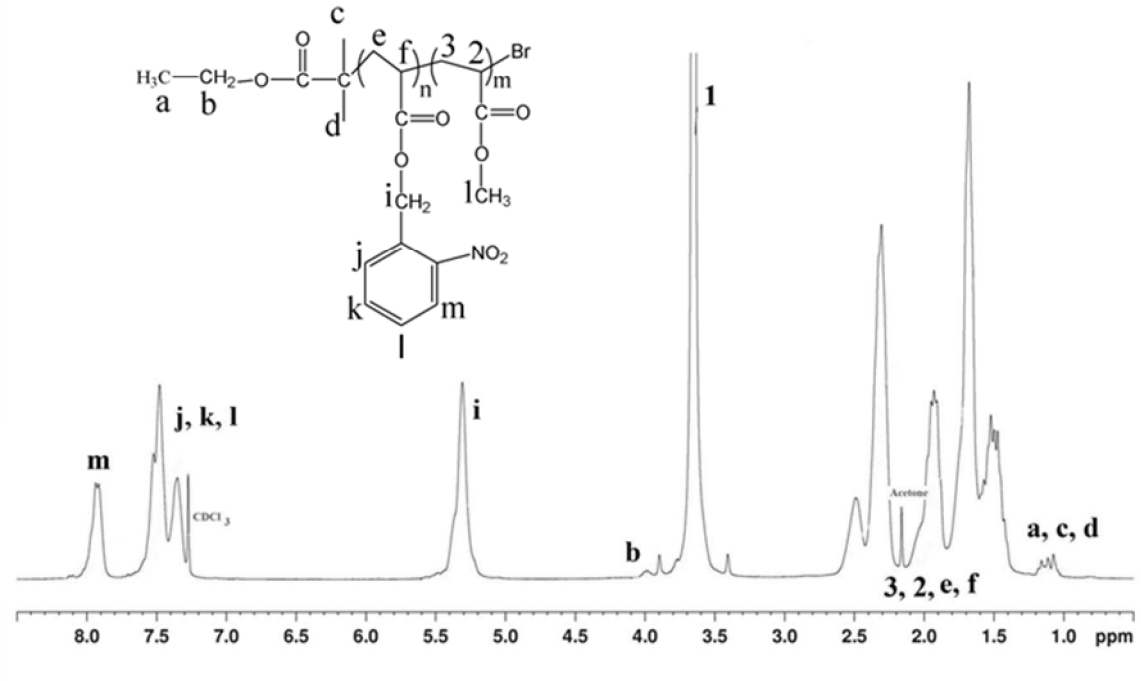

Figure S4. Evolution of the SEC traces (Differential refractive index detection) at various monomer conversion during SET-LRP of NBA (Entry 4, Table 1). $[NBA]_0/[EBiB]_0/[Me_6TREN]_0/[CuBr_2]_0$ = 100/1/1/0.1 in DMSO at 20°C

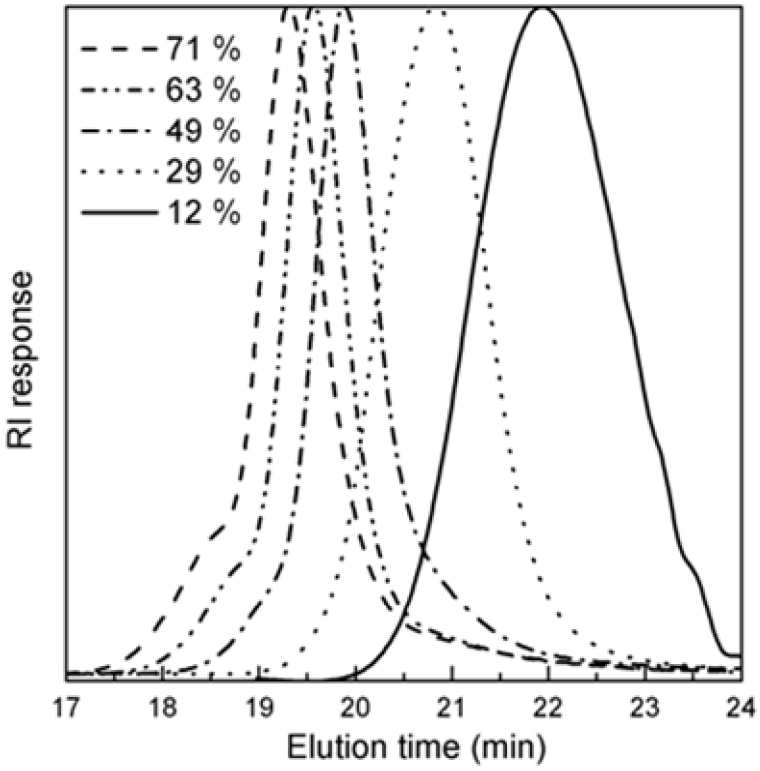

Part (II)

Synthesis of Photo-sensitive Amphiphilic Glycopolymers

In this part, we will discuss the syntheses of grafted and diblock glycopolymers. Firstly, bromide-end chain functionality of PNBA was modified using sodium azide. Secondly, alkynated dextran (with many alkyne groups all long the dextran chain) or α-alkyne dextran (one alkyne group at the reducing-end) were produced. Finally, the click chemistry between PNBA with azido function group and modified dextran will be presented. We chose the grafting onto approach using Huisgens 1,3 dipolar cycloaddition involving the azide end-group of PNBA and alkynyl functions located onto the polysaccharide. This `click_ reaction is stereospecific, easy to implement, very fast even at room temperature and has a great performance. Moreover, although the alkynyl and azide are mutually highly reactive, they are individually virtually inert. Thus, the reaction is orthogonal to many functional groups such as esters or alcohols that are present on dextran and PNBA chains. Therefore, in case of the synthesis of grafted glycopolymer, this click chemistry exhibits a very high reactivity and selectivity, should allow us to obtain a quantitative grafting and thus a good control of PNBA/dextran ratio in the final glycopolymers.

Synthesis of Amphiphilic Light-Responsive Dextran-g-poly(*o*-nitrobenzyl acrylate) Glycopolymers

Soliman Mehawed Abdellatif SOLIMAN[1,2], *Cécile NOUVEL*[1,2], *Jérôme BABIN*[1,2], *Jean-Luc SIX*[1,2]*

1) Université de Lorraine, Laboratoire de Chimie Physique Macromoléculaire LCPM, FRE 3564, Nancy F-54000, France

2) CNRS, Laboratoire de Chimie Physique Macromoléculaire LCPM, FRE 3564, Nancy F-54000, France

KEYWORDS

o-nitrobenzyl acrylate, SET-LRP, dextran, grafted copolymer, click chemistry; light-responsive polymer, glycopolymer, biodegradable.

EXPERIMENTAL

Materials

Dextran T40 (= 34,000 g mol^{-1} and = 1.2) was purchased from Pharmacia Biotech and dried under reduced pressure at 100 °C overnight. No degradation of chains was evidenced under these drying conditions as attested by Size exclusion chromatography (SEC) analysis. Tris(2-aminoethyl)amine (TREN, 96%), formaldehyde solution (36.5-38.0 %wt), formic acid solution (49-51 %wt), Cu(II)Br_2 (99 %), Cu(I)Br (99.999 %), propargylamine (98 %), sodium azide (> 99.5), 2-(2-chloroethoxy)ethanol (99%) 1,1-Carbonyldiimidazole (CDI) (> 97%) and sodium cyanoborohydride (> 95 %) were obtained from Aldrich and used without any further purification. Ethyl 2-bromoisobutyrate (EBiB, Aldrich, 98 %) was dried on CaH_2 overnight and vacuum distillated at 70 °C. 2-(2-azidoethoxy)ethyl 2-bromoisobutyrate synthesis and activation of hex-5-ynoic acid with CDI were described in supplementary information. 2-(2-azidoethoxy)ethanol was synthesized as previously reported.[1] *O*-nitrobenzyl acrylate (NBA) synthesis was previously described[2]. Tris(2-(dimethylamino)ethyl)amine (Me_6TREN) was synthesized as previously reported.[3] Surface of Cu(0) wire (0.25 mm diameter) was polished. Then Cu(0) was immersed in concentrated H_2SO_4 (Aldrich, 95-98 %) for 20 min, washed with ethanol and finally dried.

Synthesis of Alkynated Dextran

9.71g (59.94 10^{-3} mol of glucopyranosic units) of dried dextran were dissolved in 97 ml of distilled DMSO with vigorous stirring at 60 °C. 1.37 g (0.15 eq of glucopyranosic units, 8.991 10^{-3} mol) of activated 5-hexynoic acid were added after complete dissolution of dextran. The reaction was stirred at 60 °C for 2.5 days. Crude product was precipitated in 1.5 L ethanol and filtrated. Then product was washed by vigorous stirring in ethanol for 30 min. Finally, 10.61 g of alkynated dextran were obtained after vacuum drying with a yield of substitution ( ) equal to 15%. Yield of substitution is the number of alkyne groups per 100 glucopyranosic units and was calculated by ^{1}H NMR in DMSO-d_6 (Fig. 1) using Eq. (1)

where A_8 and A_9 are the areas of 4 methylene protons of alkyl chains (centered at 1.7 and 2.25 ppm). A_1 is the area of the anomeric proton centered at 4.7 ppm.

$$= \frac{\square\square\square}{\square} \square\times \frac{\square\square\square}{\square\square} \qquad \text{Equation 1}$$

Homopolymerization of NBA by SET-LRP using non-functional initiator: Synthesis of PNBA-Br.

As previously reported[2] , schlenk tube was evacuated and filled by nitrogen. NBA (4 g, 0.193 mole, 26 eq), EBiB (108 µL, 0.74 10^{-3} mol, 1 eq), Me_6TREN (32 µL, 0.133 10^{-3} mol, 0.16 eq.), $CuBr_2$/Me_6TREN solution in DMSO (0.11 mol/L, 135 µl, 0.0148 10^{-3} mol of Me_6TREN, 0.02 eq of $CuBr_2$ and of Me_6TREN) and 4 mL DMSO were successively added under N_2 flow. Consequently, the final equivalent of Me_6TREN (0.18 eq) has to be taken in consideration. Then, medium was purged with N_2 gas for 10 minutes. 6.8 cm of activated metallic Cu(0) wire were added under nitrogen to initiate the polymerization at 20°C. After 3.5 hrs, a sample was withdrawn under nitrogen atmosphere from the polymerization mixture and quenched by cooling with liquid nitrogen to determine the monomer conversion from ^{1}H NMR spectrum in $CDCl_3$. A conversion of 60 % was estimated by comparing the peaks integrals of the aromatic protons of both the monomer and the polymer (7.3-8.2 ppm) with those of the ethylenic protons of the monomer (5.9, 6.2 and 6.3 ppm).[2] Polymer called PNBA-Br was precipitated from cold methanol and filtrated. $PNBA_{3500}$-Br was dried using vacuum oven and characterized by SEC: $\square_{n(SEC)}$ = 3,500 g mol^{-1} and dispersity $\square$ = 1.06. $\square_n$ was also estimated from ^{1}H NMR ($\square_{n(NMR)}$) taking account the peaks (a, c, d) and (g) : $\square_{n(NMR)}$ = 3,510 g mol^{-1} (Fig. 3 (a)).

Synthesis of ω-Azido-Terminated PNBA (PNBA-N_3)

1.465 g of $PNBA_{3500}$-Br (0.418 10^{-3} mol, 1 eq) was dissolved with 0.136 g sodium azide (2.09 10^{-3} mol, 5 eq) in 10 mL of anhydrous DMSO at room temperature. The reaction was leaved in dark place for 24 hrs. The solution was precipitated twice from cold methanol and filtrated. PNBA-N_3 was dried using vacuum oven. 1.0 g of pure $PNBA_{3500}$-N_3 was obtained (yield = 68 %). As shown on ^{1}H NMR spectrum (Fig 3(b)),

peak at 4.35 ppm that was characteristic of CH-Br end chain was no more observed. CH-N_3 peak is now overlaping with peak (b) from initiator group at 4 ppm. No degradation of PNBA was observed as confirmed by SEC traces (not shown).

Homopolymerization of NBA by SET-LRP using functional initiator: Synthesis of α-Azido-Terminated PNBA (N_3-PNBA-Br).

This polymerization was carried out according the experimental conditions above given. In this particular case, for instance, 2-(2-azidoethoxy)ethyl 2-bromoisobutyrate (146 µL, 0.74 10^{-3} mol, 1 eq) was used as functional initiator instead of EBiB. Me_6TREN (16 µL, 0.133 10^{-3} mol, 0.08 eq.), $CuBr_2$/Me_6TREN solution in DMSO (0.11 mol/L, 676 µl, 0.0742 10^{-3} mol of Me_6TREN, 0.1 eq of $CuBr_2$ and of Me_6TREN) and 4 mL DMSO were successively added under N_2 flow. A conversion of 88 % was estimated from ^{1}H NMR spectrum of crude product. Polymer was precipitated from cold methanol and filtrated. N_3-$PNBA_{4500}$-Br was dried using vacuum oven and then was characterized by SEC: $M_{n(SEC)}$ = 4,500 g mol^{-1} and dispersity Đ = 1.05. M_n was also estimated from ^{1}H NMR taking account the peaks (a, b, c, d) and (i) : $M_{n(NMR)}$ = 4600 g mol^{-1} (Fig. 3 (c)).

Synthesis of Dex-g-PNBA by CuAAC

For instance, in case of Dex(15)-g-$14PNBA_{3500}$ the reaction was carried out as follow: 1.86 g (0.532 10^{-3} mol, 1.04 eq) of $PNBA_{3500}$-N_3 and (0.6 g, 0.51 10^{-3} mol of alkyne groups) of alkynated dextran were dissolved in 20 mL of DMSO. Then, solution was purged using N_2 for 10 min. 0.076 g (0.532 10^{-3} mol, 1 eq) of CuBr and 3.4 mg (0.0532 10^{-3} mol, 0.1 eq) of Cu(0) were added under nitrogen. Solution was left stirring for 48 hrs in dark place to avoid photolysis of PNBA. Then, solution was precipitated using syringe filter (to remove Cu(0)) from cold mixture of methanol/water (8/2, v/v), containing 5 eq of EDTA to remove all copper salts. Powder was filtered and dried using vacuum oven. The prepared grafted glycopolymer may contain some ungrafted $PNBA_{3500}$-N_3. Thus, powder was washed with a mixture of acetone/diethyl ether (8/2, v/v). 2.12 g (yield = 89 %) of pure Dex(15)-g-$14PNBA_{3500}$ copolymer were

finally obtained. (15) was yield of substitution of alkynated dextran, 14 are the number of PNBA grafts ($M_{n(SEC)}$ = 3500 g. mol^{-1}) per 100 glucopyranosic units.

Irradiation of Dex-g-PNBA

Solution of Dex-g-PNBA was prepared in DMSO with concentration 0.07 mg/mL. 3 mL of stirred solution was irradiated in 1 cm x 1 cm quartz cuvette with a OmniCure® S1000 UV spot cure lamp at 1150 mw/cm² power. A light guide of 8 mm diameter equipped with a 320-500 nm filter was used. UV-Visible absorbance spectra of solution were measured before and after various irradiation time.

Characterization Techniques

^{1}H NMR, ^{13}C NMR and 2D DOSY ^{1}H NMR spectra were recorded on a Bruker Avance 300 apparatus (300,13 MHz, 25°C) in DMSO-d_6 or $CDCl_3$.

FTIR spectra were performed using Tensor 27 (Brucker Optics) equipped with MIR source (middle-infrared light) and DLaTGS detector.

Size Exclusion Chromatography (SEC) in THF was performed at 40°C with a Multi Angle Laser Light Scattering detector (MALLS - Mini Dawn Treos, Wyatt), a differential refractometer detector (OPTILab rex, Wyatt), a HPLC pump (Waters 515), a degazer AF (waters In-Line) and three PLgel 5 ≋ (10^5 A°, 10^3 A° and 100 A°) columns (300mm x 7.5mm). Elution rate was 1 ml/min. SEC in DMSO (0.1 M $NaNO_3$) was performed at 70°C with MALLS - Mini Dawn Treos detector, a differential refractometer detector (RID - 10A, Shimadzu), a UV detector (SPD - 20A, Shimadzu), a HPLC pump (LC - 20AD, Shimadzu), a degazer (DGU - $20A_{3R}$, Shimadzu) and three PLgel 5 ≋ (10^5 A°, 10^3 A° and 100 A°) columns (300mm x 7.5mm). Elution rate was 0.7 ml/min. Solutions (10 mg/mL) were prepared by dissolution in THF or DMSO and left under vigorous stirring for 24 h. Filtration of solutions was carried out right before injection. Refractive index increments (dn/dc) was measured with a differential refractometer (Waters 410). For PNBA-N_3 and N_3-PNBA-Br, dn/dc equal to 0.137 mL/g and 0.152 mL/g were respectively

measured in THF at 40°C. dn/dc was found equal to 0.1 mL/g in DMSO at 50°C. dn/dc = 0.07 mL/g for dextran and alkynated dextran was measured in DMSO at 50°C. dn/dc of each Dex-g-PNBA was estimated in DMSO at 50°C

UV-Visible spectra of Dex-b-PNBA and of photolysis product were measured using Uvikon-XL Bio-Tek Spectrophotometer. The absorbance was recorded in the 250-450 nm range.

RESULTS AND DISCUSSION

Dextran Backbone Modification

Dextrans are polysaccharides synthesized from sucrose by micro-organisms. The most studied dextrans are produced by *Leuconostoc mesenteroides* strain B-512(F) and hydrolyzed under acidic conditions by controlled way. The resulting linear polysaccharides consist of α-D glucopyranosic units having preponderant α(1→6) linkages, while few percents of α(1→3) linkages provide short side chains.

Many modifications of dextran have been reported to either increase its thermal stability at high temperature or its solubility in organic solvents. For instance, silylation[4, 5] or acetylation[6] have been reported. According a precise study, the reactivity order of all the glycopyranosic alcohol functions was found.[4, 6] In a parallel way, some dextran-based surfactants have been obtained by dextran modification with alkyl or aromatic epoxides.[7] Recent developments of the Huisgen-type Copper (I)-catalyzed Azide-Alkyne Cycloaddition (CuAAC) click-chemistry have opened new ways of polysaccharides modification.

The introduction of azide or alkyne functionalities onto dextran chain can be obtained by tosylation/azidation[8], urethanization[9], etherification[10-14], carbonation[9, 10, 15, 16] and esterification[10, 17, 18]. Alkynated dextran has been synthesized through an esterification reaction described in Scheme 1 and adapted from a previous study[18]. First, activated 5-hexynoic acid (1) was prepared and isolated in good yield (see supplementary information). Then, alkyne groups were introduced all long the dextran chain in DMSO at 60°C according Scheme 1.

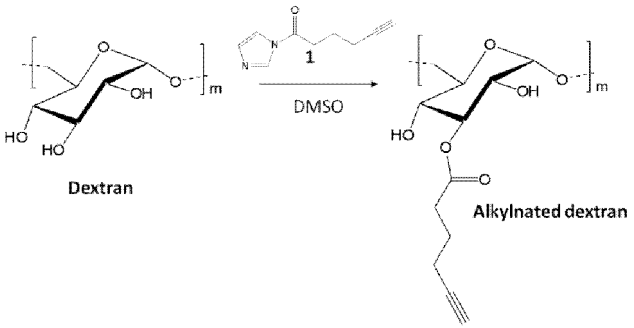

Scheme 1. Alkynated Dextran Synthesis.

Size Exclusion Chromatographie traces (Figure S2) confirmed the non-degrading character of this modification step. ^{1}H NMR spectra of dextran and alkynated dextran (Fig 1) revealed the apparition of the alkynyl proton peak at 2.75 ppm and 3 methylene peaks of the alkyl spacer between 1.5 to 2.5 ppm. A yield of substitution ( ) equal to 15% (15 pending alkyne groups per 100 glucopyranosic units) was evaluated according to equation 1. Taking into account the equivalence of (1), a quantitative reaction was achieved. Moreover, FTIR spectrum of alkynated dextran (Fig 2) showed a small band around 2100 cm^{-1} corresponding to the alkynyl groups.

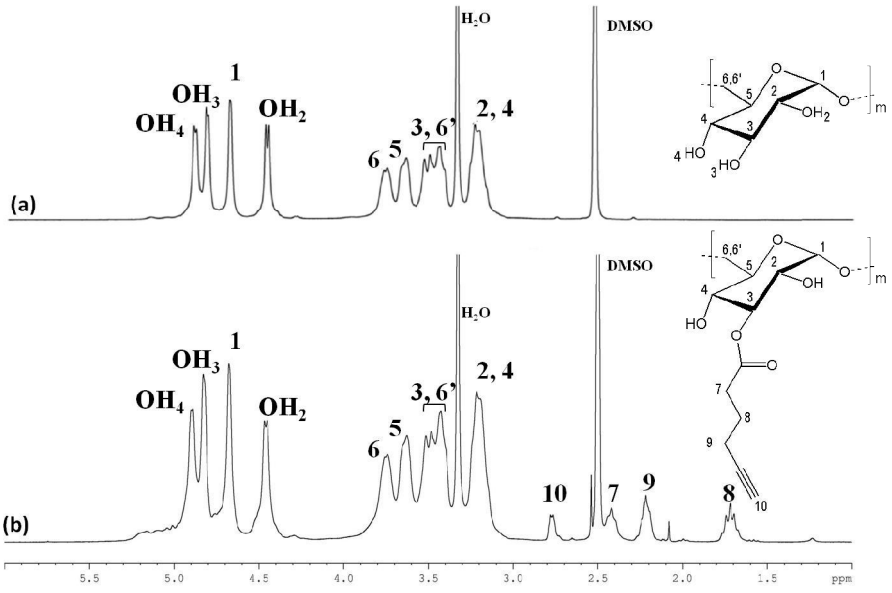

Figure 1. ^{1}H NMR spectra of dextran (a) and alkynated dextran (b) in DMSO-d_6. (Formula drawn in (b) is not the real formula but just a schematic representation)

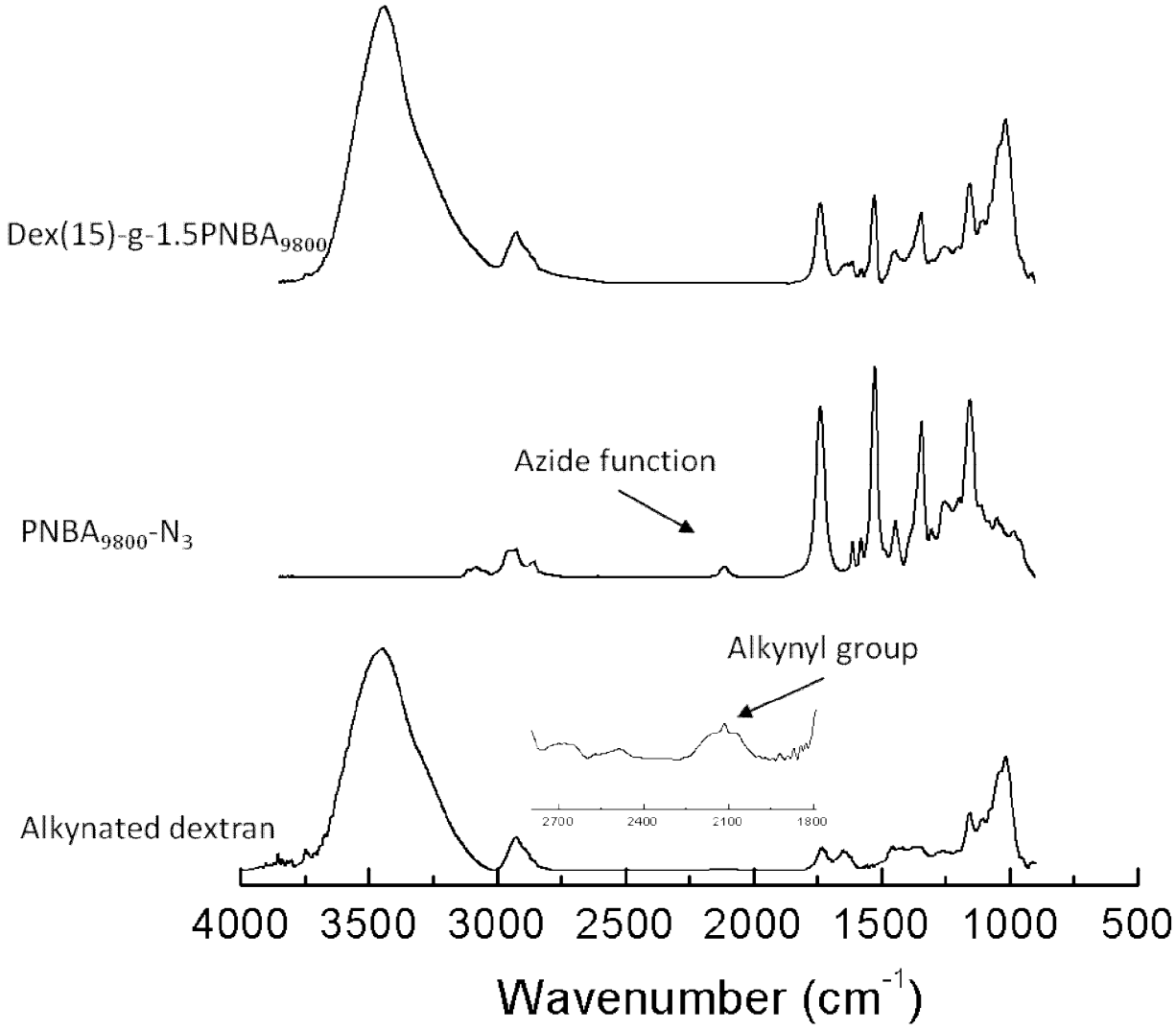

Figure 2. FTIR spectra of alkynated dextran, $PNBA_{9800}$-N_3 and Dex(15)-g-1.5$PNBA_{9800}$.

ω-Azido-Terminated PNBA (PNBA-N_3)

Several attempts to polymerize *o*-nitrobenzyl acrylate (NBA) by atom transfer radical polymerization (ATRP) in various solvents and different temperatures have been made but gave uncontrolled polymerization. Same behavior was described in the literature using ATRP and other controlled radical polymerization techniques such as radical addition-fragmentation transfert (RAFT) and nitroxyde mediated polymerization (NMP)[19]. Inhibition and retardation effects coming from the nitro-aromatic

groups[19-22] were designated as the origin of this lack of control. In a recent study, we demonstrated for the first time that NBA could be polymerized by SET-LRP in a controlled way using ethyl 2-bromoisobutyrate (EBiB) as non-functional initiator[2]. A first-order kinetics with respect to the NBA concentration was observed. Moreover, up to 50 % conversion, the SET-LRP proceeded with a linear evolution of molecular weight with a narrow distribution (dispersity < 1.2).

$PNBA_{3500}$-Br and $PNBA_{9800}$-Br were prepared by SET-LRP (Scheme 2-a) using the respective molar ratios $[NBA]_0/[EBiB]_0/[Me_6TREN]_0/[CuBr_2]_0$ = 26/1/0.18/0.02 (Entry 1, Table 1) and $[NBA]_0/[EBiB]_0/[Me_6TREN]_0/[CuBr_2]_0$ = 100/1/1/0.1 (Entry 2, Table 1) in DMSO at 20°C. After purification, PNBA-Br were analyzed by ^{1}H NMR (Fig 3-a) and SEC. A really good agreement was obtained between the theoretical molecular weight calculated from the conversion ($M_{n(th)}$), the molecular weight determined by ^{1}H NMR ($M_{n(NMR)}$) and the molecular weight estimated by SEC ($M_{n(SEC)}$) (Table 1). From these data, an initiation efficiency equal to 98% and 94% were calculated respectively for $PNBA_{3500}$-Br and $PNBA_{9800}$-Br . The good control of the NBA polymerization was confirmed by the low dispersity of the sample (仔H1.10).

SET-LRP provides an access to high halogen-functionality at the chain-end, even at high monomer conversion[23, 24]. From the ^{1}H NMR areas (Fig 3-a) of peak (b) corresponding to the -CH_2- initiator group and the peak (m) corresponding to -CHBr, chain end functionalities beyond 96 % were calculated for both experiments. The terminal bromide atom of PNBA-Br was further replaced by azide function as shown in Scheme 2-a. A classical nucleophilic substitution with sodium azide in DMSO was performed[25] . After purification, analysis of FTIR spectrum of $PNBA_{9800}$-N_3 (Fig 2) revealed an absorption peak at about 2100 cm^{-1} characteristic of the azide function. Moreover, the complete shifting of the terminal methyl proton peak (m) from 4.3 ppm to 4 ppm (Fig 3-b) was also a strong indication of the quantitative azidation of the PNBA-Br end chain. SEC chromatograms of PNBA chains after azidation shown a monomodal

distribution of the molecular weight with low dispersity (仔Ħ1.10), indicating no degradation under this treatment (Fig 4).

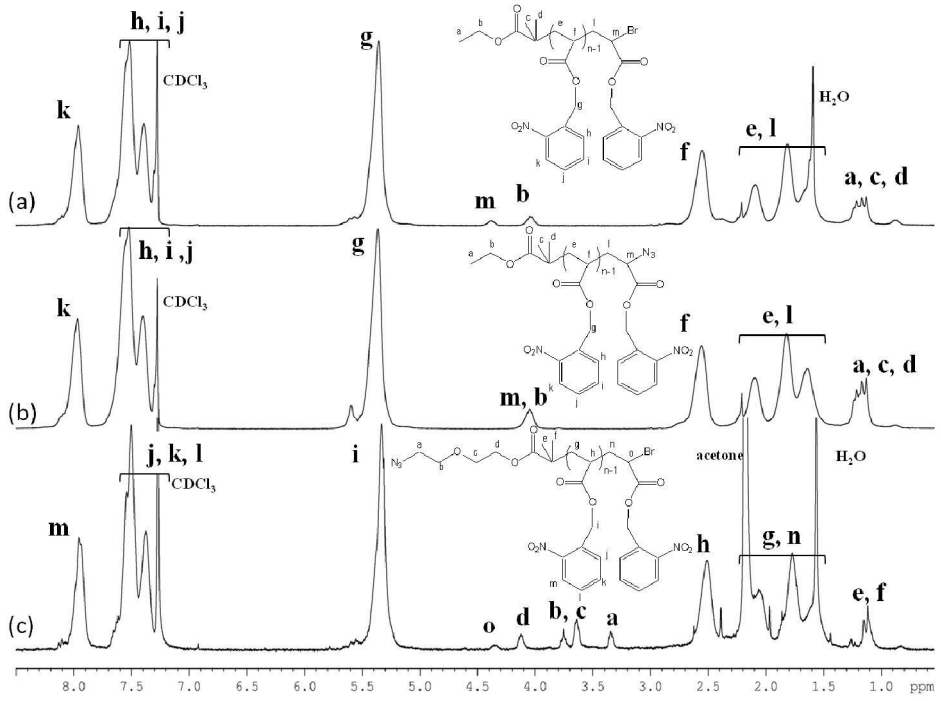

Figure 3. ^{1}H NMR spectra of (a) $PNBA_{9800}$-Br, (b) $PNBA_{9800}$-N_3 and (c) N_3-$PNBA_{4500}$-Br in $CDCl_3$.

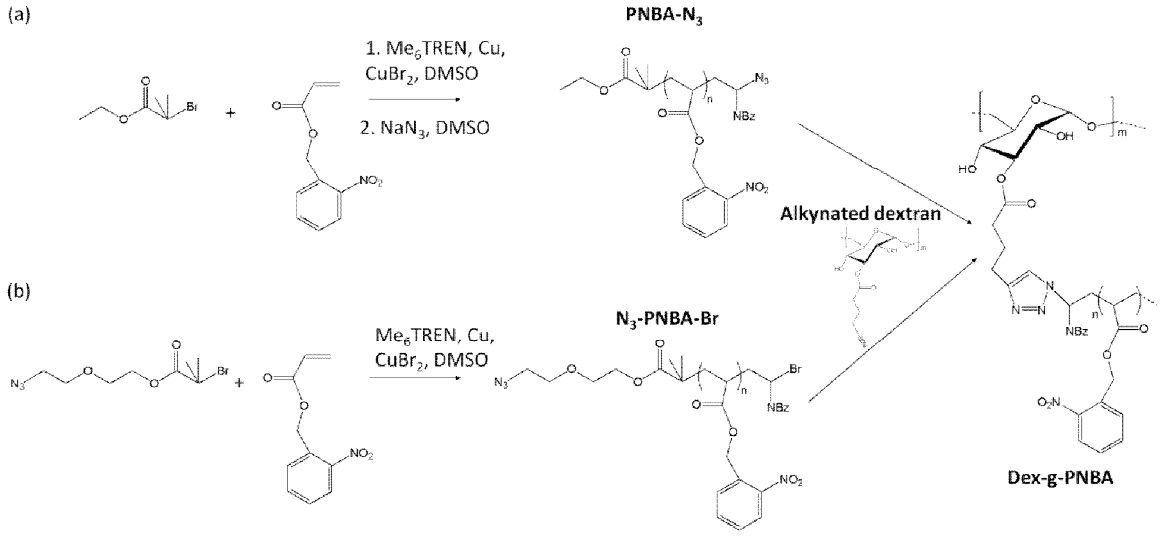

Scheme 2. Dex-g-PNBA Synthesis.

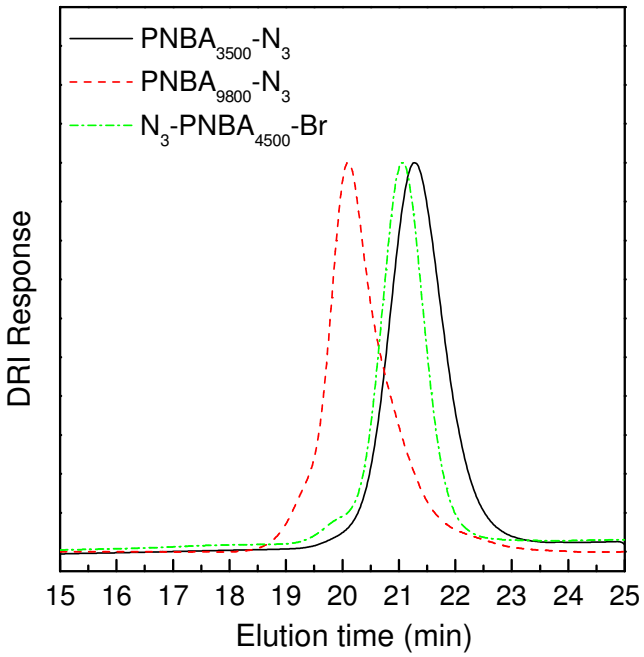

Figure 4. SEC chromatograms in THF of $PNBA_{3500}$-N_3, $PNBA_{9800}$-N_3 and N_3-$PNBA_{4500}$-Br (Differential Refractive Index Response).

α-Azido-Terminated PNBA (N_3-PNBA-Br)

Clickable macromolecules can also be obtained in one step by controlled radical polymerizations using functional initiators.[26] We used an appropriate initiator with an azide function in α-position to initiate the SET-LRP of NBA (Scheme 2 (b)). 2-(2-azidoethoxy)2-bromoisobutyrate (N_3RBr) initiator was obtained in good yield (see supporting information) and its purity was checked by ^{1}H NMR (Figure S3). Polymerizations were carried out at low temperature (20°C) to prevent side reactions such as cylization of azide function with the propagating radical or/and the 1,3-cycloaddition between the azide group and the double bond of the monomer.[26] In a first set of experiment, optimized molar ratio previously used with the non-functionalized initiator was applied ($[NBA]_0/[N_3RBr]_0/[Me_6TREN]_0/[CuBr_2]_0$ = 26/1/0.18/0.02). Unfortunately, uncontrolled polymerization was obtained. SEC analysis of polymer samples at various conversion revealed the presence of two populations as shown on figure S4 . The first one at high elution time is evolving with monomer conversion and corresponds to the desired PNBA. The second one, at low elution time, was stationary whatever the monomer conversion and corresponds to an uncontrolled high

molecular weight PNBA formed in the early stages of the reaction. Similar results have been described by Haddleton and coll. studying SET-LRP of methyl acrylate.[27, 28] An increase of $CuBr_2$ from 0.02 eq to 0.1eq (Entry 3, Table 1) prevented the formation of the high molecular weight contaminant as shown on the SEC chromatograms overlay (Fig. 5 (c)) where only one peak corresponding to the expected PNBA is present, even at low monomer conversion. Moreover, as conversion increases, the elution volume of this population decreases. No significant bimolecular termination reaction was detected (Fig. 5(c)). From this termination reaction, α,ω-azido PNBA bearing two azide functions would be produced that could act as an undesired crosslinking agent during the following click chemistry step. After an apparent induction period around 40 min a linear evolution of $\ln [M]_0/[M]_t$ *versus* time was observed (Fig. 5 (a)). This indicates a constant concentration in radical species during this period. $M_{n,SEC}$ determined by SEC increase linearly with conversion and are slightly above than the theoretical M_n (Fig. 5 (b), accordingly an initiation efficiency equal to 82%. Dispersities ($Đ$) decrease with conversion to stabilize to 1.03 confirming the good control of the NBA polymerization (Fig. 5 (b)). N_3-PNBA-Br sample isolated at 88% conversion ($M_{n,(SEC)}$ = 4,500 g/mol, $Đ$= 1.07) was purified and analysed by ^{1}H NMR spectroscopy (Fig. 2 (c)). Signals (a,b,c) and (d) corresponding to the 4 methylenes of the initiator fragment clearly appeared between 3.3 and 4.2 ppm, which confirmed the obtaining of N_3-PNBA-Br (Fig. 2(c)). FTIR spectrum (Figure S5) showed also an absorption peak at about 2100 cm^{-1} characteristic of the azide function.

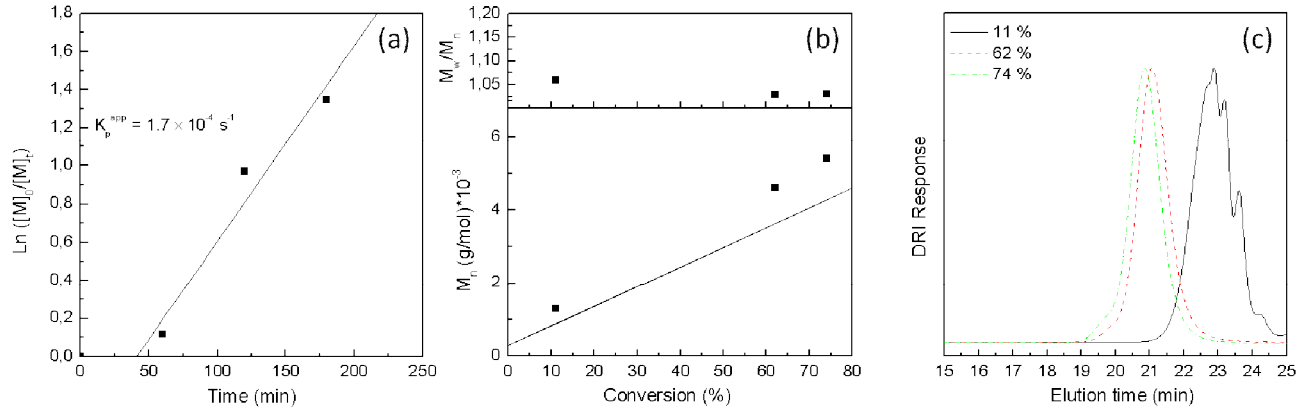

Figure 5. SET-LRP of NBA with $[NBA]_0/[N_3RBr]_0/[Me_6TREN]_0/[CuBr_2]_0$ = 26/1/0.18/0.1 in DMSO at 20°C (Entry 3, Table 1). (a) Plots of ln $[M]_0/[M]_t$ *versus* time. (b) Plots of $M_{n(SEC)}$ (square), theoretical M_n (line) and dispersities Đ *versus* conversion. (c) Evolution of the SEC traces (Differential Refractive Index response) at various conversion.

Table 1. Synthesis of ω-Azido-Terminated PNBA (PNBA-N_3) and α-Azido-Terminated PNBA (N_3-PNBA-Br) by SET-LRP of NBA.

Entry	PNBA	Initiator	$([NBA]_0/[Initiator]_0/[Me_6TREN]_0/[CuBr_2]_0)$	Cu(0) Wire Length (cm)	Time (min)	Conversion (%) [a]	$M_{n(theo)}$ (g mol^{-1}) [b]	$M_{n(NMR)}$ (g mol^{-1}) [c]	$M_{n(SEC)}$ (g mol^{-1}) [d]	Đ [d]
1	$PNBA_{3500}$-N_3	EBiB	(26 /1 /0.18 /0.02)	6.8	210	60	3,425	3,510	3,500	1.06
2	$PNBA_{9800}$-N_3	EBiB	(100/1/1/0.1)	11.9	240	44	9,300	9,100	9,800	1.10
3	N_3-$PNBA_{4500}$-Br	N_3RBr	(26 /1 /0.18 /0.1)	6.8	180	88	4,930	4,600	4,500	1.07

a) Estimated from ^{1}H NMR spectrum of crude product

b) Estimated using $M_{n(theo)} = M_{initiator} + (conv. \times ([NBA]_0/[Initiator]_0) \times M_{NBA}$, w*here M_{EBiB}, M_{N3RBr} and M_{NBA} are equal to 195, 280 and 207 g. mol^{-1}, respectively.*

c) Estimated from ^{1}H NMR spectrum of purified product

d) Evaluated from SEC-MALLS in THF

Synthesis of Dex-g-PNBA by CuAAC

Dextran-g-poly(*o*-nitrobenzyl acrylate) (Dex-g-PNBA) amphiphilic glycopolymers were elaborated by a "grafting onto" method depicted on Scheme 2. Coupling between the alkynated dextran (= 15%) and azido-terminated poly(*o*-nitrobenzyl acrylate) was realized by the copper(I)-catalyzed azide-alkyne cycloaddition (CuAAC).[18, 29-31] CuAAC was performed using CuBr/Cu(0) in anhydrous DMSO and different ratios between PNBA-N_3 and alkynated dextran (Table 2). After reaction, grafted copolymers were purified by extraction of free PNBA-N_3 by washing with a acetone/diethyl ether (8/2, v/v) mixture. As a first evidence of the coupling reaction between ω-azido-terminated PNBA and alkynated-dextran, FTIR spectroscopy of Dex(15)-g-1.5$PNBA_{9800}$ revealed the disappearance of the azide and the alkyne peaks around 2100 cm^{-1} (Fig 3) originally present in the spectra of both precursors. Moreover, the ^1H NMR spectrum of Dex(15)-g-1.5$PNBA_{9800}$ (Fig. 6 (a)) showed typical signals of both parts especially the aromatic protons peaks at 7.3-8.1 ppm attributed to the PNBA grafts and the glucosidic (3-5 ppm) and anomeric protons at 4.65 ppm from dextran. No direct evidence of the triazole ring formation was displayed due to the overlap of the aromatic protons peaks (k) at 8.0 ppm with that of triazole proton generally localized around 8.1 ppm.[18] Same FTIR (Fig. S5) and ^1H NMR (Fig. S6) characterizations were made with the glycopolymer Dex(15)-g-14.5$PNBA_{4500}$ elaborated from N_3-PNBA-Br. PNBA weight fraction (F_{PNBA}) and number of PNBA grafts along the dextran chain (n_{graft}) in glycopolymers have been estimated from ^1H NMR spectra and reported in Table 2. Typical ^{13}C NMR spectra of $PNBA_{3500}$-N_3, alkynated dextran and resulting grafted copolymer were drawn on Figure S7.

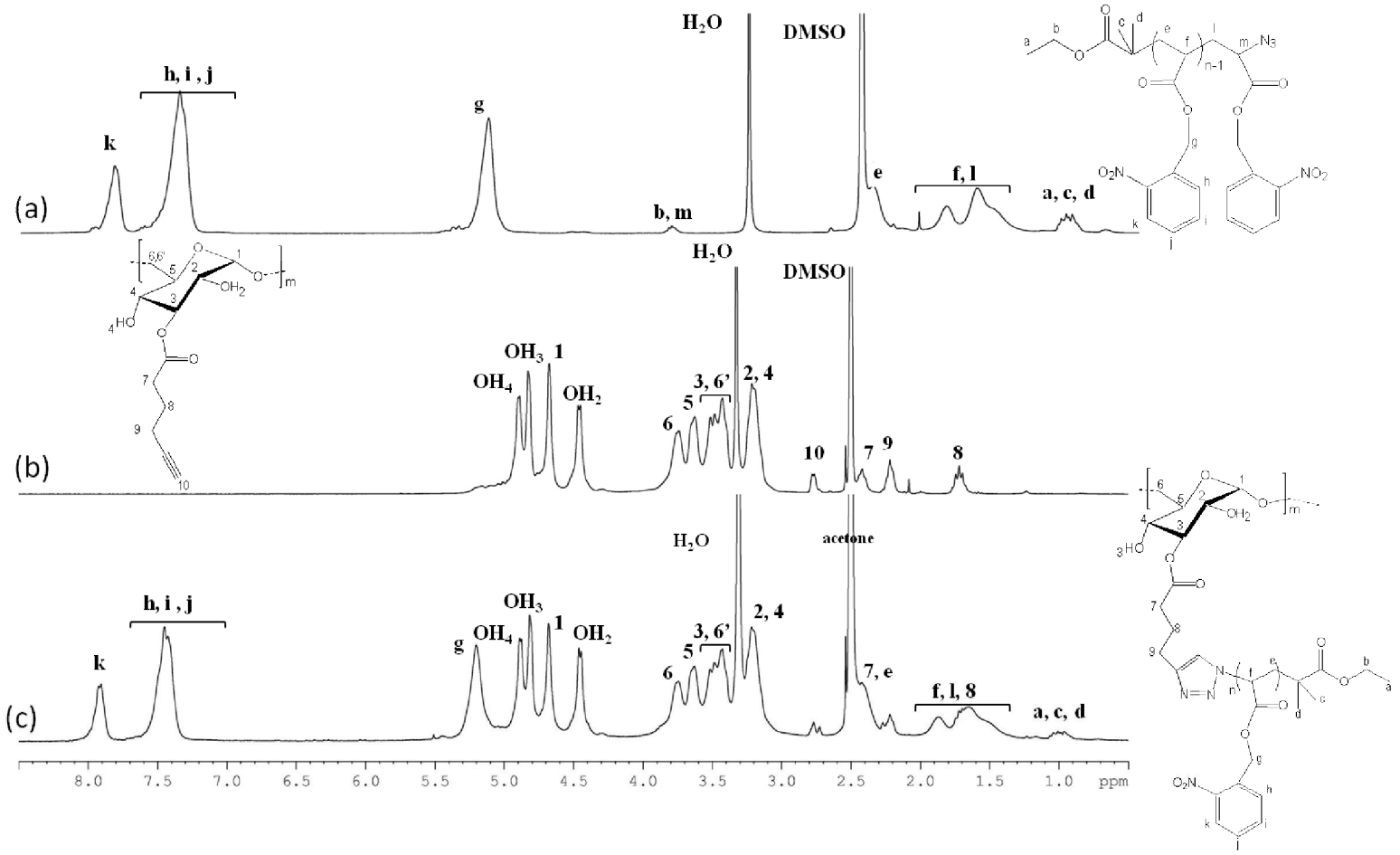

Figure 6. ^{1}H NMR spectra of (a) $PNBA_{9800}$-N_3, (b) alkynated dextran and (c) Dex(15)-g-1.5$PNBA_{9800}$ in DMSO-d_6.

Table 2. Characteristics of Dex-g-PNBA grafted copolymers

Entry	Glycopolymers	$M_{n(SEC)}$ PNBA-N_3 (g mol^{-1}) [a]	*N_3/alkyne molar ratio*	$M_{n(theo)}$ (g mol^{-1})	$M_{n(SEC)}$ (g mol^{-1}) [b]	Đ [b]	dn/dC (mg mL^{-1}) [c]	F_{PNBA} (wt%) [d]	n_{graft} [e] (^{1}HNMR)
4	Dex(15)-g-1.5PNBA$_{3500}$	3,500	0.104	46,160	40,640	1.34	0.07	22	3
5	Dex(15)-g-14PNBA$_{3500}$	3,500	1.040	144,400	149,400	1.59	0.08	75	28
6	Dex(15)-g-1.5PNBA$_{9800}$	9,800	0.104	65,820	75,800	1.09	0.07	44	3
7	Dex(15)-g-12PNBA$_{9800}$	9,800	1.040	341,000	324,900	1.59	0.08	85	24
8	Dex(15)-g-14.5PNBA$_{4500}$	4,500	1.040	175,640	167,500	1.40	0,08	79	29

a) Evaluated from SEC-MALLS in THF

b) Evaluated from SEC-MALLS analysis in DMSO (0.1M $NaNO_3$)

c) Measured in DMSO (0.1M $NaNO_3$) at 50°C

d) Weight fraction of PNBA in the grafted copolymers calculated from ^{1}H NMR using:

$$F_{PNBA} = \frac{\frac{A_g}{2} \times 207}{\frac{A_g}{2} \times 207 + A_1 \times 176.1} \times 100$$

Where A_g and A_1 are areas under peak (g) and (1), respectively (Fig. 6c). 207 is the molecular weight of one NBA monomer unit and 176.1 the average molecular weight of repeating unit of alkynated dextran

e) Number of PNBA grafts along dextran chain was estimated from ^{1}H NMR spectrum (Fig. 6c) using

$$n_{graft} = \frac{\frac{M_{n(native\ dextran)}}{162} \times \frac{A_{ar}}{3}}{DP_{graft} \times A_1}$$

Where $M_{n(native\ dextran)}$ is the M_n of native dextran (see materials part), A_{ar} area under peak (h, i, j) (Fig. 6c), 162 the molecular weight of one glucopyranosic unit and DP_{graft} the average polymerization degree of PNBA grafts.

Indirect confirmation of the covalent triazole link between parts was proved by 2D Diffusion-Ordered Spectroscopy (DOSY) ^{1}H NMR. This technique allows to measure the self-diffusion coefficient of each molecular species in a mixture. With polymers, it's a powerful method to discriminate between a block copolymer and the corresponding blocks mixture.[33] 2D DOSY ^{1}H NMR spectrum of Dex(15)-g-1.5PNBA$_{9800}$ was recorded in dilute DMSO-d_6 (Fig. 7 (a)). A single self-diffusion coefficient was observed for all the protons from dextran and PNBA segments ($D = 1.66 \times 10^{-10}$ m^2 s^{-1}) which is consistent with an efficient coupling CuAAC reaction between parts. A mixture of PNBA$_{9800}$-N$_3$ and alkynated dextran with similar weight composition than the Dex(15)-g-1.5PNBA$_{9800}$ was studied by 2D DOSY ^{1}H NMR (Fig. 7 (b)). As shown, two separate diffusion coefficients were observed ($D = 1.26 \times 10^{-10}$ m^2 s^{-1} and $D = 2.39 \times 10^{-10}$ m^2 s^{-1}) for alkynated dextran and PNBA, respectively. The presence of 2 separate diffusion coefficients shown on 2D DOSY ^{1}H NMR of the mixture, while only one (at one another value) is observed in case of grafted copolymers spectra, proved that analyzed copolymers are really composed by covalently linked PNBA grafts onto dextran backbone.

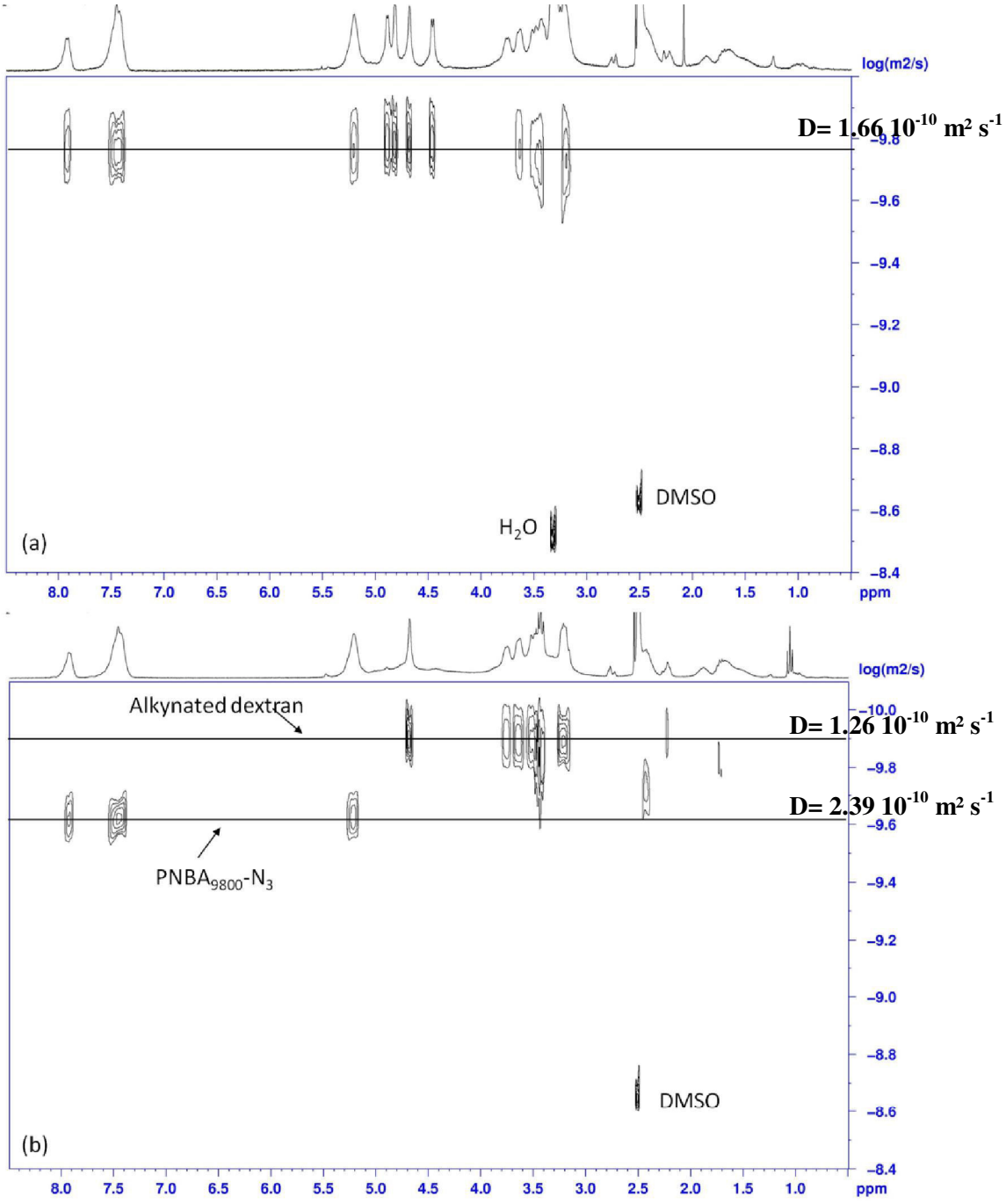

Figure 7. 2D DOSY ^{1}H NMR spectra of Dex(15)-g-1.5PNBA$_{9800}$ (a) and a mixture of PNBA$_{9800}$-N$_3$ and alkynated dextran (1:1; w:w) (b) in DMSO-*d*$_6$.

Finally, Dex-g-PNBA glycopolymers were characterized by SEC using DMSO/$NaNO_3$ as eluent (Fig. 8). Chromatograms of Dex(15)-g-1.5$PNBA_{3500}$ and Dex(15)-g-14$PNBA_{3500}$ clearly indicated a shift of the molecular weight distribution compare to the $PNBA_{3500}$-N_3 and alkynated dextran starting materials (Fig. 8 (a)). No peak of residual unlinked $PNBA_{3500}$-N_3 was observed. Therefore, one can conclude that $PNBA_{3500}$-N_3 grafts were linked to dextran during the CuAAC click reaction. Same evolution of chromatograms was observed with the Dex(15)-g-14.5$PNBA_{4500}$ elaborated from N_3-$PNBA_{4500}$-Br (Fig. 8 (b)). From MALLS detector, absolute molecular weights were determined ($M_{w,abs}$) and were in really good agreement with the theoretical molecular weights ($M_{w,theo}$) (Table 2). These results confirmed the high yield of the click reaction.

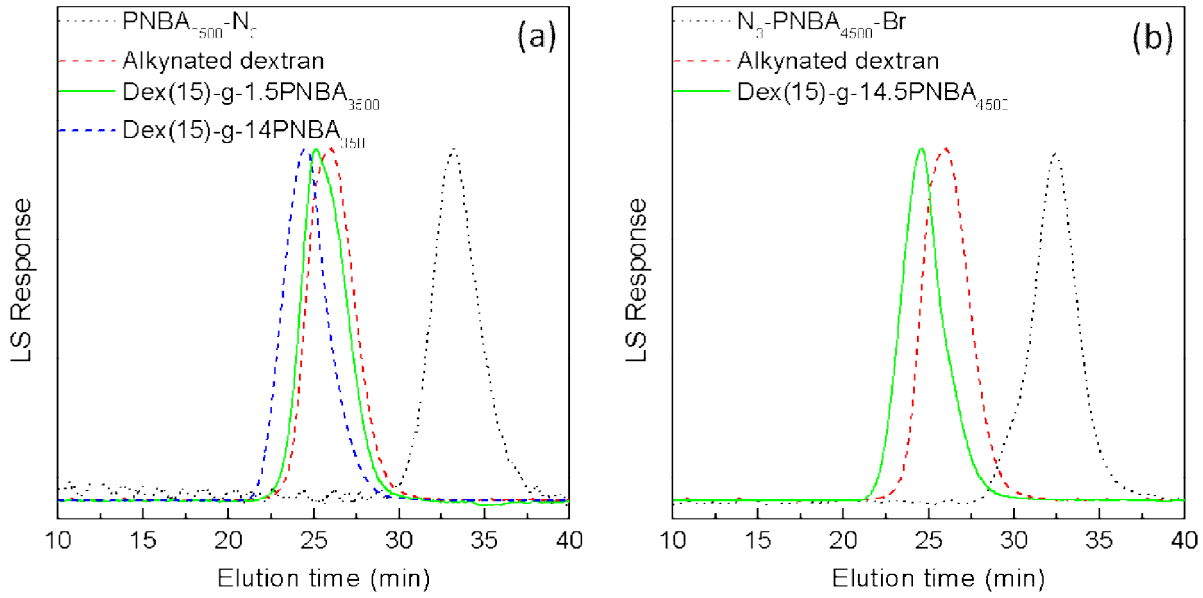

Figure 8. SEC chromatograms of PNBA and alkynated dextran precursors and Dex-g-PNBA glycopolymers. a) Case of $PNBA_{3500}$-N_3. b) Case of N_3-$PNBA_{4500}$-Br.

Light Irradiation of Dex-*g*-PNBA

Photosensitive property of dextran-g-poly(*o*-nitrobenzyl acrylate) was evaluated with a light irradiation experiment. Upon one photon irradiation, 2-nitrobenzyl esters are known to be cleaved liberating carboxylic acid groups and 2-nitrosobenzaldehyde byproducts[34]. This photocleavage can be easily followed on UV-visible absorption spectra, where 2-nitrobenzyl ester and 2-nitrosobenzaldehyde present two different bands. Light irradiation of Dex(15)-g-12PNBA$_{9800}$ was carried out in DMSO (0.07 mg/mL) with a UV light (spectra range from 320 nm to 500 nm; 1150 mW/cm² power). UV-Visible absorbance spectra of solution were measured before and after different irradiation times (Fig. 9 (a)). Before irradiation, a band at 275 nm was detected that corresponds to the absorption of 2-nitrobenzyl ester of each NBA monomer unit. After UV irradiation, the intensity of this band decreased while another band appeared at 325 nm characteristic of the formation of 2-nitrosobenzaldhyde. Plot of the absorbance at 325 nm *versus* irradiation time shows a fast photocleavage that evolves no more after 5 min (Fig. 9 (b)). By comparison with the irradiation study of PNBA homopolymers, one can conclude that dextran part in the copolymer didn't prevent the PNBA photolysis but slow down it as the absorbance at 325 nm reach a plateau value after 400 s in case of PNBA homopolymers. [2]

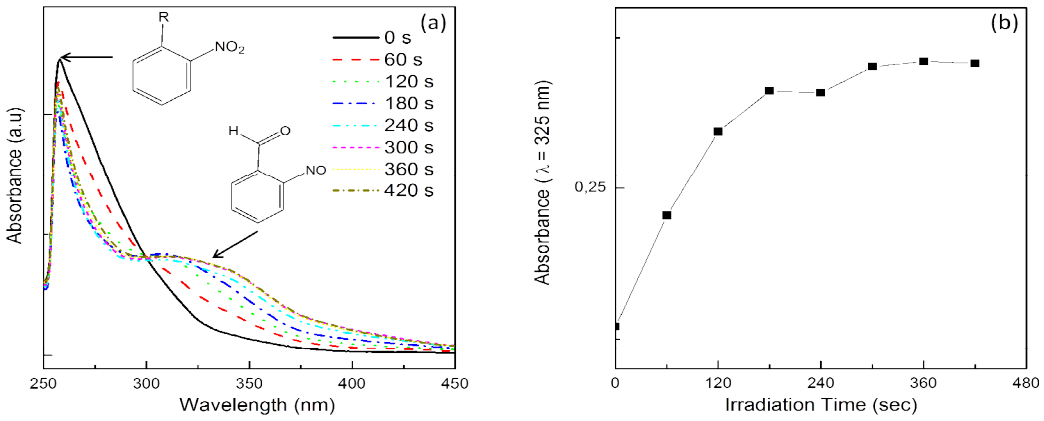

Figure 9. Light irradiation of Dex(15)-g-12PNBA$_{9800}$ in DMSO (0.07mg/mL) with a UV lamp equipped with a 320 -500 nm filter (power 1150 mw/cm²). (a) UV-Vis spectra after various irradiation times. (b) Absorbance at 325 nm *versus* irradiation time

ACKNOWLEDGMENT

The authors express their highest gratitude to Marie-Christine Grassiot for help in SEC measurements and Olivier Fabre for NMR measurements. S.M.A. Soliman gratefully acknowledges support from an Erasmus Mundus External Cooperation Windows ¯ Flow by Flow EU-Egypt Bridge Building (FFEEBB) Graduate Research Fellowship.

SUPPORTING INFORMATIONS FOR

Synthesis of Amphiphilic Light-Responsive Dextran-g-poly(*o*-nitrobenzyl acrylate) Glycopolymers

Soliman Mehawed Abdellatif SOLIMAN[1,2], *Cécile NOUVEL*[1,2], *Jérôme BABIN*[1,2], *Jean-Luc SIX*[1,2]*

1) Université de Lorraine, Laboratoire de Chimie Physique Macromoléculaire LCPM, FRE 3564, Nancy F-54000, France

2) CNRS, Laboratoire de Chimie Physique Macromoléculaire LCPM, FRE 3564, Nancy F-54000, France

KEYWORDS

o-nitrobenzyl acrylate, SET-LRP, dextran, grafted copolymer, click chemistry; light-responsive polymer, glycopolymer, biodegradable.

Activation of hex-5-ynoic acid

8.69g (53.508 10^{-3} mol) of 1,1˘-carbonyldiimidazole (CDI) was suspended in 40 ml of dichloromethane with stirring at 37 °C. 5g (44.59 10^{-3} mol) of hex-5-ynoic acid in 10 ml of dichloromethane was added to the reaction medium drop by drop under nitrogen. The reaction (Scheme S1) was stopped after 2 hrs and the crude product was washed 3 times using 50 ml of distilled water. Finally, product was dried over anhydrous $MgSO_4$. 6.45 g of pure activated hex-5-ynoic acid was obtained and the yield of reaction = 96%. ^{1}H NMR spectrum of activated hex-5-ynoic acid is given on Fig. S1.

Scheme S1. Activation of hex-5-ynoic acid with CDI

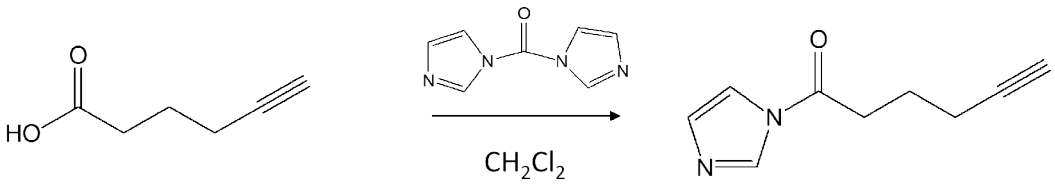

Figure S1: ^{1}H NMR spectrum ($CDCl_3$) of activated hex-5-ynoic acid

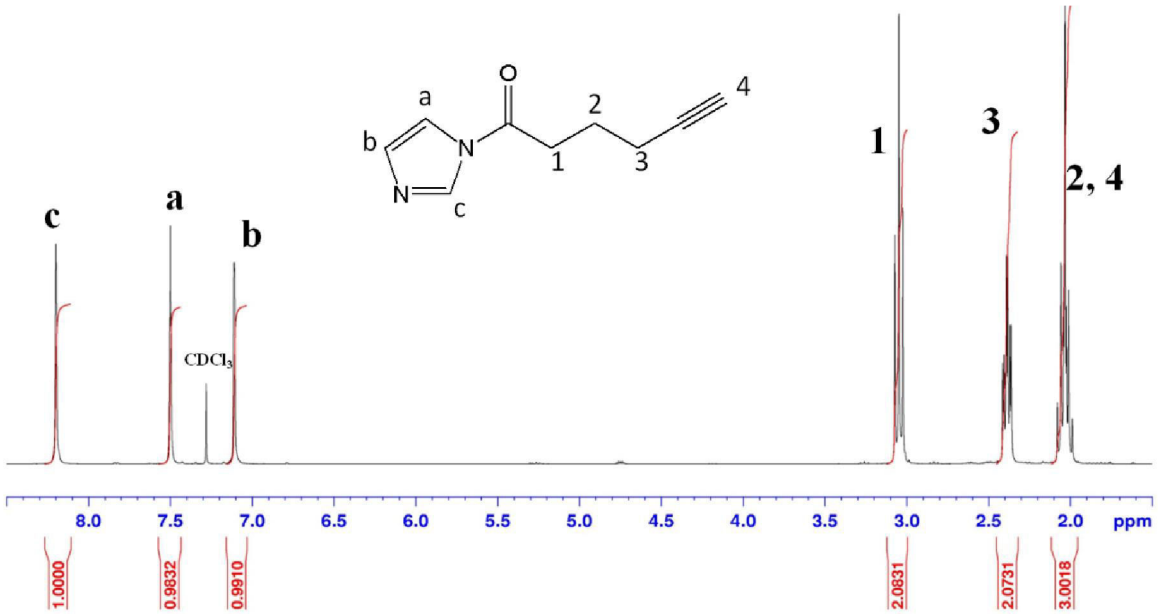

Figure S2. SEC chromatograms in DMSO (0.1M $NaNO_3$) of dextran and alkynated dextran. (Differential Refractive Index response).

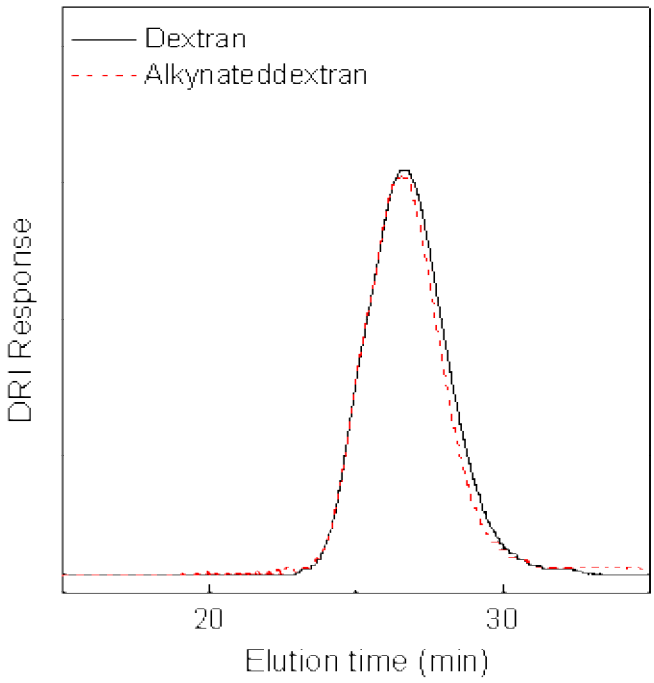

Synthesis of azide functionalized initiator (N_3RBr) (Scheme S2)

2-(2-Azidoethoxy)ethanol (2g, 15.25 10^{-3} mol) was dissolved in 25 ml of dichloromethane (DCM). Et_3N (1.5 eq, 3.2 mL) was added at 0 °C with stirring. 2-Bromo-2-methylpropionyl bromide (1.5 eq, 2.83 mL) was diluted by 15 ml of DCM and was added drop by drop with stirring at 0 °C. Solution was left stirring at 0 °C for 1 hr, then 2 hrs at room temperature. Medium was filtrated to remove ammonium salts, washed 2 times with $NaHCO_3$ saturated solution and finally with distilled water. Organic phase was dried over anhydrous $MgSO_4$. Crude product was purified by column chromatography (Petroleum Ether/ EtOAc, 7/3) to yield 73 % (3.13 g) of colorless oil. ^1H NMR spectrum of this functionalized initiator is given on Fig. S3.

Scheme S2. Synthesis of functionalized initiator (N_3-R-Br)

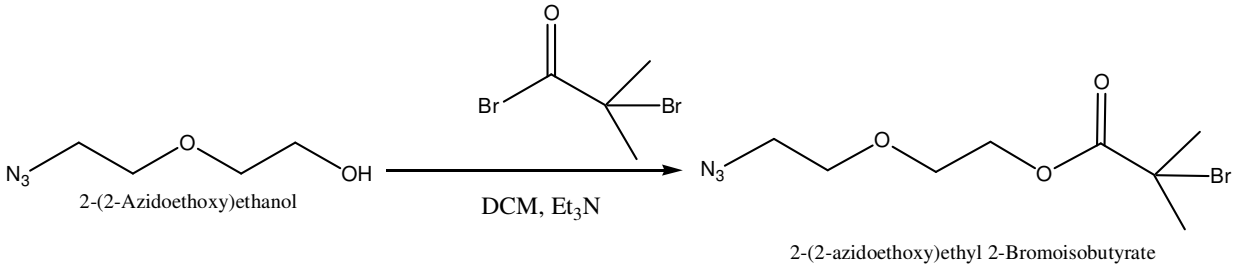

Figure S3: ^{1}H NMR spectrum ($CDCl_3$) of functionalized initiator

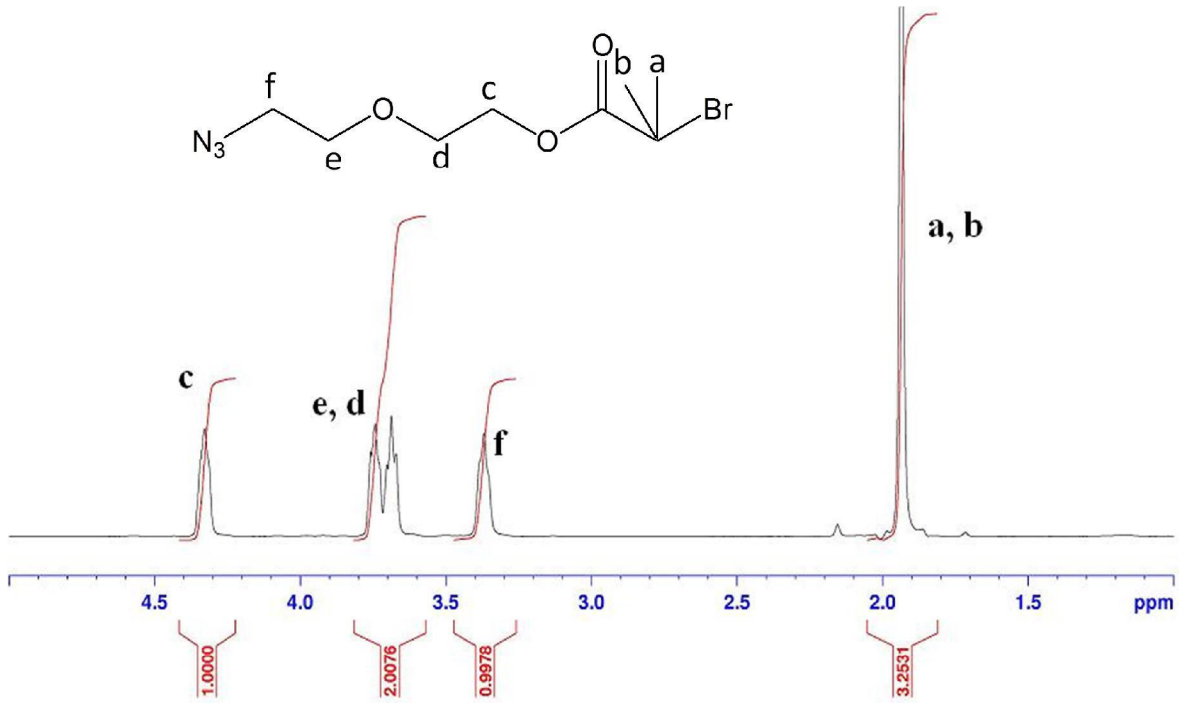

Figure S4. SET-LRP of NBA with $[NBA]_0/[N_3RBr]_0/[Me_6TREN]_0/[CuBr_2]_0$ = 26/1/0.18/0.02 in DMSO at 20°C. Evolution of the SEC traces (Differential Refractive Index response) at various conversion.

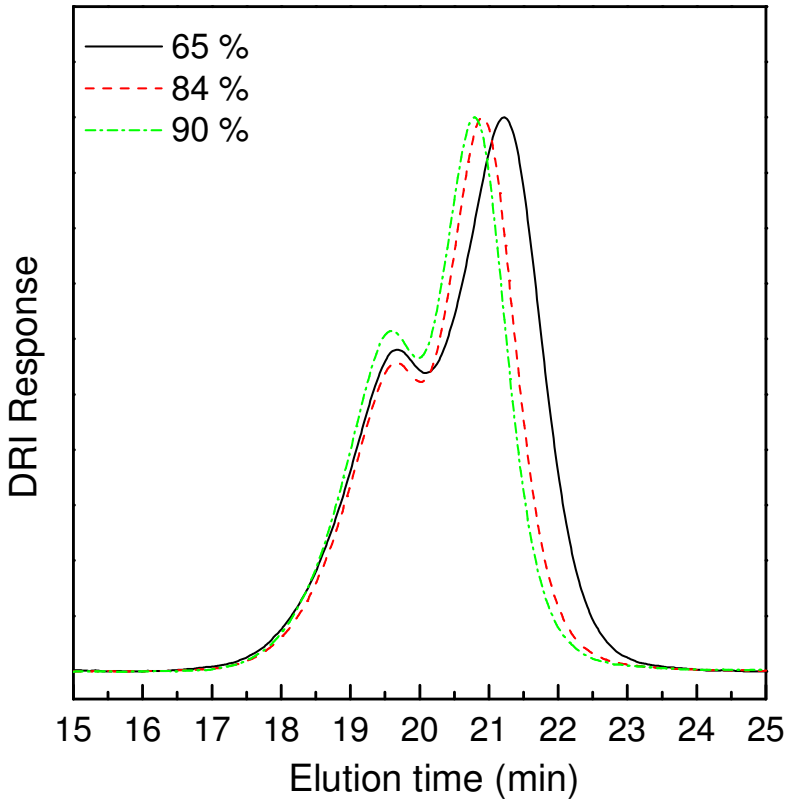

Figure S5. FTIR spectra of alkynated dextran, N_3-$PNBA_{4500}$-Br and Dex(15)-g-14.5$PNBA_{4500}$.

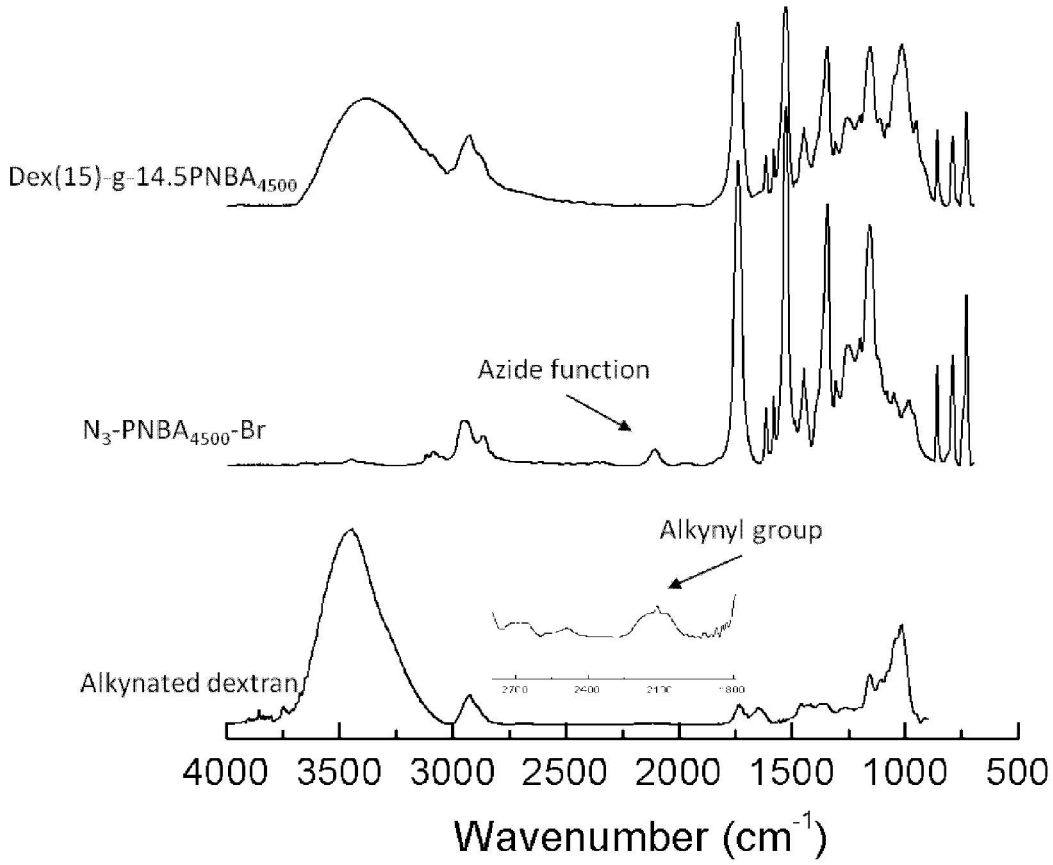

Figure S7. ^{13}C NMR spectra of (a) $PNBA_{3500}$-N_3, (b) alkynated dextran and (c) Dex(15)-g-14$PNBA_{3500}$ in DMSO-d_6.

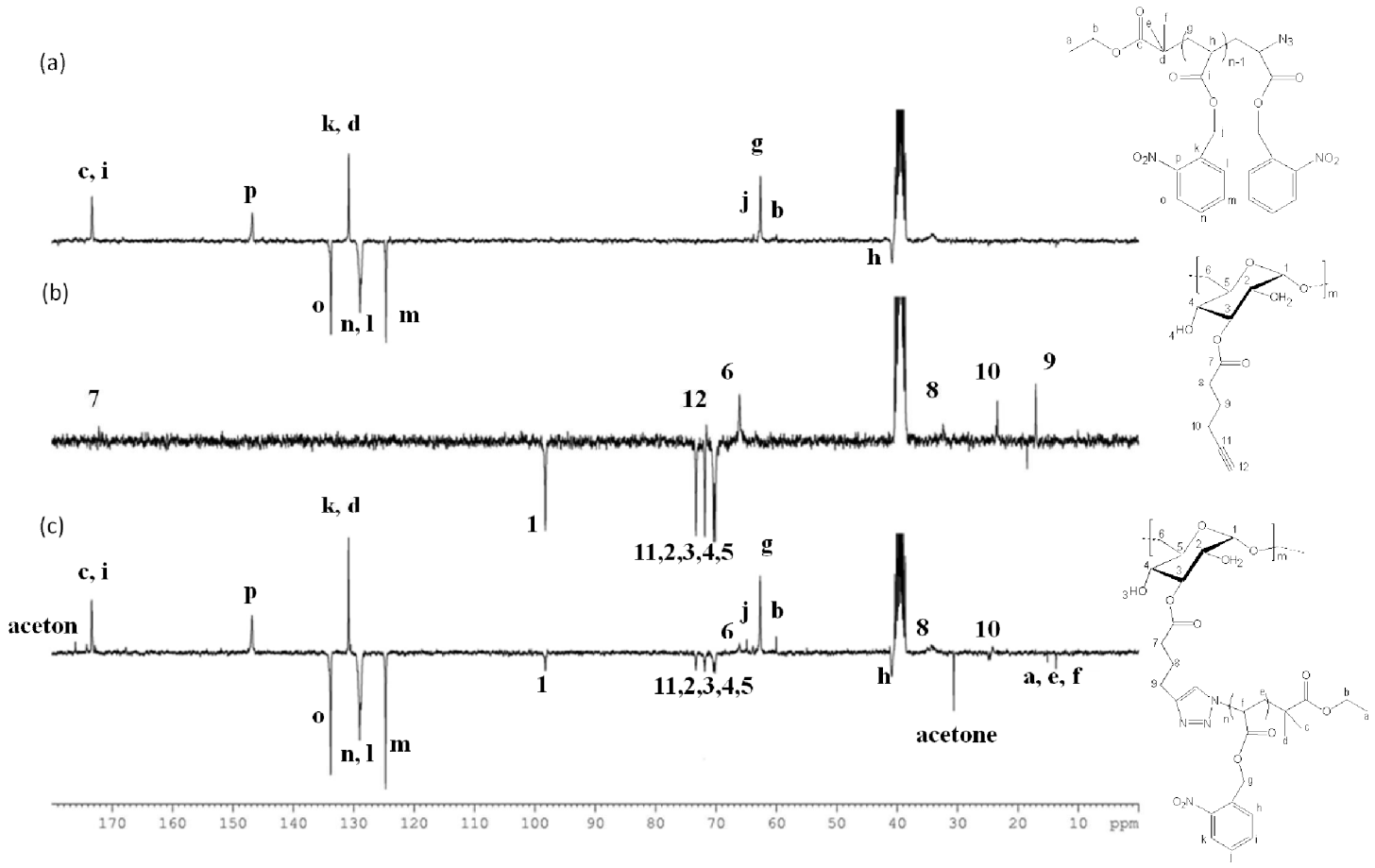

Figure S6. ^{1}H NMR spectra of (a) N_3-$PNBA_{4500}$-Br ($CDCl_3$), (b) alkynated dextran (DMSO-d_6) and (c) Dex(15)-g-14.5$PNBA_{4500}$ (DMSO-d_6).

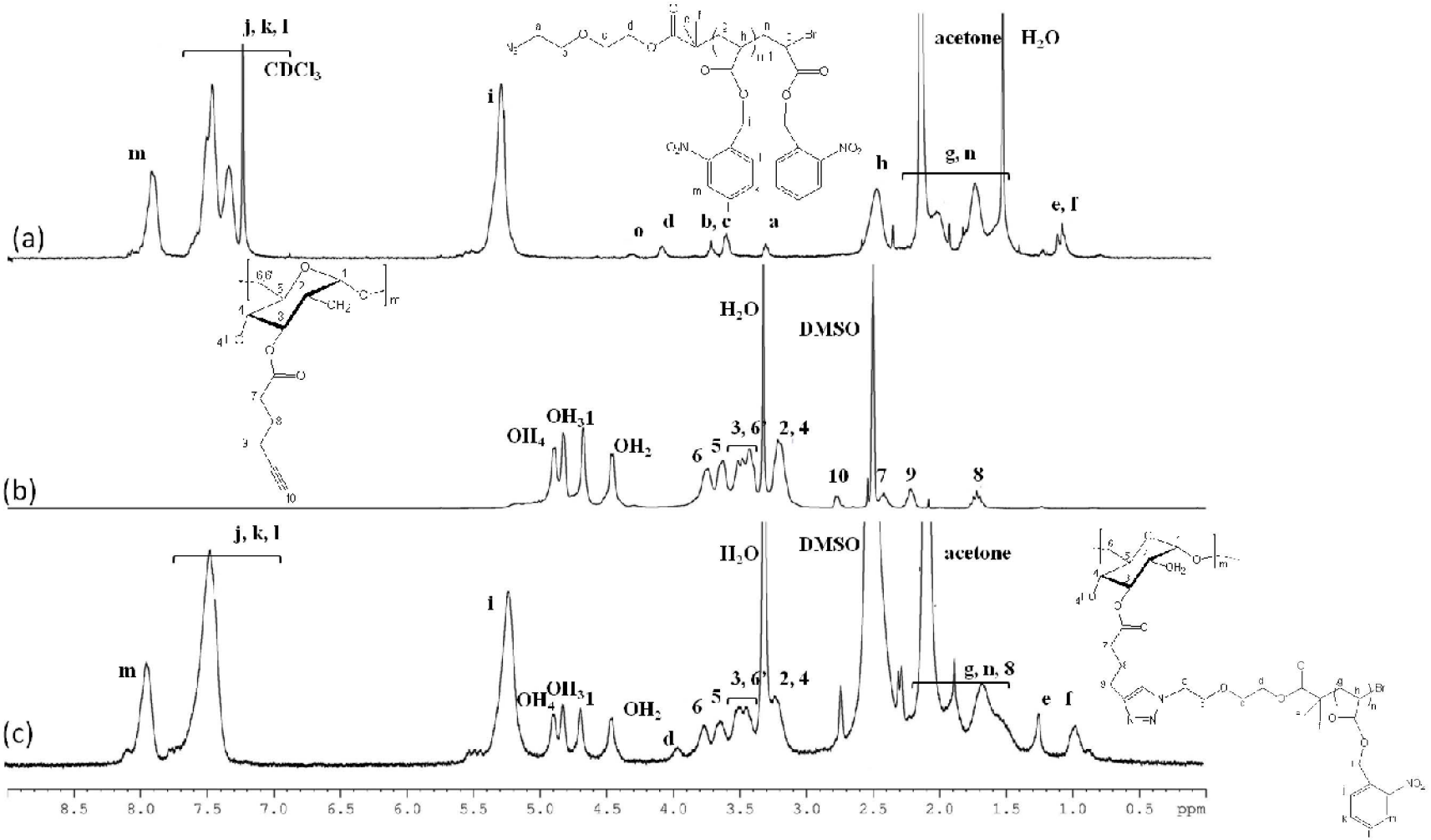

REFERENCES

1 X. Qiu, -P., F. Tanaka, F. M. Winnik, *Macromolecules* **2007**, *40*, 7069-7071.

2 S. M. A. Soliman, C. Nouvel, J. Babin, J.-L. Six, *J. Polym. Sci. Part A: Polym. Chem.* **2014**, *24*, 2192-2201.

3 M. Ciampolini, N. Nardi, *Inorg. Chem.* **1966**, *5*, 41-44.

4 C. Nouvel, P. Dubois, E. Dellacherie, J.-L. Six, *Biomacromolecules* **2003**, *4*, 1443-1450.

5 C. Nouvel, I. Ydens, P. Degée, P. Dubois, E. Dellacherie, J.-L. Six, *Polymer* **2002**, *43*, 1735-1743.

6 L. Dupayage, C. Nouvel, J.-L. Six, *J. Polym. Sci. Part A: Polym. Chem.* **2011**, *49*, 35-46.

7 E. Rotureau, M. Leonard, E. Marie, E. Dellacherie, T. A. Camesano, A. Durand, *Colloids and Surfaces A: Physicochem. Eng. Aspects* **2006**, *288*, 131-137.

8 H. Li, X. Xu, Y. Li, Y. Geng, B. He, Z. Gu, *Polym. Chem.* **2013**, *4*, 2235-2238.

9 D. A. Heller, Y. Levi, J. M. Pelet, J. C. Doloff, J. Wallas, G. W. Pratt, S. Jiang, G. Sahay, A. Schroeder, J. E. Schroeder, Y. Chyan, C. Zurenko, W. Querbes, M. Manzano, D. S. Kohane, R. Langer, D. G. Anderson, *Adv. Mater.* **2013**, *25*, 1449-1454.

10 T. T. Nielsen, V. Wintgens, C. Amiel, R. Wimmer, K. L. Larsen, *Biomacromolecules* **2010**, *11*, 1710-1715.

11 N. Pahimanolis, A.-H. Vesterinen, J. Rich, J. Seppala, *Carbohydrate polymers* **2010**, *82*, 78-82.

12 X. Dong, R. Qi, Y. Huang, X. Jing, *Journal of Controlled Release* **2011**, *152*, e192-e269.

13 M. N. Tahir, N. Lämmerhardt, P. Mischnick, *Carbohydrate polymers* **2012**, *88*, 154-164.

14 S. C. Abeylath, M. M. Amiji, *Bioorganic & Medicinal Chemistry* **2011**, *19*, 6167-6173.

15 B. G. De Geest, W. Van Camp, F. E. Du Prez, S. C. De Smedt, J. Demeester, W. E. Hennink, *Macromol. Rapid Comm.* **2008**, *29*, 1111-1118.

16 M. Jain, R. Rajan, S.-H. Hyon, K. Matsumura, *Biomater. Sci.* **2014**, *2*, 308-317.

17 S. Samatya, E. Orthan, N. Kabay, A. Tuncel, *Colloids and Surfaces A: Physicochem. Eng. Aspects* **2010**, *372*, 102-106.

18 M. Laville, J. Babin, I. Londono, M. Legros, C. Nouvel, A. Durand, R. Vanderesse, M. Leonard, J.-L. Six, *Carbohydrate polymers* **2013**, *93*, 537-546.

19 J.-M. Schumers, C.-A. Fustin, A. Can, R. Hoogenboom, U. Schubert, J.-F. Gohy, *J. Polym. Sci. Part A: Polym. Chem.* **2009**, *47*, 6504-6513.

20 G. S. Hammond, P. D. Bartlett, *J. polym. Sci.* **1951**, *6*, 617-624.

21 G. Odian, *Principles of Polymerization, 4th ed.*, Wiley, New York **2004**.

22 C. C. Price, D. A. Durham, *J. Am. Chem. Soc.* **1943**, *65*, 757-759.

23 V. Percec, T. Guliashvili, J. S. Ladislaw, A. Wistrand, A. Stjerndahl, M. J. Sienkowska, M. Monteiro, S. Sahoo, *J. Am. Chem. Soc.* **2006**, *128*, 14156-14165.

24 B. M. Rosen, V. Percec, *Chem. Rev.* **2009**, *109*, 5069-5119.

25 K. Matyjaszewski, Y. Nakagawa, S. G. Gaynor, *Macromol. Rapid Comm.* **1997**, *18*, 1057-1066.

26 U. Mansfeld, C. Pietsch, R. Hoogenboom, C. R. Becer, U. S. Schubert, *Polym. Chem.* **2010**, *1*, 15601598.

27 M. E. Levere, I. Willoughby, S. O'Donohue, A. de Cuendias, A. J. Grice, C. Fidge, C. R. Becer, A. J. Haddleton, *Polym. Chem.* **2010**, *1*, 1086-1094.

28 M. E. Levere, I. Willoughby, S. O'Donohue, P. M. Wright, A. J. Grice, C. Fidge, C. R. Becer, D. M. Haddleton, *J. Polym. Sci. Part A: Polym. Chem.* **2011**, *49*, 1753-1763.

29 V. V. Rostovtsev, L. G. Green, V. V. Fokin, K. B. Sharpless, *Angew. Chem. Int. Ed.* **2002**, *41*, 2596-2602.

30 W. H. Binder, R. Sachsenhofer, *Macromol. Rapid Comm.* **2007**, *28*, 15-24.

31 M. Meldal, *Macromol. Rapid Comm.* **2008**, *29*, 1016-1051.

32 E. Lallana, E. Fernandez-Megia, R. Riguera, *J. Am. Chem. Soc.* **2009**, *131*, 5748-5750.

33 Y. Bakkour, V. Darcos, S. M. Li, J. Coudane, *Polym. Chem.* **2012**, *3*, 2006-2010.
34 H. Zhao, E. S. Sterner, E. B. Coughlin, P. Theato, *Macromolecules* **2012**, *45*, 1723-1736.

Synthesis of Amphiphilic Light-Responsive Dextran-b-poly(*o*-nitrobenzyl acrylate) Copolymers

Soliman Mehawed Abdellatif SOLIMAN[1,2], *Cécile NOUVEL*[1,2], *Jérôme BABIN*[1,2], *Jean-Luc SIX*[1,2]*

1) Université de Lorraine, Laboratoire de Chimie Physique Macromoléculaire LCPM, FRE 3564, Nancy F-54000, France

2) CNRS, Laboratoire de Chimie Physique Macromoléculaire LCPM, FRE 3564, Nancy F-54000, France

KEYWORDS

o-nitrobenzyl acrylate, SET-LRP, dextran, diblock, click chemistry; light-responsive polymer, biodegradable surfactant.

EXPERIMENTAL

Materials

Dextran T10 ($M_{n(SEC)}$ = 8,900 g/mol, $Đ$=1.20) was purchased from Pharmacia Biotech and dried under reduced pressure at 100 °C overnight. No degradation of chains was evidenced under these drying conditions as attested by Size Exclusion Chromatography (SEC) analysis. Tris(2-aminoethyl)amine (TREN, 96%), formaldehyde solution (36.5-38.0 %wt), formic acid solution (49-51 %wt), Cu(II)Br_2 (99 %), Cu(I)Br (99.999 %), propargylamine (98 %) and sodium cyanoborohydride (> 95 %) were obtained from Aldrich and used without any further purification. Ethyl 2-bromoisobutyrate (EBiB, Aldrich, 98 %) was dried on CaH_2 overnight and vacuum distillated at 70 °C. *O*-nitrobenzyl acrylate (NBA) synthesis was previously described.[1] Tris(2-(dimethylamino)ethyl)amine (Me_6TREN) was synthesized as previously reported.[2] Surface of Cu(0) wire (0.25 mm diameter) was polished. Then Cu(0) was immersed in concentrated H_2SO_4 (Aldrich, 95-98 %) for 20 min, washed with ethanol and finally dried.

Synthesis of α-alkyne dextran (α-alkyne Dex)

The alkyne end-functionalization was conducted as previously described[3]. Dextran T10 (4 g, 0.454 10^{-3} mol of chains) was dissolved in 2% (w/v) acetate buffer (pH 5.0) at 50 °C. Propargylamine (2.5 g, 54.4 10^{-3} mol) and sodium cyanoborohydride (2.85 g, 45.4 10^{-3} mol) were added under stirring. The mixture was stirred at 50 °C for 96 h with daily addition of 25 equivalents per chain of sodium cyanoborohydride. Solution was concentrated by rotator evaporator and dialyzed against milli-Q water (MWCO 3.5 kDa) for 4 days. 2.25 g of pure -alkyne dextran (yield 75%) was recovered by lyophilization.

Homopolymerization of NBA by SET-LRP (PNBA-Br)

As previously reported [1], schlenk tube was evacuated and filled by nitrogen. NBA (4 g, 0. 193 mole, 26 eq), EBiB (108 µL, 0.74 10^{-3} mole, 1 eq), Me_6TREN (32 µL, 0.133 10^{-3} mole, 0.16 eq.), $CuBr_2$/Me_6TREN solution in DMSO (0.11 mol/L, 135 µl, 0.0148 10^{-3} mole, 0.02 eq of $CuBr_2$ and of Me_6TREN) and 4 mL

DMSO were successively added under N_2 flow. Consequently, the final equivalent of Me_6TREN (0.18 eq) has to be taken in consideration. Then, medium was purged with N_2 gas for 10 minutes. 6.8 cm of activated metallic Cu(0) wire were added under nitrogen to initiate the polymerization at 20°C. After 3.5 hrs, a sample was withdrawn under nitrogen atmosphere from the polymerization mixture and quenched by cooling with liquid nitrogen to determine the monomer conversion from ^{1}H NMR spectrum in $CDCl_3$. A conversion of 60 % was estimated by comparing the peaks integrals of the aromatic protons of both the monomer and the polymer (PNBA-Br) (7.3-8.2 ppm) with those of the ethylenic protons of the monomer (5.9, 6.2 and 6.3 ppm) [1]. Polymer was precipitated from cold methanol and filtrated. $PNBA_{3500}$-Br was dried using vacuum oven and characterized by SEC: $\overline{M}_{n(SEC)}$ = 3,500 g mol^{-1} and dispersity Đ = 1.06. $\overline{M}_n$ was also estimated from ^{1}H NMR taking into account the peaks (a,e,f) and (j) : $\overline{M}_{n(NMR)}$ = 3,510 g mol^{-1} (Fig. 3 (a)).

Synthesis of Azido-Terminated PNBA (PNBA-N_3)

1.465 g of $PNBA_{3500}$-Br (0.418 10^{-3} mol, 1 eq) was dissolved with 0.14 g sodium azide (2.15 10^{-3} mol, 5 eq) in 10 mL of anhydrous DMSO at room temperature. The reaction was leaved in dark place for 24 hrs. The medium was precipitated twice from cold methanol and filtrated. PNBA-N_3 was dried using vacuum oven. 1.0 g of pure PNBA-N_3 was obtained (Yield = 68 %)

Synthesis of Dex-b-PNBA by CuAAC

0.5 g (0.143 10^{-3} mol) of $PNBA_{3500}$-N_3 and 1.41 g (0.144 10^{-3} mol) of -alkyne dextran were dissolved in 20 mL of DMSO. Then, solution was purged using N_2 for 10 min. 0.02 g (0.144 10^{-3} mol) of CuBr and 0.9 mg (0.0144 10^{-3} mol) of Cu(0) were added under nitrogen. Solution was leaved stirring for 48 hrs in dark place to avoid photolysis of PNBA. Then solution was precipitated from cold mixture of methanol/water solution (8/2, v/v), containing 5 eq of EDTA to remove all copper salts. Powder was filtered and dried using vacuum oven. The prepared diblock glycopolymer was dialyzed against milli-Q water for 7 days to remove, if there is, uncoupled -alkyne dextran (MWCO 3.5 kDa). After dialysis step and lyophilization,

glycopolymer may also contain some ungrafted PNBA-N_3.Thus, powder was washed with a mixture of acetone/diethyl ether (8/2, v/v). 1.8 g (yield = 94 %) of pure diblock copolymer were finally obtained.

Irradiation of Dex-b-PNBA

Solution of Dex-b-PNBA was prepared in DMSO with concentration 0.1 mg/mL. 3 mL of stirred solution was irradiated in 1 cm x 1 cm quartz cuvette with a OmniCure® S1000 UV spot cure lamp at 1150 mw/cm² power. A light guide of 8 mm diameter equipped with a 320-500 nm filter was used. UV-Visible absorbance spectra of solution were measured before and after various irradiation time.

Characterization Techniques

^{1}H NMR, ^{13}C NMR and 2D DOSY ^{1}H NMR spectra were recorded on a Bruker Avance 300 apparatus (300,13 MHz, 25°C) in DMSO-d_6 or $CDCl_3$.

FTIR spectra were performed using Tensor 27 (Brucker Optics) equipped with MIR source (middle-infrared light) and DLaTGS detector.

Size Exclusion Chromatography (SEC) in THF was performed at 40°C with a Multi Angle Laser Light Scattering detector (MALLS - Mini Dawn Treos, Wyatt), a differential refractometer detector (OPTILab rex, Wyatt), a HPLC pump (Waters 515), a degazer AF (waters In-Line) and three PLgel 5 ≴ (10^5 A°, 10^3 A° and 100 A°) columns (300mm x 7.5mm). Elution rate was 1 ml/min. SEC in DMSO (0.1 M $NaNO_3$) was performed at 70°C with a MALLS - Mini Dawn Treos detector, a differential refractometer detector (RID - 10A, Shimadzu), a UV detector (SPD - 20A, Shimadzu), a HPLC pump (LC - 20AD, Shimadzu), a degazer (DGU - $20A_{3R}$, Shimadzu) and three PLgel 5 ≴ (10^5 A°, 10^3 A° and 100 A°) columns (300mm x 7.5mm). Elution rate was 0.7 ml/min. Solutions (10 mg/mL) were prepared by dissolution in THF or DMSO and left under vigorous stirring for 24 h. Filtration of solutions was carried out right before injection. Refractive index increments (dn/dc) was measured with a differential refractometer (Waters 410). dn/dc of $PNBA_{3500}$-Br and $PNBA_{9800}$-Br were measured in THF at 40°C and were found equal to

0.137 mL/g and 0.152 mL/g, respectively. dn/dc equal to 0.1 mL/g was estimated for PNBA in DMSO at 50°C. dn/dc = 0.07 mL/g for dextran and α-alkyne Dex was measured in DMSO at 50°C. dn/dc of each Dex-b-PNBA diblock copolymers was measured in DMSO at 50°C.

UV-Visible spectra of Dex-b-PNBA and of photolysis product were measured using Uvikon-XL Bio-Tek Spectrophotometer. The absorbance was recorded in the 250-450 nm range.

RESULTS AND DISCUSSION

Dextran End-Chain Modification

Derivatization of the dextran end-chain can be obtained by oxime click[4, 5] or most commonly by reductive amination[3, 6-9]. The latter approach was performed to introduce the alkyne function to the reducing-end of dextrane T10 by treatment with sodium cyanoborohydride ($NaBH_3CN$) and propargylamine in acetate buffer (pH 5.0) as shown in Scheme 1. The low concentration of the reactive aldehyde function in dextran chain in equilibrium with the cyclic unreactive hemiacetal forms of the glucopyranosic end-chain unit (Fig 1-a) imposed a long reaction time and a daily addition of the reducing agent $NaBH_3CN$, which reduces imine double bond (Schiff bases) selectively [10] . After purification, ^{1}H NMR spectrum of α-alkyne Dex (Fig 1-b) shows the complete disappearance of signals at 6.7 ppm and 6.3 ppm originally present on the spectrum of native dextran T10 (Fig 1-c). These missing peaks are corresponding respectively to the anomeric protons in and ∮ stereoisomer of the terminal glucopyranosic cycle. That indicates the quantitative modification of the reducing end of dextran chain by the propargylamine. Moreover, analysis of the FTIR spectrum of the α-alkyne Dex (Fig 2) revealed a broad band at 2130 cm^1 corresponding to the alkyne function. Finally, Size Exclusion Chromatographie analysis in DMSO (Figure S1) confirmed that this modification step didn't lead to the degradation of the native dextran T10 ($\overline{M}_{w(SEC)}$ of α-alkyne Dex = 9,300 g/mol, 仔=1.21).

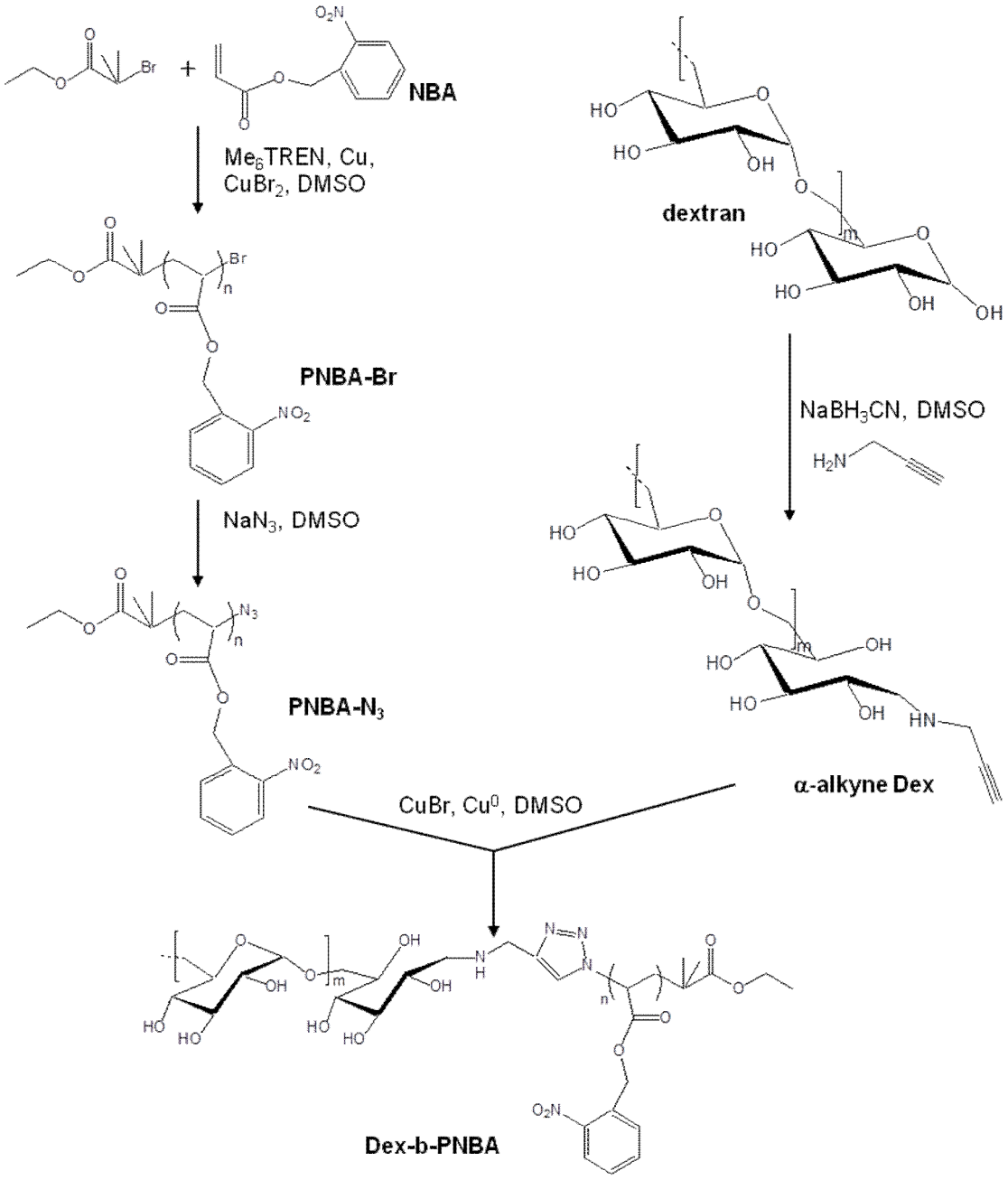

Scheme 1. Synthetic Route to Dex-b-PNBA Diblock Copolymers.

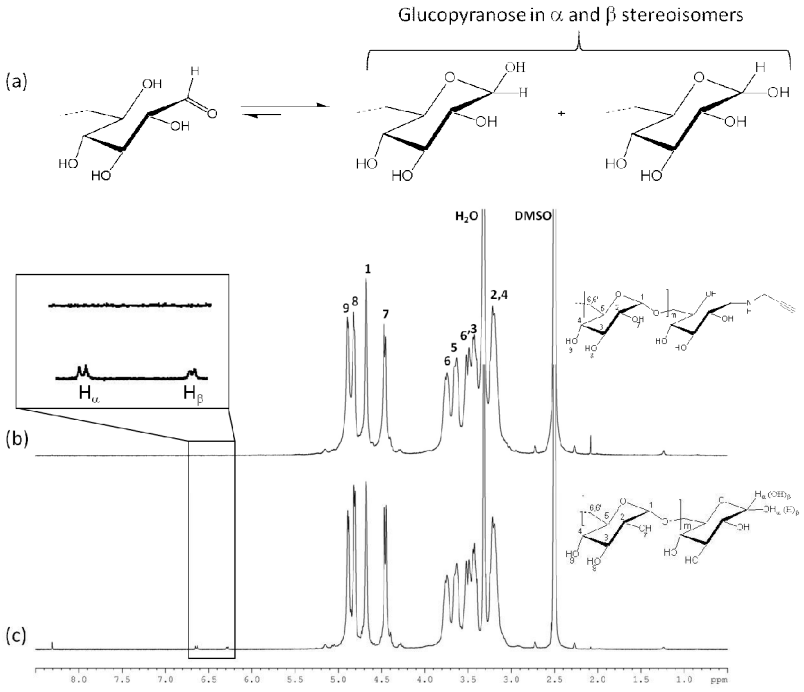

Figure 1. (a) Equilibrium between open and closed glucopyranosic end-uint. ^{1}H NMR spectra of -alkyne Dex (b) and dextran (c) in DMSO-*d*$_6$.

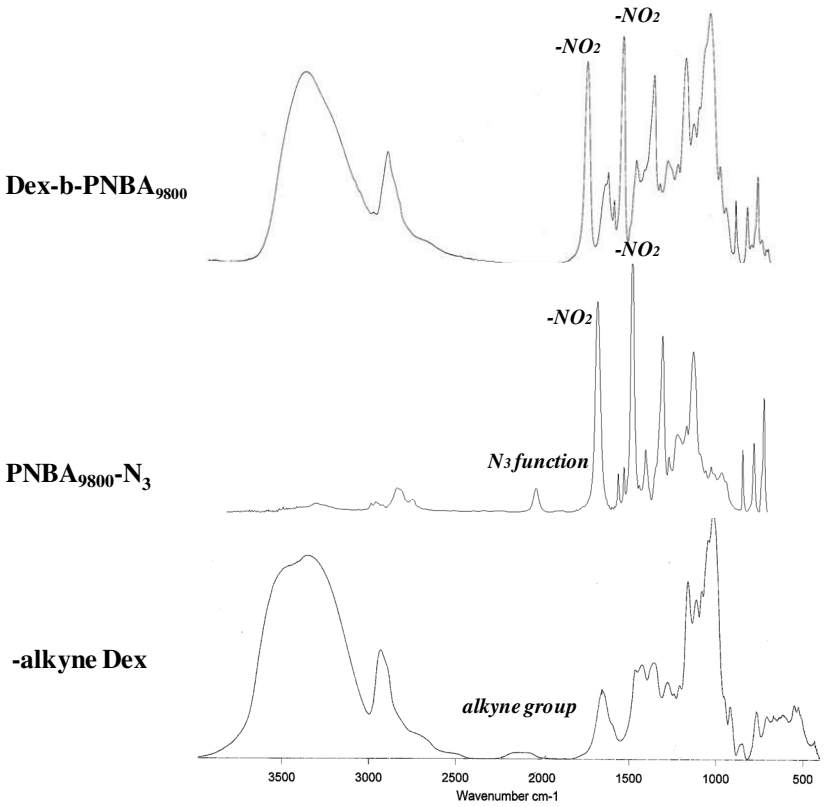

Figure 2. FTIR spectra of -alkyne Dex, PNBA$_{9800}$-N$_3$ and Dex-b-PNBA$_{9800}$.

PNBA-N_3 Synthesis

O-nitrobenzyl acrylate was considered as capricious monomer that is difficult to polymerize by controlled radical polymerization techniques such as RAFT, ATRP or NMP. This lack of control was mainly attributed to inhibition and retardation effects coming from the nitro-aromatic groups.[11-14] In a recent study, we demonstrated for the first time that NBA could be polymerized by controlled SET-LRP [1]. A first-order kinetics with respect to the NBA concentration was observed. Moreover, up to 50 % conversion, the SET-LRP proceeded with a linear evolution of molecular weight with a narrow distribution (dispersity < 1.2).

After purification, $PNBA_{3500}$-Br was analyzed by ^{1}H NMR (Fig. 3) and SEC (Fig. 4). A really good agreement was obtained between the theoretical molecular weight calculated from the conversion ($M_{n,th}$) the molecular weight determined by ^{1}H NMR ($M_{n,NMR}$ = 3,510 g.mol^{-1}) and the molecular weight estimated by SEC ($M_{n,SEC}$ = 3,500 g.mol^{-1}) (Table 1). From these data, an initiation efficiency equal to 98% was calculated. The good control of the NBA polymerization was confirmed by the low dispersity of the sample (Đ = 1.06). Moreover, an approximate 2:1 ratio between the ^{1}H NMR areas (Fig 3-a) of signal (b) corresponding to the -CH_2- initiator group and the signal (r) corresponding to the -CHBr located at the chain end was obtained indicating a total chain end functionality. Higher molecular weight ($PNBA_{9800}$-Br) was obtained using the molar ratio $[NBA]_0/[EBiB]_0/[Me_6TREN]_0/[CuBr_2]_0$ = 100/1/1/0.1 (Entry 2, Table 1). Again a good agreement was obtained between the theoretical molecular weight calculated from the conversion ($M_{n,th}$ = 9,300 g.mol^{-1}), the molecular weight determined by ^{1}H NMR ($M_{n,NMR}$ = 9,100 g.mol^{-1}) and the molecular weight obtained by SEC ($M_{n,SEC}$ = 9,800 g.mol^{-1}) (Table 1). The good control of the NBA polymerization was again confirmed by the low dispersity of the sample (Đ = 1.10). For both experiments, polymerizations were stopped at moderate conversions do avoid the bimolecular coupling termination using CuBr/Cu(0).[1] Absence of significant bimolecular coupling reaction was confirmed by SEC using light-scattering detector where no notable shoulder was observed at low elution volume (Fig S2).

Firstly, low molecular weight $PNBA_{3500}$-Br (PNBA-Br with $M_{n,th}$ = 3500 g.mol^{-1}) was prepared by SET-LRP of NBA (Scheme 1) using the molar ratio $[NBA]_0/[EBiB]_0/[Me_6TREN]_0/[CuBr_2]_0$ = 26/1/0.18/0.02 in DMSO at 20°C (Entry 1, Table 1).

Table 1. SET-LRP of NBA.

Entry	$([NBA]_0/[EBiB]_0/[Me_6TREN]_0/[CuBr_2]_0)$	Cu(0) Wire Length (cm)	Time (min)	Conversion (%) [a]	$M_{n,th}$ (g mol^{-1}) [b]	$M_{n,NMR}$ (g mol^{-1}) [c]	$M_{n,SEC}$ (g mol^{-1}) [d]	$Đ$ [d]
1	(26 /1 /0.18 /0.02)	6.8	210	60	3,425	3,510	3,500	1.06
2	(100/1/1/0.1)	11.9	240	44	9,300	9,100	9,800	1.10

a) Estimated from ^{1}H NMR spectrum of crude product

b) Estimated using $M_{n,th(theo)} = M_{EBiB} + (conv. \times ([NBA]_0/[EBiB]_0) \times M_{NBA}$, where M_{EBiB} and M_{NBA} are equal to 195 and 207 g/mol, respectively.

c) Estimated from ^{1}H NMR spectrum of purified product

d) Evaluated from SEC-MALLS in THF

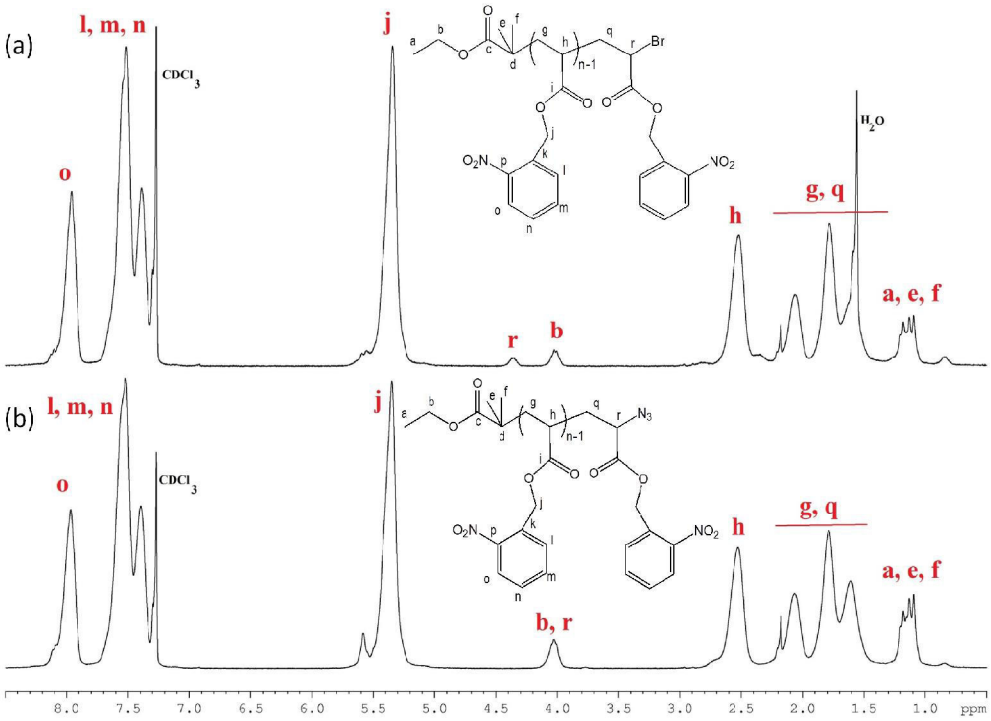

Figure 3. ^{1}H NMR spectra of $PNBA_{9800}$-Br and $PNBA_{9800}$-N_3 in $CDCl_3$.

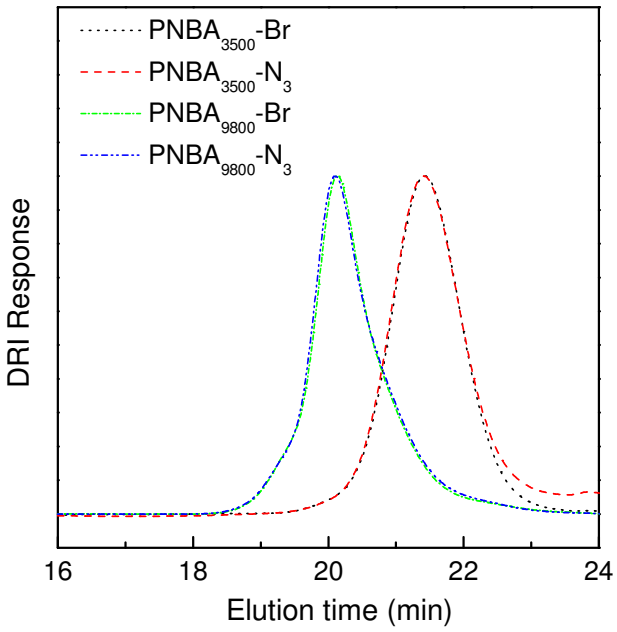

Figure 4. SEC chromatograms in THF of PNBA-Br and PNBA-N_3 with $M_{n,NMR}$ = 3,500 g/mol and 9,800 g/mol (Differential Refractive Index Response).

Secondly, the terminal bromide atom of PNBA-Br was further replaced by azide function as shown in Scheme 1. A nucleophilic substitution with sodium azide in DMSO was performed. After purification, FTIR spectrum of $PNBA_{3500}$-N_3 (Fig 2-b) revealed an absorption peak at about 2100 cm^{-1} characteristic of the azide function. Moreover, the complete shifting of the terminal CH peak (r) from 4.3 ppm to 4 ppm on Figure 3 was also a strong indication of the quantitative azidation of the PNBA-Br end chain. SEC chromatograms of PNBA chains before and after azidation remained identical, indicating no degradation under this treatment (Figure S4 and S2).

Coupling by CuAAC

Dextran-b-poly(*o*-nitrobenzyl acrylate) (Dex-b-PNBA) light-responsive diblock copolymers were elaborated by a coupling approach as shown on Scheme 1. Coupling between the alkyne-terminated dextran (α-alkyne Dex) and the azido-terminated poly(*o*-nitrobenzyl acrylate) (PNBA-N_3) was realized by the Copper(I)-catalyzed Azide-Alkyne Cycloaddition (CuAAC), the most common click reaction in polymer chemistry.[15-18] CuAAC was performed using CuBr/Cu(0) in anhydrous DMSO because polysaccharide chain cleavage may occur using Cu^{II}/ascorbic acid couple in water that catalyzes the formation of highly reactive HO° peroxide. [19] In this paper, Cu^{I} catalyst was provide by copper bromide and any ligand was used. Molar ratio between PNBA-N_3 and α-alkyne Dex was kept at 1:1. After reaction, diblock copolymers were purified by dialysis against water to ensure complete removal of unreacted α-alkyne Dex, followed by extraction of free PNBA-N_3 by washing with a acetone/diethyl ether (8/2, v/v) mixture. 94 % and 86 % yields were respectively obtained for Dex-b-$PNBA_{3500}$ and Dex-b-$PNBA_{9800}$ denoting a high efficiency of the end to end coupling reaction. FTIR spectrum of Dex-b-$PNBA_{3500}$ revealed the disappearance of the azide and the alkyne group peaks around 2100 cm^{-1} (Fig 2). For instance, Dex-b-$PNBA_{3500}$ FTIR spectrum (Fig 2-c) includes the broad stretching band at 3000-3600 cm^{-1} characteristic of alcohol functions of dextran and the stretching band at 1548 cm^{-1} and 1358 cm^{-1} from the nitro groups of PNBA. The ^{1}H NMR of Dex-b-$PNBA_{3500}$ (Fig 5) shows typical signals of both blocks especially the aromatic protons peaks at 7.3-8.1 ppm attributed to the PNBA block and the

glucosidic (3-5 ppm) and anomeric proton at 4.65 ppm from dextran part. No direct evidence of the triazole ring formation was possible due to the overlap of the aromatic (o) protons peaks at 8.0 ppm with that of triazole proton generally localized around 8.1 ppm.[18] PNBA weight fraction in diblock copolymers (F_{PNBA}) has been estimated from ^{1}H NMR spectra and reported in Table 2. ^{13}C NMR spectra of $PNBA_{3500}$-N_3, α-alkyne Dex and resulting diblock copolymer were drawn on Figure S3.

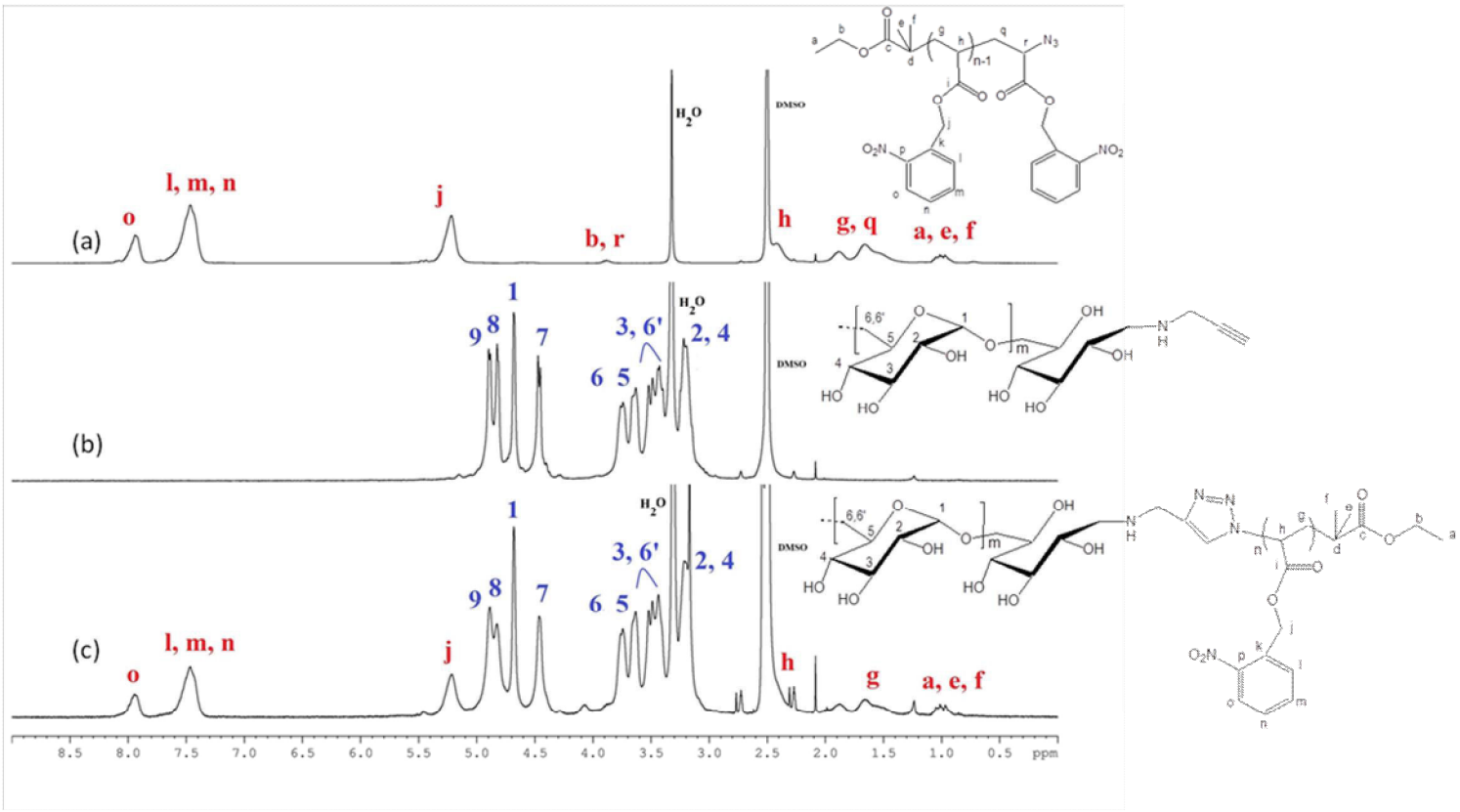

Figure 5. ^{1}H NMR spectra of (a) $PNBA_{9800}$-N_3, (b) α-alkyne Dex (c) Dex-b-$PNBA_{3500}$ in DMSO-d_6.

Table 2. Characteristics of Dex-b-PNBA diblock copolymers

Entry	[illegible] (g mol^{-1}) [PNBA-N_3 (g mol^{-1}) [a]	[illegible] (g mol^{-1}) [α-alkyne Dex (g mol^{-1}) [b]	[illegible] (g mol^{-1}) [Dex-b-PNBA (g mol^{-1})	[illegible] (g mol^{-1}) [Dex-b-PNBA (g mol^{-1}) [b]	伊[b]	dn/dc (mg mL^{-1}) [c]	F_{PNBA} (wt%) [d]
3	3,500	9,300	12,800	13,890	1.12	0.071	27
4	9,800	9,300	19,100	18,310	1.07	0.080	47

a) Evaluated from SEC-MALLS in THF

b) Evaluated from SEC-MALLS analysis in DMSO (0.1M $NaNO_3$)

c) Measured in DMSO (0.1M $NaNO_3$) at 50°C

d) Weight fraction of PNBA in the diblock copolymers calculated from ^{1}H NMR (Fig. 5c) using:

$$F_{[illegible]} = \frac{\frac{[illegible]}{[illegible]} \times [illegible]}{\frac{[illegible]}{[illegible]} \times [illegible] + [illegible] \times [illegible]} \times 100 \quad \text{Equation 1}$$

Where A_j and A_1 are areas under the peaks (j) and (1), respectively. 207 and 162 are the molecular weights of NBA and glucopyranosic monomer units, respectively.

Indirect confirmation of the covalent link between blocks was proved by 2D Diffusion-Ordered Spectroscopy (DOSY) ^{1}H NMR. This technique allows to measure the self-diffusion coefficient of each molecular species in a mixture. With polymers, it's a powerful method to discriminate between a block copolymer and the corresponding blocks mixture.[20] 2D DOSY ^{1}H NMR spectrum of Dex-b-PNBA$_{9800}$ was recorded in dilute DMSO-d_6 (Fig. 6 (a)). A single self-diffusion coefficient was observed for all the protons from dextran and PNBA parts (D = 1.66 × 10^{-10} m^2 s^{-1}) which is consistent with an efficient coupling reaction between blocks. A mixture of PNBA$_{9800}$-N_3 and α-alkyne Dex with the same weight composition than the Dex-b-PNBA$_{9500}$ was studied by 2D DOSY ^{1}H NMR (Fig. 6 (b)). Clearly, two separate diffusion coefficients were measured D = 1.28 × 10^{-10} m^2 s^{-1} and D = 1.55 × 10^{-10} m^2 s^{-1} for α-alkyne Dex and PNBA, respectively. The presence of 2 separate diffusion coefficients shown on 2D DOSY ^{1}H NMR of the mixture, while only one (at one another) is observed in case of diblock copolymers spectra, proved that analyzed copolymers are really composed by covalently linked dextran and PNBA$_{9800}$ blocks. Same conclusion, was made from Dex-b-PNBA$_{3500}$ study.

Finally, Dex-b-PNBA copolymers were characterized by SEC using DMSO/$NaNO_3$ as eluent (Fig. 7). While DRI response (Fig. 7 (a)) showed only a small shift to lower elution time of the Dex-b-PNBA$_{9800}$ distribution compare to α-alkyne Dex precursor, UV response (Fig 7(b)) clearly indicated a strong displacement of the copolymer distribution (absorbance due to the PNBA part) compare to the PNBA$_{9800}$-N_3 starting material. No peak of residual unlinked PNBA$_{9800}$-N_3 was observed. Therefore, one can conclude that PNBA$_{9800}$ block was linked to dextran one during the CuAAC click reaction. Moreover, a really good agreement was obtained between the theoretical molecular weight ($M_{n(theo)}$ = 19,100 g.mol) and the absolute molecular weight determined with MALLS detector ($M_{n(MALLS)}$) (Table 2).

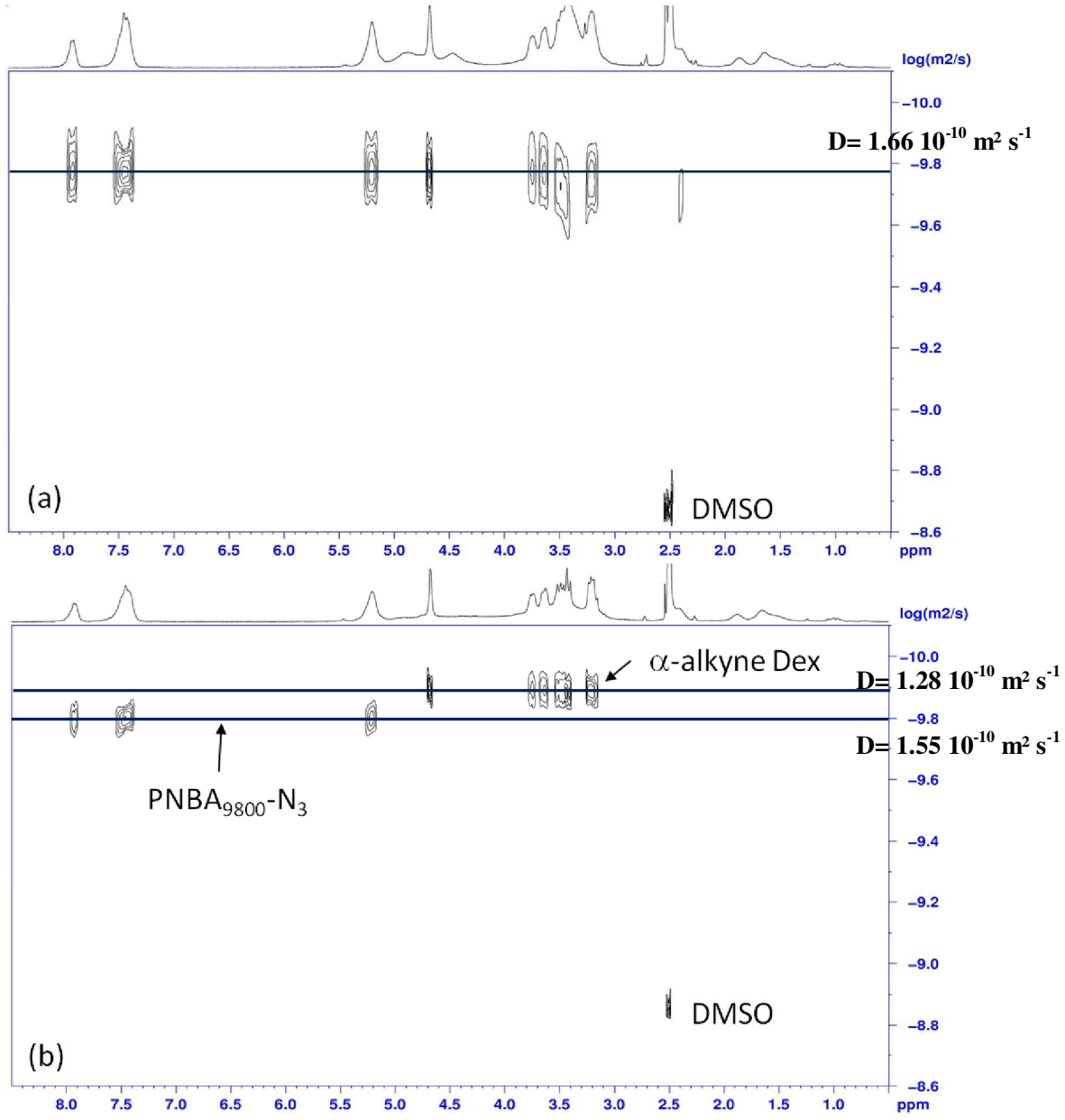

Figure 6. 2D DOSY ^{1}H NMR spectra of Dex-b-PNBA$_{9800}$ (a) and a mixture of PNBA$_{9800}$-N$_3$ and α-alkyne Dex (1:1; w:w) (b) in DMSO-*d*$_6$.

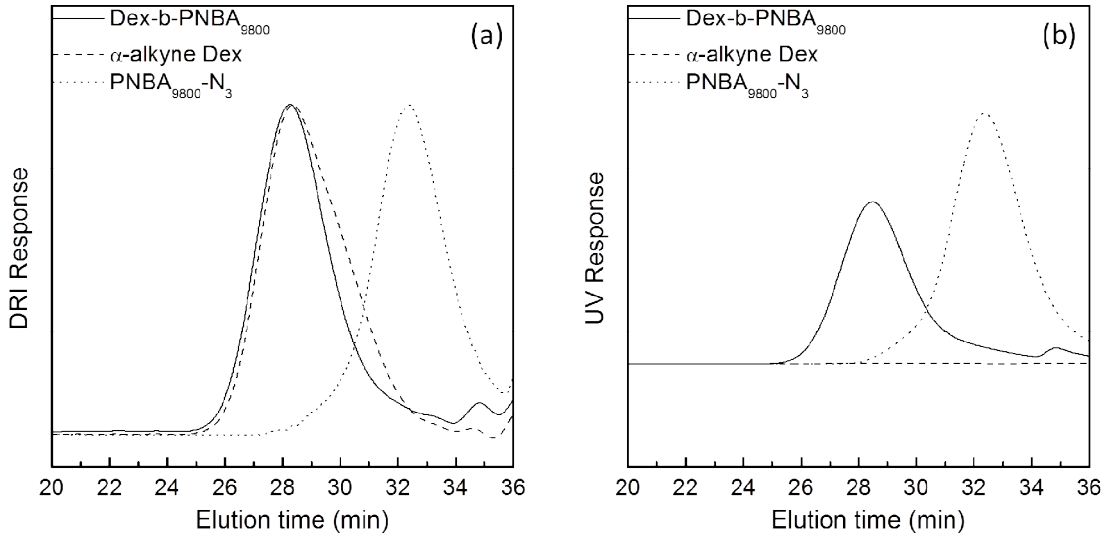

Figure 7. SEC chromatograms of $PNBA_{9800}$-N_3, -alkyne Dex and Dex-b-$PNBA_{9800}$. (a) Differential refractive index response and (b) UV response at 350 nm.

Light Irradiation of Dextran-*b*-PNBA

Photosensitive property of dextran-b-poly(*o*-nitrobenzyl acrylate) was evaluated with a light irradiation experiment. Upon one photon irradiation, 2-nitrobenzyl esters are known to be cleaved liberating carboxylic acid groups and 2-nitrosobenzaldehyde byproducts[21]. This photocleavage can be easily followed on UV-visible absorption spectra, where 2-nitrobenzyl ester and 2-nitrosobenzaldehyde present two different bands. Light irradiation of Dex-b-$PNBA_{9800}$ was carried out in DMSO (0.1 mg/mL) with a UV light (spectra range from 320 nm to 500 nm; 1150 mW/cm² power). UV-Visible absorbance spectra of solution were measured before and after different irradiation times (Fig. 8-a). Before irradiation, a band at 275 nm was detected corresponding to the absorption of 2-nitrobenzyl ester of each NBA monomer unit. After UV irradiation, the intensity of this band decreased while another band appeared at 325 nm characteristic of the formation of 2-nitrosobenzaldhyde. Plot of the absorbance at 325 nm *versus*

irradiation time shows a fast photocleavage that evolves no more after18 min (Fig. 8-b). By comparison with the irradiation study of PNBA homopolymers, one can conclude that dextran part in the copolymer didn't prevent the PNBA photolysis but slow down it as the absorbance at 325 nm reach a plateau value after 400 s in case of PNBA homopolymers. [1]

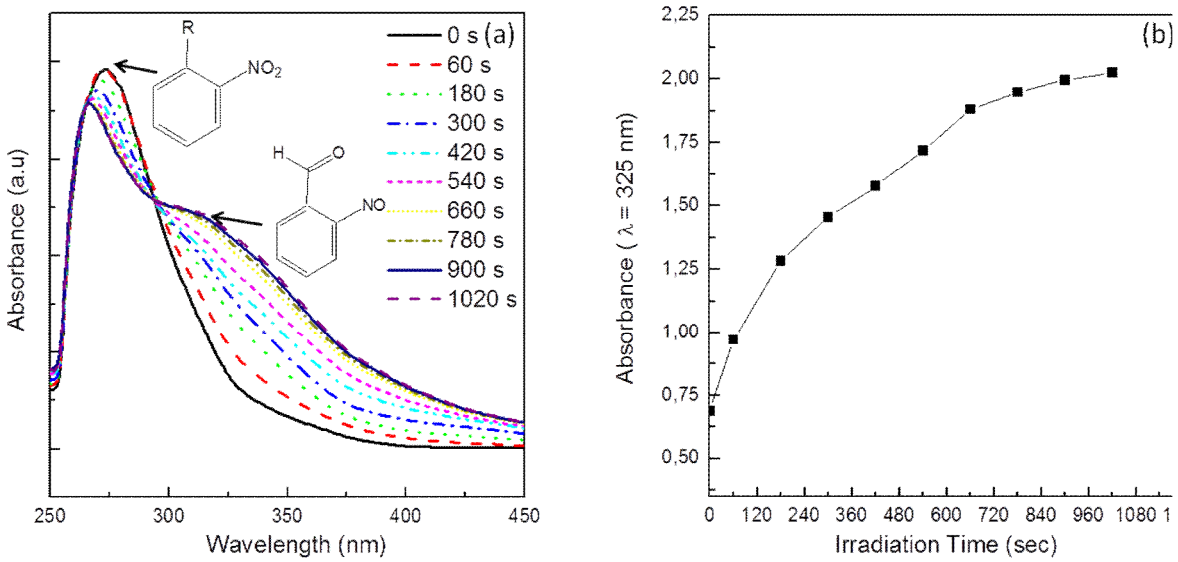

Figure 8. Light irradiation of Dex-b-PNBA$_{9800}$ in DMSO (0.1mg/mL) with a UV lamp equipped with a 320 - 500 nm filter (power 1150 mw/cm²). (a) UV-Vis spectra after various irradiation times. (b) Absorbance at 325 nm *versus* irradiation time

ACKNOWLEDGMENT

The authors express their highest gratitude to Marie-Christine Grassiot for help in SEC measurements and Olivier Fabre for NMR measurements.

S.M.A. Soliman gratefully acknowledges support from an Erasmus Mundus External Cooperation Windows ¯ Flow by Flow EU-Egypt Bridge Building (FFEEBB) Graduate Research Fellowship.

SUPPORTING INFORMATIONS FOR

Synthesis of Amphiphilic Light-Responsive Dextran-b-poly(nitrobenzyl acrylate) Copolymers

*Soliman Mehawed Abdellatif SOLIMAN[1,2], Cécile NOUVEL[1,2], Jérôme BABIN[1,2], Jean-Luc SIX[1,2]**

1) Université de Lorraine, Laboratoire de Chimie Physique Macromoléculaire LCPM, FRE 3564, Nancy F-54000, France

2) CNRS, Laboratoire de Chimie Physique Macromoléculaire LCPM, FRE 3564, Nancy F-54000, France

KEYWORDS

o-nitrobenzyl acrylate, SET-LRP, dextran, diblock, click chemistry; light-responsive polymer

Figure S1. SEC chromatograms in DMSO (0.1M $NaNO_3$) of dextran (T10) and α-alkyne Dex. (a) Differential Refractive Index Response and (b) Light Scattering Response.

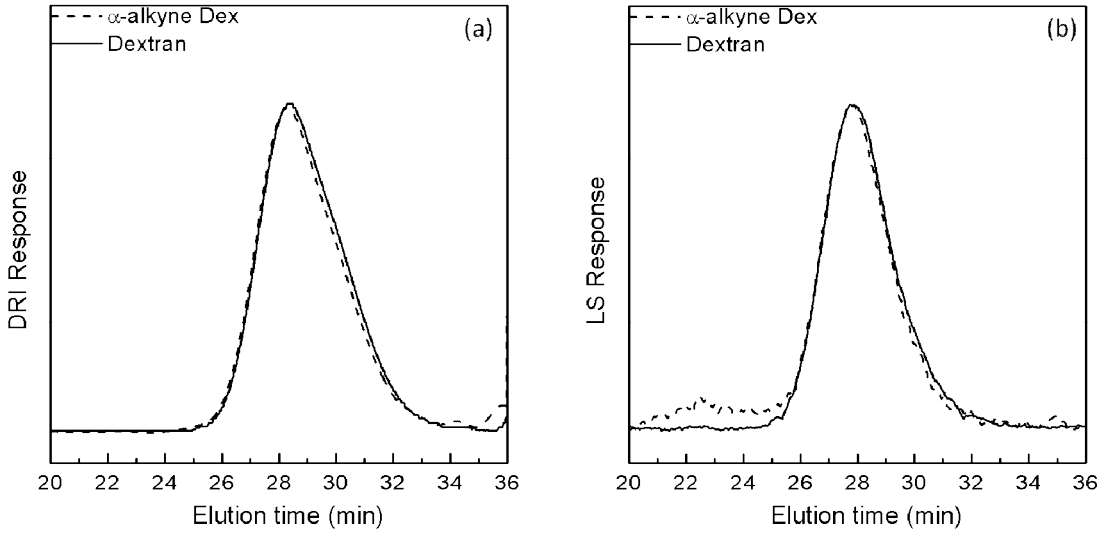

Figure S2. SEC chromatograms in THF of PNBA-Br and PNBA-N_3 with $M_{n(GPC)}$ = 3,500 g/mol and 9,800 g/mol (Light-Scattering Response)

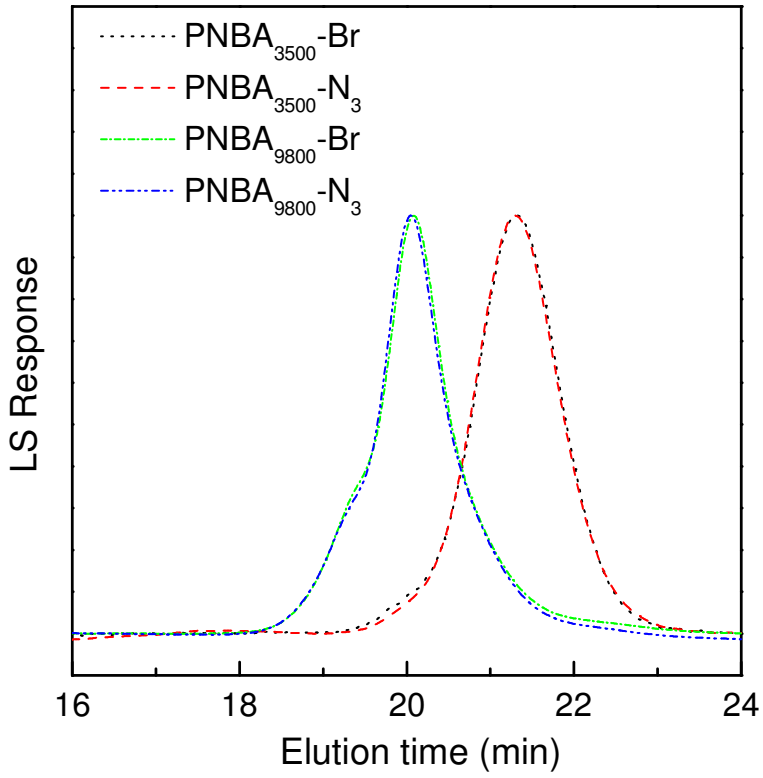

Figure S3. ^{13}C NMR spectra of (a) $PNBA_{3500}$-N_3, (b) α-alkyne Dex (c) Dex-b-$PNBA_{3500}$ in DMSO-d_6.

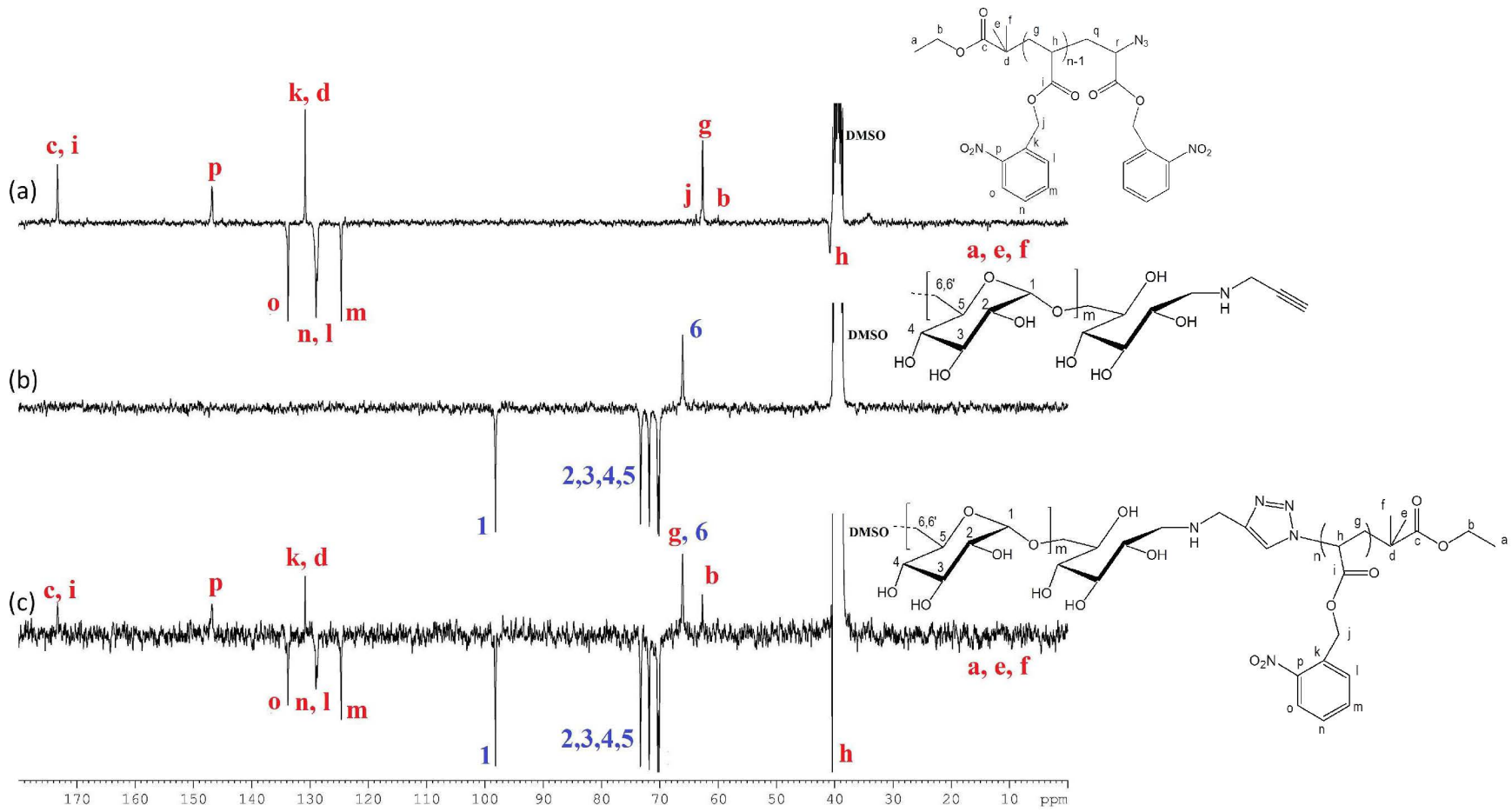

REFERENCES

1 S. M. A. Soliman, C. Nouvel, J. Babin, J.-L. Six, *J. Polym. Sci. Part A: Polym. Chem.* **2014**.
2 M. Ciampolini, N. Nardi, *Inorg. Chem.* **1966**, *5*, 41-44.
3 C. Schatz, S. Louguet, J. F. Le Meins, S. Lecommandoux, *Angew. Chem. Int. Ed.* **2009**, *48*, 2572-2575.
4 R. Novoa-Carballa, A. H. E. Müller, *Chem. Commun.* **2012**, *48*, 3781-3783.
5 R. Novoa-Carballa, A. Pfaff, A. H. E. Müller, *Polym. Chem.* **2013**, *4*, 2278-2285.
6 C. Houga, J. F. Le Meins, R. Borsali, D. Taton, Y. Gnanou, *Chem. Commun.* **2007**, 3063-3065.
7 B. Li, Q. Wang, X. Wang, C. Wang, X. Jiang, *Carbohydrate polymers* **2013**, *93*, 430-437.
8 Z. Zhao, Z. Zhang, L. Chen, Y. Cao, C. He, X. Chen, *Langmuir* **2013**, *29*, 13072-13080.
9 A. R. Fajardo, A. Guerry, E. A. Britta, C. V. Nakamura, E. C. Muniz, R. Borsali, S. Halila, *Biomacromolecules* **2014**, *dx.doi.org/10.1021/bm5005355*.
10 R. F. Borch, M. D. Bernstein, H. D. Durst, *J. Am. Chem. Soc.* **1971**, *93*, 2897-2904.
11 G. S. Hammond, P. D. Bartlett, *J. polym. Sci.* **1951**, *6*, 617-624.
12 G. Odian, *Principles of Polymerization, 4th ed.*, Wiley, New York **2004**.
13 C. C. Price, D. A. Durham, *J. Am. Chem. Soc.* **1943**, *65*, 757-759.
14 J.-M. Schumers, C.-A. Fustin, A. Can, R. Hoogenboom, U. Schubert, J.-F. Gohy, *J. Polym. Sci. Part A: Polym. Chem.* **2009**, *47*, 6504-6513.
15 V. V. Rostovtsev, L. G. Green, V. V. Fokin, K. B. Sharpless, *Angew. Chem. Int. Ed.* **2002**, *41*, 2596-2602.
16 W. H. Binder, R. Sachsenhofer, *Macromol. Rapid Comm.* **2007**, *28*, 15-24.
17 M. Meldal, *Macromol. Rapid Comm.* **2008**, *29*, 1016-1051.
18 M. Laville, J. Babin, I. Londono, M. Legros, C. Nouvel, A. Durand, R. Vanderesse, M. Leonard, J.-L. Six, *Carbohydrate polymers* **2013**, *93*, 537-546.
19 E. Lallana, E. Fernandez-Megia, R. Riguera, *J. Am. Chem. Soc.* **2009**, *131*, 5748-5750.
20 Y. Bakkour, V. Darcos, S. M. Li, J. Coudane, *Polym. Chem.* **2012**, *3*, 2006-2010.
21 H. Zhao, E. S. Sterner, E. B. Coughlin, P. Theato, *Macromolecules* **2012**, *45*, 1723-1736.

CHAPTER (III)
NANOPARTICLES FORMATION

I) Introduction

Photosensitive glycopolymers (Figure 1) such as grafted and diblock glycopolymers were successfully prepared and characterized using different techniques as we presented in ***the Chapter II***. Grafted glycopolymers (Dex-g-PNB) exhibit weight fraction of PNBA (F_{PNBA}) equal to 85 %, 75 %, 44 % and 22 % as shown in Table 1, while this fraction is equal to 49 % and 27 % in case of diblock glycopolymers (Dex-b-PNBA).

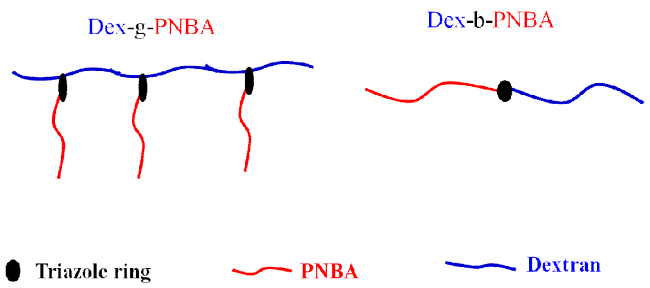

Figure 65. Schematic representation of grafted and diblock glycopolymers based on dextran and PNBA

Solubility of these glycopolymers in various solvent or mixture is given in Table 1. Whatever the PNBA weight fraction, all grafted and diblock glycopoymers are insoluble in water, even with a low F_{PNBA} such as 22 % and 27 %. We also tested Acetone/H_2O mixtures that are commonly used in nanoprecipitation method but none of the glycopolymers were soluble in such media. Grafted glycopolymers (Dex-g-PNBA) with high weight fraction of PNBA (75% and 85%) are soluble in mixture THF/H_2O (95/5, v/v) and will be used to formulate nanoparticles by nanoprecipitation method. Unfortunately, other grafted and diblock glycopolymers were proved to be insoluble in such THF/H_2O mixtures, whatever the THF/H_2O ratios. In parallel, all the grafted and diblock glycopolymers were soluble in DMSO that is a common solvent from dextran and PNBA parts. Consequently, their self-assemblies using dialysis method from DMSO solutions began to be studied, but these preliminary results will not be discussed further in this chapter.

In the present chapter, we will discuss following items:

a) The formation of nanoparticles using two methods:

- By nanoprecipitation for grafted glycopolymers (Dex-g-PNBA) with high weight fraction of PNBA (75% and 85%).

- With the emulsion / organic solvent evaporation method by carrying out an *in situ* Huisgen-type Copper (I)-catalyzed Azide- Alkyne Cycloaddition (CuAAC click chemistry). This reaction occurs at the liquid/liquid interface between several hydrophobic PNBA homopolymers that are end functionalized by an azide function and modified dextran carrying several alkyne groups (alkynated dextran).

b) All the prepared nanoparticles will be characterized using Dynamic Light Scattering and Zeta potential measurements. With these techniques, Z-average diameter, Zeta potential as well as shell thickness will be estimated.

c) The stability of these colloidal systems against ionic strengths will be studied. The advantage of covalent links (triazole rings) between core and shell will be proved using a competitive surfactant.

d) The effect of light on glycopolymers nanoparticles loaded by an hydrophobic fluorescent probe such as Nile Red dye will be studied.

e) Preliminary results on nanoparticles cyctotoxicity will be presented at the end of this chapter.

Table 19. Solubility of dextran, PNBA, grafted and diblock glycopolymers

Polymers[(a)]	F_{PNBA} % [(b)]	**DMSO**[(c)]	**Acetone/H_2O**[(c)] **(Different ratios)**	**THF/H_2O**[(c)] **(95/5)**	**Method used to produce nanoparticles**
PNBA	100	+	-	+	
Dextran	0	+	-	-	
Alkynated dextran	0	+	-	-	
Dex(15)-g-14PNBA$_{3500}$	75 %	+	-	+	Nanoprecipitation
Dex(15)-g-12PNBA$_{9800}$	85 %	+	-	+	Nanoprecipitation
Dex(15)-g-1.5PNBA$_{3500}$	22 %	+	-	**-**	Dialysis
Dex(15)-g-1.5PNBA$_{9800}$	44 %	+	-	**-**	Dialysis
Dex-b-PNBA$_{3500}$	27%	+	-	**-**	Dialysis
Dex-b-PNBA$_{9800}$	49%	+	-	**-**	Dialysis

(a)Dex(15)-g-1.5PNBA$_{3500}$ where 15 is the yield of alkyne substitution ( ), 1.5 is the number of PNBA grafts per 100 glucosidic units and 3500 is the $\overline{M}_n$ of each PNBA graft.

(b) PNBA weight fraction estimated from ^{1}H NMR spectrum

(c) (+) and (-) mean soluble and insoluble, respectively.

II) Elaboration and characterization of nanoparticles

II.1) Nanoprecipitation of Dex-g-PNBA

Nanoparticles based on Dex-g-PNBA glycopolymers, that have weight fraction of PNBA (F_{PNBA}) equal to 75% and 85%, were formed using nanoprecipitation method [1, 2]. To formulate nanoparticles, glycopolymers were dissolved in THF/H_2O (95/5,v/v), then the solution was slowly added to excess of water using micropipette (0.1 mL per minute) under moderate stirring. On one hand, after complete solution addition, THF was slowly removed by evaporation at room temperature under stirring for 24 hrs. For instance, polydispersity index (PDI) of nanoparticles based on Dex(15)-g-14PNBA$_{3500}$ were determined before and after evaporation using Dynamic Light Scattering (DLS) and was found to increase from 0.16 to 0.251, respectively. Therefore, on another hand, we tried to remove THF by centrifugation. Consequently, after formulation, nanoparticles were centrifuged then washed twice with distilled water to completely remove THF during centrifugation. Nanoparticles suspensions prepared by this way were characterized using DLS (Figure 2,A). For both glycopolymers only one population of the size distribution was obtained with low PDI (Table 2). The Z-Average diameter of nanoparticles based on Dex-g-PNBA with F_{PNBA} = 85% was larger than that of nanoparticles based on the other Dex-g-PNBA.

Table 20. Z-Average diameter and polydispersity index (PDI) values of Dex-g-PNBA- based nanoparticles estimated using dynamic light scattering (DLS). Nanoparticles were produced by nanoprecipitation.

Used copolymers	[(a)] F_{PNBA} in glycopolymers (%)	[(b)] Wt of dextran (mg) equivalent to 1g of PNBA	Z-Average diameter (nm)	PDI
Dex(15)-g-14PNBA$_{3500}$	75	310	118±3	0.08
Dex(15)-g-12PNBA$_{9800}$	85	153	185±2	0.04

(a) F_{PNBA} was estimated using the following equation

$$F_{PNBA}\ (\%) = \left(\frac{A_{CH2_2} \times 207}{A_{CH2_2} \times 207 + A_{Ha} \times 176.1} \right) \times 100$$

(b) Wt of dextran (mg) was calculated from $\left(\frac{A_{Ha} \times 162}{A_{CH2_2} \times 207} \right) \times 1000$

Where A is areas under peaks, Ha is anomeric proton, CH_2 is benzylic methylene of NBA monomer units, 207 is the molecular weight of NBA monomer unit, 176.1 the average molecular weight of repeating unit of alkynated dextran, 162 is the molecular weight of glucosidic unit

Such nanoparticles were also characterized by Transmission Electron Microscopy (TEM) that provides precise information about morphology, size and size distribution of nano-objects. As shown in the Figure 2, TEM pictures show almost spherical nanoparticles based on Dex-g-PNBA with B) F_{PNBA} =75% (Z-diameter 118 nm, with PDI= 0.08) and C) F_{PNBA} =85% (Z-diameter 185 nm, PDI= 0.04).

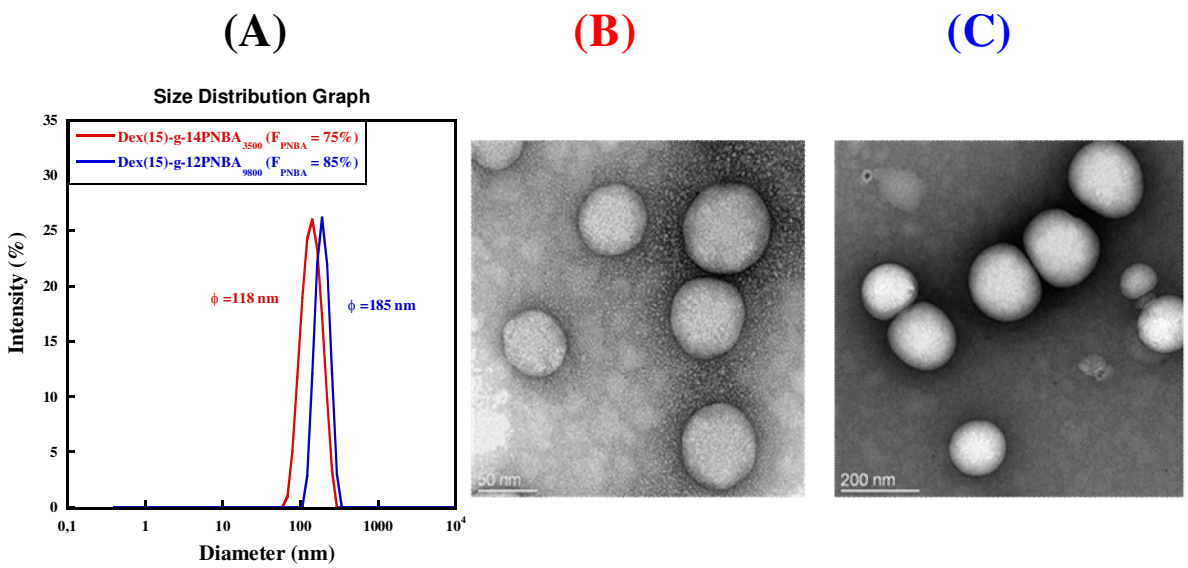

Figure 66. (A) Size distribution curves obtained from DLS of nanoparticles. TEM pictures of nanoparticles based on (B) Dex(15)-g-14PNBA$_{3500}$ (F_{PNBA} = 75%) and (C) Dex(15)-g-12PNBA$_{9800}$ (F_{PNBA} = 85%).

II.2) Emulsion/Organic Solvent Evaporation method

Emulsion/organic solvent evaporation method is one of techniques commonly used to form nanoparticles dispersion with narrow polydispersity. In this case, the hydrophobic polymer was dissolved in common organic solvent such as dichloromethane or ethyl acetate while surfactants or amphiphilic copolymers were in the aqueous phase. After the emulsion/evaporation process, a colloidal system based on hydrophobic polymer as core surrounded by surfactant as shell is obtained. The surfactant shell ensure the colloidal stability. In another way, one can dissolve amphiphilic copolymers in the organic phase without using an additional surfactant in the water [36]. Unfortunately, no grafted or diblock copolymers we elaborated were soluble in dichloromethane or ethyl acetate. Consequently, we suggested producing nanoparticles by another way.

Poly(o-nitrobenzyl acrylate) (PNBA) end-functionalized by azide function was firstly dissolved in dichloromethane. Surfactant we used was a alkynated dextran (shown chapter II, scheme 1) and was dissolved in aqueous phase. By this way, a Huisgen-type Copper(I) catalyzed Azide-Alkyne Cycloaddition (CuAAC click chemistry) will occur at the liquid/liquid interface between azide and alkyne groups, *in situ,* during the emulsification. Before running this CuAAC, we checked the surface tension properties of alkynated dextran to confirm their surfactant properties and their ability to stabilize the emulsion.

II.2.1) Surfactant properties of alkynated dextran

As shown in chapter II, we modified dextran T40 by introducing hydrophobic groups all along the dextran chain (Figure 3). Each hydrophobic tail is carrying one alkyne function and the yield of substitution was equal to 15% (15 alkynes per 100 glucosidic units). As some other hydrophobically modified dextran, we expected that alkynated dextran has surface tension properties, as shown in Figure 3, a. To confirm that, surface tension of aqueous solutions containing alkynated dextran was studied using `*Du Noüy Ring*_ method (Figure 3,b).

Figure 67. a) Alkynated dextran at water/air interface and b) Du Noüy Ring method

We measured water/air surface tension for native and modified dextran at several polymer concentrations. As shown in Figure 4, increasing the concentration of native dextran don˘t influence the surface tension of water/air. Moreover, the measured value of surface tension is equal to 72 mN/m, which is the same value of pure water. In case of alkynated dextran, surface tension of water/air decreases with increasing the concentration of alkynated dextran, as conventionnal molecular surfactants (Figure 4). Unfortunately, at higher concentration than 10 mg/mL, alkynated dextran was no more soluble in water as observed in case of several other derivatives of dextran or of amphiphilic glycopolymers [3].

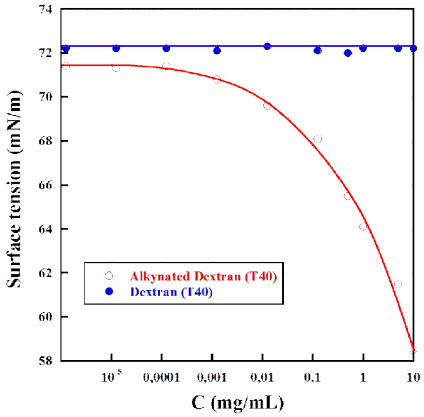

Figure 68. Surface tension against concentration. Case of native dextran and alkynated dextran (= 15%) dissolved in water phase.

II.2.2) Formation of nanoparticles without or with an *in situ* CuAAC

To obtain nanoparticles using this emulsion/ organic solvent evaporation process, we dissolved on one hand the alkynated dextran, which was modified at 15%, in the water phase. On other hand, we dissolved PNBA in dichloromethane phase. Two different PNBA carrying different end functionalities were tested: PNBA-Br ($M_{n(SEC)}$ = 7900 g/mol with $Đ$= 1.12) and PNBA-N_3 ($M_{n(SEC)}$ = 8100 g/mol with $Đ$= 1.07). We studied the influence of PNBA-Br/PNBA-N_3 ratio on the preparation and characteristics of nanoparticles. When PNBA-Br was only used, the emulsion/ organic solvent evaporation method was running without click chemistry. On the contrary, PNBA-N_3 enables us to carry out an *in situ* CuAAC during the emulsification step. After preparation, nanoparticles were washed several time by centrifugation to removed residual dextran, and then dried via lyophilization . By using ^{1}H NMR in DMSO-d_6 a good solvent for both dextran and PNBA (Figure 5), we could calculate the weight of dextran (mg) per gram of PNBA present in nanoparticles according to equation 1. Peak of anomeric proton (Ha) from glucosidic units and peak of benzylic methylene protons (CH_2) in NBA units, were used (Figure 5). We have now to precise that PNBA is located in the core of the nanoparticle and that shell is based on dextran. But, we have no proof that core is not containing dextran derivates too. As already mentioned in chapter II, we can't observe triazole protons peak in Figure 5A as its chemical shift coincides with that of some aromatic protons.

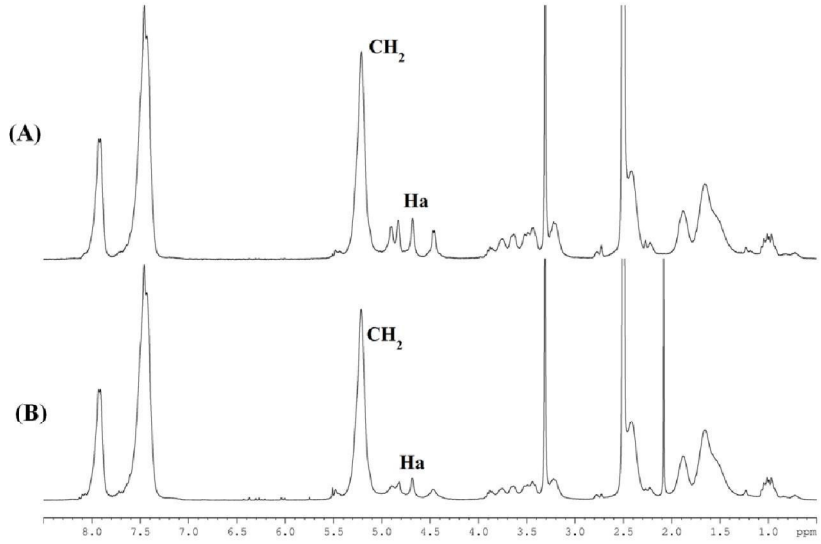

Figure 69. ^{1}H NMR spectra of nanoparticles prepared by emulsion evaporation (A) with CuAAC and (B) without CuAAC.

$$\text{Dextran weight (mg)} = \frac{A_{Ha} \times 162}{A_{CH_2} \times 207} \times 1000 \qquad \textit{Eq. 1}$$

Where AHa and ACH_2 are the peak areas of anomeric proton (4.6 ppm) and of the benzylic methylene protons (5.3 ppm), respectively. 162 and 207 are the molecular weights of glucosidic unit and NBA unit, respectively.

Two runs were made without click chemistry using different PNBA-Br/PNBA-N_3 ratios such as (1/0) and (0.5/0.5). As shown in Table 3, entries 1 and 6, we observed that the amount of dextran per gram of PNBA is equal to 140 and 109 mg, respectively. When using PNBA-Br only, we observed a higher weight of dextran that may be due to the higher hydrophobicity of bromide end function than azide group. Therefore, decreasing the hydrophobicity of end function will decrease the hydrophobic interaction between PNBA chains and alkynyl groups along backbone of dextran. Nevertheless, we have to moderate this hypothesis because obtained nanoparticles have not the same Z-average diameter (Table 3).

When using 0.5 PNBA-Br/0.5 PNBA-N_3 mixture we can produce nanoparticles carrying out or not an CuAAC at the liq/liq interface (Table 3, entries 3 and 6). After formulation of nanoparticles and dissolution in DMSO-d_6, we estimated the weight of dextran to be equal to 185 (entry 3) and 109 (entry 6). Carrying out an *in situ* CuAAC improves the chemical

linkage/adsorption of alkynated dextran at the liq/liq interface. Indeed, after CuAAC, Dex-g-PNBA that are produced are more hydrophobic than initial alkynated dextran. All of this leads to increase the amount of dextran inside nanoparticles.

Different nanoparticles dispersions were prepared with an *in situ* CuAAC, using different ratios between PNBA-Br and PNBA-N_3. As shown in Table 3, similar amount of dextran into nanoparticles has been estimated whatever the used PNBA-Br/PNBA-N_3 ratio when CuAAC occurred (Wt of dextran=175-185 mg). Consequently, no trend between PNBA-Br/PNBA-N_3 ratio and the weight of dextran was found. Moreover, from DLS, we observed that all dispersions exhibit approximately similar Z-average diameter in range 120-140 nm with narrow polydipsersity.

Table 21. Weight of dextran (mg) equivalent to 1 g of PNBA, Z-average diameter and PDI of nanoparticles dispersions

Entry	*Ratio*		*Wt of dextran(mg) equivalent to 1 g of PNBA*	*Z-average Diameter* [c] *(nm)*	*PDI* [c]
	PNBA-Br $\overline{M_n}$(SEC) = 7900 g/mol	**PNBA-N_3 $\overline{M_n}$(SEC) = 8100 g/mol**			
[a]1	**1**	**0**	140	109±2	0.144
[b]2	**0.75**	**0.25**	174	131±3	0.107
[b]3	**0.5**	**0.5**	185	125±1	0.069
[b]4	**0.25**	**0.75**	174	117±1	0.047
[b]5	**0**	**1**	**185**	**118±1**	**0.103**
[a]6	**0.5**	**0.5**	109	132±2	0.124
[a]7	**0**	**1**	**114**	**140±0**	**0.170**

[a] *Emulsion/solvent evaporation without click chemistry*
[b] *Emulsion/solvent evaporation with click chemistry*
[c] *Estimated by DLS*

Nanoparticles prepared by emulsion/organic solvent evaporation process, carrying out or not an *in situ* CuAAC are characterized by TEM (Table 3, Entry 5, 7, respectively). As shown in Figure 6, all nanoparticles have regular spherical shape. DLS size distribution graphs for nanoparticles prepared without and with *in situ* CuAAC with PDI = 0.170 and 0.103, respectively, were drawn in Figure 6.

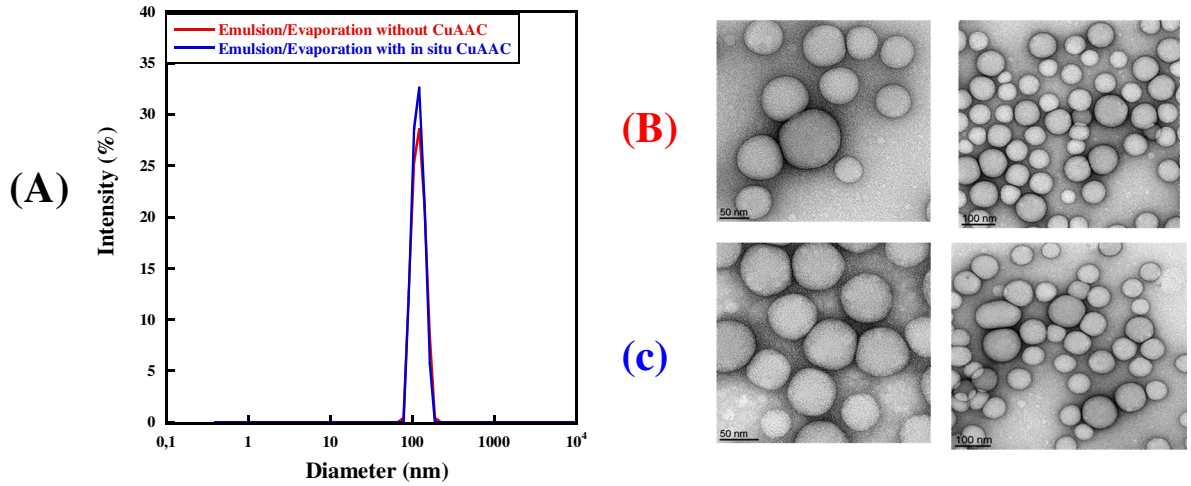

Figure 70. A) DLS size distribution graphs of nanoparticles produced by emulsion/evaporation method. B) Without click chemistry and C) with click chemistry, (Table 3, Entry 7, 5, respectively)

III) Zeta potential and thickness of dextran shell

Once the nanoparticles were produced, whatever the method previously shown, we estimated the shell thickness. That was done via zeta potential measurements. This thickness may influence the colloidal stability as well as the stealthy of the nanoparicles.

III.1) Zeta potential theory

Measuring zeta potential of charged nanoparticles is carried out after nanoparticles dispersion in aqueous phase containing salts (ions). Consequently, a Stern layer is rapidly formed on the surface of charged nanoparticles by adsorption of counter-ions (cationic ions onto the negatively charged particles for instance) (Figure 7). Anionic counter ions are diffusing in the bulk solution as far as a distance near to Stern layer that is called diffuse Gouy-Chapman layer as shown in Figure 7. The potential decreases from the Stern layer through the diffuse one to reach the neutrality between anion and cation. At this point, there is the slipping plane. The thickness of the diffuse layer is estimated from the Stern layer to the slipping plane. In parallel, zeta potential is the difference between the Stern layer potential and the slipping plane potential. There are many factors affecting the zeta potential of a suspension of nanoparticles like stabilizer concentration, pH of the medium and electrolyte concentration [4]. We can quantify zeta potential by measuring the electrophoretic particles velocity or mobility when applying an electric field across nanoparticles dispersion according to Helmholtz ¯ Smoluchowski (equation 2):

$$\zeta(\mathrm{mV}) = 25.7\ \square\frac{\square}{\square_1} - \left|\frac{\square_3\square\frac{\square}{\square_1}\square^{3} + \square_4\square\frac{\square}{\square_1}\square^{4}}{\square_1 + 3\square_3\square\frac{\square}{\square_1}\square^{2} + 4\square_4\square\frac{\square}{\square_1}\square^{3}}\right|\square \qquad \textit{Eq. (2)}$$

Where, ζ is the zeta potential, E the electrical intensity, $\square_{\square}$ is the correction factor of Henry. The relaxation effects are taken into consideration by the coefficients $\square_{\square}\square\square\square\square_{\square}$.

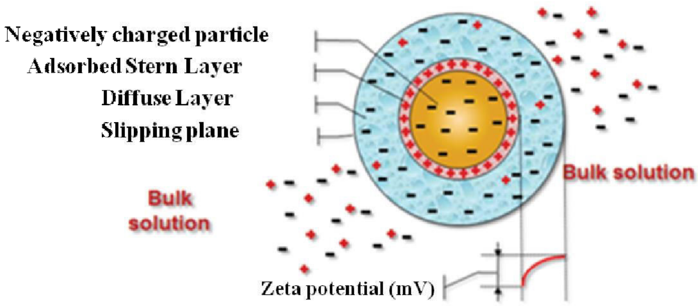

Figure 71. Negatively charged nanoparticles in salty solution.

When one nanoparticle is covered by neutral polymer chains and when this polymeric shell is thicker than the slipping plane, one can observed a moving of this slipping plane from the initial distance to a new one called shell thickness of surfactant ($ǎ_{PZ}$). Consequently, we can observe a decrease of zeta potential to reach zero as the surfactant amount and $ǎ_{PZ}$ are increasing.

Gouy and Chapman demonstrated one relation to evaluate the zeta potential as a function of Debye-Huckel parameter k_H (nm^{-1}) and of the shell thickness of surfactant ($ǎ_{PZ}$) [5]. Shell thickness of surfactant was consequently estimated from the equation 3.

$$\ln\square\square\square\square\ \square\frac{\square\square\square}{4\square_{\square}\square}\square\square = -\ln\square\square\square\square\ \square\frac{\square\square\square_{\square}}{4\square_{\square}\square}\square\square .\ k_H\ .\ ǎ_{PZ} \qquad \textit{Eq. (3)}$$

Where, ψ_o is the potential nanoparticles core. Z is the valence of the salt solution. e is the elementary charge of the electron (equal to 1.602176565 X 10^{-19} C). k_B is the Boltzman constant (equal to 1.381 X 10^{-23} J.K^{-1}). T is the absolute temperature of the medium.

The thickness of the diffuse layer is equal to the inverse of parameter k_H and depends on the ionic strength of the medium according to equation 4.

$$k_H\ (nm^{-1}) = 10^9 \left[\frac{1000.e^2.Z^2.\sum C_i Z_i^2}{\varepsilon k_B T}\right]^{1/2} \qquad \textbf{\textit{Eq. (4)}}$$

Where, C_i and Z_i are the concentration and the valence of the ions in the solution, respectively.

To calculate the thickness of surfactant shell (δ_{PZ}), the zeta potential values were measured with different ionic strength solutions, then the relation between $\ln\left[\tan\left(\frac{Ze\zeta}{4K_BT}\right)\right]$ and k_H was drawn as shown in the Figure 8. The slope of the curve at lower k_H values is obtained from this relation and is equal to δ_{PZ}.

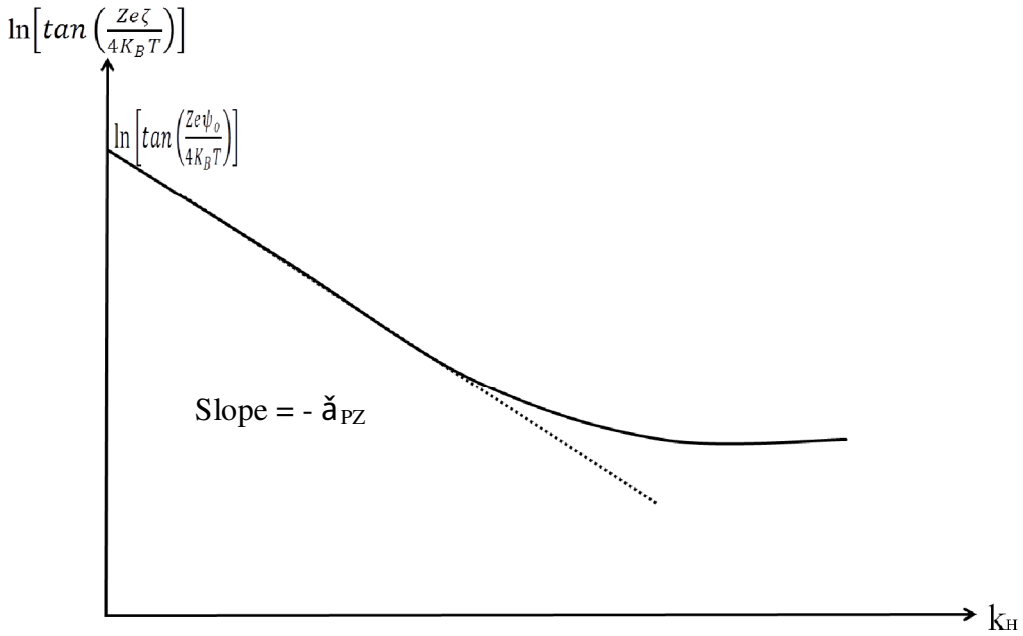

Figure 72. Determination of shell thickness (δ_{PZ}) from equation 3.

III.2) Case of nanoparticles based on Dex-g-PNBA (F_{PNBA} %= 75% and 85%) prepared by nanoprecipitation

These grafted glycopolymers were nanoprecipitated from a THF/H_2O (95/5, v/v) solution into distilled water. To measure zeta potential of nanoparticles, 2 mL of nanoparticles dispersion (1.15 mg/mL) and 2 mL of NaCl solutions were mixed. Different concentrations of NaCl solutions like 10^{-1}, 10^{-2}, 10^{-3} and 10^{-4} M were used. For each dilution, we estimated average zeta potential using Zetasizer instrument. The relation between zeta potential against concentration of NaCl was studied as shown in Figure 9. In case of low concentration (5 $X10^{-5}$ M) of NaCl solution, we observed zeta potential values equal to -31.7 and -42,6 mV for nanoparticles made on Dex-g-PNBA with F_{PNBA} equal to 75% and 85%, respectively. These values indicate the presence of negative charges at nanoparticles surface according to the nitro and ester groups of PNBA grafts. Increasing the NaCl concentration leads to decrease the distance between particle surface and bulk solution. In this case, diffuse layer will become thinner and, as we mentioned previously, diffuse layer is related to zeta potential. Consequently, values of zeta potential were decreasing with increasing ionic strength of NaCl solutions, as shown in the Figure 9.

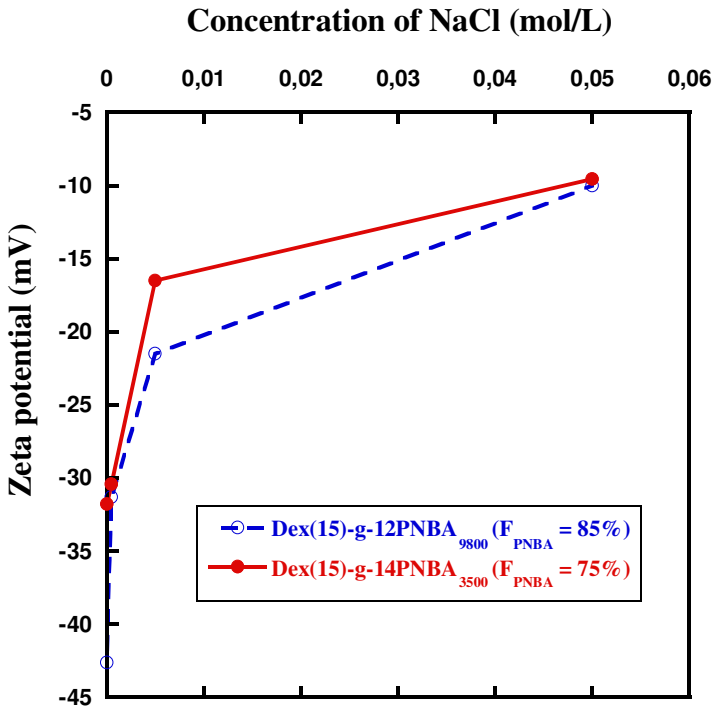

Figure 73. Evolution of zeta potential for nanoparticles made on Dex-g-PNBA (F_{PNBA}= 75 and 85%) against concentration of NaCl.

We estimated thickness of dextran shell (δ_{PZ}) for each of nanoparticles batch according to equation 3, as shown in the Figure 10. Slopes were determined at lower k_H values for each grafted glycopolymers nanoparticles. We found that nanoparticles made on Dex-g-PNBA (F_{PNBA} = 75%) have dextran shell thickness equal to 5 nm that is larger than other nanoparticles made from Dex-g-PNBA with F_{PNBA} = 85 % (δ_{PZ} = 3 nm).

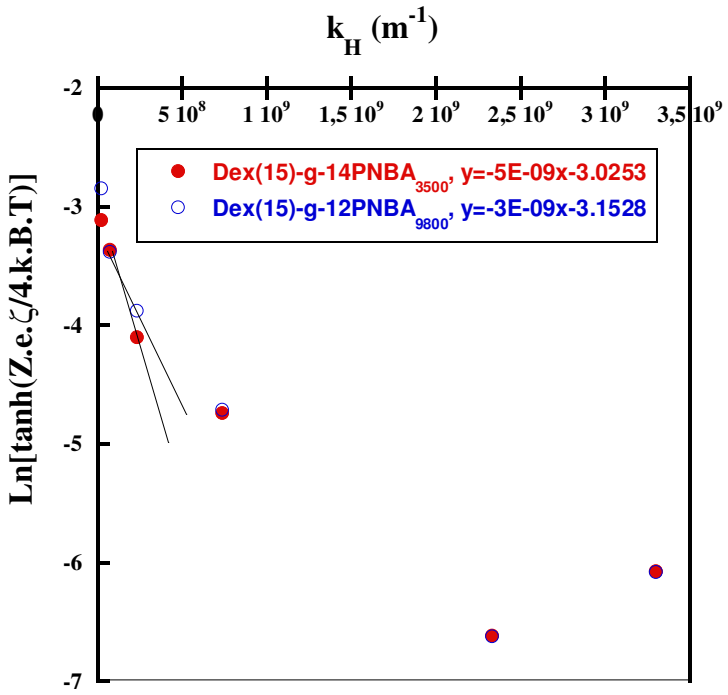

Figure 74. Determination of the thickness of dextran shell according to equation 3. Case of Dex-g-PNBA nanoparticles. (Equation of line at lower k_H is given)

III.3) Case of nanoparticles prepared via the emulsion/organic solvent evaporation

In this case, we prepared nanoparticles dispersions based on the same PNBA-N_3 ($\overline{M}_{n(SEC)}$ = 8100 g/mol) and alkynated dextran, carrying out or not an *in situ* CuAAC. The relation between zeta potential against concentration of NaCl was studied as shown in Figure 11. At low concentration of NaCl solution, we observed zeta potential values equal -15.6 and -25.6 mV corresponding to nanoparticles dispersions prepared with and without *in situ* click chemistry, respectively. Nanoparticles prepared with an *in situ* CuAAC have smaller zeta-potential than nanoparticles prepared without click. That could be due to the higher amount of dextran per gram of PNBA (see Table 3 entries 5 and 7). In other words, nanoparticles made with click chemistry are more covered by neutral dextran than other nanoparticles prepared without click. The value of zeta-potential decreases with increasing value of ionic strength as shown in the Figure 11.

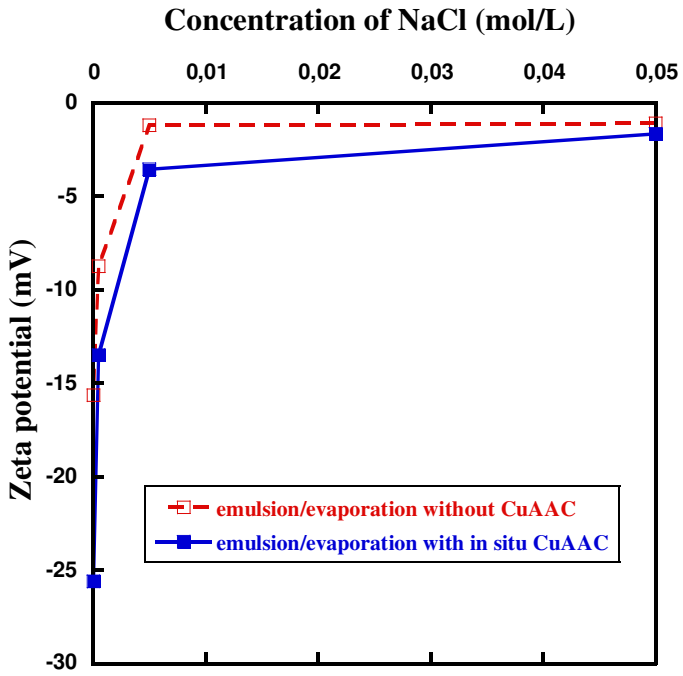

Figure 75. Evolution of zeta potential of nanoparticles prepred via emulsion/evaporation method versus NaCl concentration.

We calculated thickness of dextran shell of nanoparticles according to the equation 3, as shown in the Figure 12. We estimated $\check{a}_{PZ}$ for each nanoparticles to be equal to 9 and 10 nm, which is indicating that carrying or not an *in situ* CuAAC do not significantly influence the $\check{a}_{PZ}$ in this case.

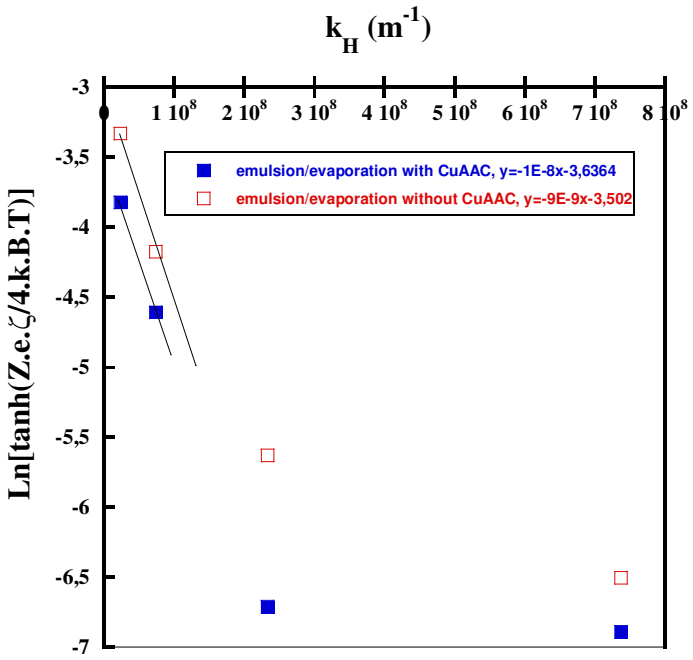

Figure 76. Determination of dextran shell thickness according equation 3. Nanoparticles were prepared by emulsion/evaporation method carrying out or not click chemistry. PNBA-N_3 ($\overline{M}_{n(SEC)}$ = 8100 g/mol) was used. (equation of line at lower k_H in given in brackets)

Carrying out an *in situ* CuAAC during emulsification step leads to the formation of grafted glycopolymers with PNBA grafts having $\overline{M}_{n(SEC)}$ = 8100 g/mol. So we chose to compare the results obtained in this case with those of nanoparticles produced by nanoprecipitation of Dex(15)-g-$PNBA_{9800}$. A thicker and more compact dextran shell was obtained in case of an *in situ* CuAAC by comparison with nanoparticles produced by nanoprecipitation of grafted glycopolymers, as proved by the $\check{a}_{PZ}$ values (10 nm and 3 nm in case of CuAAC and nanoprecipitation, respectively) and with zeta potential (-15.6 mV and -42.6 mV in case of CuAAC and nanoprecipitation, respectively).

These results could be explained by a faster formation of nanoparticles during nanoprecipitation than during emulsion/evaporation, even with CuAAC. Therefore, the core of nanoparticles made via emulsion/evaporation was more covered by neutral dextran than in case of nanoprecipitation. These results are in agreement with work done by Couvreur et. al [6] and were schematized in Figure 13.

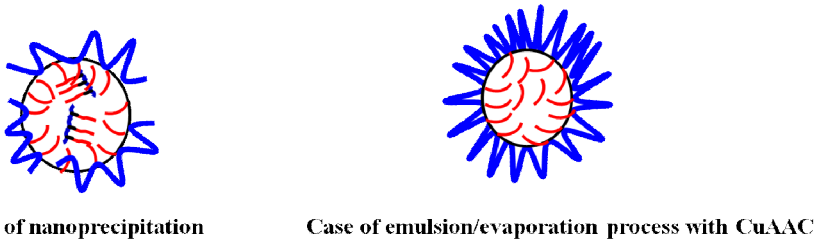

Figure 77. Schematic representation of nanoparticles prepared by nanoprecipitation or emulsion/evaporation with click chemistry

We have same conclusion if we compare zeta potentials of nanoparticles prepared by emulsion/evaporation method or by nanoprecipitation of grafted glycopolymers with lower weight fraction of PNBA, where -15.6 and -32 mV, respectively.

How these ă$_{PZ}$ values influence the colloidal dispersion stability? That ˘s what we will discuss in the following paragraph.

IV) Stability of nanoparticles

IV.1) Stability against salt

Nanoparticles based on dextran and PNBA may be used as photo-sensitive drug delivery systems in human body. From previous zeta potential measurements, we observed that nanoparticles have negatively charged surface. As the ionic strength of the blood is equal to 0.15, one can expect that these nanoparticles will be stable in such particular medium, due to the electrostatic repulsion between each other. While, with increasing ionic strength of the medium, this colloidal system may be destabilized, leading to nanoparticles aggregation then to precipitation. Therefore, stability of nanoparticles against salt must be studied.

We studied the effect of different ionic strengths on stability of our colloidal systems using UV-Visible measurement method. Indeed, when the ionic strength of medium was increased, the nanoparticles may be destabilized and aggregated themselves, so the dispersion size may increase. Consequently, the turbidity of solution will increase and lead to enhance the absorbance (Abs). For particle sizes of the order of hundreds of nanometers, visible spectrophotometer measurements are used to identify changes in stability. In our case, we made measurements of absorbance between wavelengths (≅) 400 and 600 nm, with interval of 50 nm. Long et. al. have developed a method to monitor the flocculation of dispersions

sterically stabilized as a function of ionic strength [7] The plot of log (Abs) *versus* log (≅) gives a straight line whose slope (n) can be calculated. The plot of the absolute value of this slope (n) as a function of ionic strength gives one stability curve. To follow this method, we prepared different concentrations of NaCl solutions (4, 2, 1, 10^{-1}, 10^{-2}, 10^{-3} and 10^{-4} mol/L). 2 mL of each NaCl solution were added to 2 mL of nanoparticles suspension with concentration 1.15 mg/mL, and then obtained suspension was leaved in dark place for 24 hr stirring. We measured absorbance of all solutions, then relations between log (Abs) *versus* log (≅) were studied and the slopes (n) were determined. The relation between slopes (n) and concentrations of salt inside cell of measuring was studied.

Dex-g-PNBA based nanoparticles were prepared by nanoprecipitation of Dex(15)-g-14PNBA$_{3500}$ (F_{PNBA} = 75%) and of Dex(15)-g-12PNBA$_{9800}$ (F_{PNBA} = 85%) as previously described. After adding NaCl solution to nanoparticles suspension and stirring for 24 hrs, we did not observe turbidity, whatever the NaCl concentration as shown in Figure 14. Finally, the stability of nanoparticles dispersions prepared by emulsion/evaporation method carrying out an *in situ* or not CuAAC was studied. We always observed a stable turbidity, whatever the nanoparticles we studied.

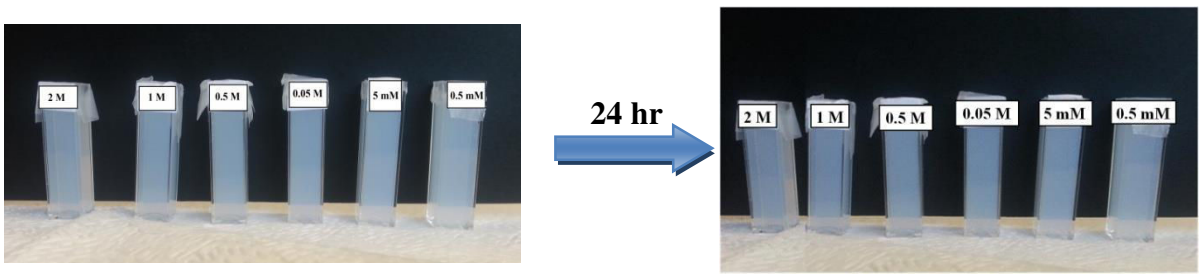

Figure 78. UV cells containing (2 mL of nanoparticles dispersion and 2 mL of xM NaCl solution). NaCl concentrations are written on cells. Case of nanoparticles produced by nanoprecipitation of Dex-g-PNBA with F_{PNBA} =75%.

As shown in Figure 15, all the values of slope (n) are constant *versus* NaCl concentration that indicates the colloidal stability of these nanoparticles in salty media. The slope value in case of nanoparticles made with Dex(15)-g-12PNBA$_{9800}$ was smaller than that in case of Dex(15)-g-14PNBA$_{3500}$ due to the Z-average diameter of nanoparticles. With Dex(15)-g-12PNBA$_{9800}$, 185 nm nanoparticles were formulated, while 118 nm diameter was observed with Dex(15)-g-14PNBA$_{3500}$. Therefore, absorbance of nanoparticles with larger Z-average diameter was

higher than with lower Z-average diameter value. On contrary, larger Z-average diameter gives smaller (n) values. This behavior was in agreement with work done by Long et. al [7].

In case of nanoparticles produced by emulsion/evaporation process with or without an *in situ* CuAAC, Figure 15 shown that, (n) slopes are also constant whatever the NaCl concentration indicating colloidal stability. We observed that (n) slope values of both nanoparticles are close to each other, due to their close Z-average diameters.

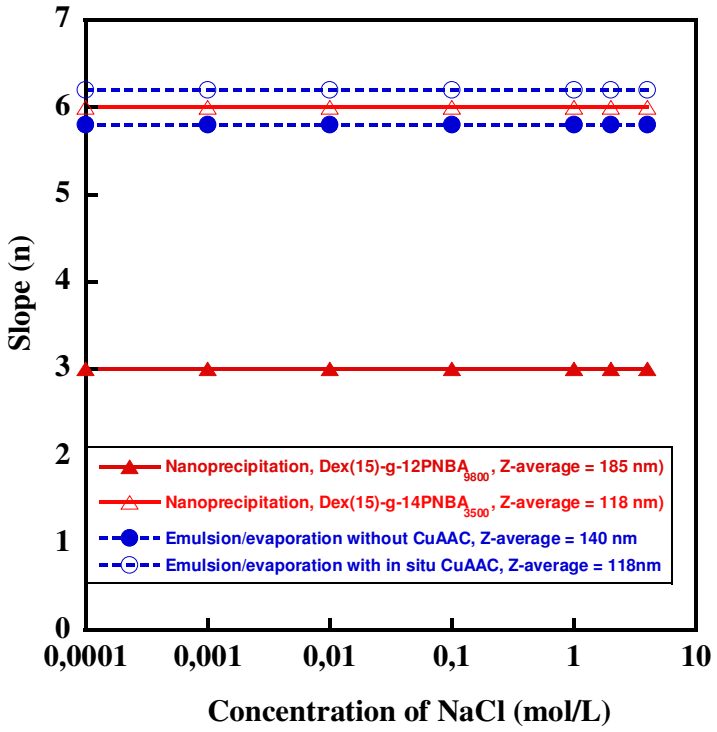

Figure 79. n (slope of Log (Abs) as a function of Log (≡)) against salt concentration for different nanoparticles prepared by nanoprecipitation and emulsion evaporation methods.

Considering results of zeta potential and UV-Visible measurements, one can suggest that stability of nanoparticles at ionic strength lower than 0.05 M comes from electrostatic and steric shell repulsion forces. Nevertheless, at higher ionic strength, nanoparticles stability comes from only steric shell repulsion due to dextran chains. According these results, injection of glycopolymers-based nanoparticles in the bloodstream may be considered. As ionic strength of blood equal 0.15, these colloidal dispersions will be stable. Nevertheless, circulating proteins may desorb the surface shell of the nanoparticles. We will estimate that in next paragraph.

IV.2) Stability against SDS

Dextran shell ensures the colloidal stability of nanoparticles against salts as shown previously. That will allow to inject these objects in blood, whatever the formulation method used. But, what will be the future of nanoparticles after injection into the bloodstream, in presence of circulating proteins as opsonins. In one recent paper, we shown that one physically absorbed dextran shell cannot ensure colloidal stability against SDS (sodium dodecyl sulfate) that is a powerful competitive surfactant mimicing the action of such proteins [3]. The effect of such surfactant was also reported by Nyström et. al on nanoparticles made of polystyrene core covered by ethyl(hydroxyethyl) cellulose (EHEC) shell [8]. The authors compared sodium dodecyl sulfate (SDS) and cetyltrimethylammonium bromide (CTAB) as anionic and cationic surfactants, respectively. They tried different concentrations of SDS and CTAB and they observed a decreasing of the shell thickness with increasing surfactant concentration. SDS or CTAB surfactants interacted with EHEC at the surface of polystyrene latex, leading to the desorption of EHEC as shown in Figure 16. On another hand, Prescott and coll. studied the effect of SDS concentrations on nanoparticles based on silica as core and poly(vinylpyrrolidone) (PVP) as shell [9]. They observed that 30 mM SDS aqueous solution is required to remove all PVP chains at the surface of silica nanoparticles. This later work is in agreement with work done on nanoparticles based on dextran and PLA by Six and coll. [3]. More precisely, they reported that 1 Wt% of SDS (equal 35 mM) is sufficient to complete desorb one physicaly adsorbed dextran shell on PLA surface.

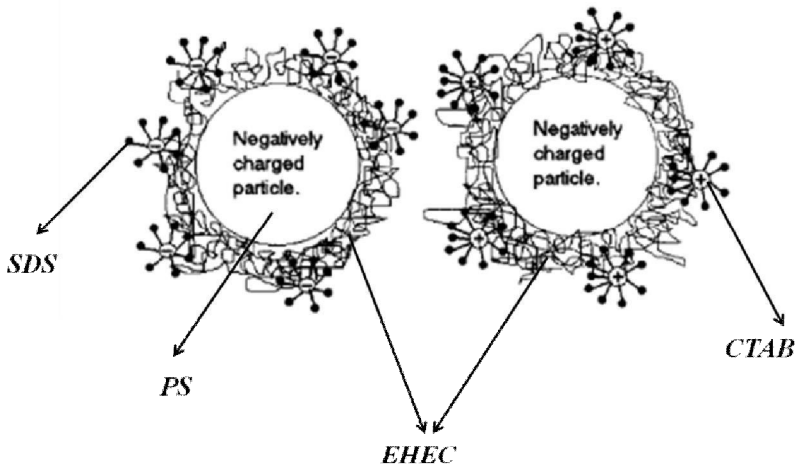

Figure 80. Schematic depiction of the adsorption of SDS or CTAB micelles on PS core/EHEC shell nanoparticles.

Therefore, we added 1% Wt of SDS onto nanoparticles based on dextran and poly(o-nitrobenzyl acrylate). In a first time, nanoparticles were prepared by emulsion/evaporation method with or without an *in situ* CuAAC. Then, each dispersion was stirred for 24 hrs with a 1 Wt% of SDS aqueous solution. After 24 hrs, dispersion was washed 2 times by distilled water using centrifugation. Finally, dispersion was completely dried from water by lyophilisation, then nanoparticles were dissolved in DMSO-d_6 and characterized by ^{1}H NMR. As previously described, when CuAAC was carried out during the sonication step, alkynated dextran was chemically linked with PNBA-N_3 leading to triazole rings formation that covalently link dextran shell onto the PNBA core. On opposite way, using emulsion/evaporation without click chemistry, dextran derivates were only physically adsorbed at the particles surface. Figure 17, A, C shows spectrum of nanoparticles made with or without CuAAC, before contact with SDS. Some peaks are characteristic of PNBA core as well as of dextran shell. As previously written in chapter II, triazole protons peak was not observed on the spectrum because having the same chemical shift than some aromatic protons. In case of nanoparticles prepared with click chemistry, dextran shell peaks were still present in spectrum after SDS contact as shown in Figure 17, B. That could be explained by the presence of triazole rings that chemically link dextran and PNBA, preventing the desorption of dextran. On another way, in case of nanoparticles prepared without click, peaks of dextran were completely disappeared after SDS contact while peaks for PNBA are still present on spectrum as shown in Figure 17, D. One can conclude that dextran physically adsorbed onto PNBA surface, is easily desorbed by SDS, as mentioned in case of Dex/PLA nanoparticles [3].

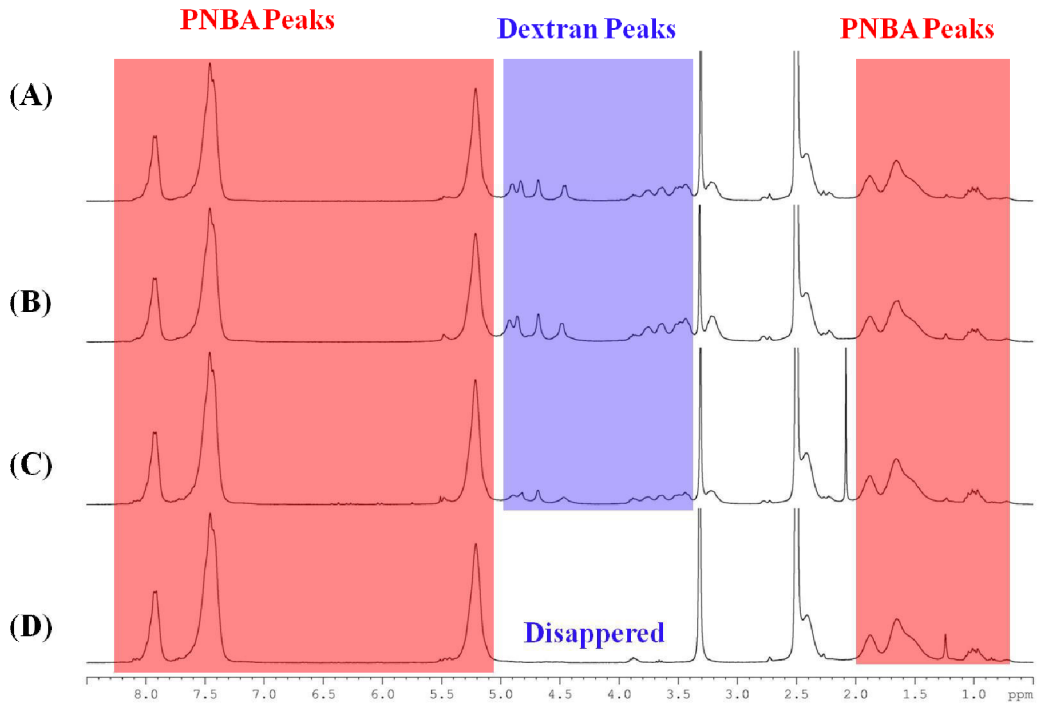

Figure 81. ^{1}H NMR spectra of nanoparticles produced with (A) or without (C) CuAAC. ^{1}HNMR spectra of nanoparticles after SDS contact, with 1 wt% SDS for 24 hrs, with (B) or without (D) CuAAC.

In case of nanoparticles produced by nanoprecipitation, no desorption of dextran shell was observed according the chemical linkages between dextran and PNBA parts in glycopolymers.

V) Effect of UV-light

Whatever the preparation methods, nanoparticles based on glycopolymers were composed of dextran and PNBA parts. PNBA was selected because of it photo-sensitive character. Due to that, nanoparticles are photo-responsive and can deliver drugs under UV-light irradiation. Firstly, we studied the effect of light on homopolymer PNBA.

V.1) Light irradiation of PNBA

Photosensitive property of poly(o-nitrobenzyl acrylate) was checked with a UV-light irradiation experiment. Upon one photon irradiation, 2-nitrobenzyl esters are known to be cleaved liberating carboxylic acid groups and 2-nitrosobenzaldehyde byproducts [10]. This photocleavage can be easily followed on UV-visible absorption spectra, where 2-nitrobenzyl ester and 2-nitrosobenzaldehyde present two different bands (Figure 18 (A)). Light irradiation of PNBA-Br ($\bar{M}_{n(SEC)}$ = 7,900g/mol, $Đ$= 1.12) was carried out in DMSO (0.1 mg/mL) with a

UV light (spectra range from 250 nm to 450 nm, 1150 mW/cm² power). UV-Visible absorbance spectra of solution were measured before and after every 60 sec of irradiation (Figure 18 (A)). Before irradiation, a band at 275 nm was detected corresponding to the absorption of 2-nitrobenzyl ester of each monomer unit. After UV irradiation, the intensity of this band decreased while another band appeared at 325 nm, characteristic of the formation of 2-nitrosobenzaldhyde. Plot of the absorbance at 325 nm *versus* irradiation time shows a fast photocleavage of o-nitrobenzyl esters after 350 seconds (Figure 18 (B)), that don't evolve after further irradiation.

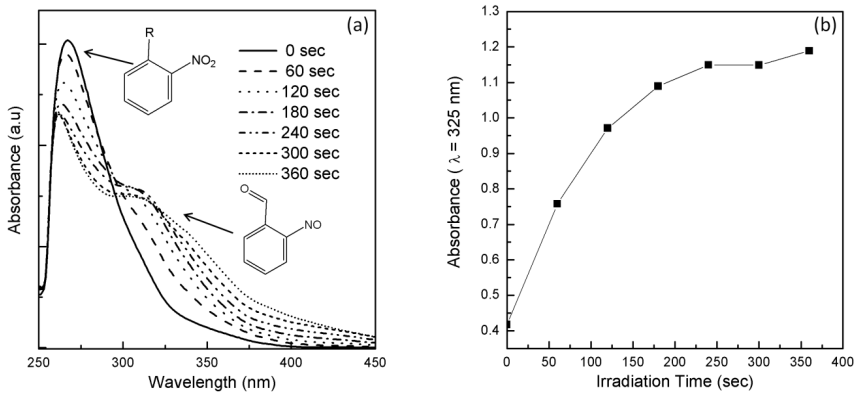

Figure 82. Light irradiation of PNBA-Br (= 7,900g/mol, 仔=1.12) in DMSO (0.1mg/mL) with a UV lamp equipped with a 320 -500 nm filter (power 1150 mW/cm²). (A) UV-Vis spectra after various irradiation time. (B) Absorbance at 325 nm *versus* irradiation time

As shown in literature, the effect of light on photo-sensitive nanoparticles is commonly studied by following the fluorescence intensity of encapsulated hydrophobic probes into such smart nanoparticles. Following the Mean Count Rate of nanoparticles with time of UV irradiation is also one study to make. Therefore, all nanoparticles we will study in the following pages were prepared via different techniques as above described. Nevertheless, during their preparation, hydrophobic Nile Red dye was selected as hydrophobic fluorescence probe and dissolved in the organic phase in order to encapsulate it. Firstly, we will study the effect of light on the nanoparticles chemistry using several techniques. Secondly, we will adjust conditions to carry out Dynamic Light Scattering and fluorescence spectroscopy measurements. Thirdly, we will discuss the effect of UV lamp power.

V.2) Light irradiation of nanoparticles made by nanoprecipitation

We prepared two different nanoparticles using nanoprecipitation method. These nanoparticles were based on grafted glycopolymers that exhibit different hydrophobic weight fractions of PNBA grafts such as F_{PNBA} =75% and 85% (Table 1) and were loaded by Nile Red dye as follows: 25 mg of grafted glycopolymer was dissolved in 5 mL mixture of THF/H_2O (95/5, v/v), then 10 µl of 5 mg/mL Nile Red dye solution in THF was added. Finally, prepared solution was nanoprecipitated from 10 mL of distilled water using 100 µL micropipette under moderate stirring. After complete addition of solution, 10 mL distilled water was added to freeze nanoparticles before centrifugation. Dispersion was centrifuged, washed two times by water to remove all THF, then nanoparticles were dispersed in 20 mL of distilled water to prepare samples for fluorescence measurements. Before studying the effect of different UV powers on nanoparticles, we characterized the photolysis products using different techniques like ^{1}H NMR, FT-IR, UV-Vis spectroscopy and pH-meter, as we will present in next section.

V.2.1) Evolution of nanoparticles chemistry *versus* irradiation

To characterize the photolysis products, we selected nanoparticles dispersion based on Dex(15)-g-14PNBA$_{3500}$ (F_{PNBA} = 75%). These nanoparticles were UV irradiated using power 1150 mW/cm² for 2, 5 and 10 min. From the literature, we known that the expected photolysis products of 2-nitrobenzyl esters are 2-nitrosobenzaldehyde and carboxylic acid groups [10]. Consequently, the excpected photolysis products of our grafted glycopolymers Dex-g-PNBA at total conversion would be Dex-g-PAA (PAA = poly(acrylic acid)) and 2-nitrosobenzaldehyde, as shown in Scheme 1. Nevertheless, if photolysis is not quantitative, PAA grafts will still contain some NBA monomer units.

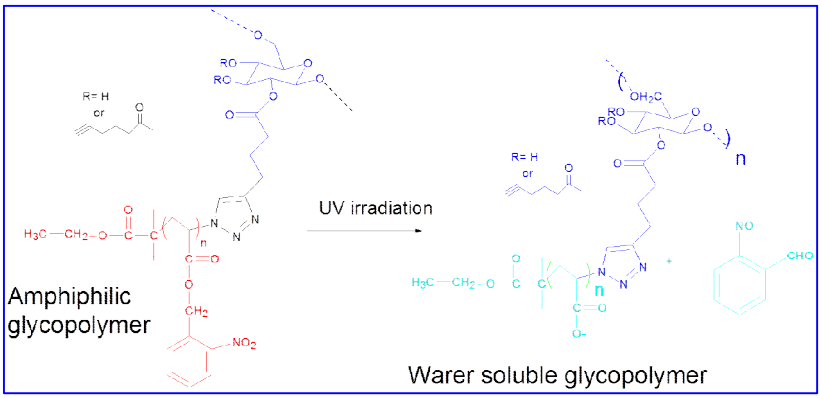

Scheme 1: Effect on the UV irradiation on amphiphilic grafted glycopolymers

After UV irradiation, dispersion was washed by dichloromethane (DCM) using separator funnel to dissolve 2-nitrosobenzaldehyde and to extract it. After extraction, residue of DCM in distilled water was evaporated using shaker oven at 37 °C for 1 hr. After complete evaporation of DCM, solution was lyophilized for 48 hrs. Finally, dried powder was characterized using different techniques as following.

V.2.1.a) ^{1}H NMR spectroscopy

During the UV-irradiation, ^{1}H NMR spectra of powder show a decrease of F_{PNBA} from 75% to 66 and 23% after 2 min and 5 min of UV irradiation, respectively, as shown in Table 4. These weight fractions of PNBA were calculated by using integration of peaks characteristic of methylene benzylic group of NBA monomer units and anomeric protons of dextran. Consequently, while photolysis is running, F_{PNBA} values are not corresponding to the NBA weight fraction in the product because F_{PNBA} didn't take account of produced acrylic acid monomer units. Nevertheless, from peaks integration, one can estimate the yield of photolysis (Table 4). As shown, 90% photolysis was reached after 5 min UV-irradiation under UV-lamp power equal to 1150 mW/cm². These results are in accordance with those on PNBA irradiation (Figure 18). Yield of photolysis *versus* irradiation time was drawn on Figure 19. After 10 min irradiation, ^{1}H NMR spectrum in DMSO shows any peak. Repeating ^{1}H NMR spectrum in D_2O leads to same observation. We thought that PNBA grafts were totally hydrolyzed in PAA grafts at this time, consequently Dex-g-PAA would be no more soluble in DMSO or in D_2O. To improve solubility of the product in water, we tried to dissolve the obtained product in D_2O by adding drops of 0.1 M NaOH in order to convert PAA grafts to poly(sodium acrylate) ones. Unfortunately, same results (no peaks) are obtained. That could be due to the strong interactions between PAA and dextran chains that were evidenced by Barbani et. al. [11] and that induced the formation of physical cross-linking between PAA and dextran [12].

Table 22. F_{PNBA} and photolysis percent of nanoparticles based on Dex(15)-g-14PNBA$_{3500}$, produced by nanoprecipitation. Before and after UV irradiation.

Times of measurement	Peak Integration		[a] F_{PNBA} %	A_{CH2}/A_{Ha}	% Photolysis [b]
	CH_2 of NBA monomer unit	Anomeric H (Ha)			
Without irradiation	2.0827	0.4120	75	5.055	0%
After UV for 2 min	1.8738	0.5547	66	3.378	33%
After UV for 5 min	0.5063	1.00	23	0.506	90%
After UV for 10 min	We didn't observe anything (***repeated two times and give same result***)				

(a) Calculated according to $F_{PNBA} = \left[\frac{A_{CH2}/2 \times 207}{A_{CH2}/2 \times 207 + A_{Ha} \times 176.1} \right] \times 100$

(b) Yield of Photolysis % $= 100 - \left[1 - \left(\frac{A_{CH2}/2}{A_{CH2}/2} \right)_{t=0} \right]$

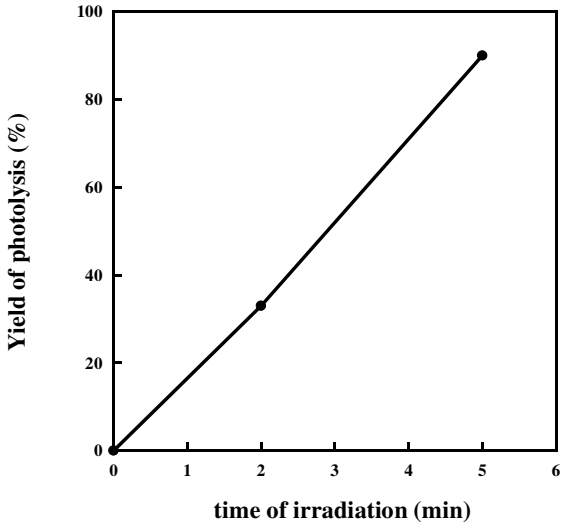

Figure 83. Yield of photolysis (%) *versus* irradiation time. Case of Dex(15)-g-14PNBA$_{3500}$ based nanoparticles

V.2.1.b) FT-IR spectroscopy

Non-irradiated and irradiated nanoparticles based on Dex-g-PNBA with F_{PNBA} = 75% were characterized using FT-IR spectroscopy. FT-IR chart of non-irradiated nanoparticles shows stretching bands at 1345 and 1579 cm^{-1} that are characteristic of NO_2 groups. Moreover, sharp band at 1739 cm^{-1} characteristic of ester carbonyl group from o-nitrobenzyl acrylate units was observed as shown in the Figure 20. OH band from 3000 to 3600 cm^{-1} is characteristic of dextran hydroxyls. Then, nanoparticles have been UV irradiated for 10 min with power equal to 1150 mW/cm². Irradiated nanoparticles FT-IR chart shows a total disappearance of above mentioned characteristic bands for nitro groups, while one new band appears at 1650 cm^{-1}, which indicates carboxylic acid groups. In addition we observed a very broad band centered at 3440 cm^{-1}, which indicates that OH of carboxylic acids band is interfering with hydroxyl groups band of dextran. Hydroxyl group band of carboxylic acids was very broad due to H-bonding interaction between carboxylic groups.

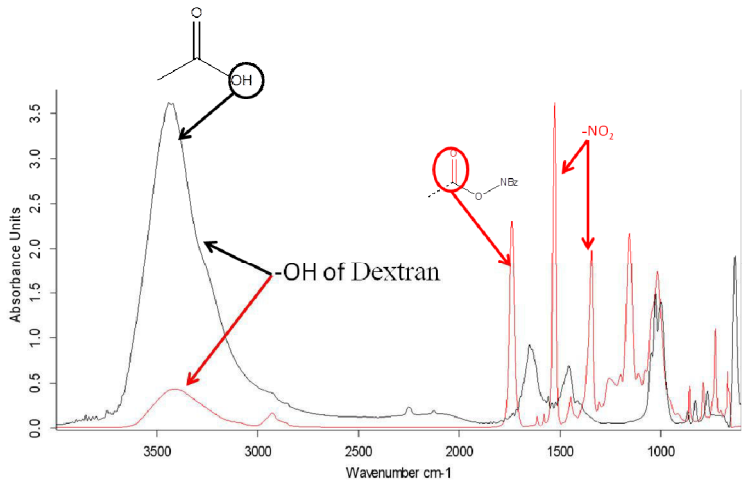

Figure 84. FT-IR charts of nanoparticles based on Dex(15)-g-14PNBA$_{3500}$ (F_{PNBA} =75%). (A) Before irradiation (red color), (B) After irradiation (black color).

V.2.1.c) pH-meter

We followed pH of the nanoparticles dispersion during UV-irradiation using pH-meter at 25 °C. The pH value of dispersion before UV irradiation indicates neutral medium, while pH of dispersion after 10 min irradiation is acidic (Table 5), confirming the formation of free carboxylic groups according to Scheme 1.

Table 23. Values of pH before and after UV irradiation of nanoparticles dispersion based on Dex(15)-g-14PNBA$_{3500}$ (F_{PNBA} = 75%) (UV lamp power = 1150 mW/cm²).

Time of irradiation	*pH value*
Zero	***7.18***
2 min	***6.40***
5 min	***5.30***
10 min	***3.81***

V.2.1.d) UV-Vis spectroscopy

As previously mentioned, dispersions of nanoparticles based on Dex(15)-g-14PNBA$_{3500}$ were irradiated using UV lamp with power 1150 mW/cm², then washed by dichloromethane (DCM) to remove 2-nitrosobenzaldehyde. After washing by DCM, the irradiated nanoparticles were dried, then we recovered UV-Vis spectra of non-irradiated and irradiated dispersions using concentration equal to 0.1 mg/mL in DMSO. Non-irradiated nanoparticles show peaks at 275 nm, which correspond to 2-nitrobenzyl ester, as shown in Figure 21, a. After 2 and 5 min of irradiation, we observed the decrease of 275 nm peak intensity with the increase of irradiation time (Figure 21, b and c). No band at 325 nm was observed according the good DCM washing. We have to remined that o-nitrosobenzaldehyde has an absorbance band at 325 nm. After 10 min of irradiation, as shown in Figure 21, d, we still observed a small band over range 250-280 nm that may correspond to electronic transition as $\pi \rightarrow \pi^*$ $n \rightarrow \pi^*$ of carboxylic acids present in PAA grafts (PAA) and ester group (that ensure the linkage of grafts onto dextran backbone) [13]. To confirm that, we prepared 0.1 mg/mL of poly(acrylic acid) (M_w = 1,800 g/mol) solution in DMSO and its UV-vis spectrum was measured. As shown in Figure 21, e, there is one UV absorbance peak over range of wavelengths from 250 to 280 nm.

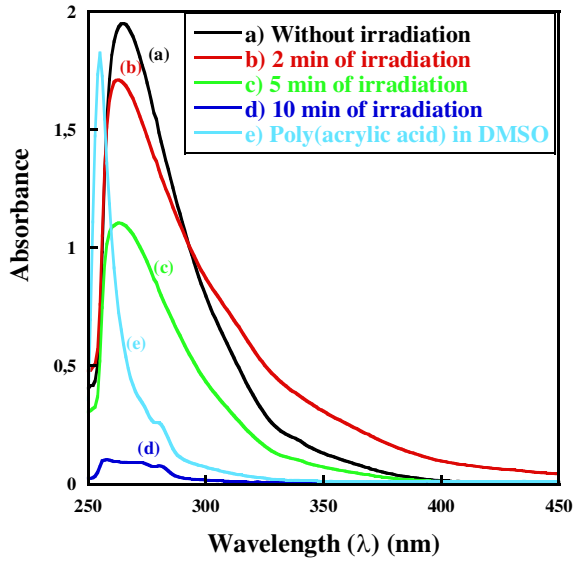

Figure 85. UV-Vis spectra of non-irradiated and irradiated nanoparticles dispersions based on Dex(15)-g-14PNBA$_{3500}$ (F_{PNBA} = 75%) and of poly(acrylic acid) solutions in DMSO (0.1 mg/mL). UV lamp equipped with a 320 ¯ 500 nm filter, power equal 1150 mW/cm².

V.2.1.e) Conclusions

Studying the kinetics of PNBA part photolysis was indirectly done by several techniques, but has to be improved by varying power and time of irradiation for instance. Unfortunately, it was not made during this thesis because lack of time. Nevertheless, based on NMR and UV-Vis spectroscopy results, kinetics of PNBA grafts photolysis was in agreement of PNBA photolysis (paragraph V.1). Moreover, total photolysis of PNBA parts seems to happened between 5 and 10 min of irradiation under UV-lamp power equal 1150 mW/cm².

V.2.2) Selection of optimum experimental conditions using DLS

V.2.2.a) Effect of the medium

As shown in Scheme 1, PNBA grafts will be converted into fully protonated poly(acrylic acid) (PAA) ones as photolysis product. That was confirmed using previously described techniques. Unfortunately, as PAA is insoluble in water, PAA grafts present in the core of nanoparticles may just swell with water after irradiation, leading to hydrogel nano-objects based on Dex-g-PAA. These nano-gels will scatter laser beam of DLS, as native Dex-g-PNBA nanoparticles and in this condition, DLS Mean Count Rate (MCR) evolution during light irradiation could be limited (Figure 22). To prove that we carried out two different experiments by studying the effect of the medium on Mean Count Rate. We chose to use nanoparticles based on Dex(15)-g-12PNBA$_{9800}$ (F_{PNBA} =85%). One sample was prepared by mixing 2 mL of distilled water and 200 µL of nanoparticles dispersion. The other one was

prepared by mixing 1 mL of distilled water with 1 mL of buffer pH= 7 (KH_2PO_4/Na_2HPO_4) and 200 µL of prepared nanoparticles dispersion. In such medium, PAA grafts will be converted to their salts that are readily soluble in water. In later case, DLS measurements will correspond to nanoparticles only. All samples were irradiated using UV lamp with power equal to 1150 mW/cm². The final particles dispersion concentration was equal to 0.11 mg/mL.

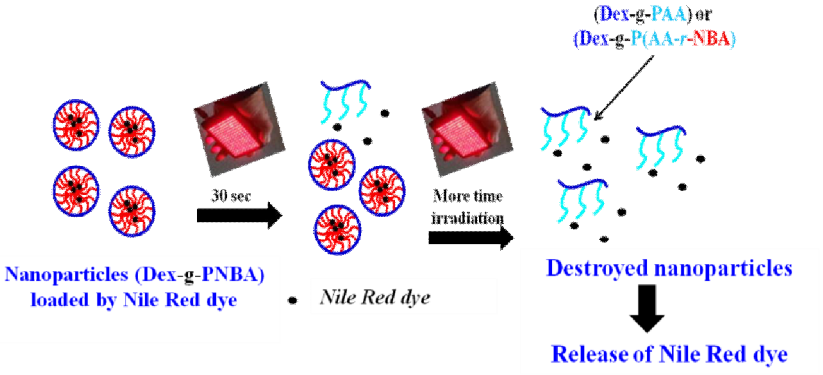

Figure 86. UV irradiation of nanoparticles loaded by Nile Red dye, in buffer solution

Firstly, initial Mean Count Rate (MCR_o, without irradiation) was measured at attenuator index equal 9 and found to be equal to 480 Kcps in case of sample without buffer. Sample was irradiated many times with 30 sec intervals and MCR was measured each time, using the same attenuator index. We studied the relation between Normalized Mean Count Rate (MCR/MCR_o) and time of irradiation as shown in Figure 23. We observed that MCR was decreasing until 120 sec. But after 150 sec irradiation, we observed that MCR value started to increase. As previously written, in absence of buffer, the formed glycopolymer Dex-g-PAA located in the core of the nanoparticles are only swelled with water leading to an increase of the Mean Count Rate values. Secondly, we repeated the previous procedure with sample prepared in buffer. After the first 30 sec of irradiation, both MCR values were very close to each other, as shown in Figure 23. But, with increasing time of UV irradiation, we observed a continuous decrease of MCR. That is due to the solubility of formed glycopolymer (Dex-g-P(AA-r-NBA)) (photolysis product) in water leading to a disruption of nanoparticles. Actually, according to previous results reported in chapter V.2, PNBA grafts were not totally converted into PAA ones after 60 sec of irradiation under this UV-lamp power. Consequently, grafts are based on NBA and acrylic acid monomer units (P(AA-r-NBA)). After 90 sec irradiation, Normalized MCR was constant in case of sample irradiated under buffer condition. At this time all nanoparticles were destroyed and converted to soluble unimer (Figure 22), meaning that no more nanoparticles in medium.

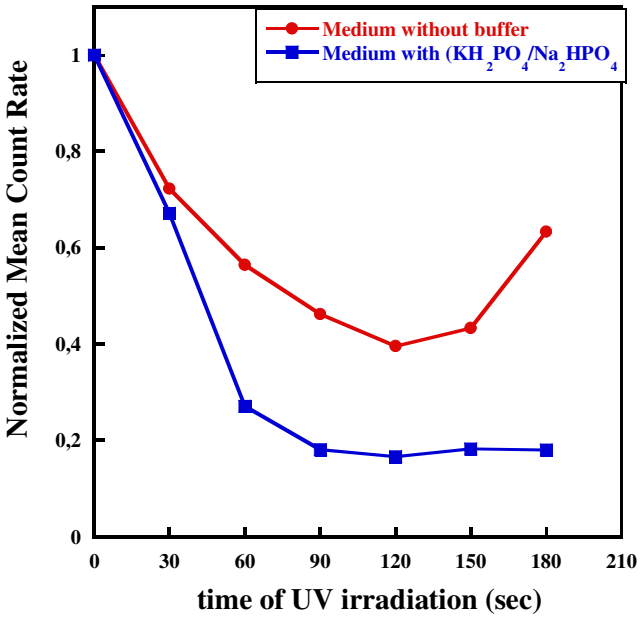

Figure 87. Normalized Mean Count Rate of irradiated (Dex(15)-g-12PNBA$_{9800}$) nanoparticles in presence and in absence of buffer (KH_2PO_4/Na_2HPO_4) against time of irradiation. (UV-lamp power 20%, 1150 mW/cm²)

V.2.2.b) Mode of irradiation

In previous pages, we show the effect of repetitive light exposure on nanoparticles. During this irradiation, nanoparticles degrade gradually leading to the Nile Red release as we will expose in future pages. But, what is the effect of repeating the UV- irradiation each 30 sec? To study that, we prepared nanoparticles dispersion based on Dex(15)-g-14PNBA$_{3500}$ (F_{PNBA} =75%) by nanoprecipitation. Sample was prepared by mixing 1 mL of distilled water, 1 mL of buffer pH= 7 (KH_2PO_4/Na_2HPO_4) and 200 µl of prepared nanoparticles. The initial Mean Count Rate was measured for non-irradiated sample (MCR_o). Then, sample was irradiated using UV lamp with low power (5%, 320 mW/cm²) for 30 sec and Mean Count Rate was measured again (MCR). A low power was selected in order to observe significant effects. After 30 sec irradiation, we observed first a decrease in Mean Count Rate value as shown in Figure 24 due to the disruption of nanoparticles. On one hand, this sample was stirred without more irradiation and we found that Mean Count Rate was increasing with increasing time of stirring. This could be due to an increase of nanoparticles diameters according to the swelling of glycopolymers. Actually, after 30 sec irradiation, photolysis is not total and consequently we have Dex-g-P(AA-r-NBA) glycopolymers. Indeed, Mean Count Rate depends on number but also on diameter of nanoparticles. On another hand, the 30 sec irradiated sample was

irradiated again with 30 sec intervals. We clearly observed a decrease of normalized Mean Count Rate due to the gradual photolysis of PNBA grafts leading to the progressive destruction of nanoparticles (number and diameter decrease) *versus* time. This test is useful to confirm that such nanoparticles can be destroyed by UV irradiation is a controlled way.

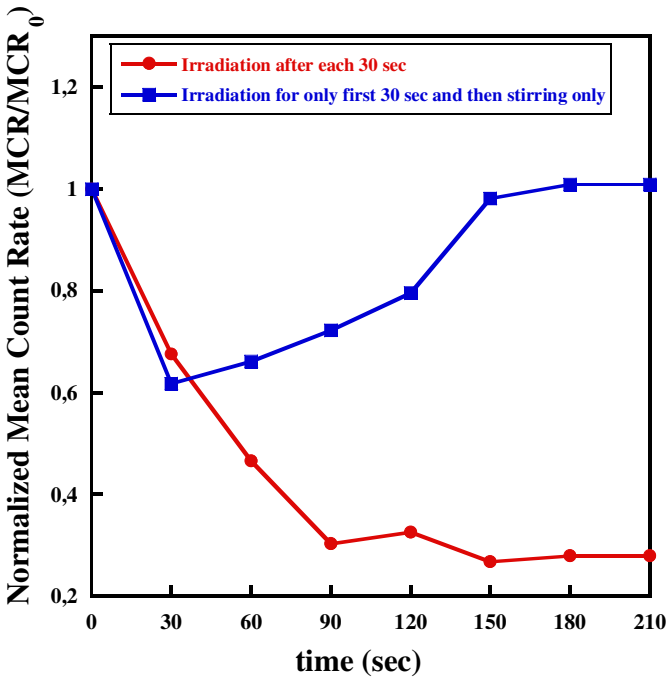

Figure 88. Effect of the mode of UV irradiation on nanoparticles based on Dex(15)-g-14PNBA$_{3500}$ (F_{PNBA} = 75%) (UV-lamp power 5%, 320 mW/cm²).

V.2.2.c) Effect of dispersions concentrations

We prepared dispersions with various concentrations of nanoparticles from the grafted glycopolymer (Dex-g-PNBA) with F_{PNBA} = 75% and loaded by Nile Red dye. The final nanoparticles concentrations were equal to 25, 12.5 and 0.11 mg/mL. All dispersions were irradiated by 30 sec interval using UV lamp power equal to 1150 mW/cm^2. To study Mean Count Rate of dispersions, we diluted irradiated samples because high concentrated samples will give false measurements. Consequently, irradiated sample with concentration 0.11 mg/mL was used as it is, while 12.5 and 25 mg/mL samples were diluted by mixing 20 and 10 µl of dispersion with 2 mL of distilled water, respectively. According these dilutions, final concentrations of all DLS samples were approximately adjusted to be 0.11mg/mL.

Initial Mean Count Rate (MCR_o) values of these different dispersions were measured before irradiation. Then, after irradiation (power 20%, 1150 mW/cm²) Mean Count Rates (MCR)

were measured again. For each dispersion, the relations between normalized mean count rates and time of irradiation were studied, as shown in Figure 25. We observed that normalized Mean Count Rate decreased with increasing time of irradiation, due to the destroy of nanoparticles. Moreover, normalized Mean Count Rate evolution depend on the dispersion concentration used to carry out UV-irradiation.

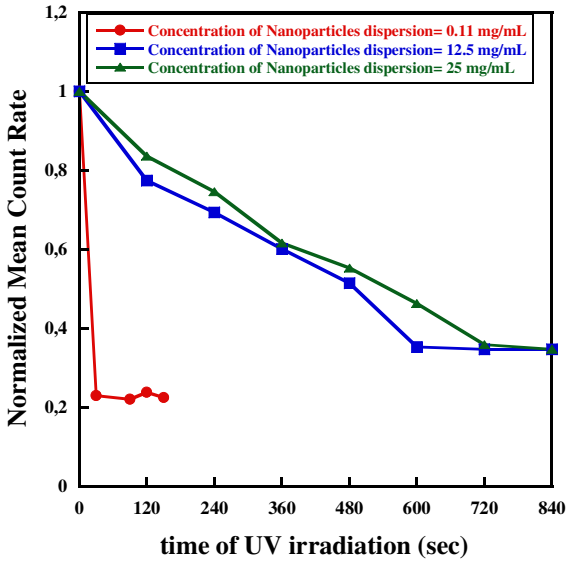

Figure 89. Normalized mean count rate against time of irradiation. Dispersion of nanoparticles based on (Dex(15)-g-14PNBA$_{3500}$) with F_{PNBA} = 75 % with different concentrations such as 0.11, 12.5 and 25 mg/mL. (power 20%, 1150 mW/cm²)

From these results, we observed that dispersions with higher concentrations show a slower decreasing of normalized MCR than dispersion with very low concentration (0.11 mg/mL). Indeed, higher number of nanoparticles in the irradiated volume needed more time to be totally destroyed than lower number (lower concentration sample). More precisely, nanoparticles located at surface of dispersion will be faster affected by light than those located in the middle or the bottom of the cell, due to the difficulty of UV irradiation to penetrate through concentrated dispersion. Consequently, to study the effect of UV-lamp power on nanoparticles dispersion, we will use lowest concentration (0.11 mg/mL) in paragraph V.2.4.

Before this experiment, we will confirm in the following pages that destruction of nanoparticles leads to the release of Nile Red dye.

V.2.2.d) Effect of the UV-lamp power

At the beginning, average Mean Count Rate (MCR_o) of non-irradiated sample based on Dex-g-PNBA with F_{PNBA} =75% was measured using DLS and MCR_o was equal to 429 Kcps with attenuator index =9. Then, sample was irradiated by UV lamp with definite power as 5%, (320 mw/cm²) for 30 sec. MCR of irradiated sample was measured equal to 290 Kcps at same attenuator index. The irradiation and measurement of average Mean Count Rate were repeated with time interval 30 sec. The relation between normalized average Mean Count Rate (MCR/MCR_o) and time of irradiation was studied. We observed that Mean Count Rate was decreasing with increasing the time of irradiation until reaching stability as described in Figure 23 and shown in Figure 26. Consequently and as written in previous pages (Chapter V.2.2.A), the number of nanoparticles was decreasing leading to the decrease of Mean Count Rate value. Same experiments were repeated using different powers of UV lamp like 10%, (620 mW/cm²) and 20%, (1150 mW/cm²). We observed that nanoparticles were destroyed with the same behavior but the kinetic of degradation depends on irradiation power. For example, in case of Dex(15)-g-$14PNBA_{3500}$ nanoparticles after 30 sec of irradiation, we observed a decrease of normalized Mean Count Rate equal to 0.32, 0.49 and 0.78 according to UV irradiation powers equal to 5%, 10%, 20%, respectively. Normalized Mean Count Rate was decreasing with time of irradiation and reach to stability at 90, 60 and 30 sec with respect to power used as 5, 10 and 20%, respectively. That behavior is due to using higher power leads to a fast destruction of higher nanoparticles number at same time of irradiation. As shown in the Figure 26, at a given UV-power, nanoparticles based on grafted glycopolymer with higher F_{PNBA} =85% show a slower decreasing of normalized MCR. That could be explained by the higher number of NBA monomer units in glycopolymers. Therefore, at same power, more irradiation time is necessary to obtain Dex-g-P(AA-r-NBA) glycopolymers soluble in water and a diruption of nanoparticles.

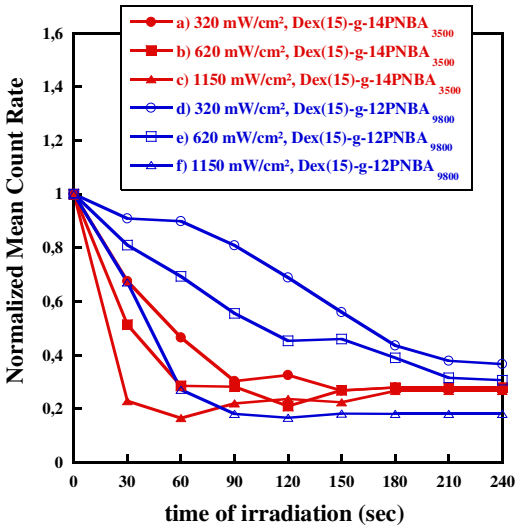

Figure 90. Normalized Mean Count Rate against time of irradiation using different UV-lamp power. Solid symbols Dex(15)-g-14PNBA$_{3500}$ (F_{PNBA} = 75 %) and open symbols Dex(15)-g-12PNBA$_{9800}$ (F_{PNBA} = 85 %)

V.2.2.e) Conclusions

As shown in previous pages, DLS measurements have to be done under buffer solution and with low dispersion concentration. Moreover a continuously UV irradiation leads to a faster destroy of nanoparticles while 30 sec irradiation followed by stirring allows the swelling of the particles. These mode and power of irradiation will probably allow us to control the release of loaded drug into particle core. Finally, composition of the glycopolymers also influence the photolysis of nanoparticles.

Comparing results obtained by DLS and NMR experiments is very fruitful. From Figure 26, one can observe that no more particles are present in suspension after 1.5 to 2 min of irradiation (power 1150 mW/cm²) whatever the chemistry of the particles while the photolysis of PNBA parts is less than 33% (Table 4). It means that, Dex-g-P(AA-r-NBA) must be water soluble at this photolysis yield. We have to mention that results from Table 4 are related to Dex(15)-g-14PNBA$_{3500}$. Consequently, and even all these studies were not be done with same glycopolymers, we can conclude that nanoparticles were destroyed before the total photolysis.

V.2.3) Nile Red Release

In order to prove that Nile Red will be released due to the photolysis of PNBA- based nanoparticles, we will study the diffusion of Nile Red outside non photosensitive particles, then under irradiation.

V.2.3.a) Release of encapsulated Nile Red dye via diffusion

We prepared various nanoparticles based on Dex(15)-g-14PNBA$_{3500}$ and an Dex-g-12PMMA$_{4400}$ already produced by LCPM [14] loaded by Nile Red dye via nanoprecipitation method. Samples were prepared as follow: mixing 1 mL of distilled water, 1 mL of buffer pH= 7 (KH_2PO_4/Na_2HPO_4) and 200 µl of prepared nanoparticles. We took in consideration that the final concentration of Nile Red dye is less than 1.00 ≈g. mL^{51}, that is the maximum solubility of Nile Red in water [15]. Nanoparticles dispersions were divided into two portions. For each nanoparticle family, one portion was kept in fridge and the other one was leaved at room temperature. Emission fluorescence spectra were followed by Fluorescence Spectroscopy. Initial emission fluorescence spectrum of Nile Red into nanoparticles was measured by using excitation wavelength equal to 570 nm. Nile Red emission wavelengths were recorded from 580 to 750 nm.

The relations between Normalized fluorescence intensity [(fluorescence intensity)$_t$/[(fluorescence intensity)$_{t0}$] against time for the two portions of Dex-g-PNBA nanoparticles were studied, as shown in Figure 27. We observed normalized fluorescence intensity values is close to one over range of days, whatever the nanoparticles. The maximum emission wavelength of Nile Red encapsulated into nanoparticles based on Dex-g-PNBA and Dex-g-PMMA was stable to 628 and 609 nm, respectively. As PMMA grafts are more hydrophobic than PNBA one, the maximum emission wavelength of Nile Red in PMMA environment is lower than that in PNBA one. These stabilities in fluorescence intensity and emission wavelength mean that no release of encapsulated Nile Red dye occurs by diffusion. As no Nile Red diffusion was observed for several days, one can studied the Nile Red diffusion during UV irradiation of nanoparticles.

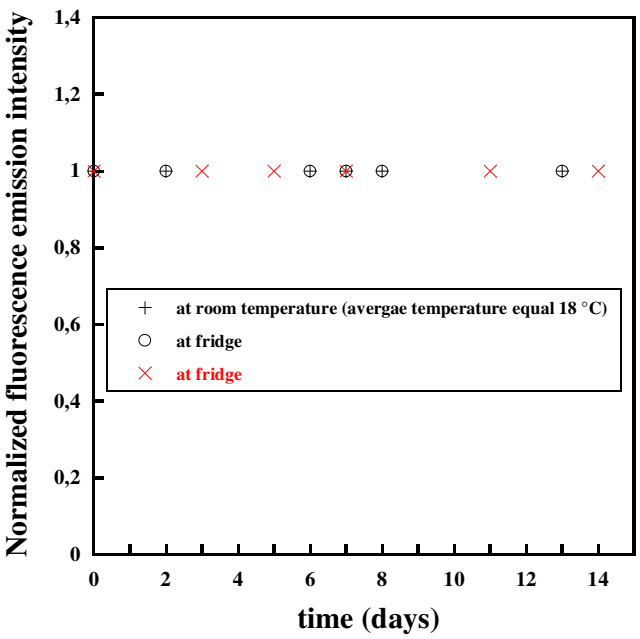

Figure 91. Fluorescence intensity of encapsulated Nile Red dye over range of days. Black symbols= Dex(15)-g-14PNBA$_{3500}$. Red symbol = Dex-g-12PMMA$_{4400}$

V.2.3.b) Release of Nile Red under irradiation

Three grafted glycopolymers were used to produce Nile Red- loaded nanoparticles by nanoprecipitation: Dex(15)-g-14PNBA$_{3500}$ (F_{PNBA} = 75%), Dex(15)-g-12PNBA$_{9800}$ (F_{PNBA} = 85%) and Dex(15)-g-12PMMA$_{4400}$ (F_{PMMA} = 76%). These nanoparticles are characterized with Z-average diameter equal 118, 185 and 144 nm with PDI = 0.08, 0.04 and 0.09, respectively. Samples were prepared by mixing 1 mL of water, 1 mL of buffer pH=7 and 200 µL of nanoparticles dispersion (with concentration 0.11 mg/ml). We studied the effect of irradiation on these nanoparticles using power of UV lamp equal to 5% (320 mW/cm²) with time interval equal 30 sec. As shown in Figure 28, A, fluorescence emission spectrum of Nile Red encapsulated into nanoparticles based on Dex(15)-g-14PNBA$_{3500}$ was determined before irradiation. Then these nanoparticles were irradiated for many times with time interval 30 sec and emission spectra were recorded after each irradiation. We observed that emission fluorescence intensities were decreasing with increasing the time of irradiation. Finally, the relations between normalized emission fluorescence intensity against time of irradiation were drawn (Figure 28, B). In case of nanoparticles based on Dex-g-PNBA, whatever PNBA weight fractions (75 and 85%), we observed a decrease of the normalized fluorescence intensities emission of Nile Red with increasing time of irradiation. That was due to the

nanoparticles destruction by UV irradiation and to the Nile Red dye release in environment with higher polarity. Consequently, its fluorescence intensity decrease. On opposite way, in case of nanoparticles based on Dex-g-12PMMA$_{4400}$, no decreasing of fluorescence intensities emission was observed during UV-irradiation, according the stability of Dex-g-PMMA products under light.

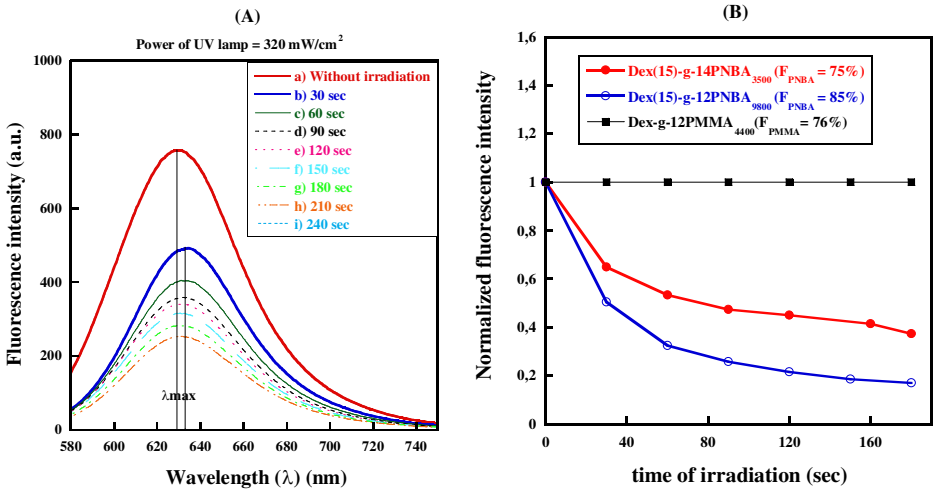

Figure 92. (A) Fluorescence spectra of Nile Red dye loaded into nanoparticles based on Dex(15)-g-14PNBA$_{3500}$, prepared by nanoprecipitation. (B) Normalized fluorescence intensity of Nile Red loaded into nanoparticles at λmax versus irradiation time. Case of Dex(15)-g-14PNBA$_{3500}$, Dex(15)-g-12PNBA$_{9800}$ and Dex-g-12PMMA$_{4400}$. Power of UV lamp was used: 320 mw/cm², (≅$_{exc}$ = 570 nm).

Then, we studied the relation between maximum emission wavelength of Nile Red *versus* irradiation time, as shown in Figure 29. We observed that the maximum wavelength of Nile Red loaded into Dex-g-PNBA nanoparticles with high F_{PNBA} (85%) was lower than dye loaded into nanoparticles with F_{PNBA} = 75% (605 and 630 nm, respectively)(Figure 29). This difference could be due to the difference in hydrophobicity of dye environment in the nanoparticles cores. Indeed, Nile Red dye encapsulated into nanoparticles based on grafted glycopolymer with F_{PNBA} = 85% is in a more hydrophobic environment. Thus, Nile Red is more protected from water and from all hydrophilic dextran chains far away. In this case, Nile Red environment exhibits a higher hydrophobicity than in case of Dex(15)-g-14PNBA$_{3500}$ based nanoparticles. In case of Dex-g-12PMMA$_{4400}$ (F_{PMMA}= 76%) based nanoparticles, the maximum emission wavelength was 609 nm. Then, samples were irradiated by UV lamp with

power equal 320 mW/cm² under stirring. We deliberately selected this low UV-power in order to observe significant effect.

We observed an increase of maximum emission wavelength after 30 sec irradiation (Figure 29). Due to irradiation, Nile Red molecules were transferred from hydrophobic environment (PNBA core) into less hydrophobic one (partially photohydrolyzed PNBA core that contains some acrylic acid monomer units) and/or into water phase (release). Consequently, Nile Red fluorescence intensity decreased as shown in Figure 28 and their wavelength undergoes Redshift, i.e. the wavelength increased. Indeed, fluorescence occurs when an orbital electron of one molecule in higher quantum state (S_1) relaxes to its ground state (S_0) by emitting a photon in accordance with:

Excitation: □□ + □□□□ ⟶ □□

Fluorescence (emission): □□ ⟶ □□ + □□□□ + □□□□□

Where, h ≥is the photon energy with h = Planck's constant and ≥= frequency of light. The specific frequencies of exciting and emitted light are depending on the studied molecule.

Thus, Redshift occurrs due to the decrease of fluorescence intensity according to Max Planck equation E=h ≥=h/≅.

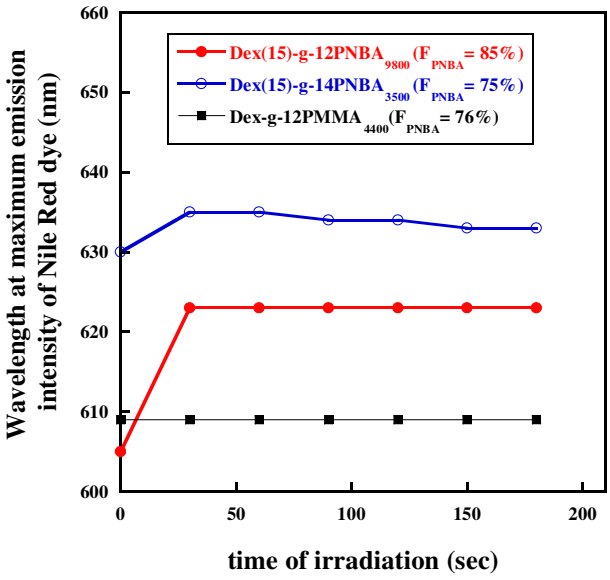

Figure 93. Wavelengths at maximum emission intensity of Nile Red dye encapsulated into Dex-g-PNBA or Dex-g-PMMA based nanoparticles against time of irradiation. Solid symbols: Dex(15)-g-14PNBA$_{3500}$ (F_{PNBA} = 75%), open symbols: Dex(15)-g-12PNBA$_{9800}$ (F_{PNBA} = 85%) and solid square: Dex-g-12PMMA$_{4400}$. Power UV lamp= 5% (320 mW/cm²).

As shown in Figure 29, maximum emission wavelengths of Nile Red didn't evolve after 30 sec of irradiation. That means the Nile Red environment didn't evolve. By comparing these results with those on the evolution of nanoparticles chemistry during irradiation (paragraph V.2.1), one can say that photolysis of PNBA core is not total after 30 sec under this UV lamp power. Consequently, Nile Red dye was released at this time, that is before the total destruction of the Dex-g-PNBA based nanoparticles. Actually, in case of Dex(15)-g-14PNBA$_{3500}$-based particles, normalized Mean Count Rate still decreased after 30 sec irradiation. In case of Dex-g-PMMA nanoparticles, no variation of the maximum emission wavelength was observed according the ineffective effect of UV-light on these particles.

In the next paragraph, we will study the effect of the UV-lamp power and we will try to answer this question: is it possible to control the Nile Red release, as we already know that UV-lamp power influences the particles photolysis.

V.2.4) Effect of power lamp

Emission fluorescence spectrum of Dex(15)-g-14PNBA$_{3500}$ nanoparticles loaded with Nile Red was measured before irradiation, then after each 30 sec irradiation. Using power equal to 5% (320 mW/cm²), we observed that fluorescence intensity of the maximum emission wavelength was decreasing with increasing time of irradiation as shown in Figure 30, A. It could be explained by the destruction of nanoparticles due to the gradual photolysis of PNBA and by the Nile Red release. Actually, fluorescence intensity of Nile Red is quenched in water (polar environment). Due to that, the fluorescence intensity we observed is mainly depending on the Nile Red concentration in the organic core of nanoparticles. We observed that initially pink dispersion turns to pale yellow after irradiation due to the release of both 2-nitrosobenzaldehyde and quenching of Nile Red by water.

(A) Dex(15)-g-14PNBA$_{3500}$ (F_{PNBA} = 75%)

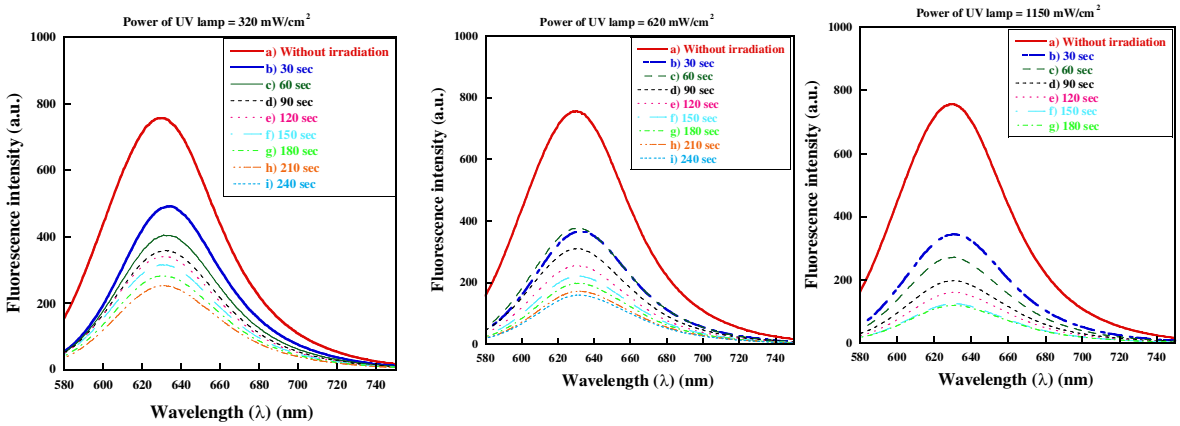

(B) Dex(15)-g-12PNBA$_{9800}$ (F_{PNBA} = 85%)

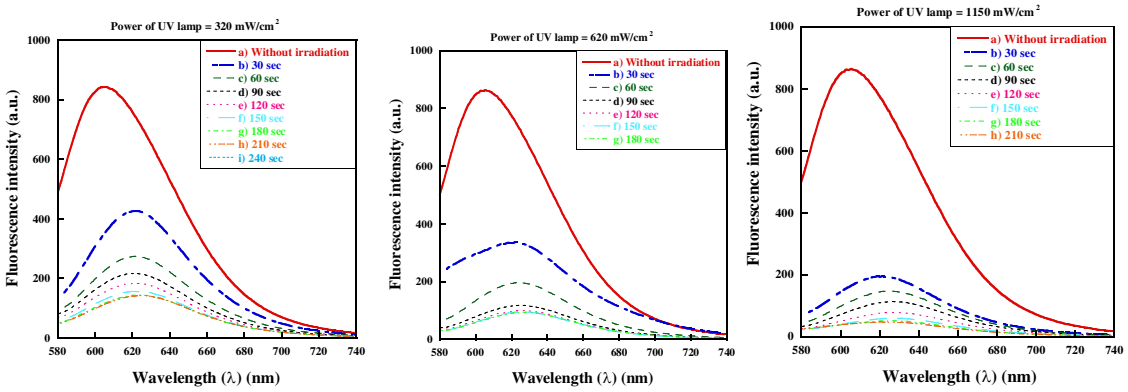

Figure 94. Fluorescence spectra of Nile Red dye loaded into nanoparticles prepared by nanoprecipitation. Different powers of UV lamp were used: 320 mw/cm², 620 mw/cm² and 1150 mw/cm² (λ_{exc} = 570 nm).

Other suspensions based on the same glycopolymer were prepared and used to study the effect of different UV irradiations powers as 10%, (620 mw/cm²) and 20%, (1150 mw/cm²). Same behavior was observed as well as for the other glycopolymer Dex(15)-g-12PNBA$_{9800}$ (F_{PNBA} =85%) (Figure 30, B)

The relations between the normalized fluorescence intensity and the time of irradiation were studied, as shown in Figure 31. In agreement with results shown in Figure 30, we observed the decreasing of fluorescence intensity, whatever the power used. But, one can observe that the rate of decrease was depending on the power of the UV lamp. For example after 30 sec of irradiation, the decrease of normalized fluorescence intensity was equal to 0.35, 0.47 and 0.55

using UV irradiation powers equal 5%, 10%, 20%, respectively (case of Dex(15)-g-14PNBA$_{3500}$). Normalized fluorescence intensity decreases with time of irradiation until reaching one plateau corresponding to the Nile Red fluorescence in aqueous phase that contains 2-nitrobenzaldehyde and photolyzed glycopolymers (Dex-g-PAA or Dex-g-P(AA-r-NBA)). This fluorescence intensity decrease is due to the change of Nile Red environment (release outside the particle). We observed that the fluorescence decreasing was faster in case of grafted glycopolymer with F_{PNBA} =85% than in case of glycopolymer with F_{PNBA} =75%. For example, after 30 sec UV irradiation, we observed a decrease equal to 0.36 and 0.49 with grafted glycopolymers having F_{PNBA} equal 75% and 85%, respectively. This is due to the higher weight fraction of PNBA, and consequently higher NBA monomer units, into Dex(15)-g-12PNBA$_{9800}$ based nanoparticles. Indeed, after irradiation such nanoparticles will produce higher PAA or its salt concentration. The Nile Red environment will be more hydrophilic than in case of glycopolymer with lower weight fraction (F_{PNBA} =75%), leading to a lower fluorescence intensity.

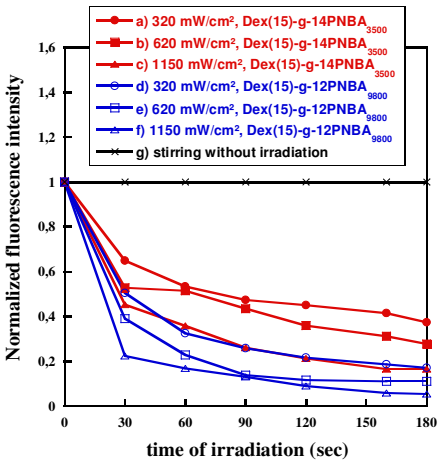

Figure 95. Normalized fluorescence intensity against time of irradiation. ***(≅$_{excitation}$ =570 nm and ≅$_{emission}$ = 580-750 nm)*** **(Solid symbols: Dex(15)-g-14PNBA$_{3500}$ (F_{PNBA} = 75%) and open symbols: Dex(15)-g-12PNBA$_{9800}$ (F_{PNBA} = 85%))**

V.2.5) Discontinuous irradiation

We chose the grafted glycopolymer based on Dex(15)-g-14PNBA$_{3500}$ (F_{PNBA}= 75%) to study the effect of discontinuous irradiation. Nanoparticles was formulated by nanoprecipitation method as mentioned previously. Sample was prepared by mixing 1 mL of water, 1 mL of pH=7 and 200 µL of dispersion of nanoparticles. Initial fluorescence intensity at maximum wavelength of non-irradiated sample was measured. Then, sample was irradiated for 30 sec using UV lamp with power 5%, 320 mW/cm². Fluorescence intensity was measured, just after

irradiation and after 10 and 20 sec stirring in the dark. This operation was repeated several time. Figure 32 clearly shows an instantaneous decrease of Nile Red fluorescence after each irradiation. During the stirring, we observed a partial recovery of the fluorescence emission intensity that may be attributed to a balancing process of Nile Red molecules between hydrated and hydrophobic parts of the disrupted nanoparticles. These results confirm the high photosensitivity of nanoparticles and its potential use as photocontrollable nanocarriers to progressively deliver hydrophobic molecules. Our results are in agreement with results were done by Zhao et. al [16].

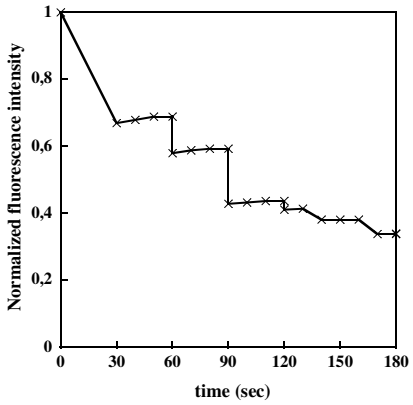

Figure 96. Normalized fluorescence emission intensity against irradiation and non-irradiation time(power 5%, 320 mW/cm²)

V.2.6) Conclusions

Based on this Nile Red release study, one can conclude:

- No release of Nile Red occurred by diffusion throughout Dex-g-PNBA based nanoparticles during two weeks. Nevertheless, this diffusion may happen at longer time.

- Under UV-irradiation, Dex-g-PNBA nanoparticles made by nanoprecipitation progressively swelled according to the photolysis of PNBA part in PAA, then were destroyed. Due to this destruction mechanism, Nile Red moved from initial hydrophobic nanoparticles core to a hydrophilic environment (water + 2-nitrosobenzaldehyde + photolyzed glycopolymers). Consequently, the maximum emission wavelength of Nile Red and it˘s fluorescence intensity decrease. These change are influenced by the chemical composition of the nanoparticles, the power of UV-lamp as well as the mode of irradiation.

All of these results demonstrate the potential applications of these nanoparticles to control the release of loaded drug.

V.3) Nanoparticles via Emulsion/Solvent Evaporation method

We prepared two different types of nanoparticles using emulsion/evaporation method as we already described. The first type of nanoparticles was prepared by a simple emulsion/solvent evaporation method `without click_ and the second type of nanoparticles was prepared with an *in situ* CuAAC. Sample for fluorescence intensity measurements was prepared as follow: 1 mL of distilled water, 1 mL of buffer pH= 7 (KH_2PO_4/Na_2HPO_4) and 200 µl of prepared nanoparticles loaded by Nile Red dye suspension. Emission fluorescence spectra of samples were measured before irradiation. Then samples were exposed for UV irradiation with various powers and emission fluorescence spectra were measured again. We repeated UV irradiation and measured corresponding emission fluorescence spectra for each time with time interval equal 30 sec. We observed that fluorescence intensities were decreasing with increasing time of irradiation as shown in Figure 33.

Emulsion/Evaporation method (without CuAAC)

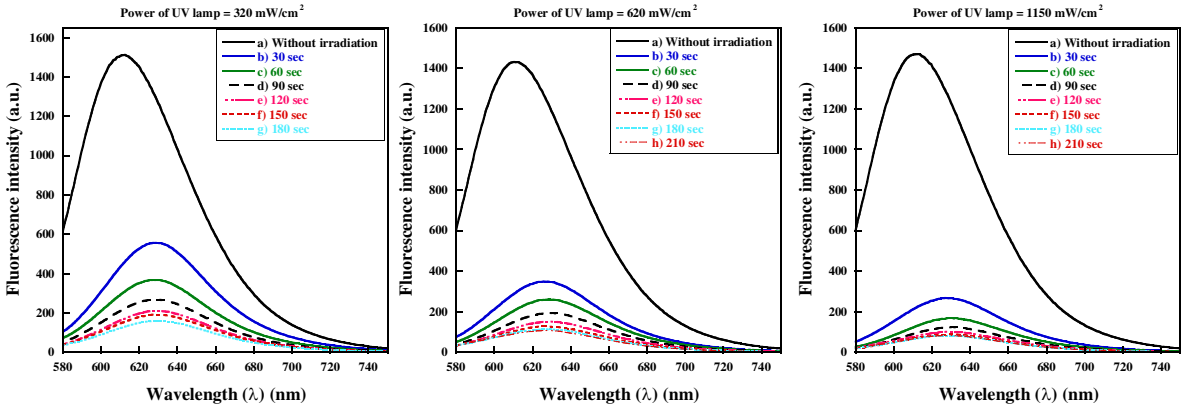

Emulsion/Evaporation method carrying an in situ CuAAC

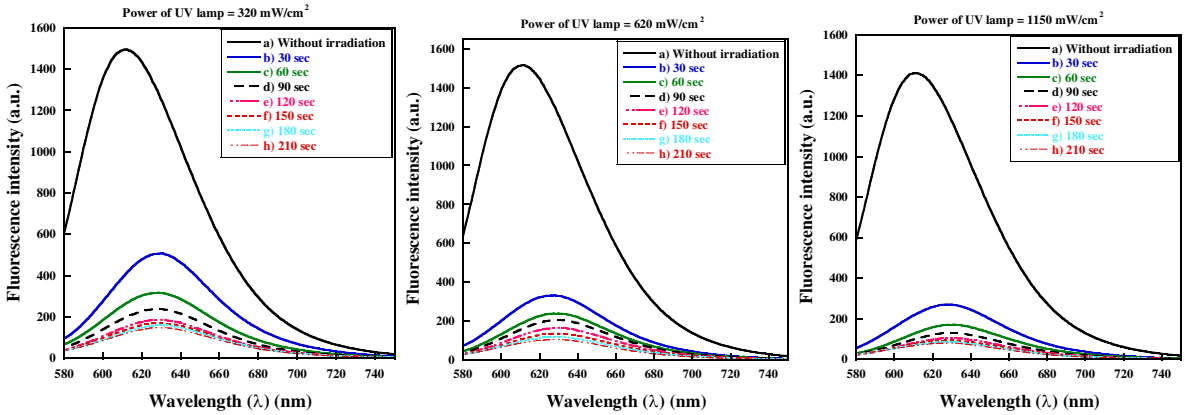

Figure 97. Fluorescence emission spectra of Nile Red loaded nanoparticles using different powers of UV lamp: 320 mW/cm², 620 mW/cm² and 1150 mW/cm². Nanoparticles were prepared by emulsion/evaporation method, with and without click chemistry.

The relations between the normalized fluorescence intensity and the time of irradiation were drawn on Figure 34. Normalized fluorescence intensity was decreasing with increasing irradiation time, whatever the power used. By comparing these curves, we observed that the decrease of fluorescence intensity was depending on the UV irradiation power used. Normalized fluorescence intensity decreases with time of irradiation until reach to plateau. More important observation, as we can observe, the presence of triazole ring linkage between PNBA core and dextran shell of the nanopartilces doesn˘t affect the destruction of the particles.

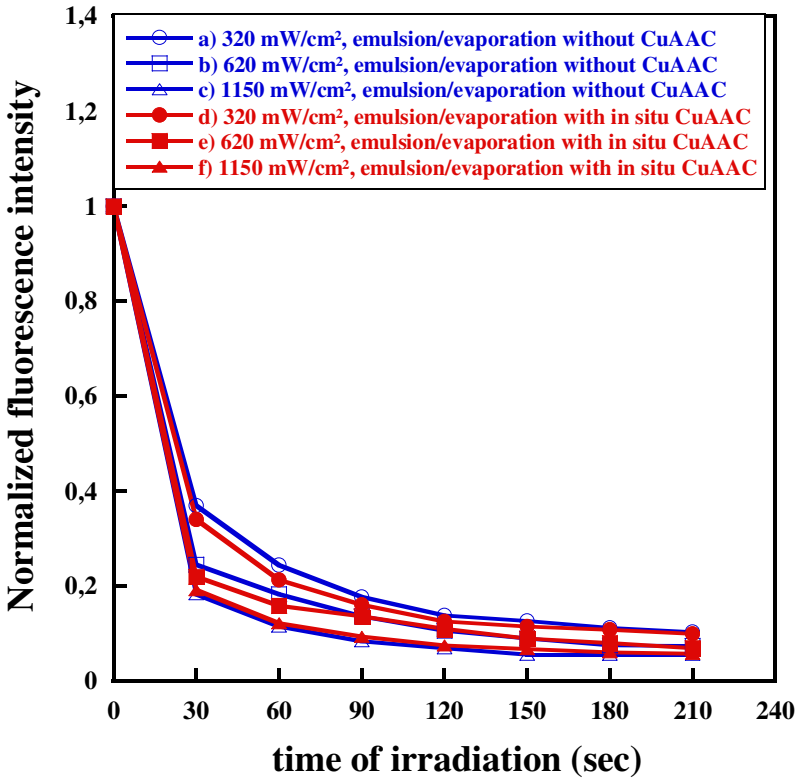

Figure 98. Normalized fluorescence intensity against time of irradiation. Open (blue) and solid (red) symbols nanoparticles were prepared via emulsion/evaporation without and with in situ CuAAC, respectively.

In parallel, Mean Count Rates (MCR_o) of nanoparticles were measured by DLS before and after UV irradiation under various UV-lamp powers. The irradiation and measuring average Mean Count Rate for same sample were repeated with time interval 30 sec. We observed that Mean Count Rate decreases with increasing the time of irradiation until reaching stability as shown in Figure 35. Nevertheless, different kinetics of degradation were observed depending on the irradiation powers. As already observed for other nanoparticles, degradation under higher UV-lamp power leads to a faster destruction of nanoparticles, at same time of irradiation.

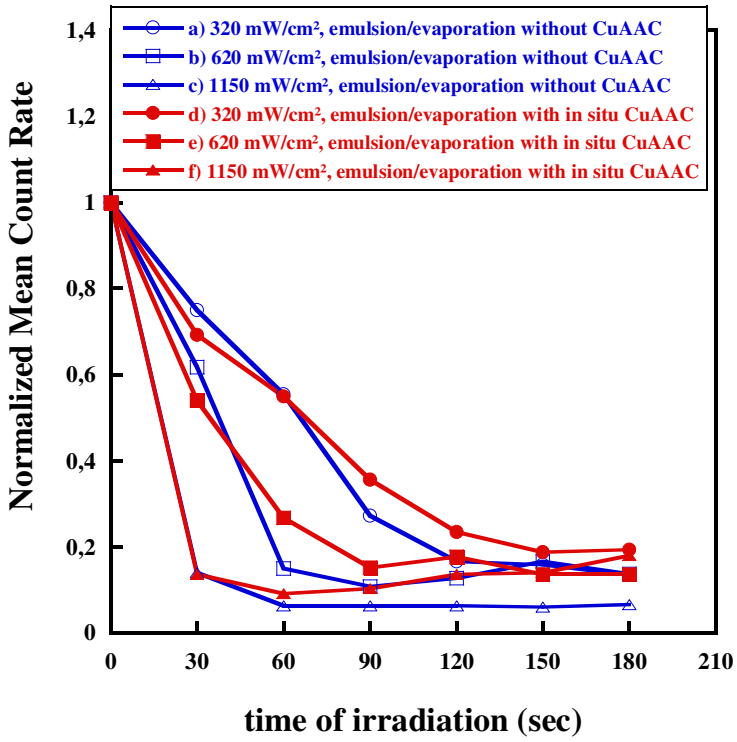

Figure 99. Normalized Mean Count Rate against time of irradiation using different irradiation powers. Open (blue) and solid (red) symbols nanoparticles were prepared via emulsion/evaporation without and with in situ CuAAC, respectively.

If we compare the decreasing of Mean Count Rates for nanoparticles made with or without *in situ* CuAAC, one can conclude that the presence of triazole ring does not prevent the destruction of the nanoparticles under UV-irradiation. Kinetics of degradation appeared close, whatever the presence or not of triazole rings. At higher irradiation time, Mean Count Rate of irradiated clicked nanoparticles seem to be higher than that observed in case of nanoparticles produced without click chemistry. That may be due to the presence of triazole ring. Indeed, carrying out on *in situ* CuAAC leads after irradiation, to produce Dex-g-PAA that may organize in aqueous phase. On other hand, in case of nanoparticles produced without CuAAC, irradiation will lead to a blend of dextran and PAA chains.

In previous pages, we studied the effect of continous UV-irradiation on the destruction of nanoparticles made via nanoprecipitation. In the following lines, we repeated this experiment using nanoparticles prepared by emulsion/evaporation carrying out an *in situ* CuAAC. Initial fluorescence intensity was measured, then sample was irradiated for 30 sec using UV lamp with power 5%, (320 mW/cm²) and corresponding fluorescence intensity was measured. Then, its fluorescence intensity was followed until 50 s, without irradiation. As shown in

Figure 36, the fluorescence intensity decreases after the 30 sec irradiation, then increases while stirring the particles. A new irradiation lead to a decrease of fluorescence intensity. As shown in Figure 36, we observed the partially recover of Nile Red fluorescence. These results are in concordance with these already discussed (Figure 32). Consequently, we can say that nanoparticles prepared by emulsion/solvent evaporation method are highly photosensitive and can be potentially used as photocontrollable nanocarriers to progressively deliver hydrophobic dyes.

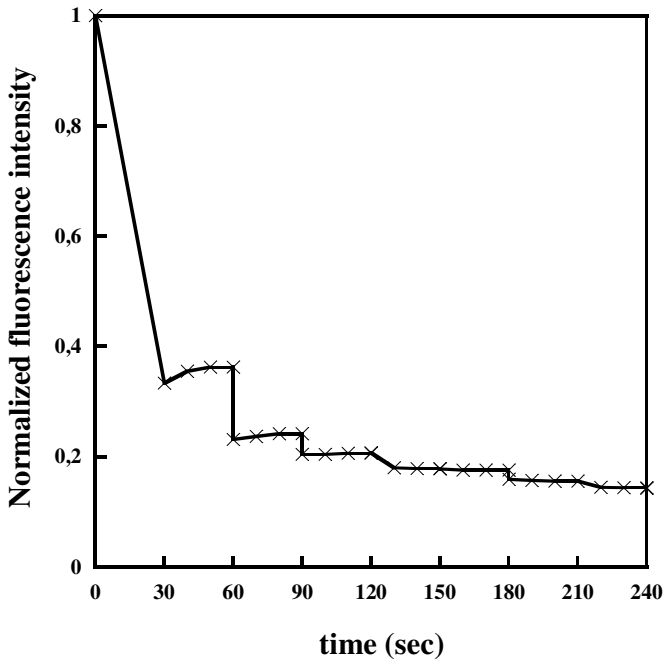

Figure 100. Normalized fluorescence emission intensity against time of irradiation and non-irradiated period. Nanoparticles prepared via emulsion/evaporation with click method (power used 5%, 320 mW/cm²).

VI) What is the future of our smart DDS after injection and irradiation?

From the results we got and described in previous pages, the photolysis products that exist after UV ¯irradiation should be Dex-g-PAA or Dex-g-P(AA-r-NBA) copolymers (in case of grafted Dex-g-PNBA). On one hand, dextran is one biodegradable polysaccharide. Actually dextran is degraded by dextranase and gives low molecular weight sugars [17]. In LCPM, we studied the biodegradation of derivatives from dextran using such dextranase. We found that biodegradation still happens until a critical degree of modification of the dextran chains that depends on the chemistry of the modification. Consequently, we can expect the degradation of Dex-g-PAA too. Elsewhere, Chiv et. al. studied and proved the biodegradation of hydrogels containing dextran and acrylic acid moieties by dextranase in pH 5.6 buffer at 37 °C [18]. On other hand, poly(acrylic acid) is one synthetic biostable polymer, even after injection into the body while it can be degradable in soil for instance [19]. Despite PAA is biostable, several papers have described it as biocompatible [20-22].

VII) Cytotoxicity test

We prepared nanoparticles dispersion (with concentration 25 mg/mL) based on Dex(15)-g-14PNBA$_{3500}$ (F_{PNBA} = 75%) by nanoprecipitation. We prepared 2 dispersions with same concentration in distilled water as medium and in Dulbecco's Modified Eagle's Medium (DMEM) as a medium. DMEM is a widely used basal medium for supporting the growth of many different mammalian cells. DMEM has a high content of glucose, sodium pyruvate and L-glutamine. One dispersion in distilled water and the one in DMEM were irradiated by UV with power lamp equal to 1150 mW/cm² for 6 min with stirring. We sent all these dispersions to Centre de Recherche en Automatique de Nancy (CRAN), University of Lorraine (Prof. Muriel Barberi-Heyob). They diluted our suspension in DMEM to prepare dispersion with final concentration equal to 2, 3 and 5 mg/ml. They put 200 µL of these new suspension over U87 cells line (grade IV human glioblastoma) seeded in a 96 wells plate (density= 6000 cells per well). Samples are tested in sixplicate. They used water-soluble tetrazolium (WST) methods for counting the number of live cells after 48 hrs incubation at 37 °C. As shown in Figure 37, A, all cells are still alive when they are cultivated onto non-irradiated nanoparticles, whatever the dispersion concentration. By this way, we proved that Dex-g-PNBA based nanoparticles are not cyctotoxic. On contrary when cells were cultivated on irradiated dispersion in distilled water, dispersions with higher concentration such as 4 and 5

mg/mL lead to cells death. In case of lower concentration, we still observed high count of cells alive. These death are due to the acidic medium that is produced during the UV-irradiation. Indeed, we measured the acidity of the medium for three samples as shown in Table 6. We found that sample irradiated in distilled water shows an acidic pH value = 3.81. Finally, third experiment concerns irradiated dispersion in DMEM that lead to maintain pH at 7.99 (Table 6). We observed higher count of cells alive at higher concentration than sample of dispersion irradiated in distilled water. According to these results, irradiated Dex-g-PNBA nanoparticles are not cyctotoxic if the irradiation was made under DMEM medium (Figure 37).

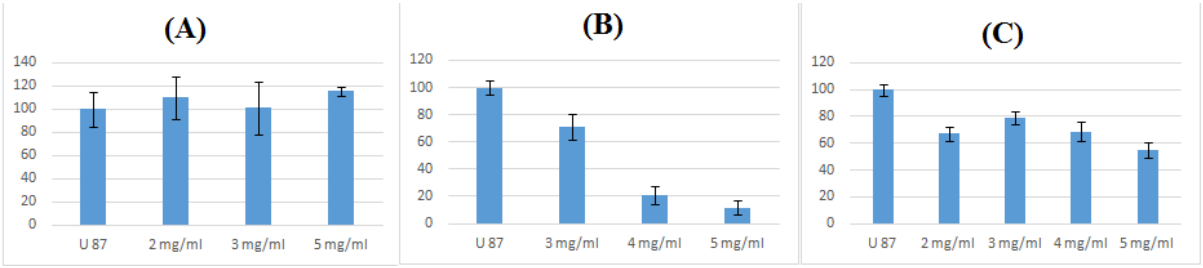

Figure 101. The relation between different concentrations of nanoparticles and count of cells (using WST method) U87 means grade IV human glioblastoma cell line.

Table 24. pH values of dispersion before irradiation in distilled water and after irradiation in distilled water and DMEM as medium.

Dispersion	***pH Value***
UV irradiation(distilled water)	***7.18***
After UV irradiation (distilled water)	***3.81***
After UV irradiation (DMEM)	***7.99***

VIII) Overall conclusions

Nanoparticles based on grafted glycopolymers with high PNBA weight fractions such as Dex(15)-g-14PNBA$_{3500}$ (F_{PNBA} = 75%) and Dex(15)-g-12PNBA$_{9800}$ (F_{PNBA}= 85%) were prepared by nanoprecipitation method. These nanoparticles have good dispersity indexes as estimated from DLS. Another type of nanoparticles were prepared by emulsion/solvent evaporation method using hydrophobic PNBA chains as a core and alkynated dextran as shell. In a first step, surfactant properties of alkynated dextan were proved. In a second step, PNBA with different end functionalities as PNBA-Br and PNBA-N_3 were synthesized. PNBA-N_3 enables us to carry out the click CuAAC reaction *in situ*, during the emulsion/evaporation method. To evaluate the *in situ* CuAAC effect, we carried out emulsion/evaporation with and without *in situ* click chemistry, using different ratios between PNBA-Br/PNBA-N_3. From ^{1}H NMR spectra of nanoparticles, we observed that nanoparticles prepared via emulsion/evaporation with an *in situ* click have a weight of dextran higher than in case of nanoparticles prepared without click. The covalent linkage (triazole ring) between alkyne group on dextran and azide end function of PNBA increases the amount of dextran in nanoparticles. Moreover, this link has another importance on the stability of nanoparticles against anionic surfactant like sodium dodecyl sulfate (SDS). As known from literature, SDS desorbs hydrophilic shell, which is physically adsorbed on hydrophobic polymer core. Actually, we proved that nanoparticles prepared by emulsion/evaporation without click chemistry are unstable under SDS medium and dextran shell was desorbed, while those prepared with *in situ* click were stable. In this latter case, no desorption of dextran shell was observed.

Zeta potential values of prepared nanoparticles were measured and dextran shell thickness were estimated. The stabilities of all the nanoparticles were studied using different ionic strengths and all nanoparticles show stability until 2 mol/L of NaCl in aqueous solution. As these nanoparticles may be used as drug delivery system and as ionic strength of the blood is equal 0.15 mol/L, we can conclude that these nanoparticles will not be destabilized by blood.

The effect of UV-irradiation on all nanoparticles prepared was studied. Firstly, the photolysis of PNBA homopolymer was proved. Then, the photolysis products of Dex-g-PNBA were characterized using different techniques such as ^{1}H NMR and FT-IR spectroscopy, UV-Vis spectroscopy and pH-meter. In agreement with literature, the photolysis products of PNBA parts were poly(acrylic acid) and 2-nitrosobenzaldehyde. Secondly, we followed the effect of UV-irradiation on nanoparticles by following the Mean Count Rate evolution during the

photolysis. Important parameters such as effect of medium composition, mode of UV-irradiation exposure, concentration of sample dispersion and optimum conditions were adapted to obtain the true measurements from DLS. In a parallel way, Nile Red loaded nanoparticles were produced and photolysis of these nanoparticles was studied by following the fluorescence of Nile Red. Whatever the particles, change in the Nile Red environment was proved during the UV-irradiation. More precisely this change occurred before the quantitative photolysis of the PNBA part. Finally, we observed that all nanoparticles based on grafted or diblock glycopolymers and those prepared by emulsion/evaporation method (without and with *in situ* click) are highly photosensitive and can be used as photocontrollable hydrophobic drug delivery systems.

Preliminary results of cytotoxcity test were done at Centre de Recherche en Automatique de Nancy (CRAN), University of Lorraine (Prof. Muriel Barberi-Heyob). Dex-g-PNBA nanoparticles, without irradiation, were no cytotoxic as nanoparticles after irradiation in DMEM. Contrary, cytotoxicity was observed for irradiated nanoparticles in water, due to the high number of acidic functions produced during photolysis of PNBA parts.

References

[1] H. Fessi, F. Puisieux, JP. Devissaguet, N. Ammoury, and S. Benita, Nanocapsule formation by interfacial polymer deposition following solvent displacement, Int. J. Pharm., 55 (1989) 1-4.

[2] C. Gavory, A. Durand, J.-L. Six, C. Nouvel, E. Marie, and M. Leonard, Polysaccharide-covered nanoparticles prepared by nanoprecipitation, Carbohydr. Polym., 84 (2011) 133-140.

[3] M. Laville, J. Babin, I. Londono, M. Legrosa, C. Nouvel, A. Durand, R. Vanderesse, M. Leonard, and J.-L. Six, Polysaccharide-covered nanoparticles with improved shell stability using click-chemistry strategies, Carbohyd. Polym., 93 (2013) 537- 546.

[4] M. G. Carneiro-da-Cunha, M. A. Cerqueira, B. W.S. Souza, J. A. Teixeira, and A.A. Vicente, Influence of concentration, ionic strength and pH on zeta potential and mean hydrodynamic diameter of edible polysaccharide solutions envisaged for multinanolayered films production, Carbohyd. Polym., 85 (2011) 522-528.

[5] W.G. Eversole and W.W. Boardman, The effect of electrostatic forces on electrokinetic potentials, J. Chem. Phys., 9(1941) 798-801.

[6] M. T. Peracchia, C. Vauthier, D. Desmaele, A. Gulik, J.-C. Dedieu, M. Demoy, J. d'Angelo, and P. Couvreur, Pegylated Nanoparticles from a novel methoxypolyethylene glycol cyanoacrylate-hexadecyl cyanoacrylate amphiphilic copolymer, Pharmaceutical Research, 15 (1998) 550-556.

[7] J. O. D. Long and B. Vincent, The equilibrium aspects of weak floculation, J. Colloid Interface Sci., 42(3) (1973) 545-553.

[8] R. A. Lauten, A.-L. Kjøniksen, and B. Nystrom, Adsorption and Desorption of Unmodified and Hydrophobically Modified Ethyl(hydroxyethyl)cellulose on Polystyrene Latex Particles in the Presence of Ionic Surfactants Using dynamic Light Scattering, Langmuir, 16 (2000) 4478-4484.

[9] B. Cattoz, T. Cosgrove, M. Crossman, and S.W. Prescott, Surfactant-Mediated Desorption of Polymer from the Nanoparticle Interface, Langmuir, 28 (2012) 2485Б2492.

[10] H. Zhao, E.S.S., E. Bryan Coughlin, and P. Theato, o-Nitrobenzyl Alcohol Derivatives: Opportunities in Polymer and Materials Science, Macromolecules, 45 (2012) 1723Б1736.

[11] M. G. Cascone, G. Polacco, L. Lazzeri, and N. Barbani, Dextran/Poly(acrylic acid) Mixtures as Miscible Blends, J. Appl. Polym. Sci., 66 (1997) 2089¯2094

[12] B. Grabowsk, M. Bulwan, S. Zapotoczny, and G. Grabowski, Biodegradation of new polymer foundry binders composition of poly(acrylic acid)/dextrin, POLIM., 57 (2012) 529-534.

[13] S. Kavlak, H. K. Can, and A. Guner, Interaction of Poly(maleic anhydride-alt-acrylic acid) with Transition Metal Cations, Ni2, Cu2, and Cd2: A Study by UV¯Vis Spectroscopy and Viscosimetry, J. Appl. Polym. Sci., 92 (2004) 2698 -2705.

[14] L. Dupayage, J.-L. Six, and C. Nouvel, Controlled elaboration of amphiphilic glycopolymers from polysaccharide: synthesis of Dextran-g-PMMA by atom transfer radical polymerization National Institution of Lorraine Polytechnique (INPL) (2009).

[15] G. R. Castro, B. K. Larson, B. Panilaitis, and D.L. Kaplan, Emulsan quantitation by Nile red quenching fluorescence assay, Appl. Microbiol. Biotechnol. , 67 (2005) 767-770.

[16] J. Babin, M. Pelletier, M. Lepage, J.-F. Allard, D. Morris, and Y. Zhao, A New Two-Photon-Sensitive Block Copolymer Nanocarrier, Angew. Chem. Int. Ed. , 48 (2009) 3329 -3332.

[17] FD. Campos, DL. Cassimiro, MS. Crespi, AE. Almeida, and M. Gremiao, Preparation and characterisation of Dextran-70 hydrogel for controlled release of praziquantel, Braz. J. Pharm. Sci., 49 (2013) 75-83.

[18] H.-C. Chiu, A.-T. Wu, and Y.-F. Lin, Synthesis and characterization of acrylic acid-containing dextran hydrogels, Polymer, 42 (2001) 1471-1479.

[19] R. J. Larson, E. A. Bookland, R. T. Williams, K. M. Yocom, D. A. Saucy, M. B. Freeman, and G. Swift, Biodegradation of Acrylic Acid Polymers and Oligomers by Mixed Microbial Communities in Activated Sludge, J. Environ. Polym. Degrad., 5 (1997) 41-48.

[20] L. J. Duan, Y. Liu, J. Kim, and D.J. Chung, Bioinspired and Biocompatible Adhesive Coatings Using Poly(acrylic acid)-Grafted Dopamine, J. Appl. Polym. Sci., 130 (2013) 131-137.

[21] E. S. Yim, B. Zhao, D. Myung, L. C. Kourtis, C. W. Frank, D. Carter, R. L. Smith, and S. B. Goodman, Biocompatibility of poly(ethylene glycol)/poly(acrylic acid) interpenetrating polymer network hydrogel particles in RAW 264.7 macrophage and MG-63 osteoblast cell lines, J. Biomed. Mater. Res. A, 91A (2009) 894-902.

[22] X. Gao, C. He, C. Xiao, X. Zhuang, and X. Chen, Biodegradable pH-responsive polyacrylic acid derivative hydrogels with tunable swelling behavior for oral delivery of insulin, Polymer, 54 (2013) 1786-1793.

CHAPTER (IV)

MATERIALS AND EXPERIMENTAL TECHNIQUES

I. Syntheses

I.1) Materials

Dimethylsulfoxide (ħ 99.7%) was purchased from Aldrich. Tetrahydrofuran (THF), Dichloromethane (DCM), Ethyl acetate (EA) and Petroleum ether were obtained from Store chemistry of Lorraine University and solvents used without further purification.

I.1.a) Synthesis of monomer (2-nitrobenzyl acrylate, NBA):

2-nitrobenzyl alcohol (97%) was supplied by Aldrich and was used without further purification. Acryloyl chloride (> 98%) was obtained from Fluka. Triethylamine (99%) and 4-dimethylaminopyridine (ħ 99%) were purchased from Aldrich.

10 g (65.3 10^{-3}mol) of 2-nitrobenzyl alcohol, 13.2 g (0.1306 mol) of triethylamine and 0.53 g (4.3 10^{-3}mol) of 4-dimethylamino pyridine were dissolved in 70 ml of anhydrous dichloromethane. The reaction medium was stirred in ice bath under nitrogen flow, then 7.09 g (78.4 10^{-3}mol) of acryloyl chloride in 30 ml of anhydrous dichloromethane was added drop wise. After complete addition of acryloyl chloride, we removed ice-bath and left the medium stirring at room temperature. The reaction was followed by thin layer chromatography, then the medium was filtrated (to remove the salt) and washed by using tetrahydrofurane (THF). Purification of monomer was carried out using separator funnel to remove residue of hydrochloride salt. Hydrochloride salt was extracted by solution of (0.065 M) of K_2CO_3 till having a basic medium then by washing with distilled water. Reaction medium was dried over $MgSO_4$ (to remove water residue), then concentrated by rotator evaporator. NBA was purified by using column chromatography (Petrolum ether / Ethyl acetate) (8: 2). Finally, monomer was dried and we got 9.23 g of oily 2-nitrobenzyl acrylate with yield= 69%. NBA must be store in the freezer because it can auto-polymerize at room temperature or in fridge, as we checked using SEC (Figure 1). Indeed SEC confirmed that free homopolymer was formed during storage even in fridge or purification of monomer.

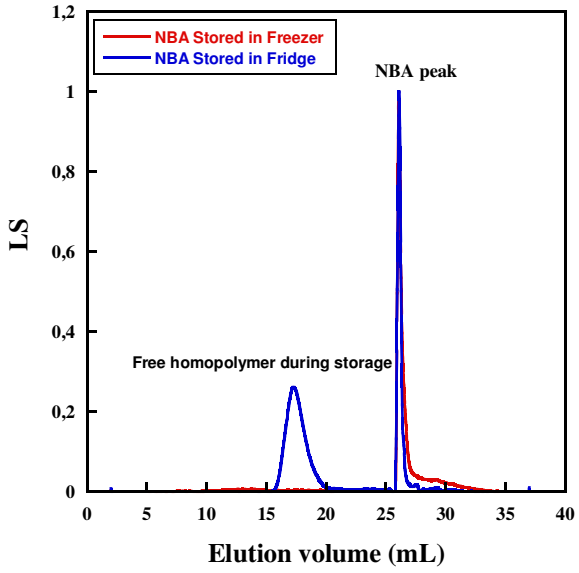

Figure 102. SEC chromatograms (LS detector) of NBA storage in Fridge (blue) and in Freezer (red)

Pure monomer was analyzed by ^{1}H NMR spectroscopy (Figure 2).

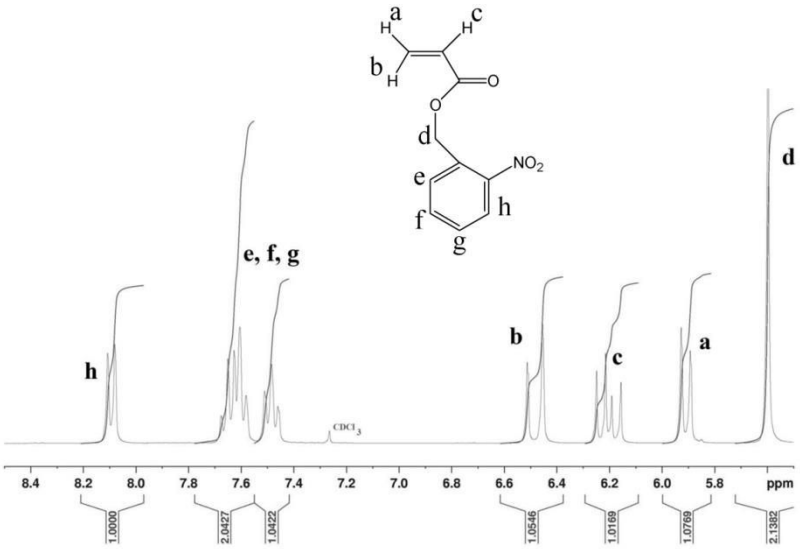

Figure 103. ^{1}H NMR spectrum of o-nitrobenzyl acrylate in $CDCl_3$

I.1.b) Synthesis of ligand Tris(2-(dimethylamino)ethyl)amine (Me_6TREN)

Tris(2-(dimethylamino)ethyl)amine (96%), Formaldehyde solution (36.5˜38.0% wt), Formic acid solution (49˜51% wt) and HCl 36.5-38.0 % were purchased from Aldrich.

Firstly, tris(2-aminoethyl) amine (TREN) (0.452 mol, 6.8 ml) in 85 ml of methanol were added dropwise into 50 ml of HCl in methanol (3 M). After that, the medium was left stirring in room temperature for 1 hr then filtrated, washed by methanol and dryied in vacuum oven overnight (weight powder with Y% = 97 %). Secondly, we dissolved 11.2424 g (0.044 mol) of TREN.HCl in 16.7 ml distilled water and added (2.22 mol) 83.6 ml of formic acid and (2.09 mol) 76.9 ml of formaldehyde. Solution was stirred for 6 hrs under reflux at 120 °C, then was stopped and neutralized using NaOH pellets (test by pH paper). Me_6TREN was extracted by dichloromethane, then dichloromethane was evaporated and pure Me_6TREN was collected by vacuum distillation at 79 °C. Pure Me_6TREN was confirmed by ^{1}H NMR spectroscopy (Figure 3).

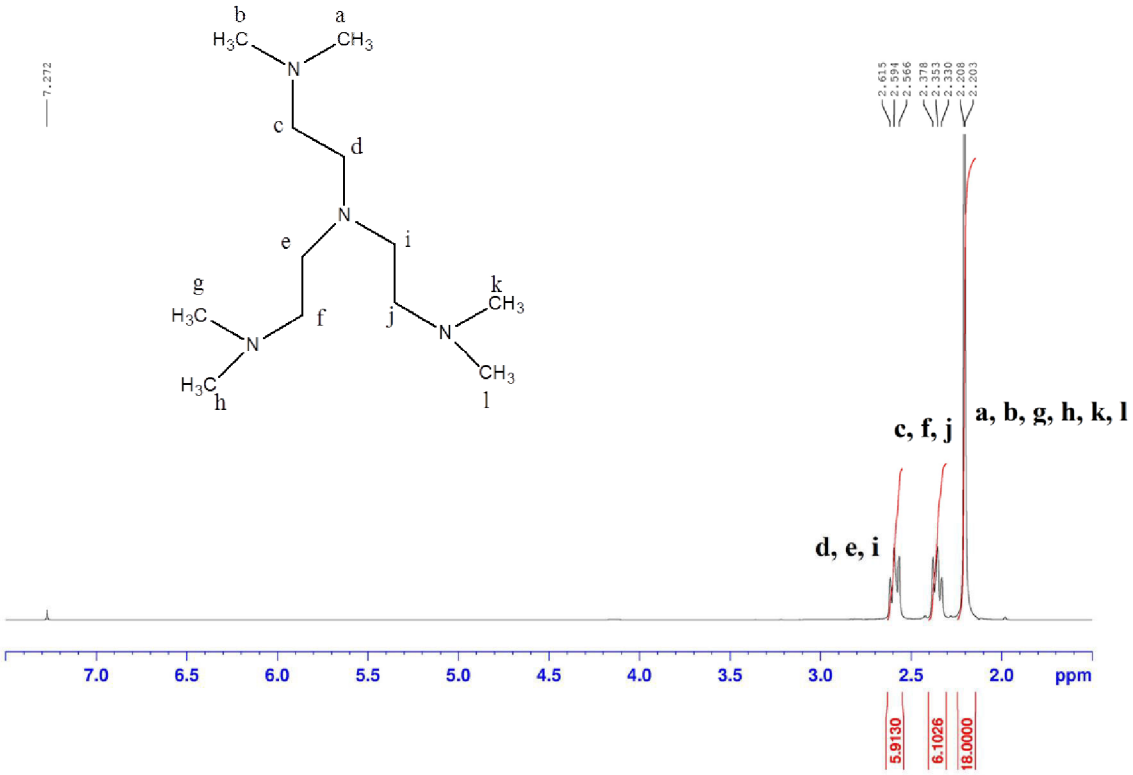

Figure 104. ^{1}H NMR spectrum of Me_6TREN in $CDCl_3$

I.2) Poly(o-nitrobenzyl acrylate)(PNBA)

I.2.a) Homopolymerization by SET-LRP

Surface of Cu(0) wire (0.25 mm = 30 gauge, according to American Wire Gauge (AWG)) was polished. Then Cu(0) was immersed in concentrated H_2SO_4 (Aldrich, 95-98%) for 20 min, washed with ethanol and finally dried. Ethyl 2-bromoisobutyrate (EBiB) (99%) was

purchased from Aldrich and was dried on CaH_2 overnight before vacuum distillation at 70 °C. Sodium azide (ħ99.5%) and Cu(II)Br_2 (99%) were obtained from Sigma-Aldrich.

Schlenk tube was evacuated and filled by nitrogen. NBA (26, 100 or 200 equiv per initiator EBiB), EBiB (1 equiv), Me_6TREN (1-x equiv), $CuBr_2$/Me_6TREN solution in DMSO (x equiv of $CuBr_2$ and of Me_6TREN) and 1 mL of DMSO per 1 gram of NBA were successively added under N_2 flow. Consequently, at the end, 1 equivalent of Me_6TREN has to be taken in consideration. Then, medium was purged with N_2 gas for 10 min. Metallic Cu(0) wire (for instance length 1.7 cm per gram of NBA) was added under nitrogen to initiate the polymerization at 20 °C. Samples were withdrawn under nitrogen atmosphere from the polymerization mixture at various time intervals and quenched by cooling with liquid nitrogen. One part of each sample was used to determine the monomer conversion from ^{1}H NMR spectrum in $CDCl_3$. Conversion was estimated by comparing the peaks areas of the aromatic protons of both the monomer NBA and the polymer PNBA (7.3¯8.2 ppm, A_{ar}) with those of the ethylenic protons of the monomer (5.9, 6.2, and 6.3 ppm, $A_{a,b,c}$) according to equation (1). The other part of the sample was diluted using THF and was precipitated then analyzed by SEC¯MALLS to determine the $M_{n(SEC)}$ and dispersity. M_n was also estimated from ^{1}H NMR($M_{n(NMR)}$) taking into account areas of peaks from 0.9 to 1.2 ppm (A_{CH3}) and the methylene benzylic protons peak (A_{CH2}) centered at 5.4 ppm according equation (3).

$$Conv = 1 - \left[\frac{A_{a,b,c} \times 4}{A_{ar} \times 3}\right] \qquad \text{equation (1)}$$

Conversion can also be estimated according equation (2)

$$Conv = \frac{A_{CH2}\,(PNBA)}{A_{CH2}\,(PNBA) + A_{CH2}\,(NBA)} \qquad \text{equation (2)}$$

Where A_{CH2} (PNBA) and A_{CH2} (NBA) are areas of methylene benzylic protons in PNBA (centered at 5.3 ppm) and in NBA (5.6 ppm), respectively.

$$M_{n\,NMR} = 207 \times \left[\frac{A_{CH2\ benz}}{2} \times \frac{9}{A_{3CH3}}\right] \qquad \text{equation (3)}$$

I.2.b) Modification of PNBA-Br by using NaN_3

Bromide end-function of PNBA-Br that is prepared via SET-LRP, was replaced by azide group by using 5 equiv of NaN_3 in DMSO at room temperature, as shown in Scheme 1. The reaction was left in dark place for 24 hrs because photolysis PNBA can be occurred by visible or sun light. The reaction medium was precipitated twice from cold methanol and filtrated. PNBA-N_3 was dried using vacuum oven. 1.0 g of pure PNBA-N_3 was obtained (Yield = 68 %)

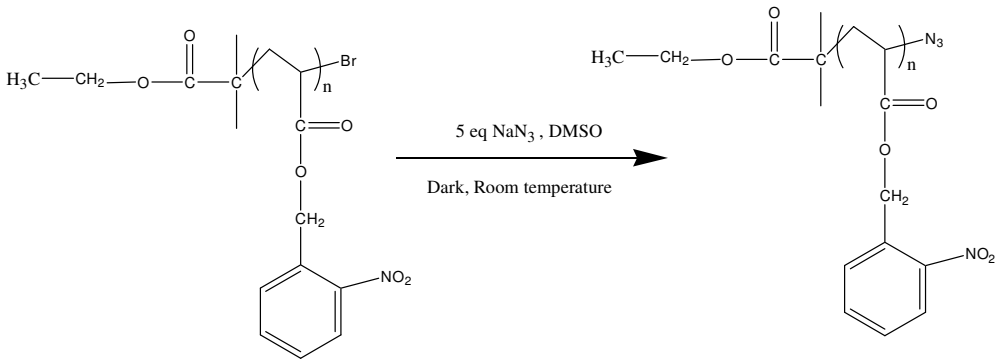

Scheme 1. Modification of PNBA-Br by using NaN_3

From ^{1}H NMR spectrum, we observed that the peak of CH-Br at 4.35 ppm was disappeared and CH-N_3 interfered with peak of CH_2 of initiator (Figure 4). From ^{1}H NMR, we observed that there is no peak at 4.9 ppm, which is characteristic of methylene group in benzyl alcohol. This proves that nucleophilic substitution reaction didn't occur. SEC traces confirm also there is no degradation of PNBA during this substitution (Figure 5).

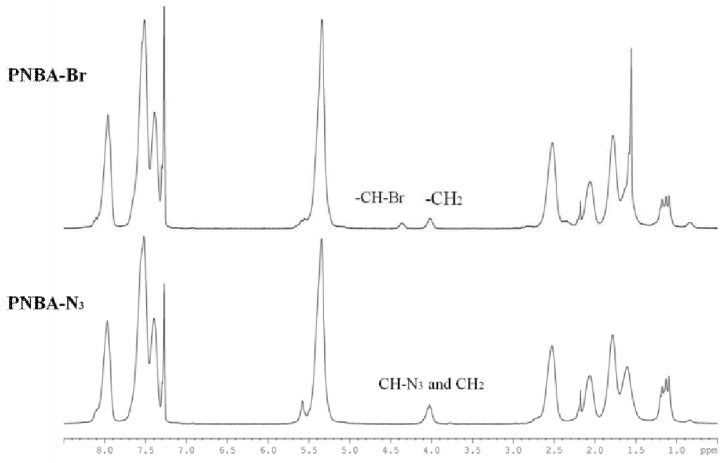

Figure 105. ^{1}H NMR spectra of PNBA-Br and PNBA-N_3

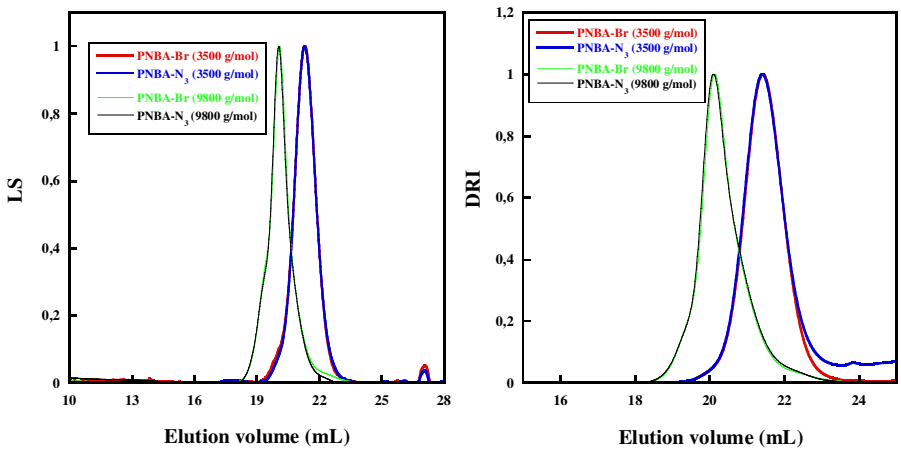

Figure 106. SEC chromatograms of PNBA-Br and PNBA-N_3 with = 3500 and 9800 g/mol. (LS and DRI detectors)

I.3) Modification of dextran

Dextran T_{40} and T10 were purchased from Pharmacia Biotech (= 34 620 g/mol and Đ = 1,10; = 8800 g/mol and Đ = 1.20, respectively. They were characterized using size exclusion chromatography coupled to multi-angle laser light scattering (SEC-MALLS) performed at room temperature using DMSO/ 0.1 M $NaNO_3$ solution as eluent. 5-hexynoic acid and 1, 1'-carbonyldiimidazole were purchased from Aldrich. Propagylamine (≥99%) and sodium cyanborohydride (95%) were obtained from Aldrich.

I.3.a) Modification of dextran (T40). Synthesis of alkynated dextran

Dextran T40 (= 34,620 g/mol, =1.26) was modified to introduce alkyne groups using activated hex-5-ynoic acid. Modification of dextran was made through two steps: a) Activation of hex-5-ynoic acid, b) Partial esterfication between activated 5-hexynoic acid and dextran.

I.3.a.1) Activation of hex-5-ynoic acid

(53.508 10^{-3}mol) of 1,1'-carbonyldiimidazole was suspended in 40 ml of dichloromethane under stirring at 37 °C. 5 g (44.59 10^{-3}mol) of hex-5-ynoic acid in10 ml of dichloromethane was added to the solution drop by drop under nitrogen. The reaction was followed by thin layer chromatography using (ethylacetate/petroleum ether, 6/4, v/v) and methoxypropyl acetate as eluents. The reaction was stopped after 2 hrs and crude product was washed using 50 ml of distilled water, then washed by dichloromethane. Finally, product was dried over

anhydrous $MgSO_4$. 6.45 g of pure activated hex-5-ynoic acid was obtained and the yield of reaction = 96%.

I.3.a.2) Partial esterfication of dextran by activated hex-5-ynoic acid

Dextran (59.94 10^{-3}mol of glucosidic units) was dried overnight at 100 °C. Dried dextran was dissolved in 97 ml of distilled DMSO with vigorous stirring at 60 °C. 0.15 eq (8.991 10^{-3}mol) of activated 5-hexynoic acid was added after complete dissolution of dextran. The reaction was left stirring at 60 °C for 2.5 days. Crude product was precipitated in 1.5 L ethanol and filterated. Then, product was washed by vigorous stirring in ethanol for 30 min. Finally, modified dextran was dried and we obtained 10.61 g of alkynated dextran with yield of substitution equal to 15%. Yield of substitution was calculated from ^{1}H NMR from peak area of anomeric proton (A_1) and that of the areas of 4 protons of alkyl chains (from 1.5 to 2.4 ppm) according to equation 4.

$$\text{Substitution Yield } (\ ) = \frac{\square_8 + \square_9}{4} \times \frac{100}{\square_1} \qquad \text{equation (4)}$$

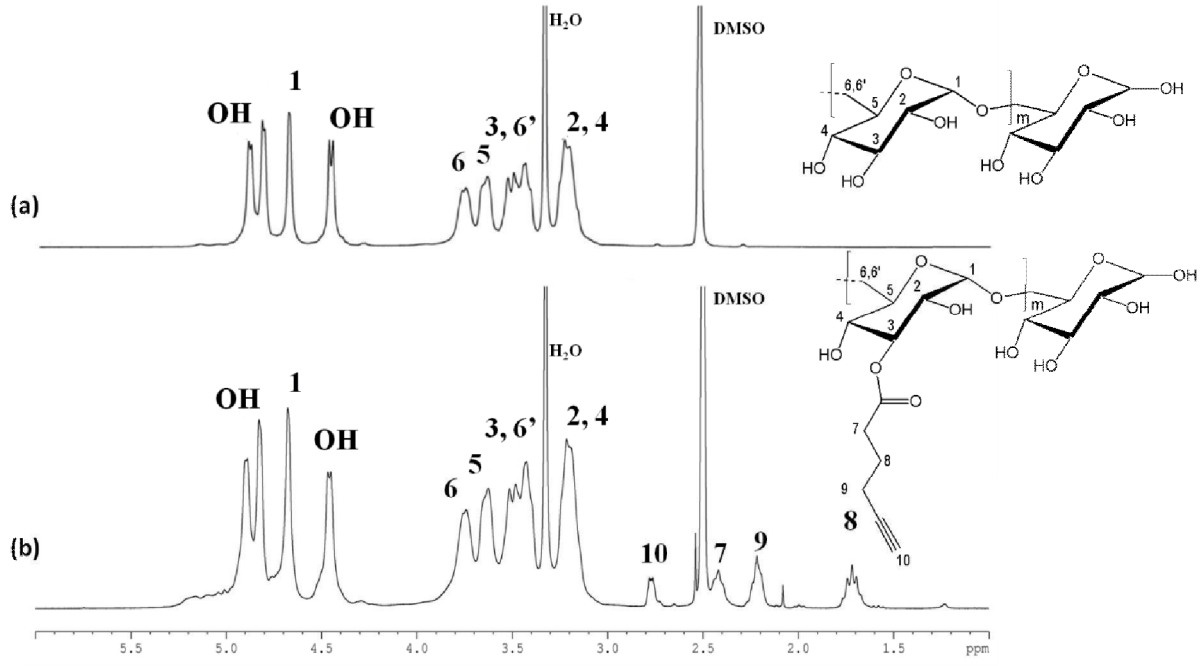

Figure 107. ^{1}H NMR Spectra of (a) native dextran and (b) alkynated dextran.

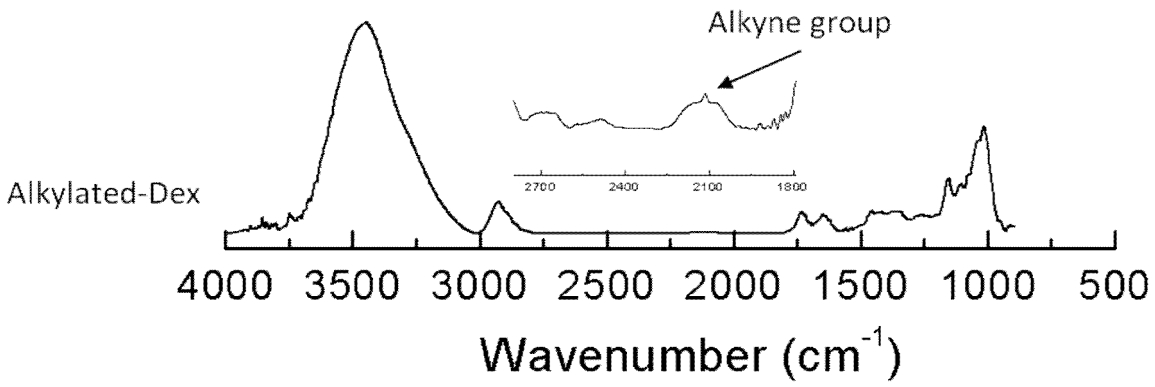

Figure 108. FT-IR chart of alkynated dextran

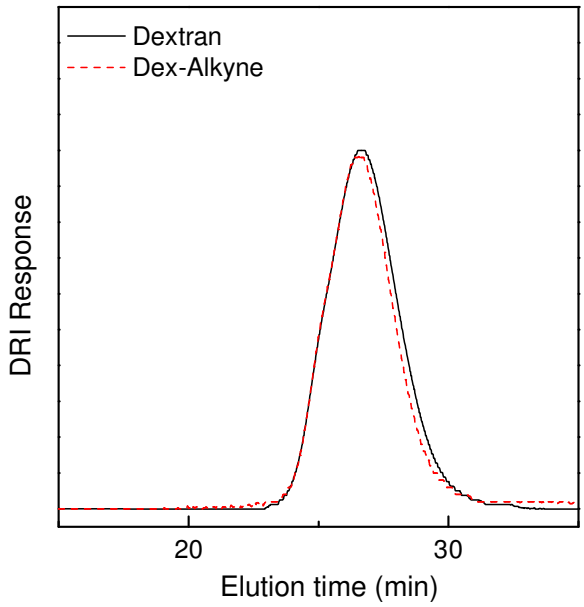

Figure 109. DRI chromatogram of native dextran and alkynated dextran

I.3.a.3) Measurement of surface tension of alkynated dextran

We measured surface tension for water solution of alkynated dextran. Firstly we prepared different solutions with different concentrations. We poured the solutions onto vessel and left it stabilize overnight to reach equilibrium. Used vessel must be carfully cleaned because surface tension of liquid was affected by dust or impurities. So we washed them using water and acetone and dried well. After equilibrium, we measured the value of surface tension using `Du Noüy Ring method_. For very low concentrations (10^{-6} till 10^{-4} mg/ml) we observed same value of pure water which equal to 71.6 (our measuring). Surface tension started to decrease when using solution at 10^{-3} mg/ml. As shown in Figure 9, minimum plateau value

was not observed. Previous procedures were repeated with unmodified dextran. In this case, we observed that surface tension values of different concentration of dextran were the same because dextran is a hydrophilic compound and is completely soluble in water. (Figure 9)

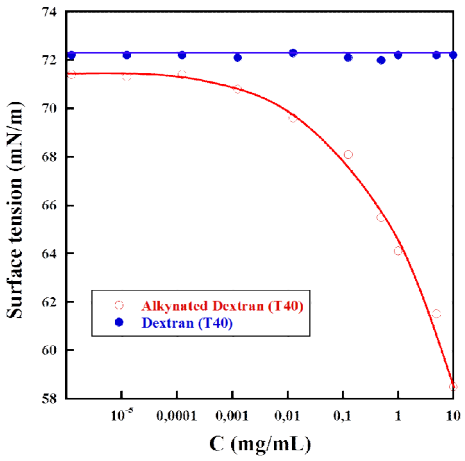

Figure 110. Surface tension against concentration. Case of native dextran and alkynated dextran (= 15%) dissolved in water phase.

I.3.b) End-chain modification of dextran (T10). Synthesis of -alkyne dextran

Dextran T10 (3g, 0.454 10^{-3}mol of chains) was dissolved in 2% (w/v) acetate buffer (to adjust pH of medium to 5) at 50 °C. Propagylamine (2.5g, 54.4 10^{-3}mol) and sodium cyanoborohydride (2.85 g, 45.4 10^{-3}mol) were added under stirring. The mixture was stirred at 50 °C for 96 h with daily addition of 25 equivalents per chain of sodium cyanoborohydride. Solution medium was concentrated by rotator evaporator and dialyzed against milli-Q water for 4 days to remove salts. Then product was lyophilized and we obtained pure 2.25 g of -alkyne dextran. Pure and dried -alkyne dextran was analyzed using ^{1}H NMR, FT-IR and Size Exclusion Chromatography. As shown in Figure 10, ^{1}H NMR spectrum of native dextran exhibits two peaks characteristic of H and H$_{\beta}$ protons from the 2 stereoisomers of closed glucopyranosic end unit. On ^{1}H NMR spectrum of -alkyne dextran, these protons peaks were disappeared.

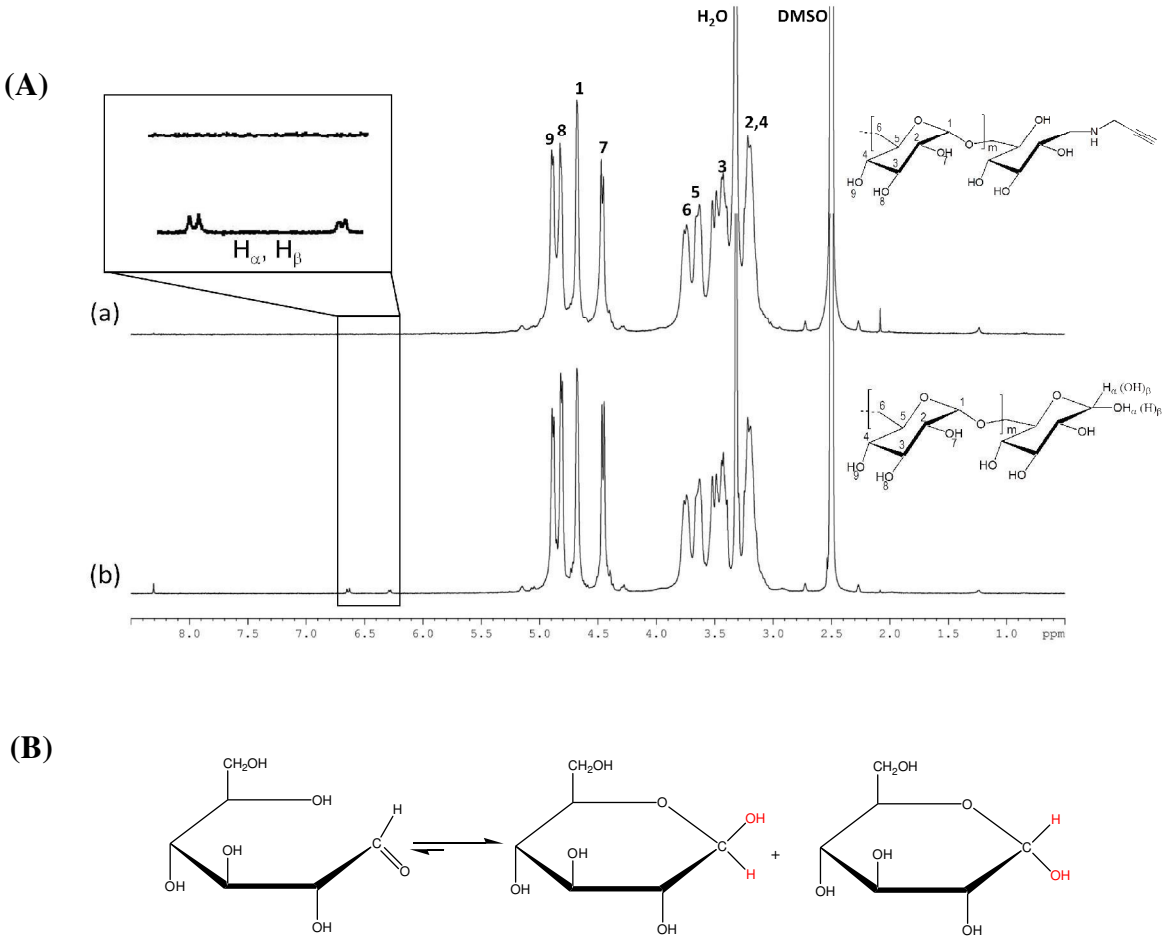

Figure 111. (A) ^{1}H NMR spectra of (a) native dextran and (b) -alkyne dextran. (B) equilibrium between open and closed form of glucopyranosic end unit

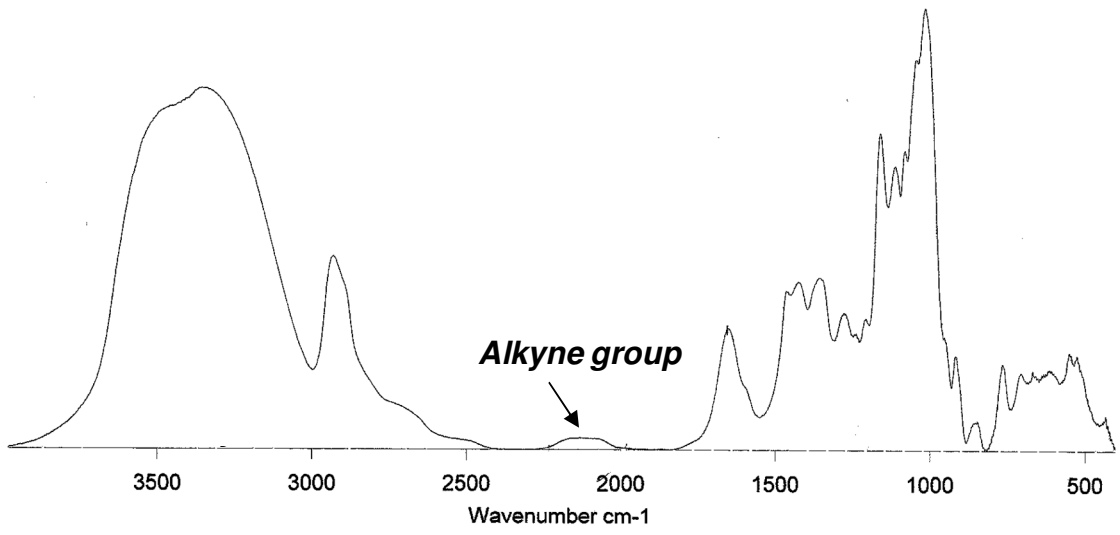

Figure 112. FT-IR chart of -alkyne dextran

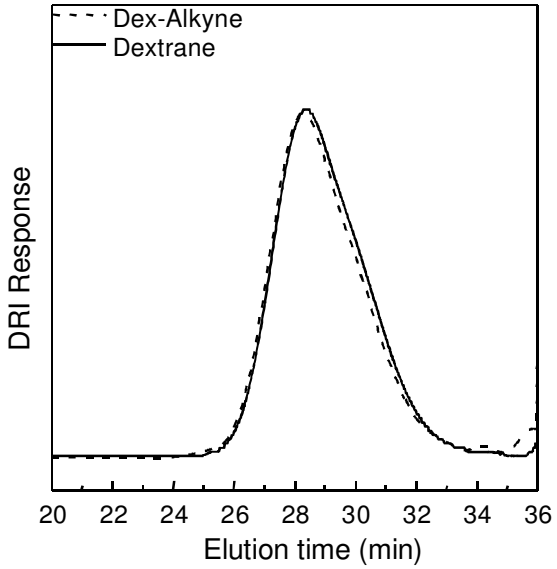

Figure 113. DRI chromatogram of native and -alkyne dextran

I.4) Click chemistry

Cu(I)Br (99.999%) was purchased from Sigma-Aldrich.

PNBA-N_3 and alkynated dextran (T40 or T10) were dissolved in DMSO and the ratio between Azide/alkyne was adjusted. Then, solution was purged by N_2 for 10 min and Cu(I)Br and Cu(0) powder were added under N_2 with 1 equiv and 0.1 equiv per mole of alkyne, respectively. The reaction was left for 48 hrs in dark place, then the medium was precipitated from cold EDTA solution (5 eq EDTA per Cu mol) to remove Cu salts. The solution was precipitated using syringe filter to remove Cu(0). Powder was dried using vacuum oven. Diblock glycopolymers were dialyzed against milli-Q water for 7 days, then washed with a mixture of acetone/diethyl ether (8/2, v/v) to remove unreacted -alkyne dextran and PNBA-N_3, respectively. In case of grafted glycopolymers, we used only acetone/diethyl ether washing. Finally, pure amphiphilic copolymer was characterized by ^{1}H and ^{13}C NMR and FT-IR spectroscopy, Size Exclusion Chromatography (SEC). As shown in Figure 13 and 14, ^{1}H spectra of grafted and diblock glycopolymers with different weight fractions of PNBA. Their spectra show the increasing of peaks characteristics of PNBA with increasing its weight fraction in glycopolymer.

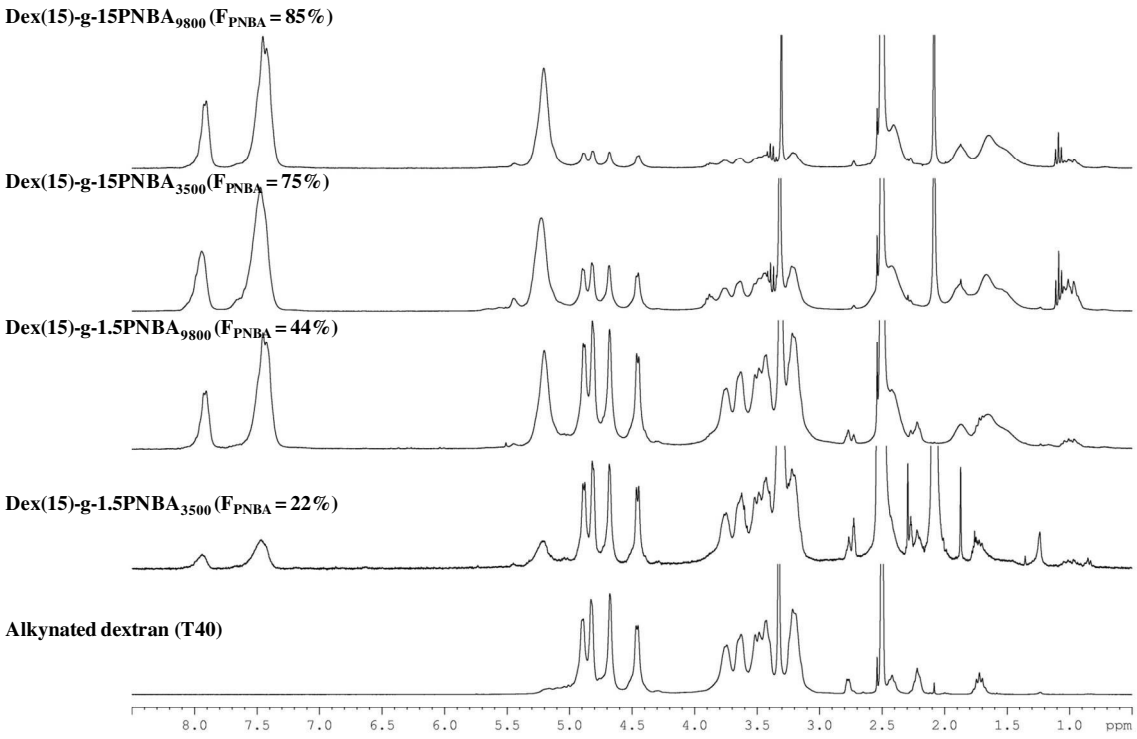

Figure 114. ^{1}H NMR spectra of grafted glycopolymers and alkynated dextran (T40)

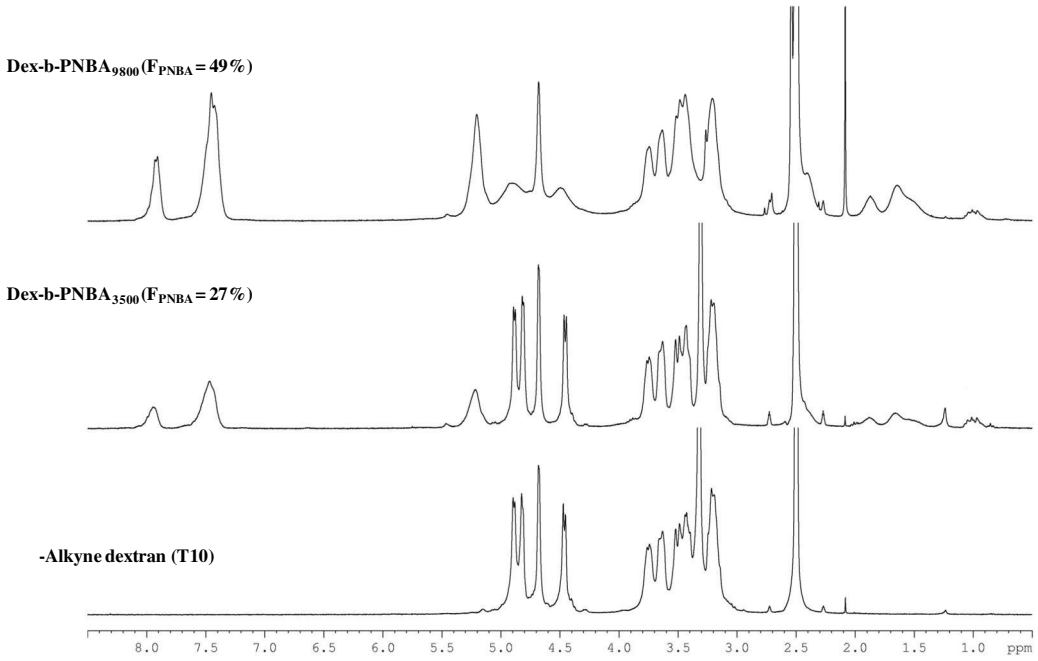

Figure 115. ^{1}H NMR spectra of diblock glycopolymers and -alkyne dextran

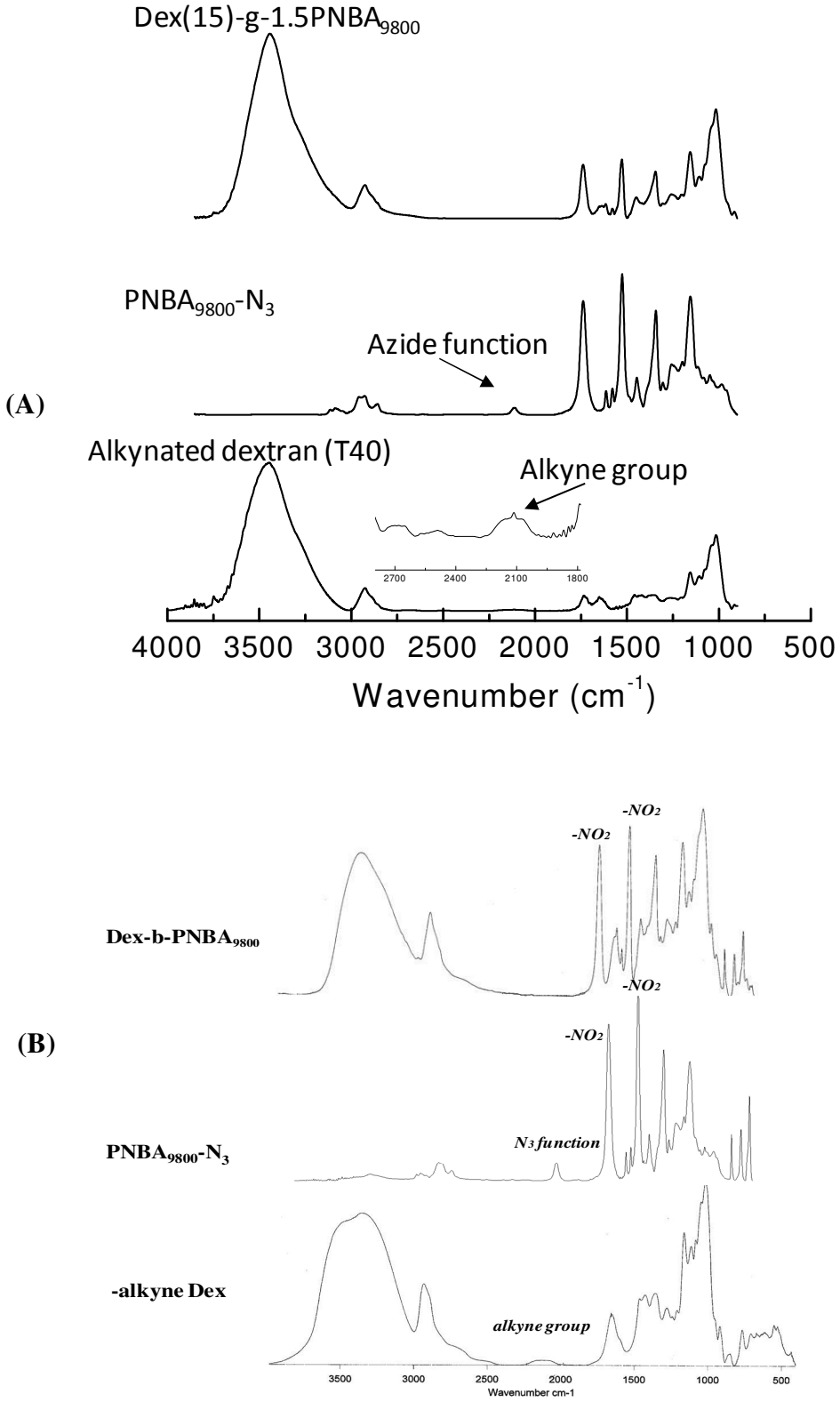

Figure 116. FT-IR charts of (A) PNBA-N_3, alkynated dextran (T40) and grafted copolymer and (B) -alkyne dextran (T10) and diblock glycopolymer.

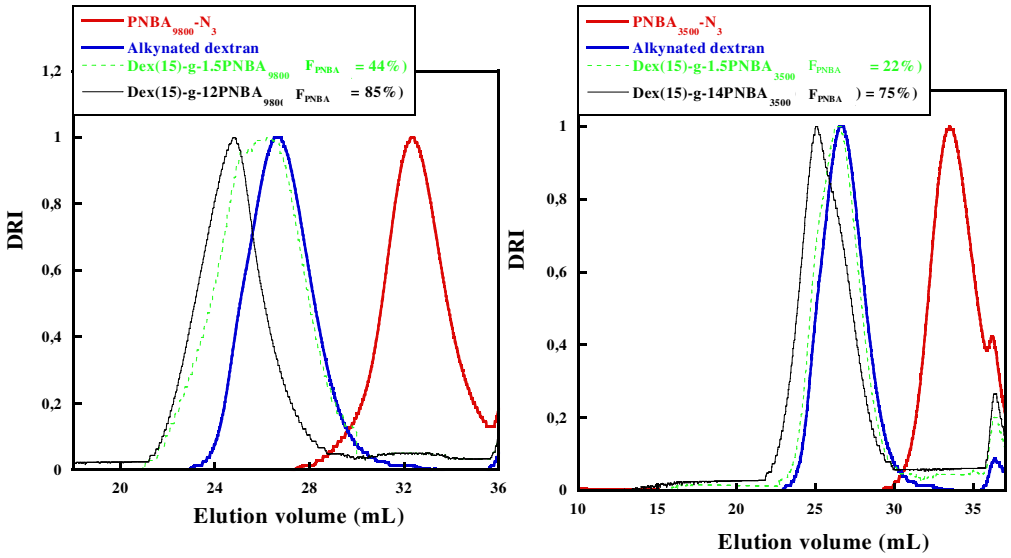

Figure 117. DRI chromatograms PNBAN_3, alkynated dextran and grafted glycopolymers

II. Methods of nanoparticles formation

Nile Red dye (>98 %) was purchased from Aldrich.

II.1) Nanoprecipitation method

To prepare dispersion of nanoparticles loaded by Nile Red we used 3 steps

(a) 25 mg of grafted glycopolymer (F_{PNBA} = 75 and 85%) were dissolved in 5 ml of mixture (THF/H_2O, (95/5) v/v).

(b) We prepared solution of Nile Red dye in THF with concentration 5 mg/ml. Then 10 µl of Nile Red solution was added to solution of glycopolymer.

(c) Organic solution was nanoprecipitated from 10 ml of distilled water (without surfactant) using micropipette by rate of addition 0.1 ml per min, with moderate stirring. The needle of syringe was immersed in H_2O as shown in Figure 17.

After complete addition, 10 ml of distilled water was added portion wise to freeze the nanoparticles dispersion. Finally, THF was removed using centrifuge, because removing of THF via evaporation leads to aggregate. Nanoparticles were washed two times by distilled water using (centrifugation: 15 000 tr/min at 15 °C for 30 min). After 2 times washing, nanoparticles were dissolved in 20 ml of distilled water and Z-average diameter was measured using Dynamic Light Scattering.

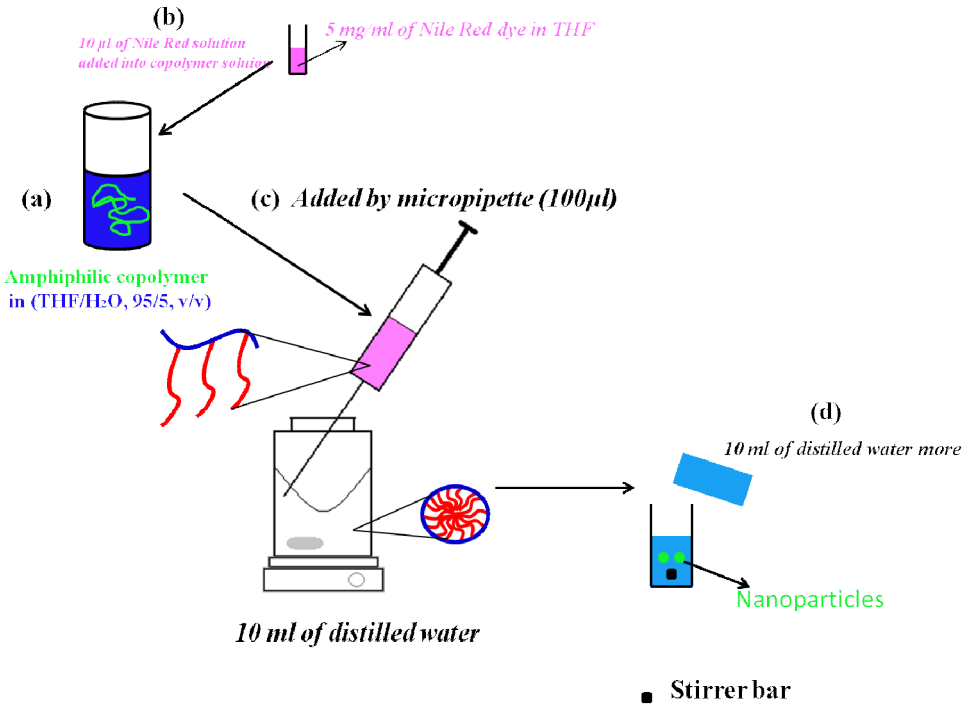

Figure 118. Nanoprecipitation method

II.2) Emulsion/Solvent Evaporation without and with CuAAC click chemistry

We dissolved 25 mg of PNBA-N_3 in 1 ml of dichloromethane. 50 mg of alkynated dextran (T40) were dissolved in 10 ml of distilled water. We saturated this solution with DCM by washing two times. Solution was purged by N_2 for 30 min. Then, we added organic solution to aqueous phase and we added 6 mg ($4.26X10^{-5}$ mol equivalent per alkyne) of CuBr under N_2 flow. Then, both phases were pre-emulsified using vortex for 40 sec under N_2. Some procedures were done without adding CuBr and without N_2 purge when the emulsion/solvent evaporation was carried out without CuAAC. Nanoemulsification of solution was realized using ultrasound (power = 46 W, percent cycle active = 50% for 2 min). After sonication, dichloromethane was completely evaporated using shaker oven for 2h30 min at 37 °C. After that, when in situ CuAAC occurred, we added EDTA (5 eq: 1 eq CuBr) to the dispersion and left stirring for 24 hr at room temperature. Finally, nanoparticles were collected using centrifugation for 1 hr with speed 10 000 tr/min at 15 °C. Nanoparticles were dispersed in water again using ultrasound for approximately 15 min. Nanoparticles were washed two times with distilled water, then were dispersed in 10 ml of distilled water. Prepared nanoparticles dispersion was characterized using dynamic light scattering. Nanoparticles dispersion was lyophilized for 24 hr, then dried nanoparticles were analyzed by ^1H NMR spectroscopy in

DMSO-d_6. Unfortunately and as already written, triazole ring proton peak cannot be observed as shown in Figure 18.

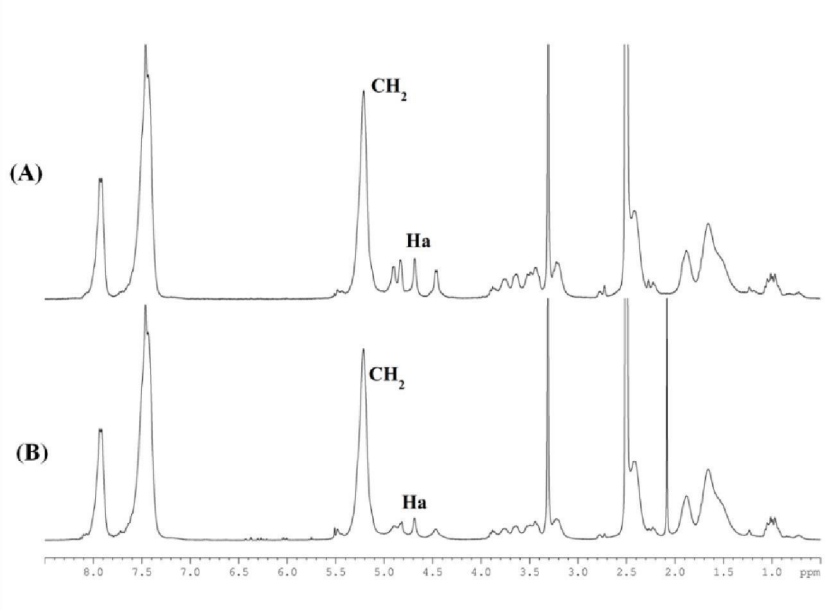

Figure 119. ^{1}H NMR spectra of nanoparticles prepared by emulsion/evaporation (A) with CuAAC and (B) without CuAAC.

III) Instruments

III.1) Nuclear Magnatic Resonance spectroscopy:

We used ^{1}H, ^{13}C and 2D DOSY ^{1}H NMR spectroscopies to elucidate structures of the products. NMR spectra were recorded on a Bruker Avance 300 apparatus (300, 13 MHz, 25 °C) in $CDCl_3$ or DMSO-d_6 depending on products solubility. We adjusted the concentration of all products equal to 10 mg/ml.

III.2) Size Exclusion Chromatography

The principle of size exclusion chromatography is to separate the molecules depending on their hydrodynamic volume. Solution was passed through column and consequently larger molecules were eluted firstly, while small molecules remain in the pores of column and then eluted. This technique enables us to determine number average molecular weight ($\overline{M}_n$) of prepared polymers and their dispersity (Đ). The values of (dn/dC) of all polymers were determined using differential refractometer.

We used in our study two modules of SEC, because we have samples soluble in DMSO/0.1 M $NaNO_3$ or in THF.

III.2.a) ***SEC used for polymer soluble in THF:***

Size exclusion chromatography coupled to multi-angle laser light scattering (SEC-MALLS) was performed at room temperature using a Merck HPLC pump (L-6200A) equipped with a degazer, three PLgel 5 lm columns [100 A °, 300 9 7.5 mm; 1000 A °, 300 9 7.5 mm and guard columns, 50 9 7.5 mm (Polymer laboratories)]. Two detectors were used online: a Multi-Angle Light Scattering detector (MALLS) and differential refractometry (Merck RI-71). SEC was performed at 40 ^{o}C and using Tetrahydrofurane (THF) as eluent (1.00 ml/min). dn/dC of PNBA depends on its average molar mass where $PNBA_{3500}$ and $PNBA_{9800}$ equal to 0.137 and 0.152.

III. 2.b) ***SEC used for polymer soluble in DMSO***

Size exclusion chromatography consists of Multi Angle Laser Light Scattering detector (MALLS - Mini Dawn Treos, Wyatt), a differential refractometer detector (RID - 10A, Shimadzu), a UV detector (SPD - 20A, Shimadzu), a HPLC pump (LC - 20AD, Shimadzu), a degazer (DGU - 20A3R, Shimadzu) and three PLgel 5 ≋ (105 A°, 103 A° and 100 A°) columns (300mm x 7.5mm). In case of DMSO, SEC were performed at 70 °C with elution rate 0.7 mL/min.

III.3) Fourier Transform InfraRed spectroscopy (FT-IR)

FT-IR spectra were recorded on Infra Red-Spectrophotometer (Tensor 27, Brucker Optics), which is equipped with a light source emitting wavelengths in the infrared and a detector DLaTGS kind. Approximately 4 mg of dried sample was blended with 200 mg of dry KBr (IR grade) and about 100 mg of the mixture was used to prepare as a pellet.

III.4) Surface tension

We used `Du Noüy Ring method_ to measure surface tension of aqueous solution with different concentration of polymer. This method established by slowly raising platinum ring from liquid and determined the related forces.

We prepared aqueous solutions with different concentrations (2, 1, 0.5, 0.25, 0.125, 0.0125, 0.00125, 0.000125, 0.0000125 and 0.00000125 mg/ml). We poured the solutions into very

clean and dried vessel, because dust or impurities affect on surface tension of liquid. So we washed them using water and acetone and dried well. We left solutions overnight to stabilize and reach equilibrium. After overnight, surface tension measurements were performed using an automatic tensiometer `Dyne Easy Kruss_. The solution is maintained at 25 ° C in a bath thermostatically during measuring.

III.5) Differential Scanning Calorimetry

Glass transition temperature of grafted and diblock glycopolymers prepared were measured using Q2000 V24.1.0 Build 122 MDSC from T.A. instruments.

Glass transition temperatures of $PNBA_{3500}$ and $PNBA_{9800}$ were measured using DSC and we found Tg were equal to 28 and 37 °C, respectively (Figure 19)

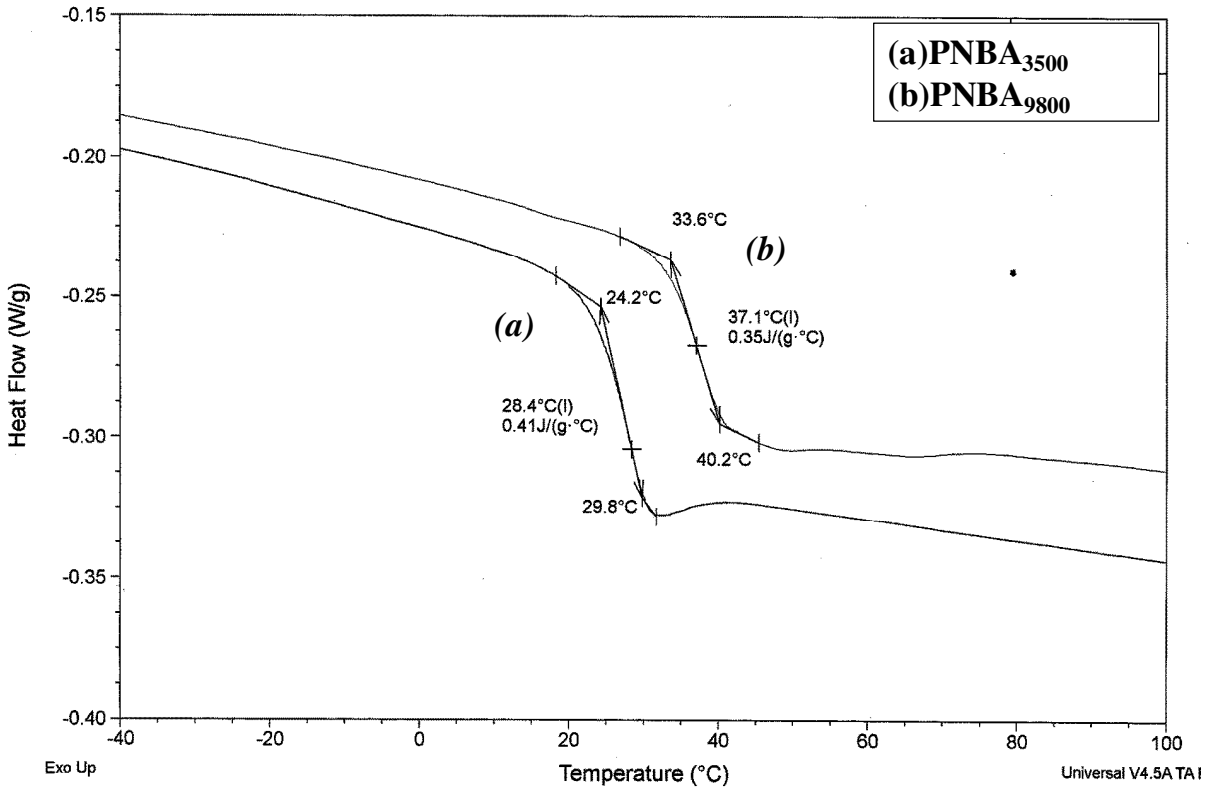

Figure 19. Thermograms DSC of $PNBAN_3$ (3500 g/mol) and $PNBAN_3$ (9800 g/mol)

We used modulated DSC (MDSC) for measuring glass transition temperatures of grafted and diblock glycopolymers. MDSC has advantage than traditional DSC, as MDSC is more

sensitive for low weight of sample and by using low weight that enables us to get on better resolution. As shown in Figure 20, each diblock glycopolymers shows one glass transition temperature (Tg) of Dex-b-PNBA$_{3500}$ with (F_{PNBA} = 27%) and Dex-b-PNBA$_{9800}$ with (F_{PNBA} = 49%).

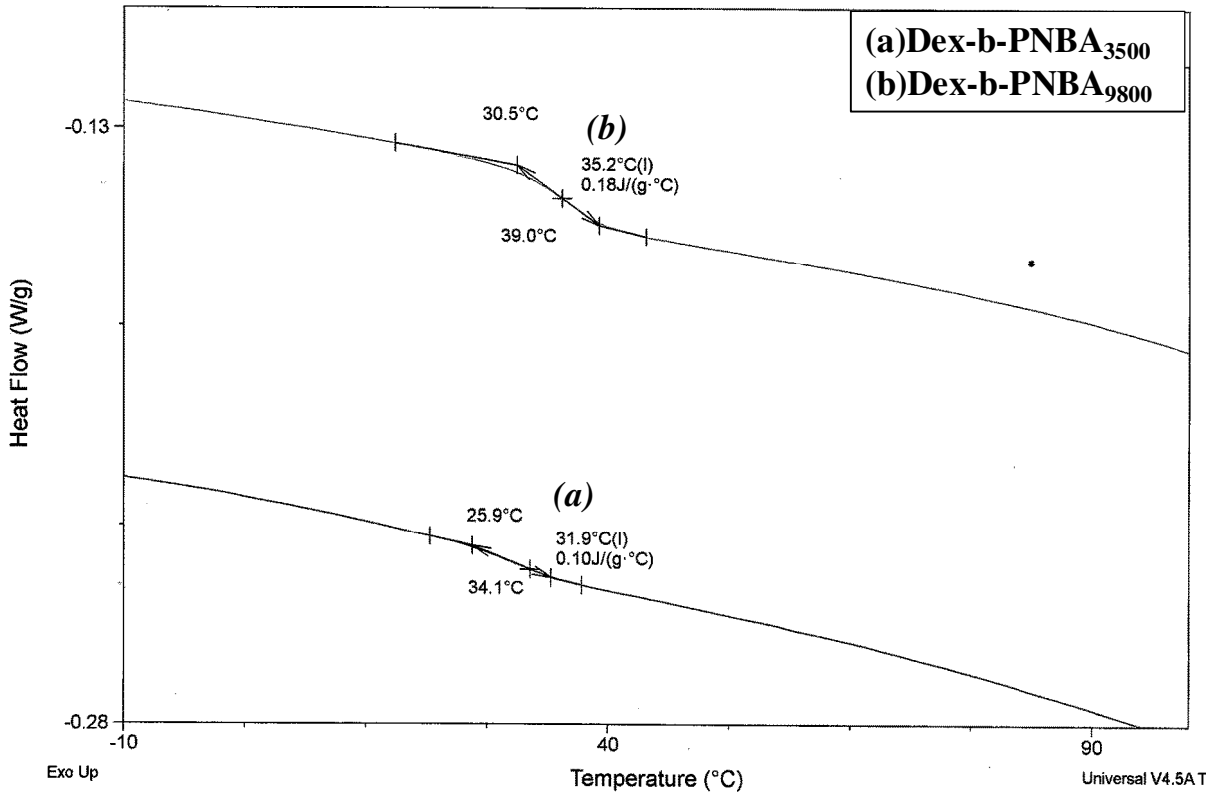

Figure 20. Thermograms MDSC of diblock glycopolymers Dex-b-PNBA$_{3500}$ (F_{PNBA} = 27%) and Dex-b-PNBA$_{9800}$ (F_{PNBA} = 49%)

The glass transition temperatures of grafted glycopolymers with different weight fractions of PNBA were measured using MDSC. As shown in Figure 21, by comparing grafted glycopolymers having close number of graft PNBA chains, we found that grafted glycopolymer with longer PNBA grafts show higher Tg. On another hand, if we compare two glycopolymers with different number of same PNBA grafts such as Dex(15)-g-12PNBA$_{9800}$ (F_{PNBA} = 85 %) and Dex(15)-g-1.5PNBA$_{9800}$ (F_{PNBA} = 44 %), we observed that Tg increase when the number of grafts decreases. Decreasing the number of graft may increase probability of hydrogen bonding formation between hydroxyl groups of glucosidic units and consequently, Tg will be higher.

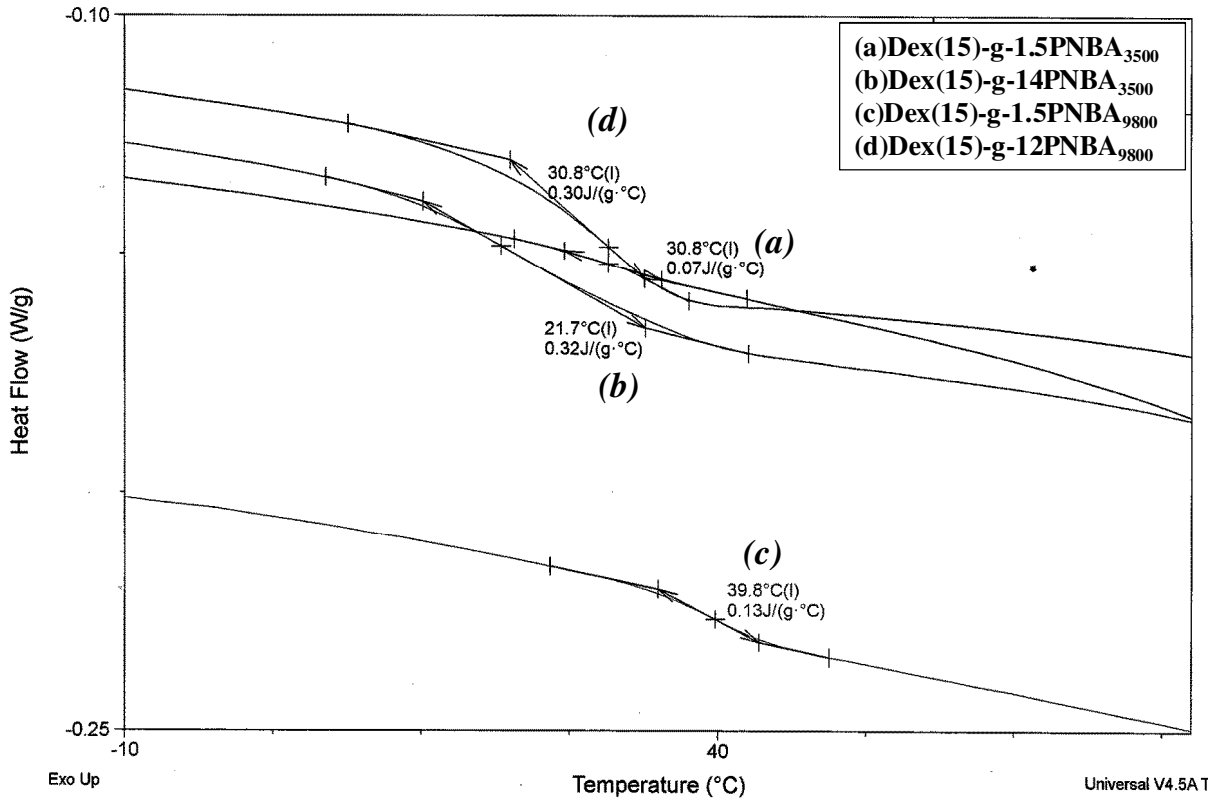

Figure 21. Thermograms MDSC of grafted glycopolymers, Dex(15)-g-1.5PNBA$_{3500}$, Dex(15)-g-14PNBA$_{3500}$, Dex(15)-g-12PNBA$_{9800}$, Dex(15)-g-1.5PNBA$_{9800}$ with F_{PNBA} = 22, 75, 85, 44 %, respectively.

III.6) High Performance Particle Sizer (HPPS)

We measure the Z-average diameter of nanoparticles using High Performance Particle Sizer (HPPS). HPPS measures diameter of nanoparticles by scattering of light. Laser beam passed through nanoparticles dispersion and small particles scattered laser beam in all directions (Rayleigh scattering). This fluctuation is due to the Brownian motion of the small nanoparticles in solutions. HPPS from Malvern Instruments has a laser (He-Ne, 3.0 mW, 633 nm), an avalanche photodiode type detector, (Q, E> 50% 633 nm), and allows a temperature control regulation between 10 ° C and 55 ° C. Measurements are in backscattering at an observation angle of 173 °, which allows the study of relatively concentrated dispersions. The measurement position of the beam is automatically adjusted according to the concentration of the sample in order to avoid multiple scattering effects. We used glass or plastic cells depending the solvent we used as organic solvent (DMSO) or aqueous, respectively.

III.7) Zetasizer instrument

This instrument was used to determine zeta potential value corresponding to each nanoparticles we prepared. Sample was prepared as follow: 1.5 mL of nanoparticles dispersion and 1.5 mL of xM NaCl solution (where x is concentration of NaCl solution from 10^{-1} to 10^{-4} mol/L) were mixed. We filled capillary zeta potential cell of Zetasizer instrument (Figure 22) with solution and zeta potential was measured. We measured zeta potential three times and then take average value. We measured all samples using same cell measuring.

Figure 120. The capillary zeta potential cell for the Malvern Zetasizer.

III.8) Transmission Electron Microscopy (TEM)

The shapes of prepared nanoparticles were characterized by transmission electron microscopy (TEM) Philips CM200 operating at 200 kV (dot resolution: 0.27 nm resolution in lines: 0.14 nm). It is equipped with two CCD cameras (fast and HR) and an energy dispersion spectrometer photons X.

A drop of the nanoparticles dispersion was deposited onto a copper grid. After 3 minutes, the excess solution was absorbed with a filter paper . One drop of a milli-Q water solution uranyl acetate (10 mg/mL) was added to the grid. After 1 minute, the excess solution is absorbed with a filter paper. The grid was finally allowed to dry for 5 minutes before measurement.

III.9) UV-Vis spectroscopy

Uvikon-XL Bio-Tek Spectrophotometer. The absorbance was recorded in the 250-450 nm range.

VI) UV-Irradiation

UV- lamp used is OmniCure® S1000 UV spot cure lamp provides a well-rounded and Lamp module is High Pressure 100 Watt mercury shot arc with light guide insertion with core is equal to 8 mm.

We studied the effect of UV-irradiation on solutions of homopolymer PNBA, diblock and grafted glycopolymers in DMSO using UV lamp power equal to 1150 mW/cm². Effect of UV-irradiation on nanoparticles prepared was also studied on their aqueous solutions containing buffer pH= 7 (KH_2PO_4/Na_2HPO_4) and using different powers of UV lamp as 5%, 320 mW/cm², 10%, 620 mW/cm² and 20%, 1150 mW/cm².

V) Cytotoxicity. WST-1 assay (done by Prof. M. Barberi-Heyob, CRAN, Nancy-France)

Day 1: U 87 cells (Grade IV human glioblastoma cell line) were seeded at a density of 6 000 cells per well in a 96 wells plate in DMEM culture medium (Gibco, Invotrogen) (10% fetal calf serum, 1% streptomycin/penicillin, 1,25% sodium pyruvate, 1% essential amino acids, 0,5% non essential amino acids, 0,4% vitamins, 1% L-glutamine/L-asparagine under standard conditions (5% CO2, 37 °C, 95% humidity).

Day 2: After 24h, culture medium is removed and 200 µl of each nanoparticles concentrations (1,2,3,4,5 mg/mL) are added in the wells. Each experiment was tested in sixplicate

Day 3: The nanoparticles and cells are incubated together for 24h at 37°C , then the wells are washed 3 times with 200 µl of DMEM. After that, cells are incubated during 24h with 150µl/well of fresh DMEM.

Day 4: 15µl of WST-1 are added in each well. After medium homogenization, the plates are incubated for 1h at 37°C. Their absorbances are measured at fixed wavelength equal to 450 nm using spectrometer titertekmultiskan (Labsystem,Cergy-pontoise, France).

GENERAL CONCLUSION AND PERSPECTIVE

General Conclusion and Perspective

Many years ago, LCPM interested in the development of one nanomedicine approach, that is drug delivery systems (DDS), to allow the administration of pharmaceutical compounds in human body. Stealthy DDS were produced by nanoprecipitation or emulsion/organic solvent evaporation techniques that require amphiphilic polysaccharide derivatives used as surfactants. The hydrophilic part of such surfactants provides the hydrophilic surface to DDS and allows the immune system bypassing. Beyond polysaccharide derivatives, one of LCPM's strength is to produce amphiphilic glycopolymers using controlled polymerizations. These compounds are based on hydrophilic polysaccharide and hydrophobic parts. In the last ten years, LCPM firstly produced dextran-g-polylactide using the "grafting from" strategy through the controlled ring opening polymerization of lactide. Then, by an ATRP/grafting from combination, dextran-g-PMMA were produced and opened the way to dextran-g-poly(diethylene glycol cholesteryl ether acrylate) that are the first liquid crystal-based glycopolymers. To shift LCPM's researches, we suggested to produce new photosensitive amphiphilic glycopolymers through the "grafting onto" strategy. Consequently, the subject of this thesis was to firstly produce several glycopolymers by controlled ways to reach various architecture. Secondly, we turned this thesis to produce new photosensitive DDS.

In the first chapter of this manuscript, we discussed the development of drug delivery systems and finally we focused on sensitive DDS, especially on light-sensitive ones. Then, in the same chapter, we expounded the controlled free radical polymerization techniques and focused on Single Electron Transfer- Living Radical Polymerization (SET-LRP). Indeed, we selected this technique to obtain photosensitive hydrophobic poly(*o*-nitrobenzyl acrylate) (PNBA) in a controlled way.

Controlled synthesis of PNBA was described in the first part of the second chapter. While the radical polymerization (even with ATRP, RAFT and NMP) of *o*-nitrobenzyl acrylate (NBA) was not controlled due to inhibition and retardation effects coming from the nitro-aromatic groups, we have benefitted from recent developments in the single-electron transfer¯living radical polymerization (SET¯LRP) to control the NBA polymerization and published it for the first time. The living character of this polymerization was demonstrated by chain extension using methyl acrylate as second monomer. Then, bromide end-function of PNBA was easily substituted by azido group.

In a parallel way, dextrans (T40 and T10) were modified by introducing several alkyne groups as side chains along the polysaccharide (alkynated dextran) or only one alkyne group at the reducing dextran end-chain (-alkyne dextran). These modified dextrans have been used to produce grafted and diblock glycopolymers (dex-g-PNBA and Dex-b-PNBA) through the "grafting onto" technique that proceeded via a Huisgen-type Copper(I) catalyzed Azide-Alkyne Cycloaddition (CuAAC click chemistry). By this strategy, we got four grafted glycopolymers with different weight fractions of PNBA (F_{PNBA}) equal to 22, 44, 75, 85 %. Two diblock glycopolymers with F_{PNBA} equal to 27 and 49% were also produced.

In the third chapter of this manuscript, we formulated nanoparticules from the previous amphiphilic glycopolymers. On one hand, grafted glycopolymers with high PNBA weight fractions (Dex(15)-g-14$PNBA_{3500}$ (F_{PNBA} = 75%) and Dex(15)-g-12$PNBA_{9800}$ (F_{PNBA}= 85%)) were successful nanoprecipitated. On the second hand, we also tried to produce nanoparticles based on grafted glycopolymers with lower PNBA weight fractions (Dex(15)-g-1.5$PNBA_{3500}$ and Dex(15)-g-1.5$PNBA_{9800}$), but these last glycopolymers are not soluble in common organic solvents used in nanoprecipitation method. Another type of nanoparticles was prepared using hydrophobic PNBA chains dissolved in an organic phase and alkynated dextrans used as surfactants in an aqueous one. After emulsion/organic solvent evaporation, nanoparticles based on hydrophobic PNBA core and hydrophilic dextran shell were produced due to the tensioactive properties of these dextran derivatives. Depending on the PNBA chains we used, alkynated dextrans are just physically adsorbed onto the particles surface (case of PNBA-Br) or covalently linked to the core (case of PNBA-N_3). More precisely, PNBA-N_3 enabled us to carry out the CuAAC click chemisty *in situ*, during the sonification step of this method. From ^{1}H NMR spectra, we observed that nanoparticles prepared with an *in situ* CuAAC have a higher content of dextran than the others prepared without click chemistry. Moreover, thes covalent linkage (triazole ring) between dextran and PNBA has another importance on the colloïdal stability against competitive anionic surfactant like sodium dodecyl sulfate (SDS). As known from literature, SDS desorbs hydrophilic shell, which is physically adsorbed onto hydrophobic surface. By carrying out an *in situ* click chemistry, SDS was unable to desorbe this dextran shell. Zeta potential values and dextran shell thickness of all prepared nanoparticles were estimated. The colloïdal stability of all nanoparticles were studied using different ionic strengths. All results proved that these nanoparticles may be used as drug delivery system.

Due the photosensitive character of PNBA, we studied the effect of UV-irradiation on all nanoparticles in the third chapter of this manuscript. Firstly, the photolysis of PNBA, then of Dex-g-PNBA, was studied using different techniques such as ^{1}H NMR, FT-IR, UV-Vis spectroscopy and pH-meter. In agreement with literature, the photolysis products of PNBA were poly(acrylic acid) and 2-nitrosobenzaldehyde. Secondly, we proved that the presence of dextran linked to PNBA did not prevent this photolysis. The effect of nanoparticles irradiation was studied by following the Mean Count Rate evolution during the irradiation, that allowed us to adapt important parameters such as the effect of medium composition, concentration of sample dispersion and mode of UV-irradiation exposure.

In a parallel way, Nile Red loaded nanoparticles were produced and were found to be stable (no Nile Red diffusion occurred during the tested period). The photolysis of these nanoparticles was studied by following the Nile Red fluorescence. Whatever the particles, change in the Nile Red environment was highlighted during the UV-irradiation. More precisely this change occurred before the quantitative photolysis of the PNBA part. With this study, we proved that all the nanoparticles based on grafted or diblock glycopolymers are highly photosensitive and can be used as photo-controllable drug delivery systems.

Preliminary results on cytotoxcity were done at Centre de Recherche en Automatique de Nancy (CRAN), University of Lorraine (Prof. Muriel Barberi-Heyob). Dex-g-PNBA nanoparticles were found to be no cytotoxic. After irradiation in DMEM medium, consequent cytotoxicity was never observed. Contrary, nanoparticles cytotoxicity was observed after irradiation in water, due to the high number of acidic functions produced during photolysis of PNBA parts.

As above summarized, during this Ph.D., we got core/shell nanoparticles that may be used as photosensitive and photo-controllable drug delivery systems. In the near future, we will study the following items:

- Self-assembly of amphiphilic glycopolymers via dialysis technique will be further studied.

- Cytotoxicity tests will be improved using the Caco-2 cells line (continuous cells of heterogeneous human epithelial colorectal adenocarcinoma). This study will be carried out in collaboration of LRGP, University of Lorraine.
- An anti-cancer hydrophobic drug will be loaded in PNBA/Dextran nanoparticles. The release of this drug, induced by the UV-irradiation, will be studied. By this way, the effect of these smart DDS to stop the Caco-2 expansion or to kill them will be estimated.
- In order to improve the adhesion of these DDS onto the Caco-2 surface, or to promote the penetration into them, specific peptides will be anchored on the nanoparticles surface. These peptides will be linked to the glycopolymers before the formulation of the particles, or nanoparticles will be post-functionalized.
- In a parallel way, these photosensitive glycopolymers will be used to formulate smart microcarriers. These microcarriers will compete commercials ones that are used to promote the expansion of Human Mesenchymal Stem Cells (multipotent progenitor cells found in bone marrow and other organism sites) required in tissue engineering.

LIST OF FIGURES

CHAPTER (I) BIBLIOGRAPHY

CHAPTER (II) LIGHT-SENSITIVE AMPHIPHILIC GLYCOPOLYMERS

I) Introduction

1) o-Nitrobenzyl Acrylate is Polymerizable by Single Electron Transfer-Living Radical Polymerization

2) Synthesis of Amphiphilic Light-Responsive Dextran-g-poly(o-nitrobenzyl acrylate) Glycopolymers

3) Synthesis of Amphiphilic Light-Responsive Dextran-b-poly(o-nitrobenzyl acrylate) Copolymers

CHAPTER (III) NANOPARTICLES BASED ON DEXTRAN AND POLY(O-NITROBENZYL ACRYLATE)

LIST OF TABLES

CHAPTER (I) BIBLIOGRAPHY

CHAPTER (II) LIGHT-SENSITIVE AMPHIPHILIC GLYCOPOLYMERS

1) o-Nitrobenzyl Acrylate is Polymerizable by Single Electron Transfer-Living Radical Polymerization

2) Synthesis of Amphiphilic Light-Responsive Dextran-g-poly(o-nitrobenzyl acrylate) Glycopolymers

3) Synthesis of Amphiphilic Light-Responsive Dextran-b-poly(o-nitrobenzyl acrylate) Copolymers

CHAPTER (III) NANOPARTICLES BASED ON DEXTRAN AND POLY(O-NITROBENZYL ACRYLATE)

LIST OF SCHEMES

CHAPTER (I) BIBLIOGRAPHY

CHAPTER (II) LIGHT-SENSITIVE AMPHIPHILIC GLYCOPOLYMERS

I) Introduction

1) o-Nitrobenzyl Acrylate is Polymerizable by Single Electron Transfer-Living Radical Polymerization

2) Synthesis of Amphiphilic Light-Responsive Dextran-g-poly(o-nitrobenzyl acrylate) Glycopolymers

3) Synthesis of Amphiphilic Light-Responsive Dextran-b-poly(o-nitrobenzyl acrylate) Copolymers

CHAPTER (III) NANOPARTICLES BASED ON DEXTRAN AND POLY(O-NITROBENZYL ACRYLATE)

TITRE Des glycopolymères photosensibles aux systèmes de libération stimulable de principes actifs

Des glycopolymères greffés et dibloc, amphiphiles et photosensibles, à base de poly(acrylate d'*o*-nitrobenzyle) (PNBA) hydrophobe et photoclivable et de dextrane hydrophile ont été préparés avec succès en utilisant notammennt une réaction d'Huisgen (Cycloaddition Azoture-Alcyne catalysée par le Cuivre (I) - CuAAC chimie click). Dans un premier temps, la polymérisation de l'acrylate d'*o*-nitrobenzyle a été contrôlée avec succès grâce aux développements récents de la polymérisation radicalaire vivante par transfert d'un seul électron (SET-LRP). Nous avons alors obtenu un PNBA fonctionnalisé à son extrémitié par un brome. Ce brome a ensuite été substitué par un groupe azido. En parallèle, le dextrane a été modifié pour y introduire plusieurs fonctions alcyne (dextrane alcyne) ou une seule sur son extrémité réductrice (dextrane α-alcyne). Nous avons ensuite fait réagir ces dérivés de dextrane avec le PNBA-N_3 pour obtenir respectivement les glycopolymères greffés et dibloc. Tous les glycopolymères ont été caractérisés par chromatographie d'exclusion stérique (SEC), Résonnance Magnétique Nucléaire ^{1}H, ^{13}C, 2D DOSY ^{1}H et par spectrométrie FT-IR. Dans un deuxième temps, nous avons optimisé les conditions pour obtenir des nanoparticules peu disperses à partir des précédents glycopolymères. Dans certains cas, des nanoparticules ont également été obtenues en utilisant le dextrane alcyne et le PNBA-N_3 dans un procédé d'émulsion/évaporation de solvant organique. La stabilité de toutes les nanoparticules vis-à-vis de solutions aqueuses de diverses forces ioniques ou d'un tensioactif compétitif a été étudiée. Enfin, l'effet de la lumière sur ces nanoparticules photosensibles a été mis en évidence à l'aide de la lampe UV. Plus précisément, nous avons pu suivre la destruction des nanoparticules par spectroscopie de fluorescence et diffusion de lumière dynamique en encapsulant le Rouge du Nil (sonde fluorescente) au sein de ces particules.

Mots-clés: glycopolymère, greffé, dibloc, photosensible, amphiphile, nanoparticule, acrylate o-nitrobenzyle, SET-LRP, dextrane, chimie click

TITLE From photosensitive glycopolymers to smart drug delivery systems

Photosensitive grafted and diblock amphiphilic glycopolymers based on hydrophobic photosensitive poly(*o*-nitrobenzyl acrylate) (PNBA) and hydrophilic dextran were successfully prepared via grafting onto techniques through a Huisgen-type Copper(I) catalyzed Azide-Alkyne Cycloaddition (CuAAC click chemistry). Firstly, recent developments in the single-electron transfer–living radical polymerization (SET–LRP) provided us an access to control the *o*-nitrobenzyl acrylate polymerization and we obtained PNBA with bromide end function. Then, this bromide end function was replaced by azido (N_3) group. In a parallel way, we modified dextran by introducing several alkyne groups all long the polysaccharide chain (alkynated dextran) or only one group at the reducing end-chain (α-alkyne dextran). In the second step, alkynated dextran and α-alkyne dextran were reacted with PNBA-N_3 by CuAAC to obtain grafted or diblock glycopolymers. All glycopolymers were characterized by Size Exclusion Chromatography, ^{1}H, ^{13}C, 2D DOSY ^{1}H NMR and FT-IR spectroscopy. Secondly, conditions to formulate nanoparticles from the previous glycopolymers were optimized. In some case, we also carried out an emulsion/evaporation process using dextran alkynated and PNBA-N_3 to produce nanoparticles. Then, stability of nanoparticles were studied over rang of ionic strengths as well as stability in presence of a competitive surfactant. Finally, the effect of light on these photosensitive nanoparticles was studied using UV-lamp. More precisely, we loaded these nanoparticules by Nile Red fluorescent dye and followed thier destruction by using fluorescence spectroscopy and Dynamic Light Scattering.

Keywords: Glycopolymer, grafted, diblock, photosensitive, amphiphilic, nanoparticle, o-nitrobenzyl acrylate, SET-LRP, dextran, click chemistry, light-responsive polymer